Rapport / Report

Åknes/Tafjord-project

Numerical simulations of tsunamis from potential and historical rock slides in Storfjorden; Hazard zoning and comparison with 3D laboratory experiments

20051018-00-1-R
24 March 2010
Rev.: 01, 21 February 2011

Project

Project:	Åknes/Tafjord-project
Document No.:	20051018-00-1-R
Document title:	Numerical simulations of tsunamis from potential and historical rock slides in Storfjorden; Hazard zoning and comparison with 3D laboratory experiments
Date:	24 March 2010
Revision:	01, 21 February 2011

Client

Client:	Åknes/Tafjord Beredskap IKS
Client's contact person:	
Contract reference:	Confirmation of orders from NGI; 2006-02-13, 2009-11-11 and 2010-12-15

For NGI

Project manager:	Carl Bonnevie Harbitz
Prepared by:	Carl Bonnevie Harbitz , Sylfest Glimsdal
Reviewed by:	Finn Løvholt

Main office:
PO Box 3930 Ullevål Stadion
NO-0806 Oslo
Norway

Trondheim office:
PO Box 1230 Pirsenteret
NO-7462 Trondheim
Norway

T (+47) 22 02 30 00
F (+47) 22 23 04 48

BIC No. DNBANOKK
IBAN NO26 5096 0501 281
Company No.
958 254 318 MVA

ngi@ngi.no
www.ngi.no

Executive Summary

This report presents the final results from the numerical modeling of tsunamis due to potential rock slides from Åknes and Hegguraksla in Storfjorden, Møre & Romsdal County, western Norway. Important contributions to the presented work are also given by the University of Oslo, the Coast and Harbor Research Laboratory at SINTEF, and Lars Harald Blikra (NGU and the Åknes/Tafjord-Beredskap IKS).

According to the guidelines from The Norwegian Water Resources and Energy Directorate (NVE) and County Governor of Møre & Romsdal County, an estimated sea level rise for the period 2010-2100 of 0.7 m is taken into account in

the calculations for the hazard zoning. The background for the estimate is found in DSB (2009).

As stated in the contract with the Åknes/Tafjord-Beredskap IKS (ÅTB), NGI has conducted detailed tsunami run-up calculations at 21 locations along Storfjorden as input to hazard zoning. All locations are evaluated for two rock slide tsunami scenarios from Åknes. At Fjøra, Vika, Valldal, and Tafjord also two rock slide tsunami scenarios from Hegguraksla are considered. For slide volumes see Table 0.1. As an example, Figure 0.1 shows the maximum inundation lines (trim lines) for the two scenarios from Åknes for Hellesylt. The largest tsunami impact for the Åknes scenarios is found at Hellesylt with simulated run-up in excess of 80 m due to the largest slide scenario. For the same scenario a run-up height in excess of 60 m is found at Geiranger. For a summary of the simulated maximum run-up heights at the 21 locations, see Table 0.1. It should be emphasised that the analyses reveal large local variations in the distribution of the run-up heights. The table only shows the maximum value.

In addition NGI has updated the run-up heights using new scenarios and wave propagation models for the outer part of Storfjorden (the previous results were presented in NGI, 2008a).

Tsunamis propagating in a fjord may propagate over large distances without being significantly reduced. In addition, local effects may lead to unexpected large run-up far from the slide area.

An important parameter for the wave loads acting on buildings and infrastructure as well as for the erosion during tsunami impact is the wave current velocity. The configuration of the topography and obstructions may focus and channelize the waves, leading to stronger localised loads or erosion during run-up.

The set of numerical models applied in the presented work is thoroughly validated against the laboratory experiments at SINTEF, Trondheim. The discrepancies between the numerical model and the laboratory experiments are remarkably small. Furthermore, the performance of the numerical run-up model is confirmed by validatoin against an independent run-up model. The run-up due to three historical events, Tafjord (1934), Skafjell (1731), and Tjelle (1756), are closely reproduced by the numerical models. We may therefore conclude that the modeling is performed with high accuracy. The largest uncertainty is related to how the slides will enter the water in a real event. In the computations we have applied "rounded box slides" that represent worst cases for each individual volume. Geological findings at Åknes confirm that simultaneous releases of large blocks or even the total volumes are not unlikely.

The new results presented in this report differ from the previous results (NGI, 2005). This is due to

- Improvements in the numerical modelling (the run-up heights are now calculated by a numerical model rather than the simplified empirical approach, and the models for the tsunami propagation are improved)
- Larger slide volumes and larger slide frontal areas
- Longer and more realistic run-out distances
- Slightly different slide directions

The results from the run-up calculations in this report are best estimate predictions, i.e. they are not taking any safety factors into account.

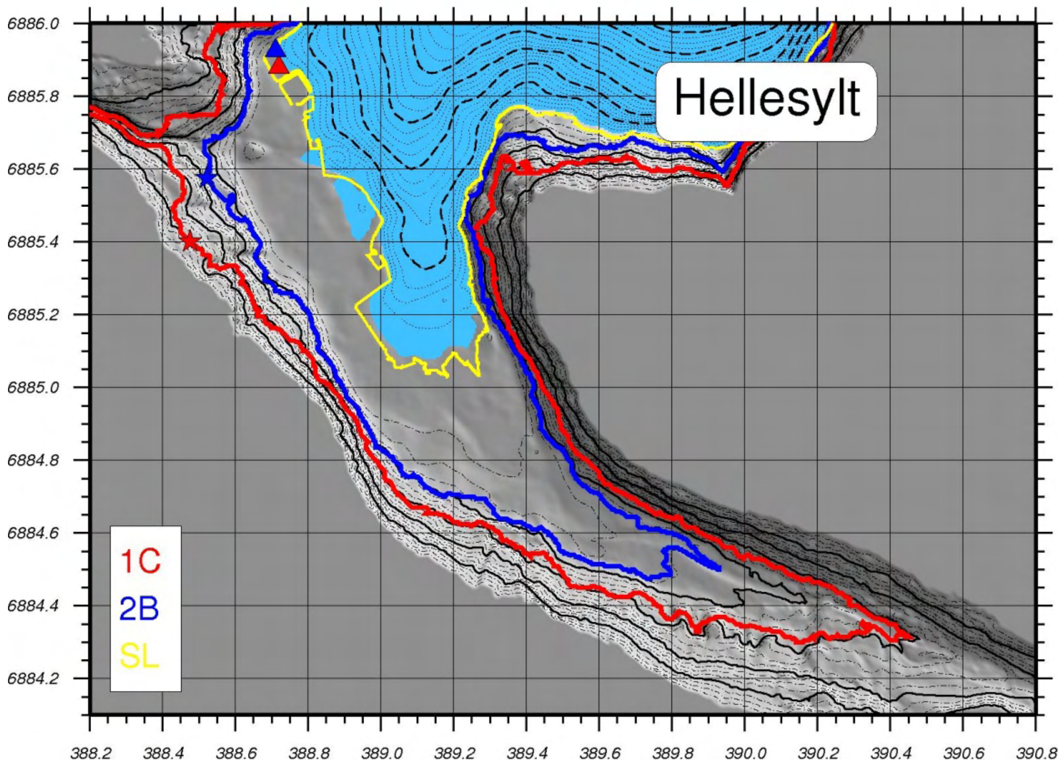

Figure 0.1: The trim lines at Hellesylt for scenarios from Åknes (1C and 2B). The yellow line represents today's coastline. The triangles and stars indicate the positions of the maximum inundation height along shoreline (for a sea level rise of +0.7 m) and of the maximum run-up height, respectively.

Table 0.1: Run-up heights given in meters above today's mean sea level (MSL) at all locations. The heights include the effect of a sea level rise of 0.7 m. For the selection of locations and scenarios we refer to ÅTB (2009a, 2009b).

Location	**Scenarios**			
Name	**1C** *54 M^3*	**2B** *18 Mm^3*	**H2** *2 Mm^3*	**H3** *3.5 Mm^3*
Dyrkorn	3	2	-	-
Eidsdal	8	4	-	-
Fjøra	6	3	17	20
Geiranger	70	30	-	-
Gravaneset	7	3	-	-
Hellesylt	85	35	-	-
Hundeidvik	2	1	-	-
Linge	6	3	-	-
Magerholm	3	1	-	-
Norddal	14	7	-	-
Oaldsbygda	100	70	-	-
Ramstadvika	3	2	-	-
Raudbergvika	13	6	-	-
Skardbøen	4	2	-	-
Stordal	8	4	-	-
Stranda	7	4	-	-
Sykkylvsfjorden	4	2	-	-
Tafjord	14	7	9	13
Vaksvik	5	3		
Valldal	7	3	6	8
Vegsundet	4	3	-	-
Vika	9	4	11	15
Ørskog	6	3	-	-

Contents

1 Introduction

This is the fourth and final NGI rock slide tsunami report for the Åknes/Tafjord-project. In agreement with the client, NGI has for the hazard zoning performed detailed tsunami run-up calculations at 21 locations along Storfjorden, Figure 2.1. All locations are evaluated for two rock slide tsunami scenarios from Åknes (Figure 4.5), see Table 2.1. At Fjøra, Vika, Valldal, and Tafjord also two rock slide tsunami scenarios from Hegguraksla (Figure 4.13) are considered.

The main purpose of this report is to contribute to the tsunami hazard zoning, see Sections 2 and 3. In Section 4 the new set of models made available for the project is described and details regarding the tsunami propagation and inundation for eight scenarios from Åknes and three from Hegguraksla are given in addition to a set of back-calculations of historical events. Furthermore, the model setup and the numerical results are validated through comprehensive comparisons with laboratory experiments and with an independent numerical (run-up) model in Sections 5 and 6, respectively. Finally, the uncertainties of the numerical modelling are discussed in Section 7.

The previous reports in this project are:

- NGI (2005) Innledende numeriske analyser av flodbølger som følge av mulige skred fra Åknes.
- NGI (2006) Semi-annual report: Preliminary results using an improved tsunami model.
- NGI (2008a) Semi-annual report: Tsunami impact in the outer part of Storfjorden, testing of numerical models for rock slide and tsunami, coupling to laboratory experiments.

In Appendix A the details for the hazard zoning is found, while the comparison between independent run-up models is found in Appendix B, C, and D. The sensitivity analyses from the previous reports are summarized in Appendix E together with the new ones.

2 Tsunami hazard zoning

For the hazard mapping at the 21 locations shown in Figure 2.1, tsunami simulations for two rock slide scenarios at Åknes and two rock slide scenarios at Hegguraksla are conducted. The deliverables are the maximum run-up heights (a single value at each location), inundation maps (trim lines and maximum water levels), flow depths and wave current velocities. In this section the hazard is presented as maximum run-up heights (single values). Further, important findings at each location and a discussion of the results are described. For discussions regarding the modelling uncertainties, we refer to Section 7.

Details of all other quantities are presented in Appendix A together with the result data for direct implementation into GIS, which is delivered as a part of this report. An example for Hellesylt showing the trim lines is given in Figure 2.3, while for the other quantities examples are found in Figure 4.16 - Figure 4.20.

According to the guidelines from NVE and County Governor of Møre & Romsdal County an estimated sea level rise for the period 2010-2100 of 0.7 m is taken into account in the calculations for the hazard zoning. The background for this estimate is found in DSB (2009).

The calculated run-up heights at all locations and for all scenarios applied in the hazard zoning is also delivered in digital form for later use in GIS-applications by the end users. The elevation of the trim lines (see definition below), which form parts of the digital deliverable of this project, refer to today's mean sea level. See Appendix E for information on the background data, etc.

For the hazard zoning we have considered the effect of the largest leading waves that do have the strongest impact during run-up. With a few exceptions the highest run-up is found for the very first positive wave.

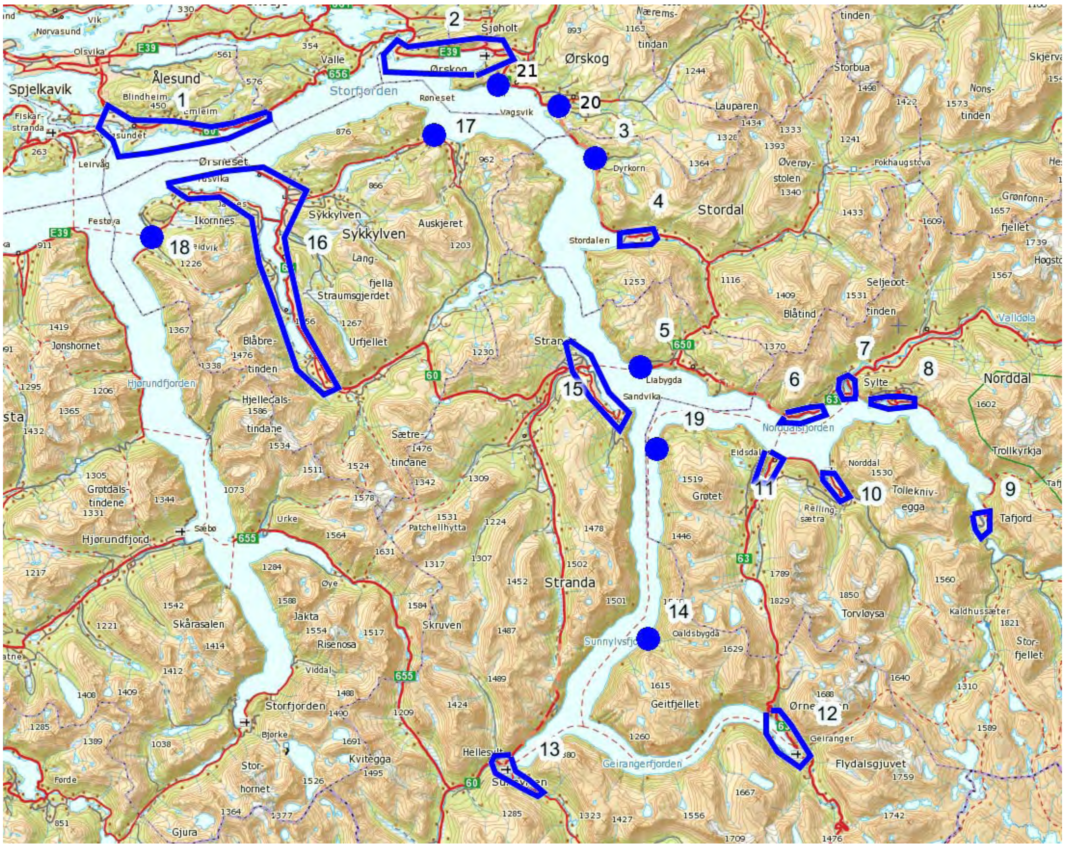

Figure 2.1: Overview of all locations for hazard zoning. Maximum run-up heights for all the locations are listed in Table 2.2.

2.1 Definitions

Below, definitions of technical key terms used in the text are presented. As far as possible, compatibility with the UNESCO-IOC tsunami glossary (UNESCO-IOC, 2006) is aspired. In addition, a definition sketch defining the parameters related to the tsunami inundation process is given in Figure 2.2.

- **Flow depth –** Water elevation above land during inundation (see Figure 2.2).
- **Hazard -** Probability that a particular danger (threat) occurs within a given period of time. Here, the tsunami hazard is the maximum water level associated with a scenario return period.
- **Inundation distance –** Maximum horizontal penetration of the tsunami from the shoreline (see Figure 2.2).
- **Maximum water level –** Here, defined as the largest water elevation above the still water level (see Figure 2.2).
- **Probability -** A measure of the degree of certainty. This measure has a value between zero (impossibility) and 1.0 (certainty). It is an estimate of the likelihood of the magnitude of the uncertain quantity, or the likelihood of the occurrence of the uncertain future event.
- **Return period -** Average time period between events of a given size in a particular region, cycle time.
- **Risk -** Measure of the probability and severity of an adverse effect to life, health, property, or the environment. Quantitatively, Risk = Hazard × Potential Worth of Loss. This can be also expressed as "Probability of an adverse event times the consequences if the event occurs".
- **Run-up height –** Water level above the still water level at the inundation limit (see Figure 2.2).
- **Surface elevation –** Here, defined as the water elevation relative to the mean sea (can be negative or positive, see Figure 2.2).
- **Trim line –** The line describing the maximum inundation (see Figure 2.2). The location of the trimline is in this report defined to where the maximum flow depth is 10 cm.
- **Vulnerability -** (1) The degree of loss to a given element at risk, or set of such elements, resulting from an event of a given magnitude or intensity, usually expressed on a scale from 0 (no loss) to 1 (total loss). (2) Degree of damage caused by various levels of loading.

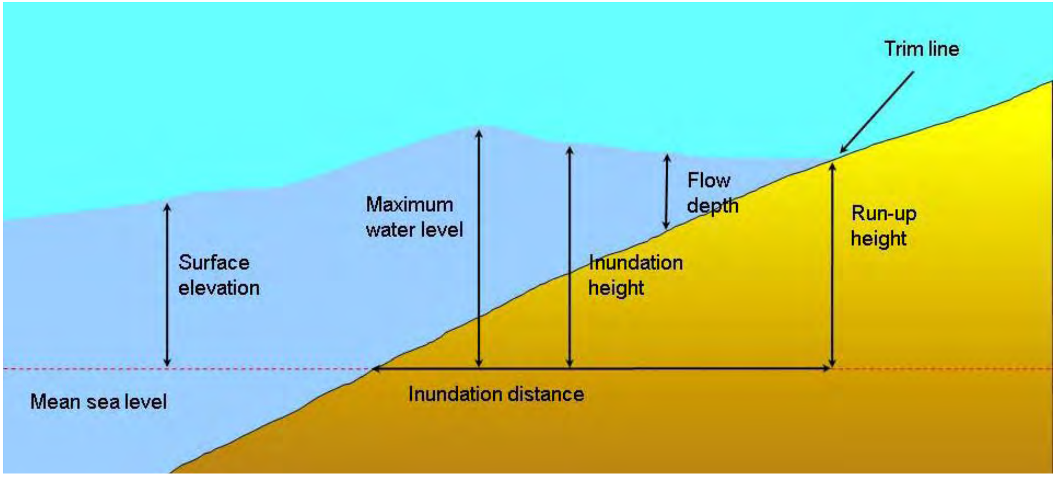

Figure 2.2: Definitions of terms used for describing the tsunami impact on land.

2.2 Slide scenarios

Altogether four scenarios are applied for the hazard zoning, see Table 2.1. From Åknes, the largest scenario of 54 Mm^3 corresponds to the credible worst case scenario (1C), while the western flank scenario (2B) is estimated to a volume of 18 Mm^3. The impact velocity for both scenarios is estimated to 45 m/s. In addition, two scenarios from the upper part of Hegguraksla are included. The volumes are 2 Mm^3 (“H2”) and 3.5 Mm^3 (“H3”), with impact velocity of 60 m/s.

For the scenarios from Åknes, the velocity progression of the slide (and hence the run-out distances) mimics the velocity progression from the laboratory experiments, while for the scenarios from Hegguraksla the velocity progression is given by NGI (2003).

The nominal annual probability is considered less than 1/1000 for scenarios 1C and H3, and equal to 1/1000 for scenarios 2B and H2, see ÅTB (2009a).

Table 2.1. Parameters for all the scenarios applied for the hazard zoning.

Scenario		**Dimensions**			**Impact velocity**	**Volume**	**Annual probability**
		Height [m]	*Width [m]*	*Length [m]*	*[m/s]*	*10^6 m^3*	
Location	Number						
Åknes	1C	120	450	1000	45	54	<1/1000
	2B	80	450	500	45	18	>1/1000
Hegguraksla	H2	40	200	250	60	2	>1/1000
	H3	46	250	300	60	3,5	<1/1000

2.3 Calculation of run-up

In Table 2.2 we present the maximum run-up heights calculated for all 21 locations. Note that there are large local variations (see, e.g., Figure 4.16) and only the maximum run-up heights are presented in the table. For the largest scenario 1C from Åknes, the maximum run-up heights for Hellesylt and Geiranger are in the range 70 - 85 m. In the outermost location, Vegsundet, the maximum run-up height is found to be about 4 m.

More details for each scenario and all locations are found in Appendix A, where the maximum inundation height and the trim lines are presented for all locations for the scenarios 1C and 2B. At Fjøra, Valldal, Vika, and Tafjord also the scenarios H2 and H3 are evaluated. Further, for the areas at Magerholm, Ørskog, Stordal, Stranda, Ikornes, and Valldal, we present in addition to the maximum inundation heigths and the trim lines also the current velocities and flow depths as well as time-histories for surface elevations and current velocities extracted at five positions at each location. Maximum values and time history of the surface elevation and current velocity give important contributions for the estimate of the wave loads acting on buildings and infrastructure as well as the erosion.

For more background regarding the modeling setup and for more examples we refer to Section 4.

Table 2.2: Run-up heights given in meters above today's mean sea level (MSL) at all locations, the numbering ("no") of the locations refers to Figure 2.1. The heights include the effect of a sea level rise of 0.7 m. For the selection of locations and scenarios we refer to ÅTB (2009a, 2009b).

Location		***Scenarios***			
Name	***no***	***1C***	***2B***	***H2***	***H3***
Dyrkorn	3	3	2	-	-
Eidsdal	11	8	4	-	-
Fjøra	8	6	3	17	20
Geiranger	12	70	30	-	-
Gravaneset	5	7	3	-	-
Hellesylt	13	85	35	-	-
Hundeidvik	18	2	1	-	-
Linge	6	6	3	-	-
Magerholm	1	3	1	-	-
Norddal	10	14	7	-	-
Oaldsbygda	14	100	70	-	-
Ramstadvika	17	3	2	-	-
Raudbergvika	19	13	6	-	-
Skardbøen	21	4	2	-	-
Stordal	4	8	4	-	-
Stranda	15	7	4	-	-
Sykkylvsfjorden	16	4	2	-	-
Tafjord	9	14	7	9	13
Vaksvik	20	5	3		
Valldal	7	7	3	6	8
Vegsundet	1	4	3	-	-
Vika	8	9	4	11	15
Ørskog	2	6	3	-	-

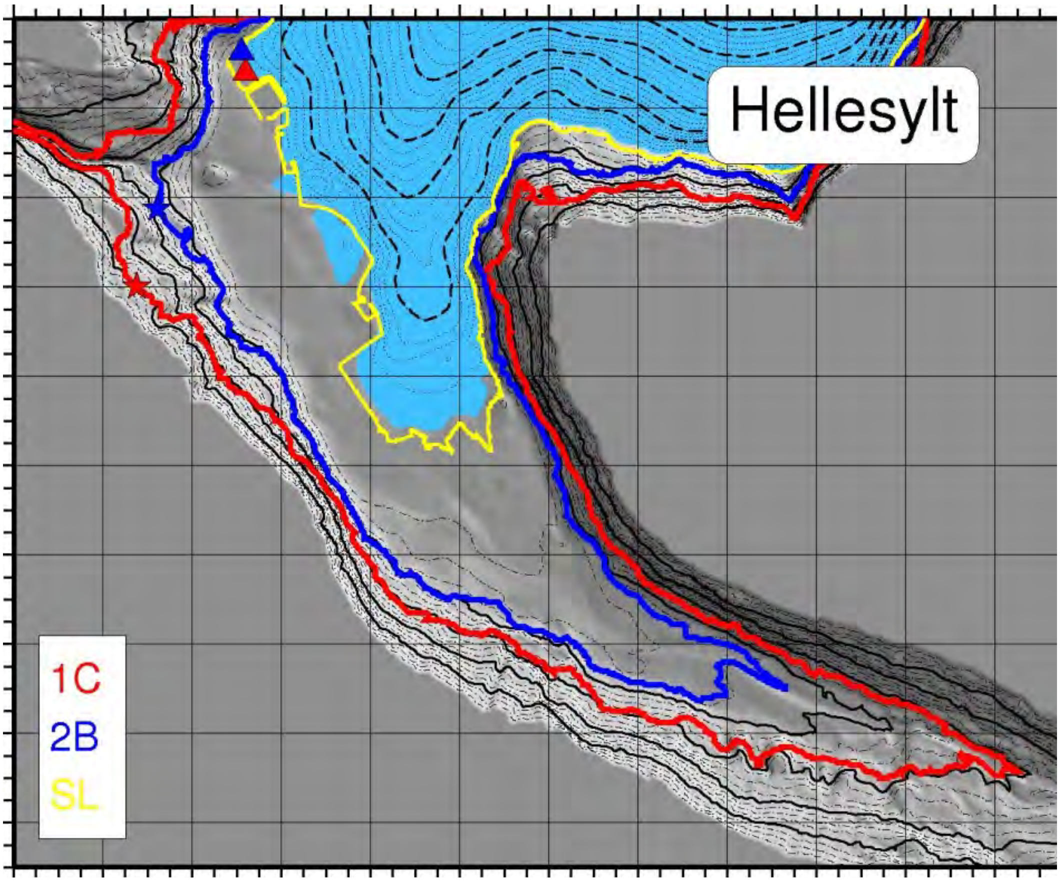

Figure 2.3: Trim lines at Hellesylt for scenaiors 1C (red line) and 2B (blue line). The yellow line represents today's coastline. The triangles and stars indicate the positions of the maximum inundation height along theshoreline (for a sea level rise of +0.7 m) and of the maximum run-up height, respectively. See also Figure 2.2. The contour line intervals are 20 m and 5 m for thick and thin contour lines, respectively.

2.4 Discussion

The main parameters influencing on the run-up heights are:

1. ***Wavelength*** of incident wave.
2. ***Bathymetric slope*** outside the shoreline (the shorter wavelength and the steeper bathymetric slope, the lower run-up height).
3. ***Shape*** of the bathymetry/topography (3D effects).
4. ***Angle*** of tsunami incidence.

Highest run-up is expected for waves impacting the shore perpendicularly. This typically happens in the heads of the fjord system, which are at the same time normally the most inhabited locations. Here the tsunami is also amplified due to shoaling and focusing. As an example see the results for Fjøra in Appendix A. The shoreline is facing towards Hegguraksla and the waves from Hegguraksla are moving perpendicularly against the shoreline and are amplified up to 5 times, while waves from Åknes are almost not amplified (a factor 1 – 1.2). As the wave enters shallower water, it will be amplified and the wave front will typically be steeper. In the last stage the wave steepening may lead to wave breaking. The highest wave current velocity is normally found for the draw-down and mainly seaside the shoreline. As observed in the simulations, the leading waves have the strongest impact in fjord heads, while at locations along the fjord the highest run-up may be related to trailing waves.

After the Tafjord 1934 event, Stranda (Sløgstad) did not observe any waves, but at both Stordal and Ørskog further out in Storfjorden the tsunami impact was severe (run-up heights of several meters), see Furseth (2006). At Stranda the fjord is extremely steep and the waves propagate more or less perpendicularly to the shoreline. However, both Ørskog and Stordal are located at shallower bays. Here the waves are forced to change direction and they tend to propagate perpendicularly towards the shoreline and are finally also more amplified due to gentler bathymetric slopes. In addition the waves are focused inside the bay, see above.

A few examples of different ways of measuring the tsunami impact are found in Section 4.4.1. Maximum inundation height is the highest value at each point at the inundation area measured during the tsunami impact. Similarly, maximum current velocity and maximum flow depth is the highest absolute value of the current velocity and the highest measured height of the water above ground, respectively. In addition, some locations were analyzed using time history of surface elevations and absolute values of the current velocity. The latter measurements are valuable for determining the tsunami impact in more detail. An important observation through these examples is that it is typically very large variations locally of both the maximum inundation height and the maximum current velocity. The shape of topography may channelize and focus the wave leading to higher current velocities and hence stronger erosion like in (narrow) river valleys. This effect may also be important to take into account when designing obstructions against a potential tsunami since such obstructions may easily get an opposite effect channelizing the flow.

2.5 Comments for results at all locations

Below we briefly describe how the bathymetry and topography influence on the wave amplification through shoaling, focusing, refraction, and inundation for all locations (in alphabetical order). We also present the approximate wave period for the different scenarios and indicate whether wave breaking takes place. The wave period is determined from the time history of the surface elevation close to the shoreline, and is an important factor for the duration of the inundation and hence for the total effect on buildings, infrastructure, etc., located in the inundation zone. An interesting observation is that the wave period is mainly increasing with increasing distance of propagation. Possible explanations are dispersive effects as well as effects of wave filtering through the bends and divides throughout the fjord system. Wave breaking is reducing the total run-up through energy dissipation, but may locally lead to stronger damage.

Note that all locations are evaluated for the scenarios 1C and 2B from Åknes. The scenarios H2 and H3 from Hegguraksla are only evaluated for Fjøra, Vika, Tafjord, and Valldal.

2.5.1 Dyrkorn

The bathymetry outside Dyrkorn (location 3, see Figure 2.1) is steep and the waves propagate almost parallel to the shoreline leading to minor amplification of the wave during run-up. The wave period is 250 s, and no wave breaking is found for any scenario.

2.5.2 Eidsdal

The inlet at Eidsdal (11) is steep and the waves are only to a minor extent refracted towards the shoreline, giving insignificant amplification of the wave from the deeper part of the fjord. Landside the shoreline the topography is gentle. The wave period is here 250 s and we revealed no wave breaking.

2.5.3 Fjøra

The bathymetry outside Fjøra (8) is also steep. For the waves from Åknes, Fjøra is partly protected by the headland, and the incident wave is only partly refracted towards the shoreline behind the headland leading to low amplification of the wave.The wave period is 320 s. However, for the waves from Hegguraksla, Fjøra is much more exposed. The waves are here heading directly towards the shoreline. The wave period for the Hegguraksla scenarios is 50 s. We discovered no wave breaking for any scenarios here.

2.5.4 Geiranger

Outside Geiranger (12) the bathymetry is gentle and the waves are focused at the fjord head. Both these effects lead to stronger amplification of the waves. The wave period is 150 s. At least for the largest scenarios intensive wave breaking occur on land close to the shoreline.

2.5.5 Gravaneset

Gravaneset (5) is located on a headland surrounded by a steep bathymetry. The topography is also steep, except for the road and the parking lane for cars waiting for the ferry. The amplification of the waves is insignificant here. The wave period is 200 s, and the waves are not influenced by wave breaking.

2.5.6 Hellesylt

At Hellesylt (13) the conditions for wave amplification are quite similar to those at Geiranger. The wave period is 150 s and on the landside of the shoreline the waves are influenced by extensive breaking. For the largest scenario (1C) the wave inundates the valley up to about 200 m above Steimshølen (easting UTM 390.4 km, see Figure 4.16).

2.5.7 Hundeidvik

Hundeidvik (18) is the outermost location for run-up evaluation. Even though the waves propagate almost perpendicular to the shoreline, the amplification is small due and steep bathymetry. The wave period is 400 s.

2.5.8 Linge

The bathymetry at Linge (6) is steep. At the ferry quay the waves propagate parallel to the shoreline leading to minor amplification of the waves. At the settlements further west, larger amplification is found due to waves propagating more perpendicular to the shoreline. The wave period is 300 s and no wave breaking is found.

2.5.9 Magerholm

The bathymetry at Magerholm (1) is also steep, and the waves are mainly propagating parallel to the shoreline leading to minor amplification. However, at some inlets along the fjord moderate amplification is found. The wave period is 600 s, and no wave breaking is found.

2.5.10 Norddal

At Norddal (10) the bathymetry is somewhat gentler, and the waves are refracted towards the shoreline. In addition the waves are focused by the inlet leading to stronger amplification. Inland the topography is almost flat, leading to extensive wave breaking at least for the largest scenarios. The wave period is about 250 s.

2.5.11 Oaldsbygda

Oaldsbygda (14) is located on the opposite side of Sunnylsfjorden at Åknes. The waves swash up to 100 m.a.s.l. for the largest scenarios even though the bathymetry and the topography are steep. The wave period is approximately 50 s, and due to the steep topography no significant wave breaking appears in the simulation for any scenario. The model does not capture local effects like for instance splashing that might be relevant this near to the rock slide area.

2.5.12 Ramstadvika

At Ramstadvika (17) the bathymetry is steep, but the waves are refracted towards the shoreline. However, the amplification is low and only minor effects of wave focusing. The wave period is about 250 s, and there are no signs of wave breaking here.

2.5.13 Raudbergvika

At Raudbergvika (19) the bathymetry is steep, but with gentler slope landside the shoreline. Since this location is situated not too far from Åknes large waves may impact the area. However, the amplification is insignificant due to the bathymetry and the wave propagation parallel to the shoreline. The wave period is 160 s, and wave breaking does not appear in the calculations.

2.5.14 Skardbøen

At Skardbøen the waves propagate along the shoreline leading to insignificant amplification of the waves. The wave period is about 300 s.

2.5.15 Stordal

The waves at Stordal (4) are focused by the inlet, and refracted towards the shoreline. The amplification is relatively strong, and due to gentle topography, the largest waves will be breaking. The wave period is 250 s.

2.5.16 Stranda

At Stranda (15) the bathymetry is steep, but at least the topography along the river course is gentle. Waves are slightly refracted towards the shoreline. The amplification of waves is relatively small, but the waves are during inundation focused and focused along the river course. This may lead to higher current velocities and thus stronger erosion. The wave period is about 250 s, and we have revealed wave breaking to some degree for the largest scenarios.

2.5.17 Sykkylvsfjorden

Sykkylvsfjorden (16) is about 10 km long, and at the outer part about 2 km wide. The depth is gradually decaying, where the fjord also becomes narrower leading to an increased amplification of the waves. However, about 2 km north of Straumgjerde there is a threshold at the narrowest part of the fjord (width 300 m). At this point the waves are to a large extent reflected. The part of the wave that is not reflected here is extensively influenced by wave breaking. Without this effect the run-up at Straumgjerde could have been much higher. The maximum run-up at the river at Straumgjerde is about 2.5 meters. If the wave enters Fetvatnet (1.6 m.a.s.l.) it will be substantially damped due to radial spread in the lake. For the outer part of Sykkylvsfjorden the waves are mainly propagating parallel to the shoreline leading to limited amplification of the waves.

2.5.18 Tafjord

Tafjord (9) is located at a fjord head with gentle bathymetry leading to stronger amplification of the waves. For scenarios from both Åknes and Hegguraksla the waves are influenced by wave breaking landside the shoreline (owing to smooth topography). The wave period is approximately 200 s and 150 s for scenarios from Åknes and Hegguraksla, respectively.

2.5.19 Vaksvik

In the bay at Vaksvik the waves are focused, and due to low terrain the waves may propagate inland along the river. North and south of Vaksvik, the waves propagate more or less along the shoreline, leading to minor amplification of the waves. The wave period is here about 200-250 s.

2.5.20 Valldal

Outside Valldal (7) the bathymetry is relatively steep, while the topography is to a great extent flat. The waves from both Åknes and Hegguraksla are hardly amplified at all. The wave period is 400 s and 200 s for Åknes and Hegguraksla scenarios, respectively. At least the waves from Hegguraksla are influenced by wave breaking.

2.5.21 Vegsundet

Vegsundet (1) is located inside a bay, with several inlets leading to focusing of the waves. The shallow bathymetry is also leading to a stronger amplification. The wave period is about 400 s. No wave breaking is found at Vegsundet.

2.5.22 Vika

Both the bathymetry (inlet) below the settlements of Vika (8) and the topography are gentle. Waves from Åknes propagate more parallel to the shoreline leading to less amplification. The headland Vikaneset is also partly protecting the settlements from the waves from south. However, stronger amplification of the waves for the Hegguraksla scenarios is found, where the waves propagates more normal to the shoreline The wave periods for scenarios from Åknes and Hegguraksla are 350 s and 130 s respectively. The waves from Hegguraksla are influenced by wave breaking.

2.5.23 Ørskog

At the inlet at Ørskog (2) the waves are focused and refracted towards the shoreline, but due to a relatively steep bathymetry the waves are not affected by strong amplification. The wave period is approximately 400 s, and no wave breaking is found.

3 Update on previous run-up estimates for the outer part of Storfjorden using a simplified approach

This update was performed using the dispersive GloBouss tsunami model and new velocity progression for the scenarios as described in Section 4.2. The sea level rise of +0.7 m was incorporated also in this analysis. The maximum values of the calculated surface elevation offshore each study location are used to find an estimate on the run-up height on land by using amplification factors (NGI 2005, 2008a). It is important to stress that this empirical approach presumably gives conservative results, and is less accurate than the results from Sections 2 and 4 in this report based on detailed inundation modelling. As examples, some of the locations listed in Table 3.1 are also covered by the most recent results presented in this report, see Section 2.3. For instance at Sykkylven (Aure), the amplification factor gave 8 m for scenario 1C while the run-up model gave 4 m (see Table 2.2), while at Vegsundet the same scenario gave 5 m and 4 m, respectively. At Sykkylven this imply that the run-up height estimate is reduced by 50 % by using the new set of models. At Vegsundet the reduction is only 20 %. An additional finding is that the amplification of the wave from the deeper part to the maximum run-up heights is clearly different for waves impacting a bay or a fjord-head (more perpendicular impact and focussing leads to stronger amplification) and for waves impacting other locations along the fjord (weaker amplification), cfr. also the discussions in Sections 2.4. The difference between the presented run-up results in NGI (2005, 2008a) and the ones given in the table below (using amplification factors) are related to:

- Model improvements (slide and tsunami propagation)
- Different (and larger) rock slide volumes and frontal areas
- Longer and more realistic rock slide run-out distances
- Slightly different rock slide directions
- A sea level rise of 0.7 m is incorporated in the analysis

Table 3.1: Updated run-up height estimates (m) for the outer part of Storfjorden applying the empirical approach as explained in the text. A sea level rise of 0.7 m is taken into account. Yellow colored values should be replaced by the most recent detailed run-up height calculations from Section 2.3. Details about the scenarios (1A, 1B,…, and H3) are found in Table 4.1, while the locations are shown Figure 3.1.

	Location	***fact***	***depth***	***old****	***1A***	***1B***	***1C***	***1D***	***2A***	***2B***	***3A***	***3B***	***H1***	***H2***	***H3***
1	Aure	5	98.0	2-3	6	7	8	7	4	4	2	2	1	2	2
2	Festoy	4	142.0	1-2	2	3	3	3	2	2	1	1	1	1	1
3	Glomset	5	87.6	3-4	6	7	8	7	4	4	2	2	1	2	2
4	Haaheimsvika	5	70.9	3-4	6	7	9	8	4	4	2	2	1	2	2
5	Hareid	5	94.7	1-2	2	3	3	3	2	2	1	1	1	1	1
6	Hjorungavaag	5	159.6	1-2	2	3	3	3	2	2	1	1	1	1	1
7	Ikornes	5	76.7	2-3	6	7	8	7	4	4	2	2	1	2	2
8	Leksnes	4	59.8	1-2	3	3	4	4	2	2	1	1	1	1	1
9	Magerholm	5	84.8	3-4	4	5	6	5	3	3	2	1	1	1	2
10	Ørsnes	4	97.0	2	4	4	5	5	2	2	2	1	1	1	2
11	Saebo	4	114.1	2-3	4	4	5	5	2	2	2	1	1	1	2
12	Solevaag	5	106.7	3	3	4	4	4	2	2	1	1	1	1	1
13	Sulesund	4	102.5	1-2	2	2	3	2	1	1	1	1	1	1	1
14	Sunde	5	98.9	2-3	3	4	4	4	2	2	1	1	1	1	1
15	Vegsundet	5	97.0	3-4	3	4	5	4	2	2	2	1	1	1	1

*From NGI (2008a), volume and slide velocity comparable to 1A.

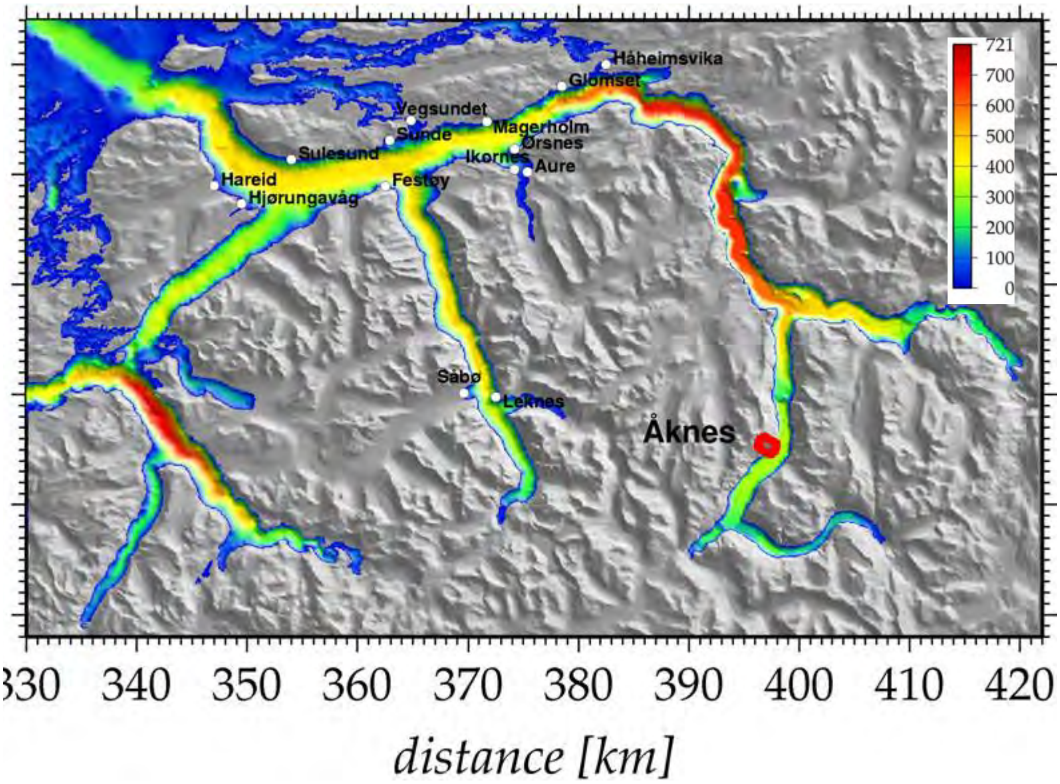

Figure 3.1: Overview over the locations found in Table 3.1.

4 Tsunami generation, propagation, and run-up

4.1 Modelling

Throughout the Åknes/Tafjord-project significantly improved numerical tsunami models have been made available to the project. In this section we present how the modelling of the generation, propagation, and run-up is performed with the new set of models, as well as the coupling of the models between the different stages.

4.1.1 Generation

In the numerical model, as well as in the now finished laboratory experiments at the Coast and Harbour Research Laboratory, SINTEF, Trondheim (SINTEF, 2008), the rock slides are described as fixed shaped boxes. For the numerical simulations the boxes are slightly rounded due to possible numerical noise and instabilities. The rounding leads to slightly larger volumes (about +10%), see also NGI (2008a). The rounding of the rock slides is probably also more correct physically. In addition, for the historical scenarios and for the scenarios from Hegguraksla, the boxes are made longer since some stability problems here occur due to the water depression at the slide tail. There is only a minor effect on the leading wave if we apply such a prolonged slide configuration, see Appendix E.

To determine the slide progression, we apply several approaches. For the scenarios from Åknes it is obvious to use the slide progression measured in the laboratory experiments (SINTEF, 2008). For the other scenarios we apply both numerical block slide models such as the PCM model (NGI, 2005) and the analytical energy-line approach, see Appendix E and references therein.

4.1.2 Propagation

For the propagation stage, we have applied two different numerical models, i.e GloBouss and DpWaves. Rock slide scenario data (ÅTB, 2009a) as well as input from laboratory experiments (SINTEF, 2008) are applied as input to the models. We refer to Appendix E for further information and references as well as convergence tests and other sensitivity tests.

The slide motion is given as input to the tsunami propagation model as a sink-source distribution taking the water volume displacement due to the slide motion into account.

4.1.3 Inundation

For calculating the tsunami inundation, we have applied the ComMIT/MOST model, see ComMIT (2010) and NGI (2008b). ComMIT/MOST is a standard model and probably the most common model applied for tsunami run-up modelling.

4.2 Definitions of slide scenarios

In this subsection we describe the various potential rock slide scenarios from Åknes and Hegguraksla, as well as the historical rock slide events Tafjord (1934), Skafjell (1731), and Tjelle (1756). The main parameters for all scenarios are listed in Table 4.1. The background for the parameter selection is found in NGI (in prep.), Harbitz et al. (1993), NGI (2003) and ÅTB (2009a). The rock slide dimensions are mainly determined by inspecting the bathymetries as well as the (potential) release areas. For the historical events, the initial rock slide locations and dimensions are supplemented from literature studies. The annual probability for the scenarios is given in the ÅTB (2009a).

The historical events are all valuable due to the well documented eyewitness observations and measured run-up and maximum inundation heights. This is particularly true for the most recent 1934 Tafjord event. For further reading about the historical events, see Harbitz et al. (1993), Furseth (2006) and Jørstad (1968).

Table 4.1. Parameters for all scenarios.

Scenario		**Dimensions**			**Impact velocity**	**Volume**	**Annual probability**
Location	Number	*Height [m]*	*Width [m]*	*Length [m]*	*[m/s]*	$10^6\ m^3$	
Åknes	1A	80	450	1000	45	36	<1/1000
	1B	100	450	1000	45	45	<1/1000
	1C	120	450	1000	45	54	<1/1000
	1D	80	450	1500	45	54	
	2A	80	450	500	65	18	
	2B	80	450	500	45	18	>1/1000
	3A	60	225	800	60	10.8	1/200
	3B	50	200	600	60	6	1/100
Hegguraksla	H1	33	150	200	50	1	1/600
	H2	40	200	250	60	2	>1/1000
	H3	46	250	300	60	3,5	<1/1000
Tafjord (1934)		75	130	400	50	3	
Skafjell (1731)		160	250	100	34	4	
Tjelle (1756)		60	500	500	45	15	

4.2.1 Potential rock slides from Åknes

The scenarios 1A-1D represent the situations if more or less the entire area of moving masses at Åknes are released simultaneously as one large slide. The volumes vary from 36 to 54 Mm^3, while the velocity of these slides entering the fjord is calculated to be 45 m/s, see NGI (in prep.). For the generation of the tsunami, the most sensitive parameter is the frontal area, see NGI (2006, 2008a) and the sensitivity tests in Appendix E. The most tsunamigenic scenario is scenario 1C, which is expected. The smaller scenarios 2A, 2B, 3A, and 3B reflect the possible collapse of the western flank. These scenarios have volumes between 6 and 18 Mm^3, and higher impact velocities due to longer distance from the initial position of the front of the slide to the shoreline and hence higher initial potential energy. The direction of the slide track is 273.3 degrees from east.

The velocity progression for the slides from Åknes is shown in Figure 4.1. The progression is taken from the measurements in the laboratory experiments, see Appendix E and SINTEF (2008). The slides accelerate until they reach the flat fjord bottom. From this point the velocity is reduced until the slide stops. In Figure 4.2 the run-out progression of the slide as a function of time is shown.

The H/L relations measured for the slides in the laboratory experiments are found to be in the range of 0.35 to 0.45. Based on the data from historical rock slides in Norway (NGU, 2001), these values are of the same order for rock slides with same volume.

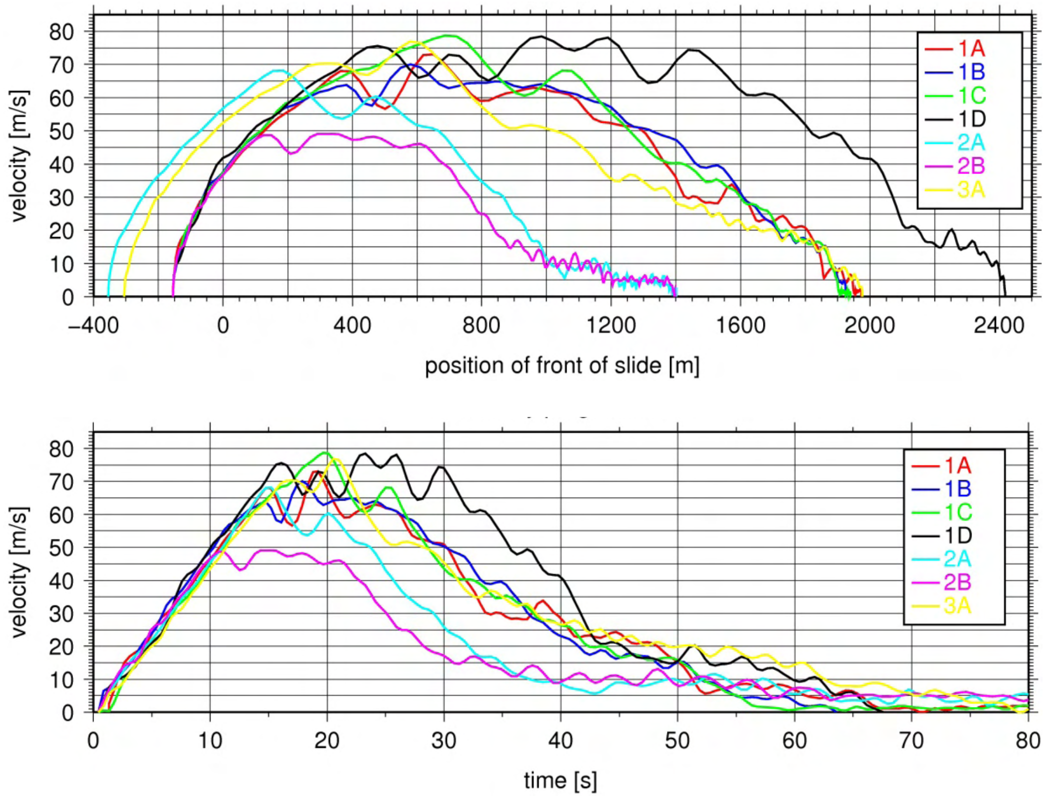

Figure 4.1: Velocity progression as a function of front position of the slide (upper panel) and time (lower panel) for slide scenarios from Åknes, as measured in the laboratory experiments (transferred to full scale). Position=0 in the upper panel is the shoreline.

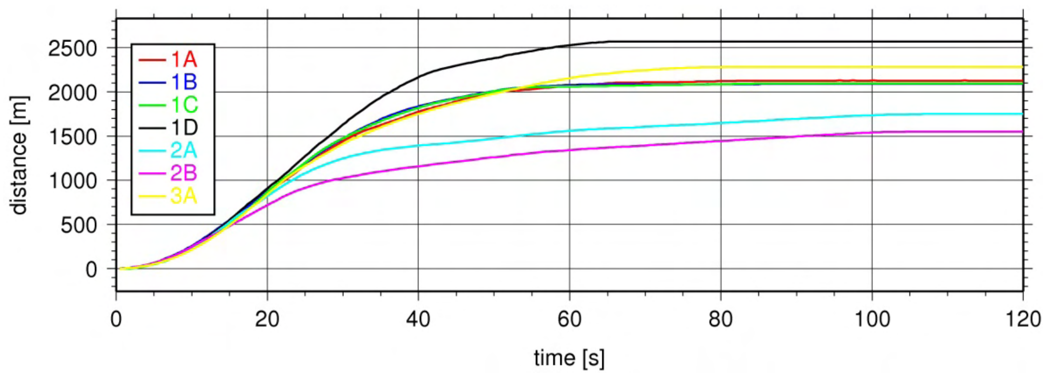

Figure 4.2: Run-out progression as a function of time for rock slide scenarios from Åknes, as measured in the laboratory experiments (transferred to full scale).

4.2.2 Potential rock slides from Hegguraksla

From Hegguraksla altogether three scenarios were evaluated. The first scenario (H1) mimics a release of the lower part of Hegguraksla. The volume estimate for H1 is 1 Mm^3 and the impact velocity is estimated to 50 m/s. The remaining two scenarios mimic releases of the upper part of Hegguraksla. These scenarios were estimated to 2 Mm^3 (H2) and 3.5 Mm^3 (H3), with an impact velocity of 60 m/s. The parameters for these scenarios are taken from NGI (2003). In the numerical tsunami model an analytical rock slide progression was applied. Due to instability problems caused by the wave depression at the tail of the slide, the slide was prolonged as described in Appendix E.

4.2.3 Tafjord, 1934

The upper part of the Tafjord rock slide (Langhammaren) was released 7th April, 1934 from about 450 to 750 m a.s.l, see Figure 4.21. The rock slide constituted a volume of 1.0-1.5 Mm^3. Beneath the rock a talus of at least the same volume was released, implying a total volume of 2-3 Mm^3. The H/L ratio is 0.57 (NGU, 2001).

The impact velocity was estimated to 50 m/s, with a total submarine run-out of 530 m. The applied parameters for the Tafjord event as well as the analytical rock slide progression are taken from Harbitz et al. (1993). Due to instability problems caused by the wave depression at the tail of the slide, the slide was prolonged as described in Appendix E. Note that we for the simulation have applied the new set of models, as described in Section 4.1.

4.2.4 Skafjell, 1731

Skafjellet is located on the opposite side of Stranda in Sunnylvsfjorden, about 2 km away, see Figure 4.26. The 8th February 1731 a rock slide with a volume of about 4 Mm^3 was released from altitude 100 to 300 m a.s.l. The H/L ratio for this scenario is close to 0.9. The reason for this short run-out is probably the abrupt transition from the steep slope to the flat seafloor.

The dimensions for the box-slide were provided by the ÅTB (ÅTB, 2009a), while the velocity progression applied in the simulations was determined through the energy-line approach (see Figure 4.3) as described in Appendix E and the references therein. The impact velocity is estimated to about 35 m/s, while the total submarine run-out distance is found to be 950 m. The velocity progression calculated by the energy-line approach is applied directly into the numerical model. Due to instability problems caused by the wave depression at the tail of the slide, the slide was prolonged as described in Appendix E.

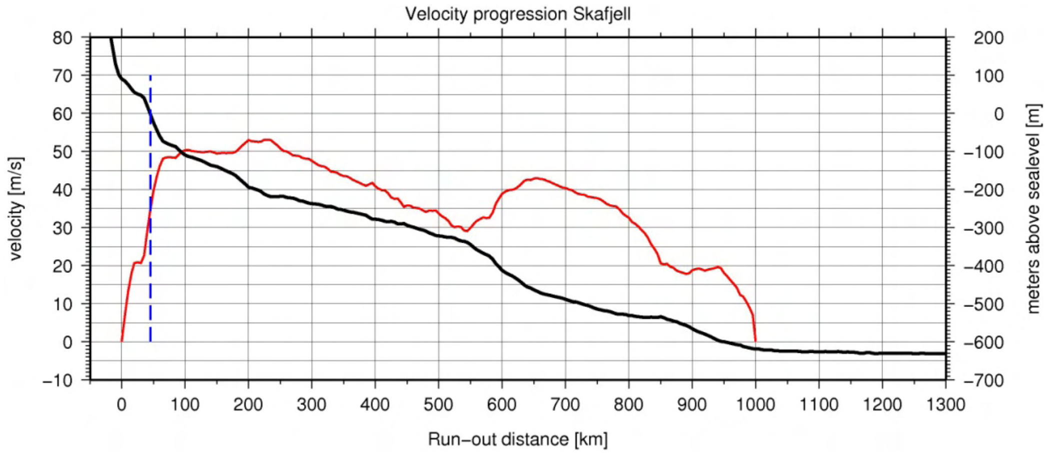

Figure 4.3: Calculated velocity progression of the 1731 Skafjell rock slide (red line, left axis). Vertical blue dashed line indicates the position of the shoreline. Black line is the bathymetry/topography (right axis).

4.2.5 Tjelle, 1756

In 22nd February 1756, 15 Mm^3 of rocks from the mountain Tjellefonna fell into the fjord Langfjorden at Tjelle, Nesset, see Figure 4.29. The upper part was released from about 200 to 380 m a.s.l. This is the largest historical rock slide tsunami known in Norway. For this event, the H/L ratio is measured to 0.38 (NGU, 2001).

The dimensions for Tjelle were provided by the ÅTB (ÅTB, 2009a), while the velocity progression was as for the Skafjell event determined through the energy-line approach (see Figure 4.4). The impact velocity is estimated to be about 45 m/s, while the total submarine run-out distance is 1650 m. Due to instability problems caused by the wave depression at the tail of the slide, the slide was prolonged as described in Appendix E.

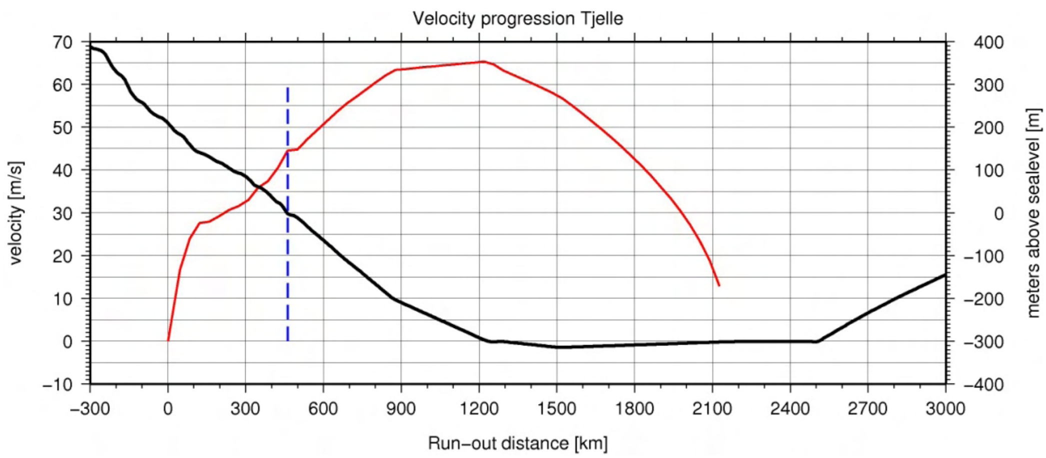

Figure 4.4: Calculated velocity progression of the 1756 Tjelle rock slide (red line, left axis). Vertical blue dashed line is the shoreline. Black line is the bathymetry/topography (right axis).

4.3 Tsunami propagation in Storfjorden for potential scenarios

There are several factors influencing the propagating tsunami. First, the alteration of the tsunami height depends on the distance from slide area, the width of the fjord, and the fjord complexity. Tsunamis propagating in a fjord without divides and almost constant width are less dependent on the distance from the slide area since the tsunami may then behave like an almost plane wave with less spread of the energy and minor variation of the height with propagation distance. However, when the fjord become narrower or wider, the tsunami height increases or decreases, respectively. In Storfjorden the largest reduction of the height occurs in fjord bends or in divides where the tsunami is partly reflected and/or split and proceeds in two different directions.

For the propagation stage a resolution of 50 m is applied while the numerical model (GloBouss) is run in linear dispersive mode for producing the results below (non-linearity has only minor effect on the maximum surface elevations and is omitted due to instability problems for longer simulation times). For results regarding the inundation, see Section 4.4 and Appendix A.

4.3.1 *Results for scenarios from Åknes*

Through Figure 4.5 to Figure 4.12 the maximum surface elevations during simulations for one hour are shown for all scenarios from Åknes. For waves travelling southward the fjord divide north of Hellesylt reduce the height slightly. From here, the waves propagate almost as plane waves with only minor reduction in height, before they are amplified outside Hellesylt and Geiranger. The waves propagating northward are reduced in height where Sunnylvsfjorden become wider a few kilometres north of Åknes. Further attenuation take place at the fjord divide where the energy is spread and waves propagate both outward to the outer part of Storfjorden and inward to Tafjord. Wave amplitudes are gradually decreasing seaward as Storfjorden become wider. The waves towards Tafjord are reduced east of Valldal, where the width of the fjord decreases abruptly from about 3 km to less than 1 km leading to wave reflection. In bays, inlets, and fjord heads the waves are clearly amplified. For the largest scenarios significant wave heights are found also at the fjord head of Hjørundfjorden (Tysseøyra) where surface elevations of more than two meters are found. An explanation for this is that Hjørundfjorden is gradually decreasing in both width and depth leading to an optimal (unfavourable) amplification of the waves entering the fjord. The distance from Åknes to Tysseøyra is about 100 km.

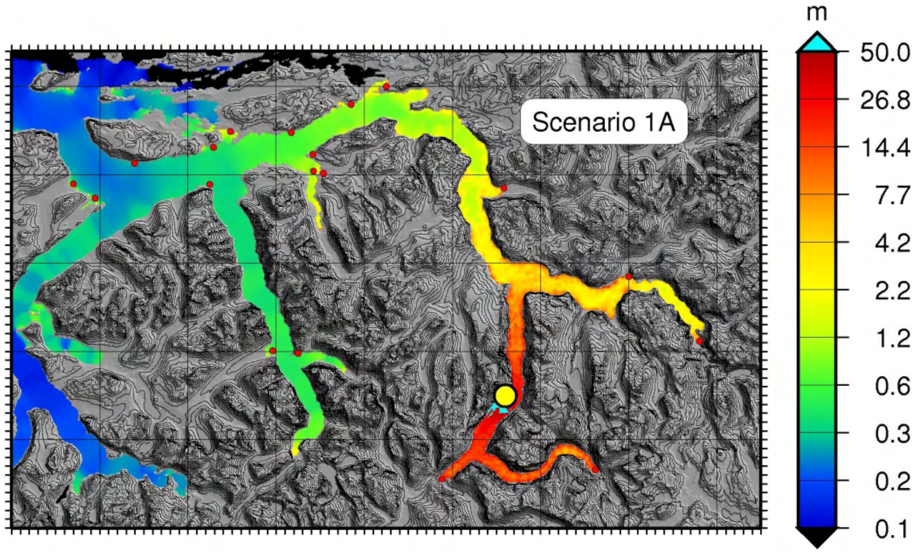

Figure 4.5: Maximum surface elevation in meters for scenario 1A. The Åknes release area is marked with a yellow bullet.

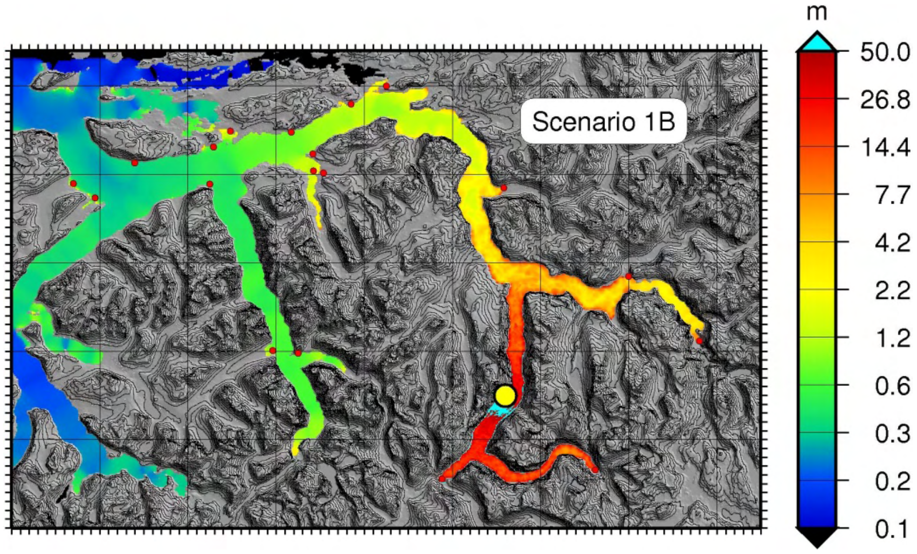

Figure 4.6: Maximum surface elevation in meters for scenario 1B.

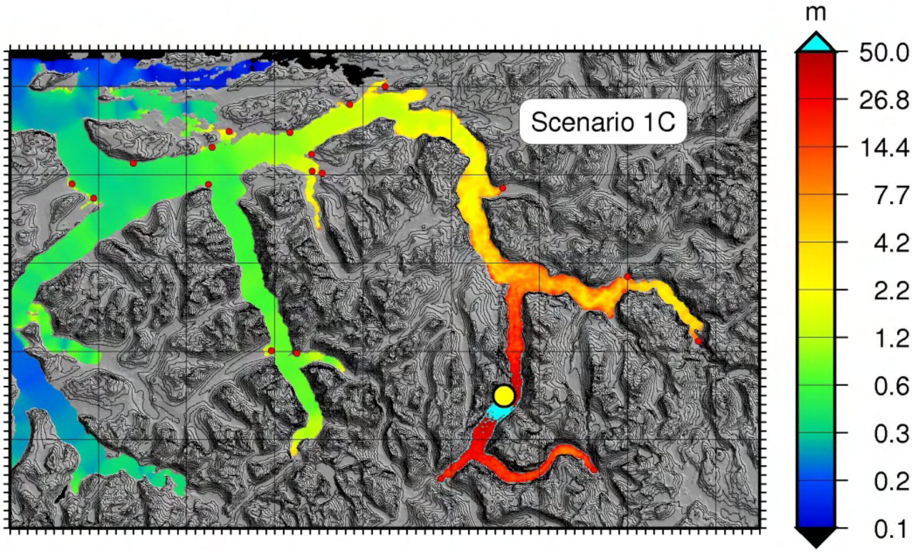

Figure 4.7: Maximum surface elevation in meters for scenario 1C.

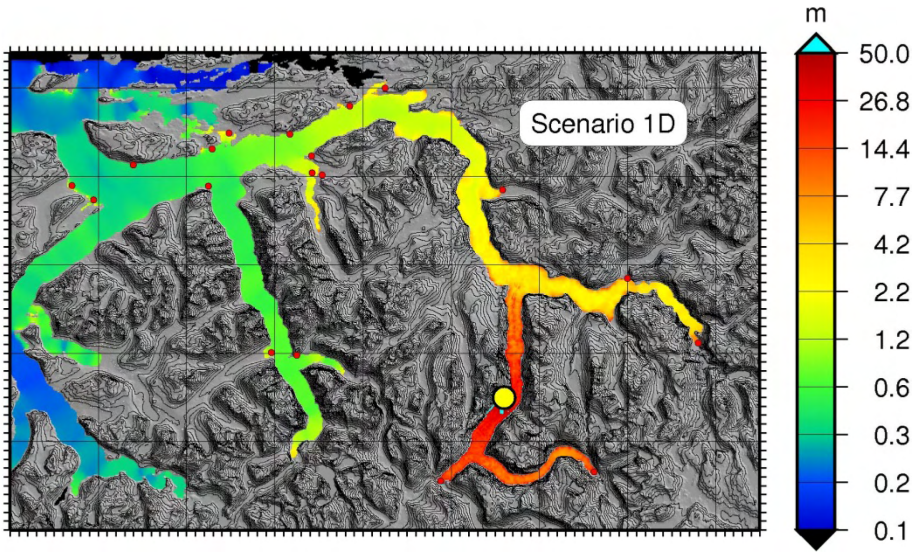

Figure 4.8: Maximum surface elevation in meters for scenario 1D.

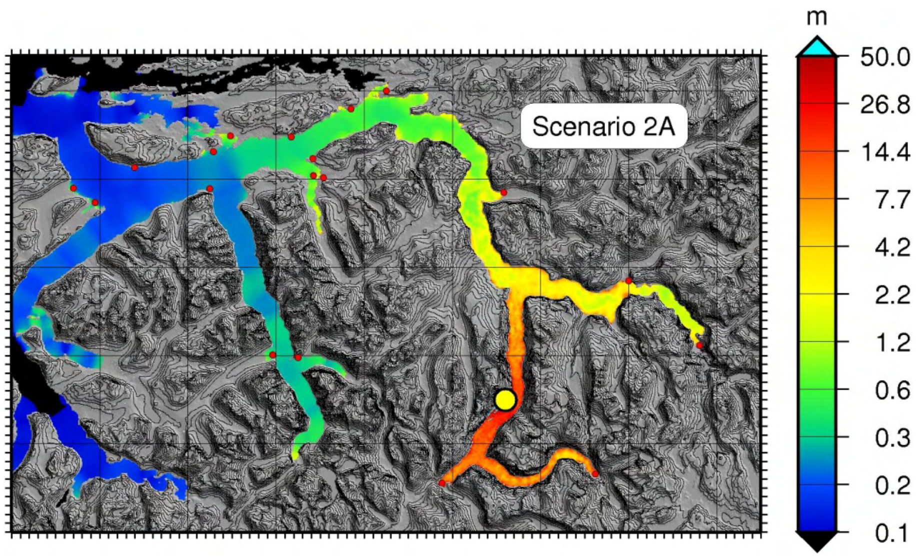

Figure 4.9: Maximum surface elevation in meters for scenario 2A.

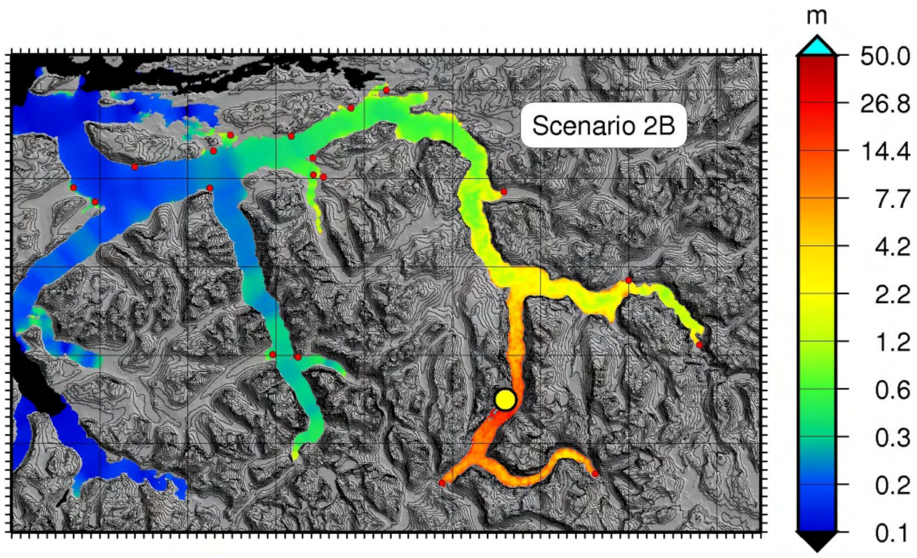

Figure 4.10: Maximum surface elevation in meters for scenario 2B.

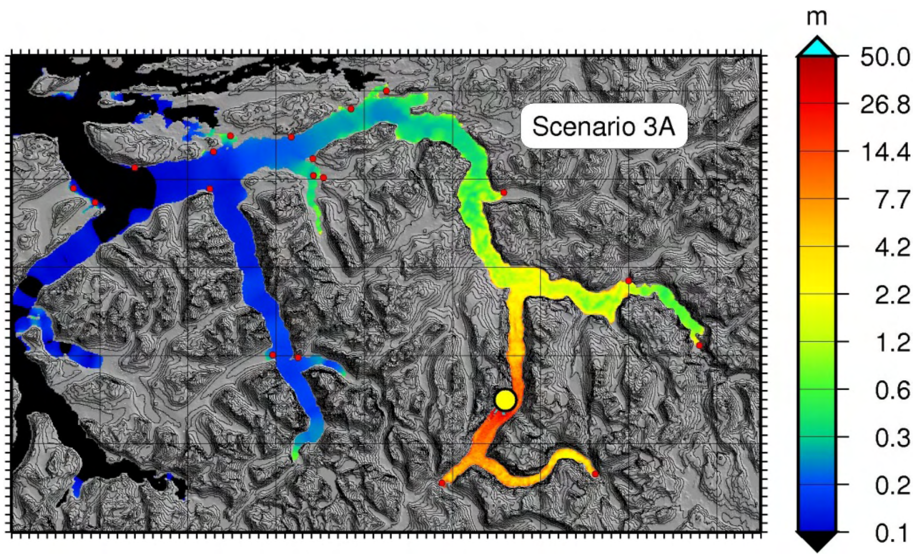

Figure 4.11: Maximum surface elevation in meters for scenario 3A.

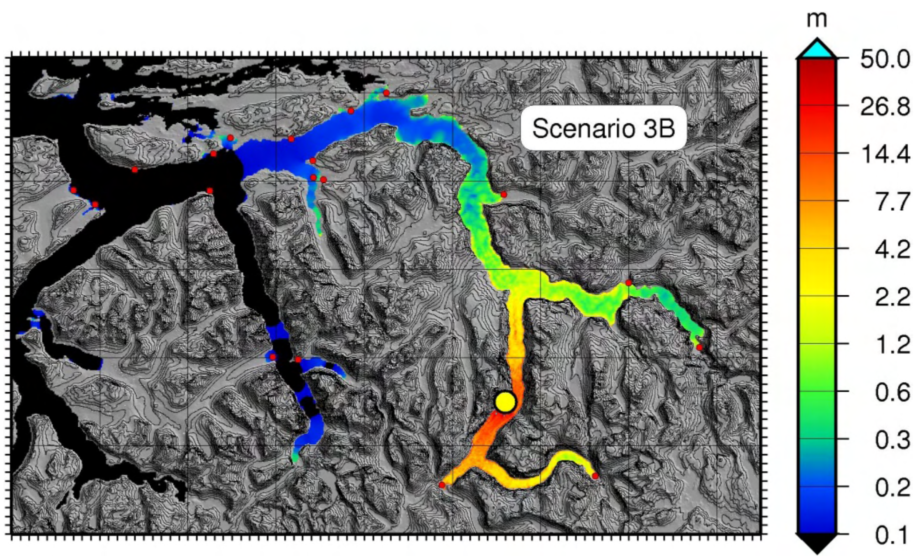

Figure 4.12: Maximum surface elevation in meters for scenario 3B.

4.3.2 Results for scenarios from Hegguraksla

The scenarios from Hegguraksla are much smaller in volume, and the potential tsunami impact is much more local. The waves propagating outwards decrease rapidly at Valldal, where the fjord becomes wider. Further attenuation is found at the divide at Sunnylsfjorden. However, for the largest scenario (H3), surface elevations up to 1-2 m are found as far out as Glomset. For results regarding the inundation, see Section 4.4 and Appendix A.

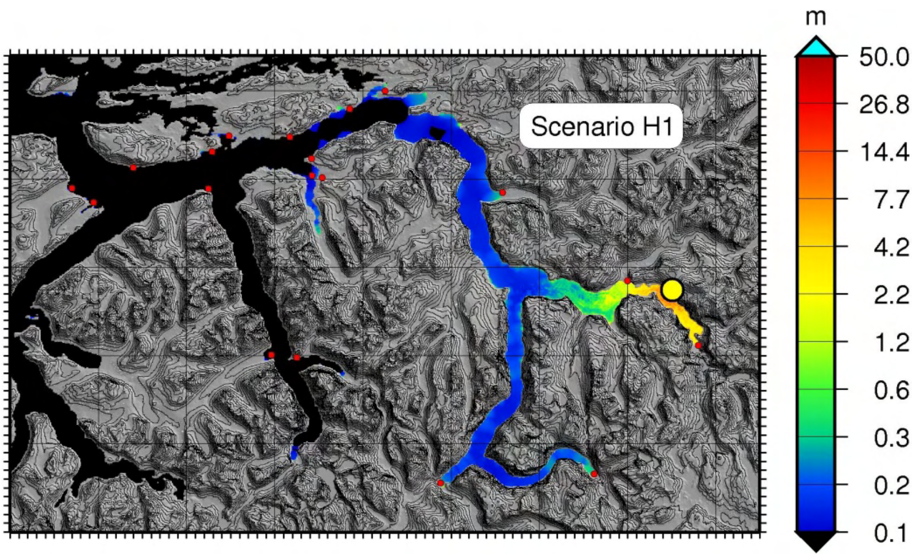

Figure 4.13: Maximum surface elevation in meters for scenario H1. The Hegguraksla release area is marked with a yellow bullet.

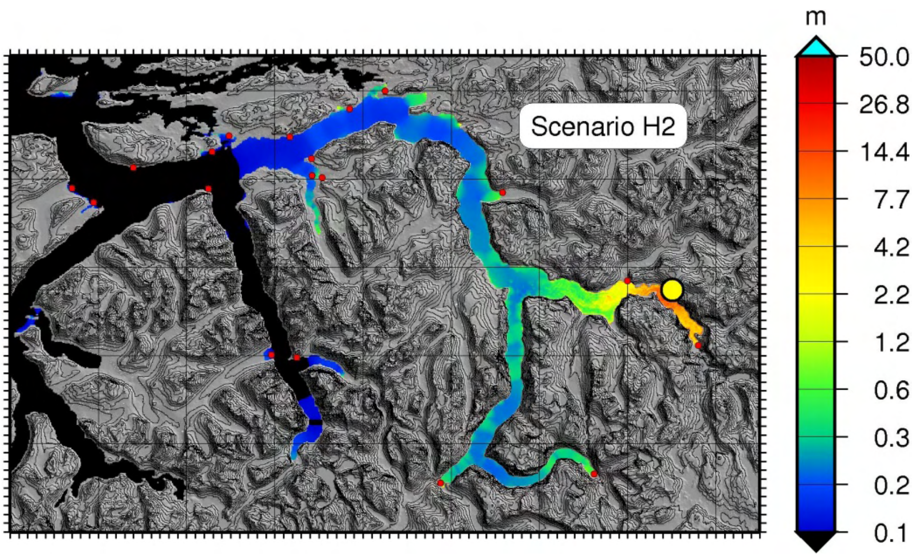

Figure 4.14: Maximum surface elevation in meters for scenario H2.

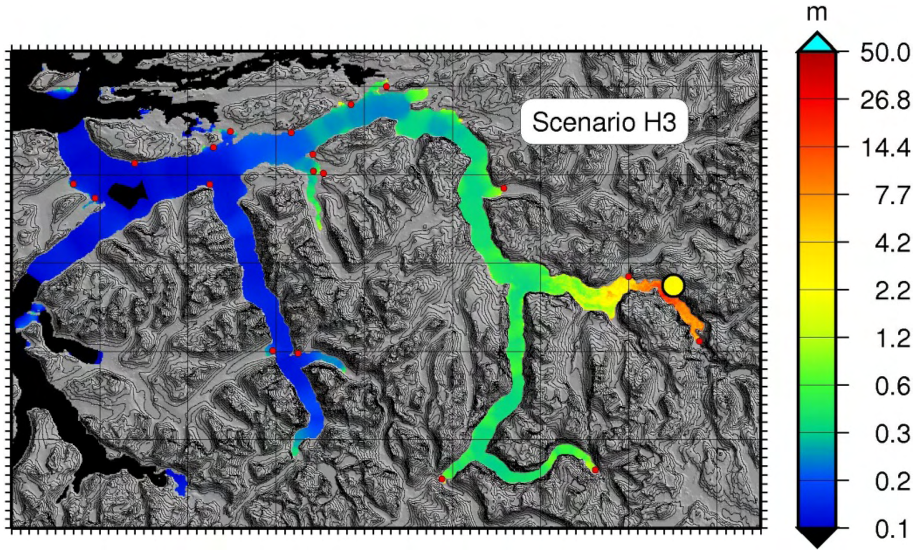

Figure 4.15: Maximum surface elevation in meters for scenario H3.

4.4 Inundation for today's sea level for potential scenarios

To investigate the potential tsunami impact during run-up, several metrics can be invoked. In this section we show some examples of such metrics in addition to maximum values for wave propagation and run-up for all potential scenarios from Åknes and Hegguraksla for Hellesylt, Geiranger, Stranda, and Tafjord. For full details of the inundation mapping for all locations and scenarios for the hazard zoning we refer to Appendix A. A discussion of important aspects related to the inundation calculations are found in Section 2.4.

The calculations are based on today's sealevel, and the data for the topography is based on high resolution data (5 m) from NGU, see also Appendix E.

4.4.1 Examples of maximum inundation heights, maximum current velocities, and maximum flow depths

An example of maximum inundation heights (as well as maximum surface elevation in the fjord) is found for scenario 1C in Figure 4.16 (Hellesylt) and in Figure 4.19 (Valldal). The maximum current velocity (see Figure 4.17, Hellesylt and Figure 4.19, Valldal) may be used to estimate of the wave loads acting on buildings and infrastructure as well as the erosion. Finally the flow depth is shown in Figure 4.18 (Hellesylt).

Time histories for the surface elevation and current velocity are exemplified for scenario 1C at Valldal in Figure 4.20

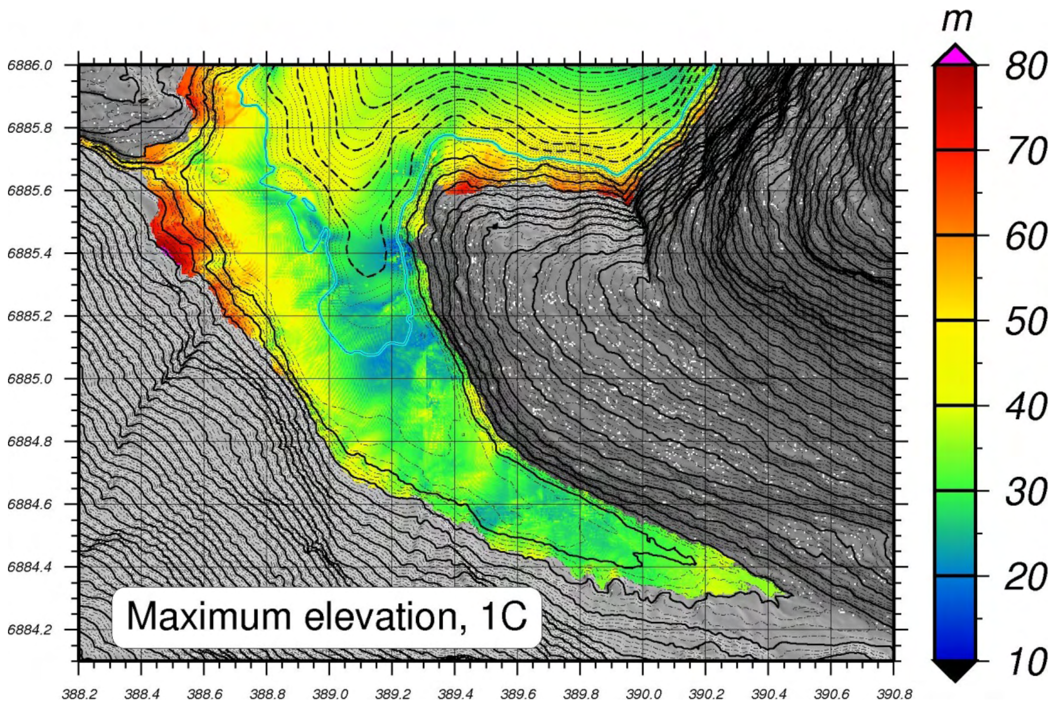

Figure 4.16: Example of maximum inundation heights (on land) and maximum surface elevation (in the fjord) at Hellesylt, scenario 1C.

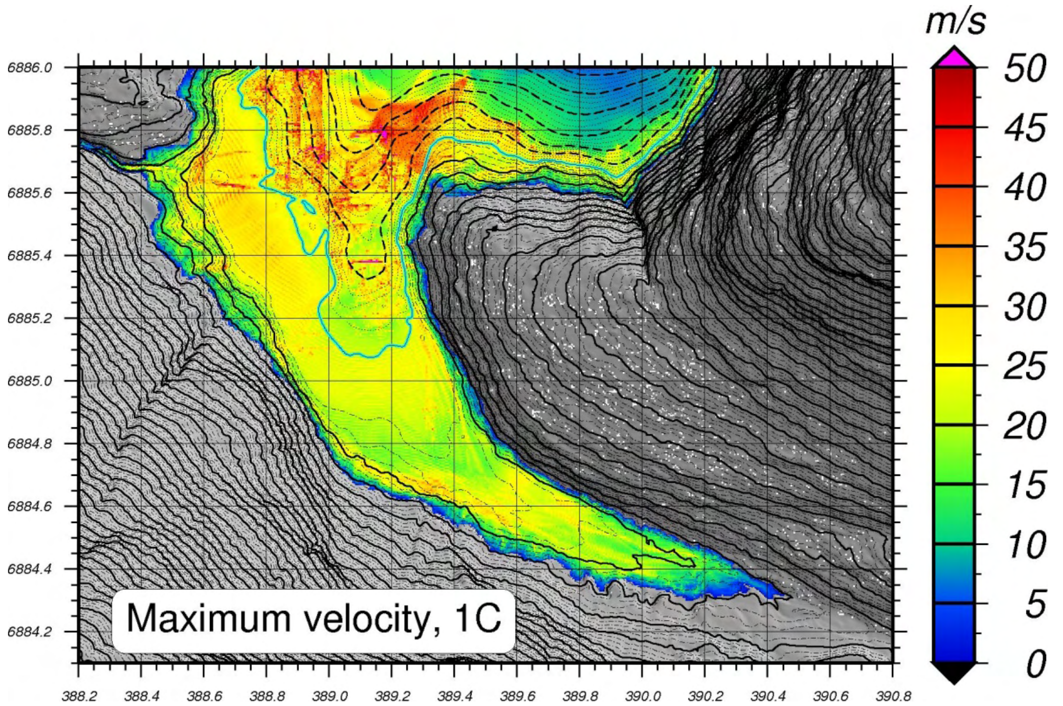

Figure 4.17: Example of maximum current velocity at Hellesylt, scenario 1C.

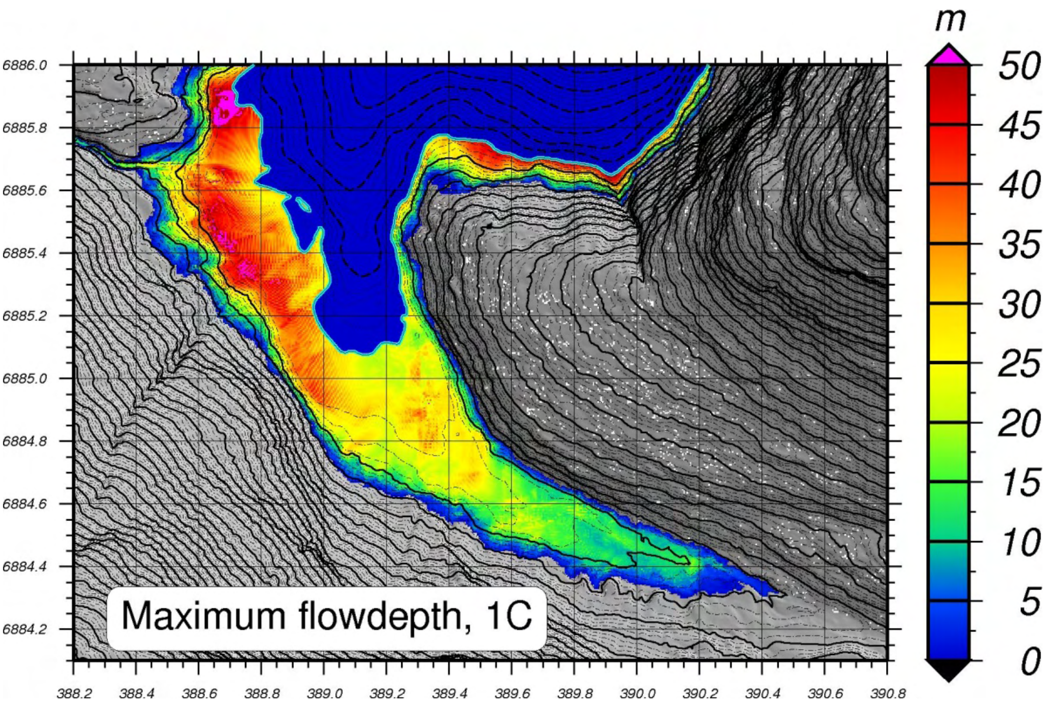

Figure 4.18: Example of maximum flow depth onshore at Hellesylt, scenario 1C.

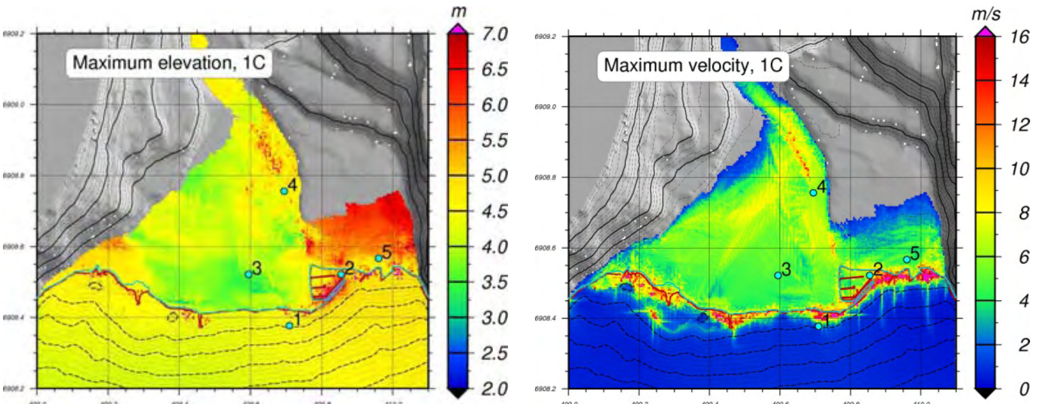

Figure 4.19: Example of maximum inundation heights (left) and maximum current velocity (right) for scenario 1C at Valldal. The numbers refer to the location of the time histories of surface elevation and current velocity in Figure 4.20

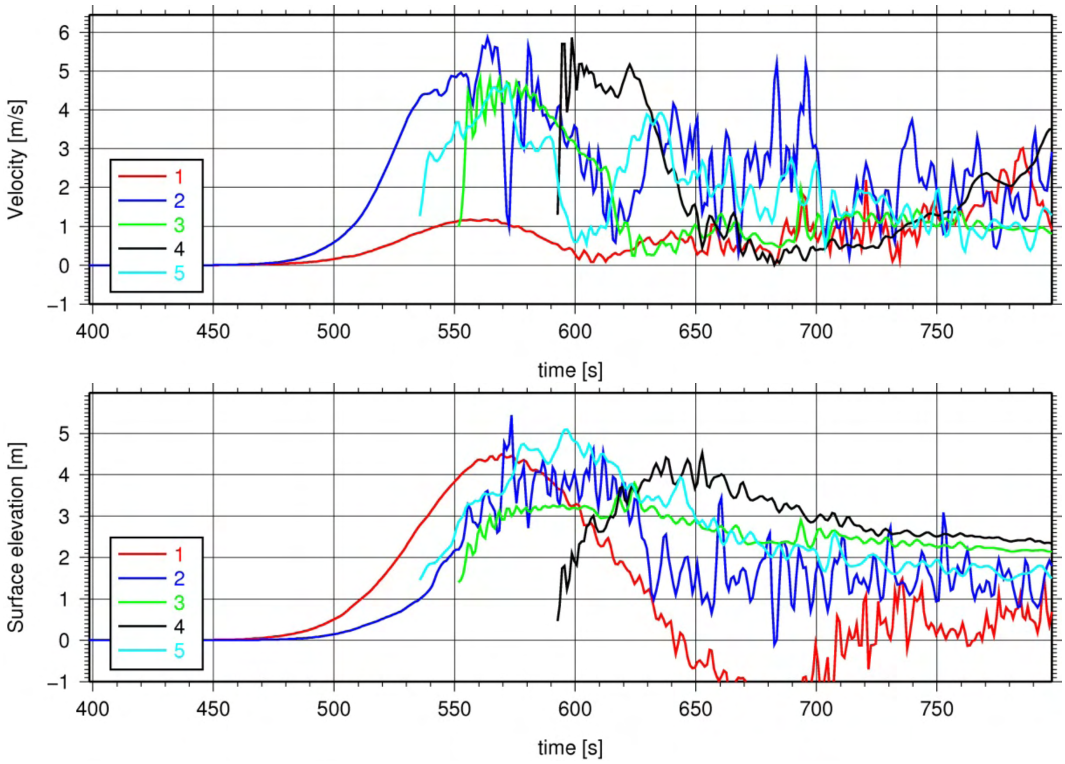

Figure 4.20:Examples of time histories of current velocity (upper panel) and inundation heights (or surface elevation for points located in the fjord) (lower panel) at Valldal for scenario 1C. The location of the gauges 1-5 is shown in Figure 4.19.

4.4.2 Results for all scenarios at Hellesylt, Geiranger, Stranda, and Tafjord

In Section 2 as well as in Appendix A the results are shown for the scenarios 1C and 2B for all locations and H2 and H3 for some selected locations. In this subsection, the maximum values from run-up height calculations for all scenarios at Stranda, Hellesylt, Geiranger, and Tafjord are presented, see Table 4.2. In addition to the maximum run-up heights, also maximum values for the water level at the shoreline and the height of the incident leading wave in deep water are given. By evaluating the amplification of the waves from deep water to the run-up stage, we are able to see how the effect of the bathymetry/topography influences on the run-up heights, see also Section 2.4. The ratio between the surface elevation in deep water and the run-up height is here labeled the amplification factor. As seen in the table the factor varies from 1.8 to 5.0 depending on which location and scenario that are evaluated. The average amplification factors for the fjord heads Hellesylt and Geiranger are 4.3 and 3.7, respectively. At Stranda the waves propagate mainly parallel to the shoreline and the bathymetry is steep, both aspects limiting the amplification and the run-up height. At this location, the amplification factor is around 2, which is expected for steep slopes. Finally, at Tafjord the amplification factors for the Åknes and Hegguraksla scenarios are in average about 4 and 3, respectively. The difference here may be due to different wave lengths.

Table 4.2: Maximum water level and run-up heights. 'Deep' is the surface elevation of the leading wave measured at the deeper part of the fjord outside each location (water depth indicated within the brackets). 'Shoreline' is the maximum inundation height measured along today's shoreline (ref. colored triangles in Figure 2.3), while 'Run-up' is the vertical distance between MSL and the highest point of the trim line (ref. colored stars in Figure 2.3 and Figure 2.2). Erroneous numbers due to noise are removed.

Scenario	Hellesylt				Stranda				Tafjord				Geiranger			
	Deep (215m)	Shoreline	Run-up	Amp. factor	Deep (615m)	Shoreline	Run-up	Amp. factor	Deep (175m)	Shoreline	Run-up	Amp. factor	Deep (150m)	Shoreline	Run-up	Amp. factor
1A	13.7	38.8	57.5	4.2	1.8	2.8	2.9	1.6	2.8	8.4	9.1	3.3	11.2	27.1	37.1	3.3
1B	18.4	45.8	73.9	4.0	2.3	-	-	-	3.5	12.1	10.5	3.0	14.7	34.2	42.9	2.9
1C	23.4	57.5	82.9	3.5	2.8	-	5.7	2.0	4.4	11.1	13.1	3.0	18.3	48.0	63.5	3.5
1D	15.2	40.3	64.3	4.2	2.7	-	4.9	1.8	4.0	10.8	12.4	3.1	12.6	30.3	41.4	3.3
2A	7.7	23.3	35.5	4.6	1.2	1.9	2.4	2.0	1.7	7.1	5.7	3.4	6.4	-	23.3	3.6
2B	7.1	26.9	32.6	4.6	1.2	1.8	2.3	1.9	1.7	8.7	5.4	3.2	6.1	22.3	22.8	3.7
3A	4.0	-	17.4	4.4	0.6	0.9	1.4	2.3	0.9	-	2.5	2.8	3.2	12.2	12.0	3.8
3B	2.3	-	10.7	4.7	0.3	-	-	-	0.5	1.8	1.7	3.4	1.9	10.5	9.5	5.0
H1	0.2	0.9	0.9	4.5	0.1	0.3	-	-	1.1	4.9	4.6	4.2	0.2	1.0	0.9	4 5
H2	0.3	-	-	-	0.3	0.5	-	-	2.1	-	7.9	3.8	0.4	-	-	-
H3	0.5	2.3	2.4	4.8	0.6	0.8	1.4	2.3	3.4	9.1	13.8	4.1	0.7	-	2.5	3.6

4.5 Hindcast of historical slide scenarios

4.5.1 Tafjord, 1934

Below Langhammaren where the disastrous Tafjord 1934 event occurred, the average width of the fjord is a little more than 1 km. The depth is about 200 to 220 m, see Figure 4.21. Altogether 40 people were killed in this event.

Field surveys after the event resulted in a map with details of the run-up, especially the inner part of Tafjorden, see Figure 4.22. Within a distance of 2.5-3 km in both directions from the slide area, all exposed locations (like peninsulas and bays) revealed run-up heights above 25 m, see Figure 4.22. Further away the run-up heights were much smaller. This is because only a limited part of the wave energy escapes from the inner semi-closed basin of Tafjorden (inside Fjøra), Harbitz et al. (1993). The dimensions and velocity progression parameters are found in Table 4.1.

In Figure 4.23, the calculated maximum surface elevation is shown. As we can see, the water is elevated to over 50 m close to the slide area, while the surface elevation is reduced to about 1 m north-westwards (in the deepest part of the fjord) 5 km away. For the inner part of the fjord (2-3 km in both directions from the slide area) the surface elevations are above 8-10 m. The results for the inundation calculations at Tafjord are found in Figure 4.24 (shown as flow depth), where also the estimated location of the run-up recordings from 1934 is plotted (there is some uncertainty related to the location of these points since they are visually determined from Figure 4.22). The flow depth is about 10 m at the shoreline and attenuates gradually landward. If we compare the measured surface elevations with the calculated ones, we observe that the numerical solution slightly underestimates the measured run-up heights at the central part of the bay, see Figure 4.25. Here the measured height is about 16 m while the calculated height is up to 12 m. However, less deviation is found at the western and eastern parts of the domain, with slightly overestimated calculated heights. We conclude that the back-calculation give reasonable results.

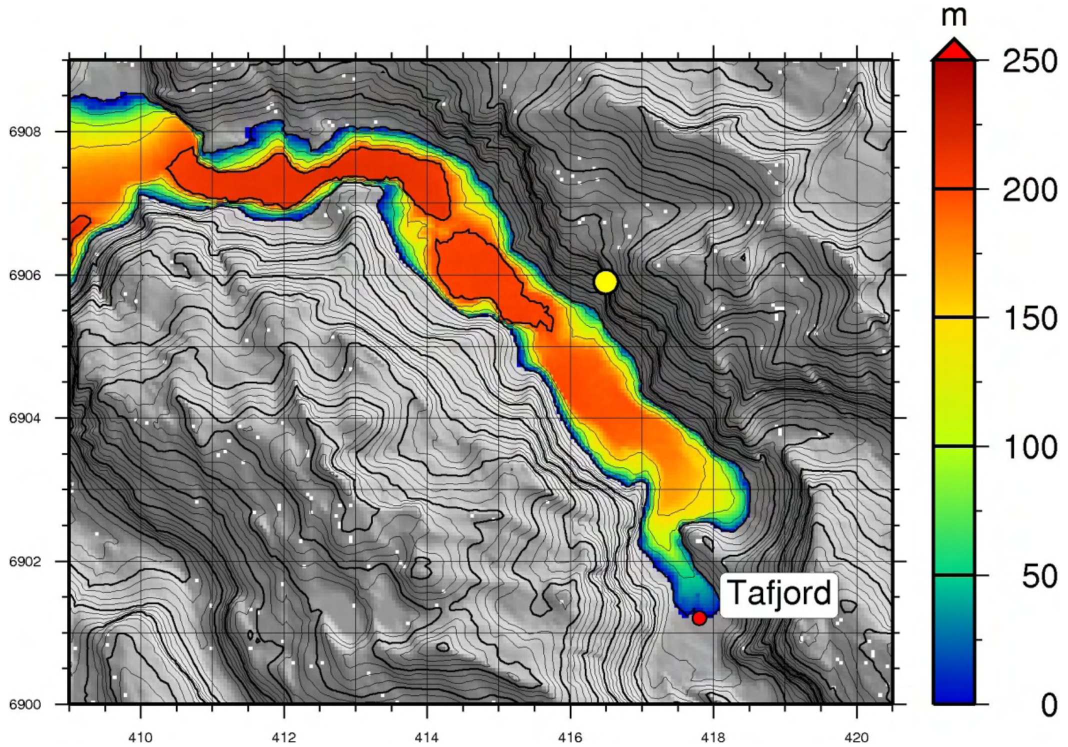

Figure 4.21: Bathymetry for the Tafjord event. The release area at Langhammaren is marked with a yellow bullet. The equidistance for thin and thick contour lines are 50 m and 200 m, respectively.

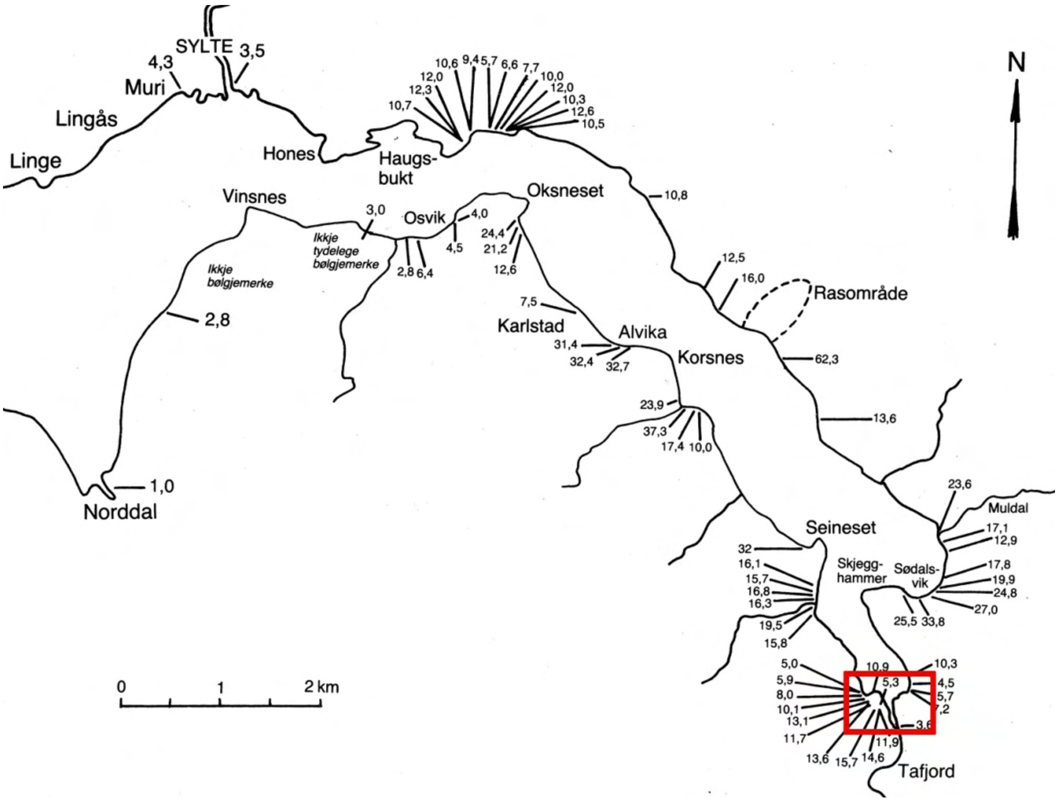

Figure 4.22: Measured maximum inundation heights and run-up heights in meters (from Furseth, 1985; based on Kaldhol and Kolderup, 1937). The comparison between the numerical simulations and the historical recordings is made within the area marked with a red rectangle. “Rasområde” is the rock slide release area.

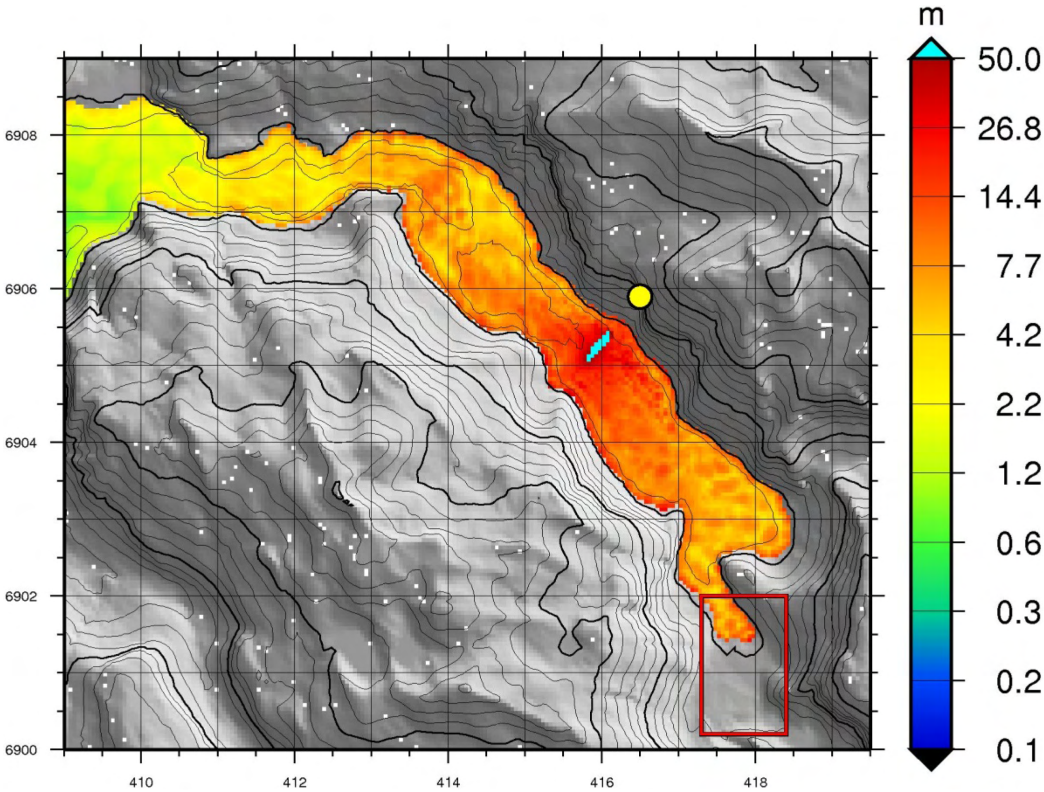

Figure 4.23: The maximum surface elevations from the back-calculation of the tsunami generated by the Tafjord rock slide, 1934. The release area is marked with a yellow bullet, while the red rectangle is the area for the run-up calculations at Tafjord village.

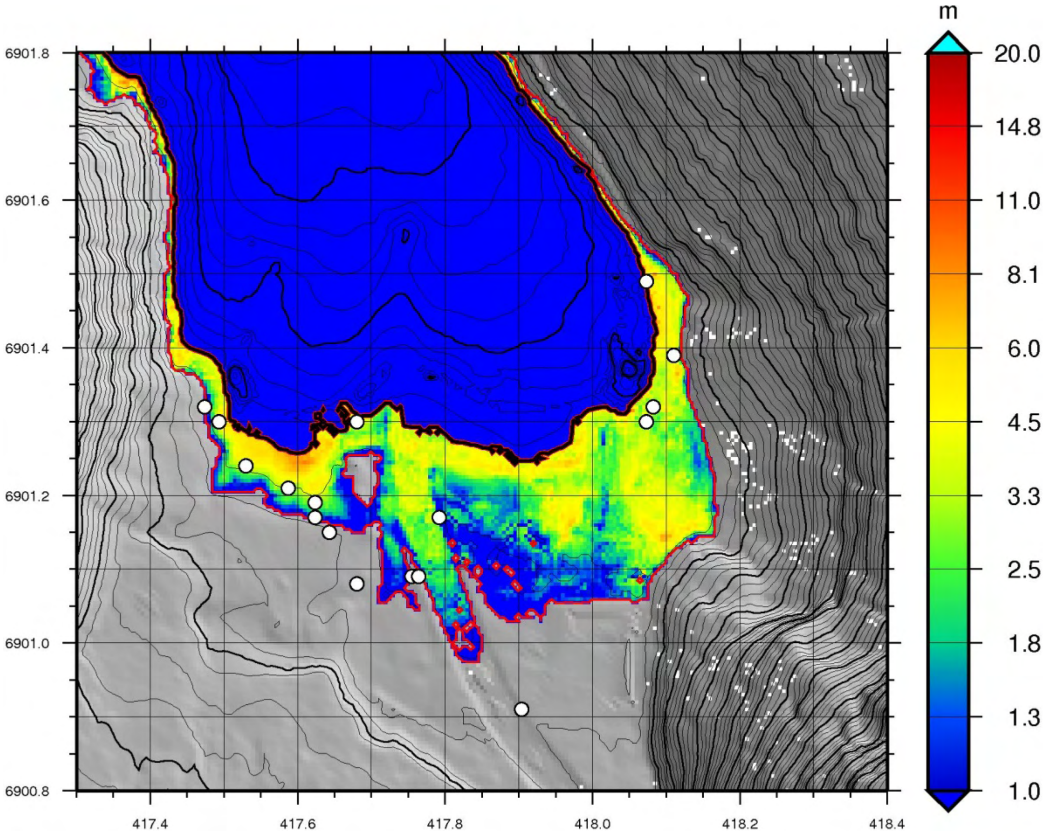

Figure 4.24: Calculated maximum flow depth during inundation at Tafjord (inside the red rectangle in Figure 4.22). White bullets are the locations where the maximum water level and run-up heights were measured (shown as yellow stars in Figure 4.25). There is some uncertainty related to the location of these points since they are visually determined from Figure 4.22. The trim line is colored red.

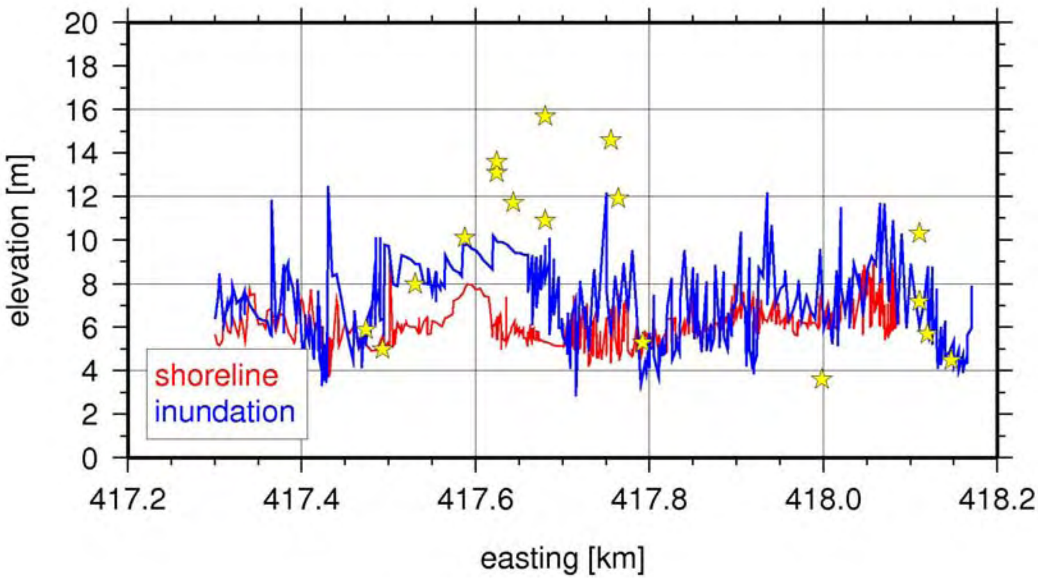

Figure 4.25: Comparison between measured and back-calculated inundation and run-up heights at Tafjord. The first axis is the east-west coordinates. 'shoreline' and 'inundation' are the maximum inundation heights at the shoreline and the height of the trim line (run-up), respectively. The yellow stars refer to the measured heights at the locations shown in Figure 4.24.

4.5.2 Skafjell, 1731

After the rock slide plunged into Sunnylvsfjorden, the wave impacted several locations along the fjord. At Sløgstad (now Stranda), only 2 km away, the church was wiped away. The first waves close to the slide area were observed to be more than 30 m high, and the waves were observed up to 70 km away. Altogether 17 people were killed in this event.

As shown in Figure 4.27 the maximum surface elevation of the tsunami outside the slide area is calculated to more than 50 m locally, but reduced to 2-5 m 2 km away. The inundation distance at Stranda is calculated to 70-300 m depending on where the inundation is measured, see Figure 4.28. The flow depth at the location of the church (A. Furseth, personal comments) was calculated to be approximately 15-20 m.

As a conclusion, the calculated waves are of same order as the eyewitness observations. The inundation distance observed at Sløgstad was "100 paces" (100 paces = 94 m). Even "100 paces" is within the interval given by the back-calculations, the most obvious place to measure the inundation distance is where the waves passing the church. The calculated distance was closer to 300 m here, and hence overestimated. This may indicate that the real rock slide was less tsunamigenic than the modelled one. Another possible factor of error is that the front of the rock slide is possibly too steep in the numerical calculations.

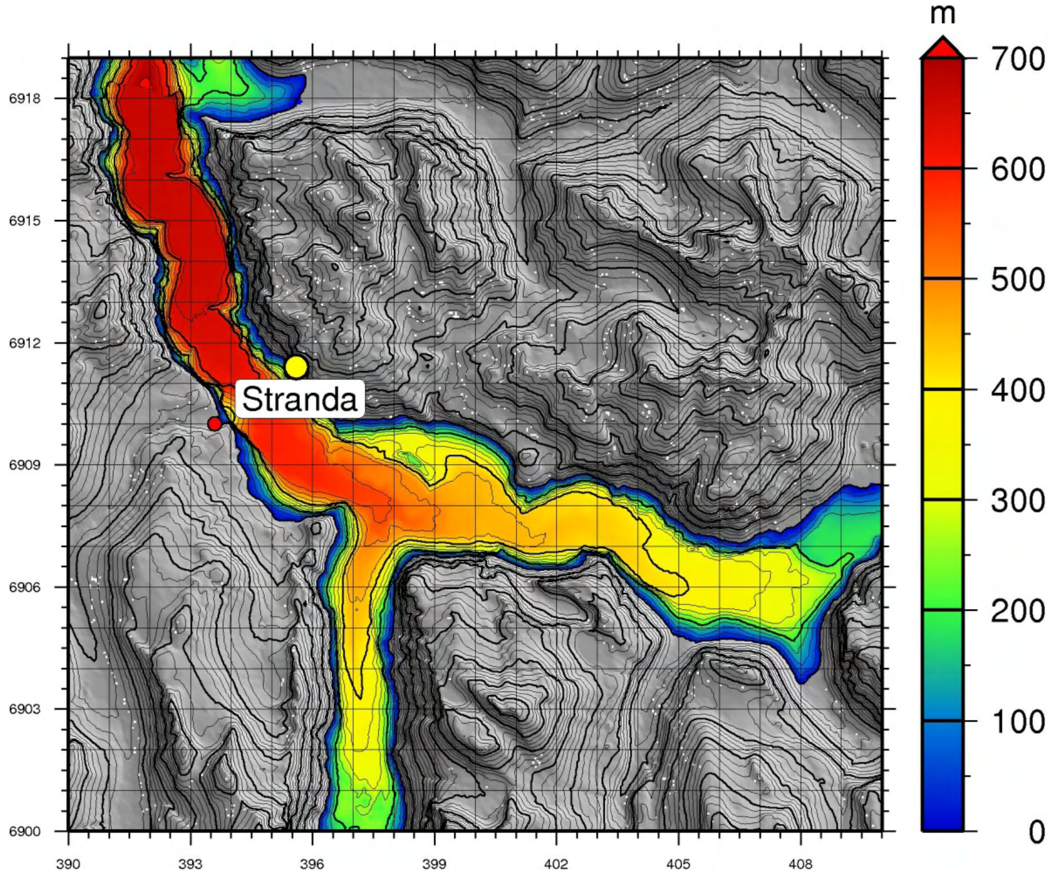

Figure 4.26: Bathymetry for the Skafjell event. The release area is marked with a yellow bullet. The equidistances for thin and thick contour lines are 50 m and 200 m, respectively.

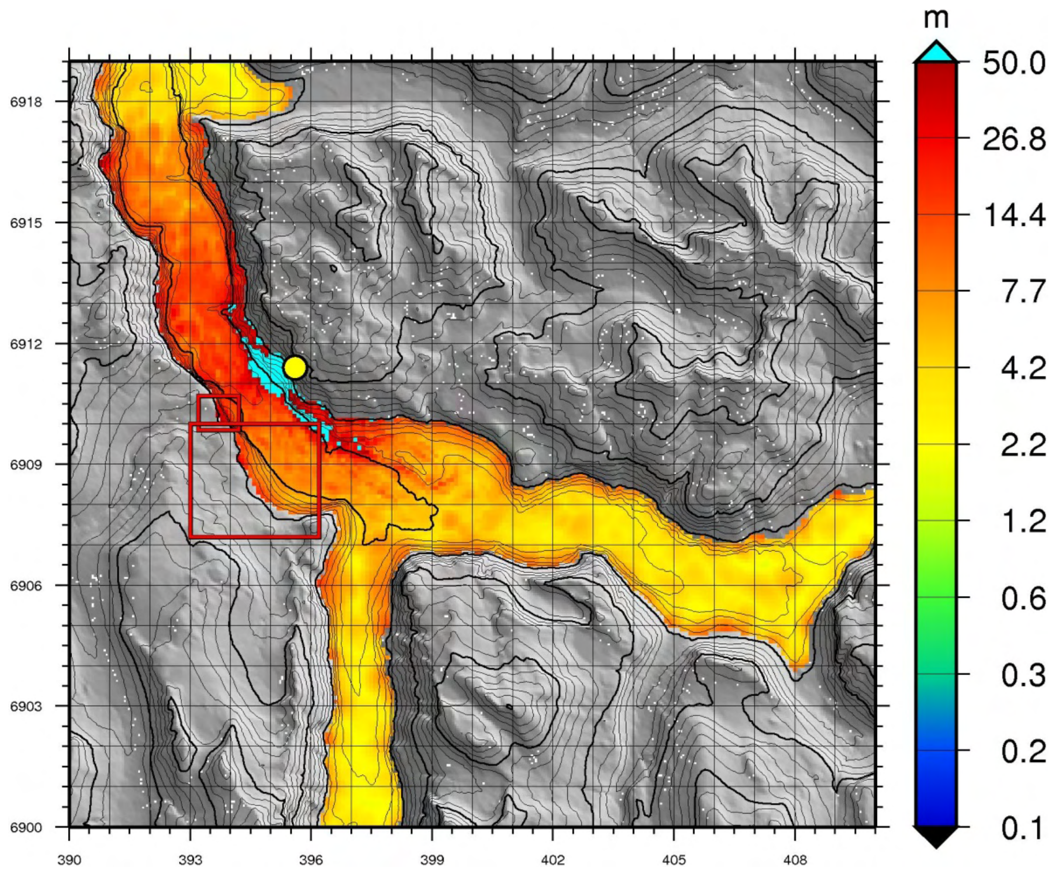

Figure 4.27: The maximum surface elevations for the back-calculation of the tsunami generated by the 1731 Skafjell rock slide. The release area is marked with a yellow bullet, while the red rectangles are the areas for run-up calculations. Only the results for the smallest rectangle are shown in this report.

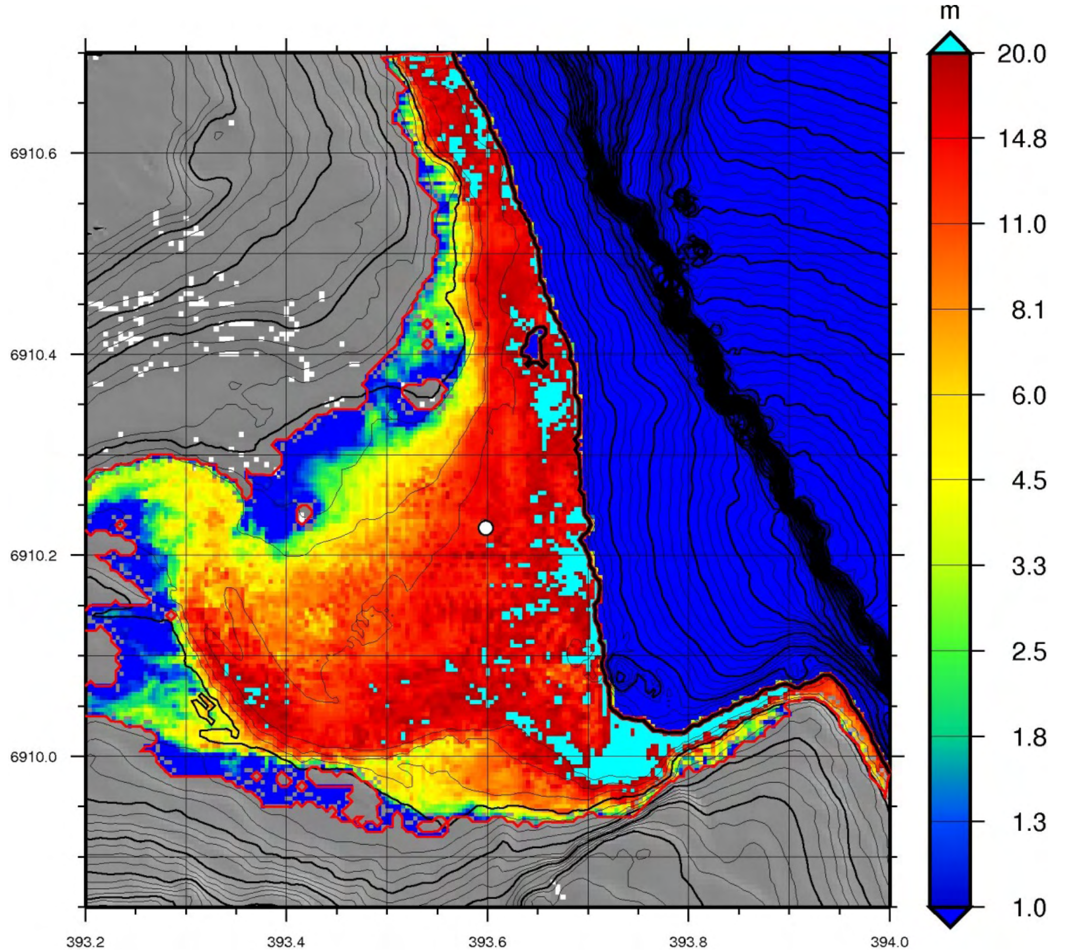

Figure 4.28: Calculated flow depth onshore for the tsunami generated by the 1731 Skafjell rock slide. The white bullet is the location of the church, while the trim line is colored red.

4.5.3 Tjelle, 1756

The waves generated by the rock slide from Tjelle were reported to reach "50 paces in height" above normal water level (no exact location specified, most likely measured along the terrain and close to the slide area). On both sides of Langfjorden and Eresfjorden the wave caused considerable damage to a height of several meters and up to "200 paces" (about 190 m) inland from the shore. At Veøy, Figure 4.30, approximately 25 kilometers from the slide area, the water reached "20 paces" higher than the highest tide level, tore down a fence, and deposited sand, seaweed, seashells, etc. Also at Gjermundnes about 40 km from the slide area, the wave was described as quite extensive. The eyewitnesses referred also to severe turbulence over the entire fjord and three incident waves.

The waves did not only wash away the soil, but also trees and houses. A number of vessels and boats were destroyed. A considerable number of deepwater fish were thrown as much as 100-200 paces on land. Altogether 32 people perished as a result of the waves.

The calculated maximum surface elevation decays from over 50 m outside the slide area, down to 8-10 m eastward and about 2 m at Veøy, see Figure 4.30. At Gjermundnes (located at coordinates 98 km east-west and 6969 km north-south) the deep sea surface elevation is calculated to be about 1 m.

The calculated inundation distance at Veøy varies from only a few meters up to 100 m. It is not known where the "20 paces" over high tide was registered.

A surface elevation of 1 m at Gjermundnes will give an assumed run-up of 2-3 m, and hence give potential damage to infrastructure and buildings close to the shoreline.

At Nesset rectory (prestegård), the inundation distance is found to be between 100 to 200 m, see Figure 4.31. At the shoreline closest to the rectory the distance is closer to 100 m.

As a conclusion the calculated wave heights close to the slide area as well as the inundation distance at Nesset rectory is close to what was observed in 1756. However, the inundation distance calculated at Veøy may indicate that the results are somewhat overestimated, but this is still uncertain since "20 paces" are still in the interval of calculated inundation distances and the location of this observation is unknown.

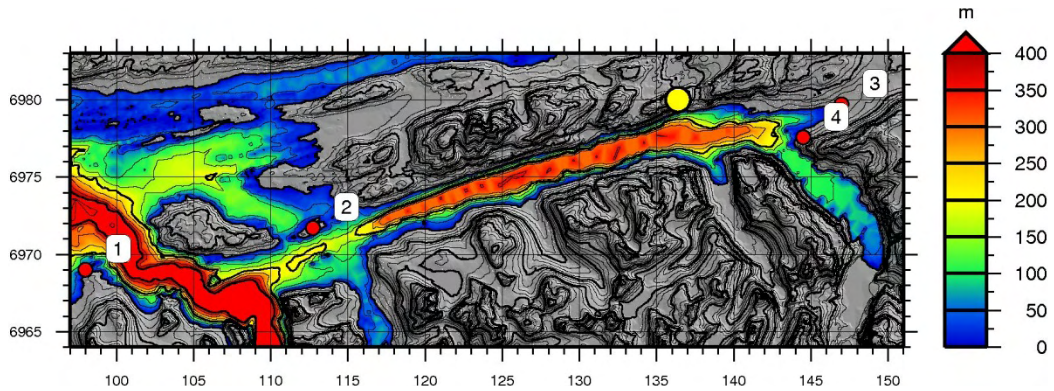

Figure 4.29: Bathymetry for the 1756 Tjelle event. The release area is marked with a yellow bullet. The equidistances for thin and thick contour lines are 50 m and 200 m, respectively. The figure also shows the location of Gjermundnes (1), Veøy (2), Nesset Rectory (3), and Nesset (4).

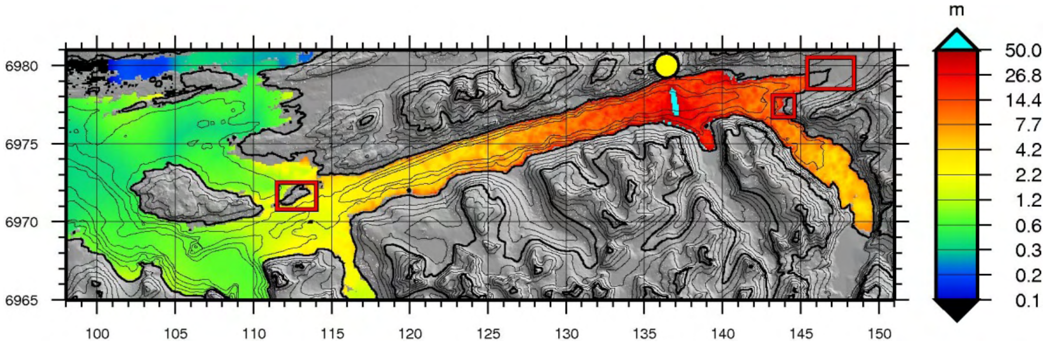

Figure 4.30: The maximum surface elevations for the back-calculation of tsunami generated by the Tjelle rock slide, 1756. The release area is marked with a yellow bullet, while the red rectangles are areas for run-up calculations (from west to east: Veøy, Nesset Rectory (prestegård) and Nesset). Results for Nesset are not shown in this report.

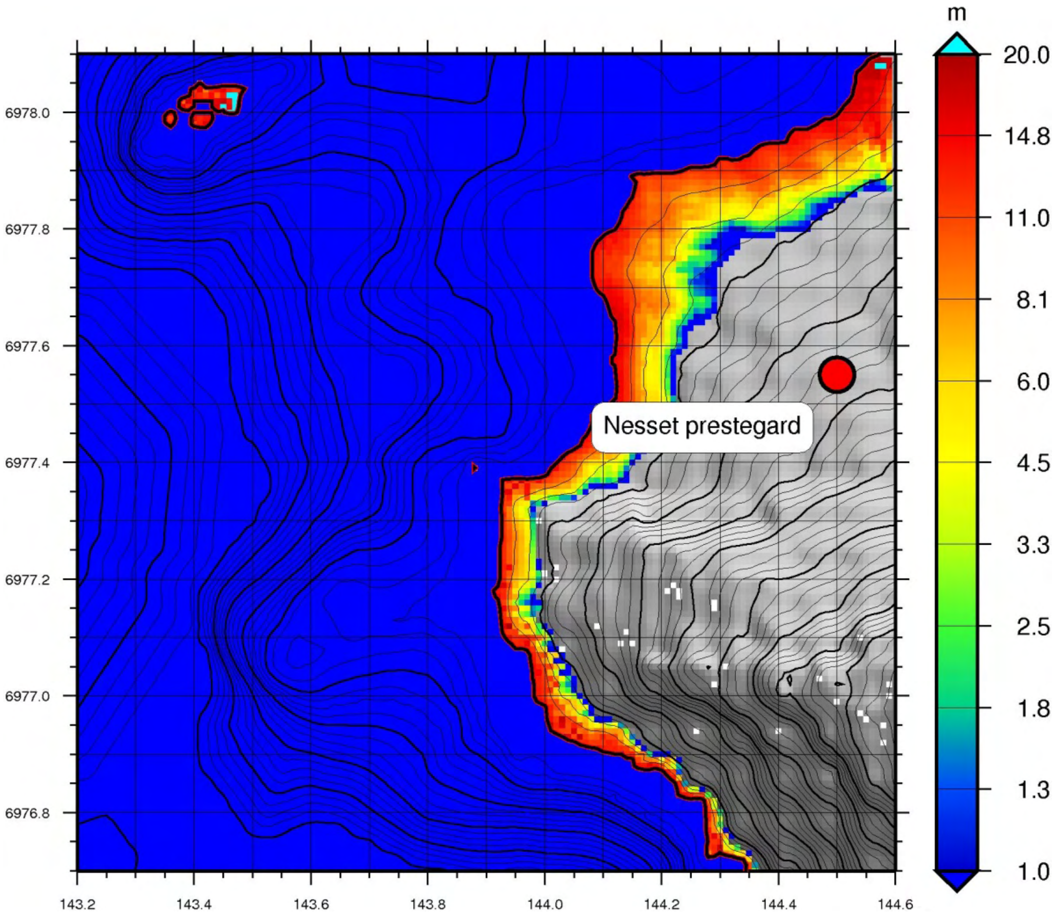

Figure 4.31: Maximum flow depth onshore during inundation at Nesset rectory ("prestegård").

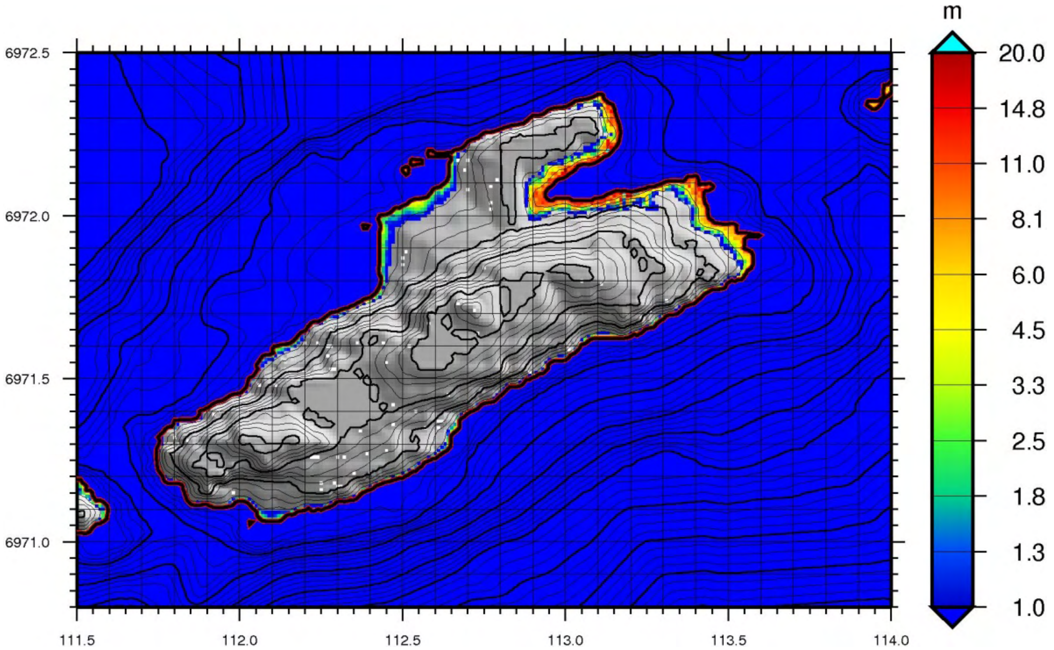

Figure 4.32: Maximum flow depth onshore during inundation at Veøy, about 25 km away from the rock slide area.

5 Comparison between the 3D laboratory experiments and the numerical simulations

In this section we will compare numerical results with the results from the three dimensional laboratory experiments at Coast and Harbour Research Laboratory/SINTEF (SINTEF, 2008). The 1:500 scale model, covers the part of Storfjorden about 3 km north of Åknes and the inner part of Storfjorden including Hellesylt and Geiranger, see Figure 5.1. The comparison is made in two different ways. First, surface elevations at the gauges 4-6 are extracted from the laboratory experiments, and given as input to the numerical model. The results from the laboratory experiments and the numerical simulations are then compared at the gauges 7-9 (towards Hellesylt) and 10-12 (towards Geiranger). Second, a comparison is made between the laboratory results and the numerical results where also the generation of the waves is done numerically, i.e., no input from the laboratory experiments. For both cases, also run-up calculation is performed.

The numerical modelling follows the configuration of the laboratory experiments as close as possible. For instance, the slide velocity progression measured in the laboratory is applied directly into the numerical model. In the numerical model we must apply a so called threshold depth, see Section 4.1.2 and Appendix E. The threshold depth may in some cases lead to higher waves for the propagation phase, but through sensitivity tests in Appendix E we reveal less influence on the run-up heights. Note that there are scale effects (viscosity, surface tension, friction, etc.) that may lead to different results for the experiments and the numerical modelling.

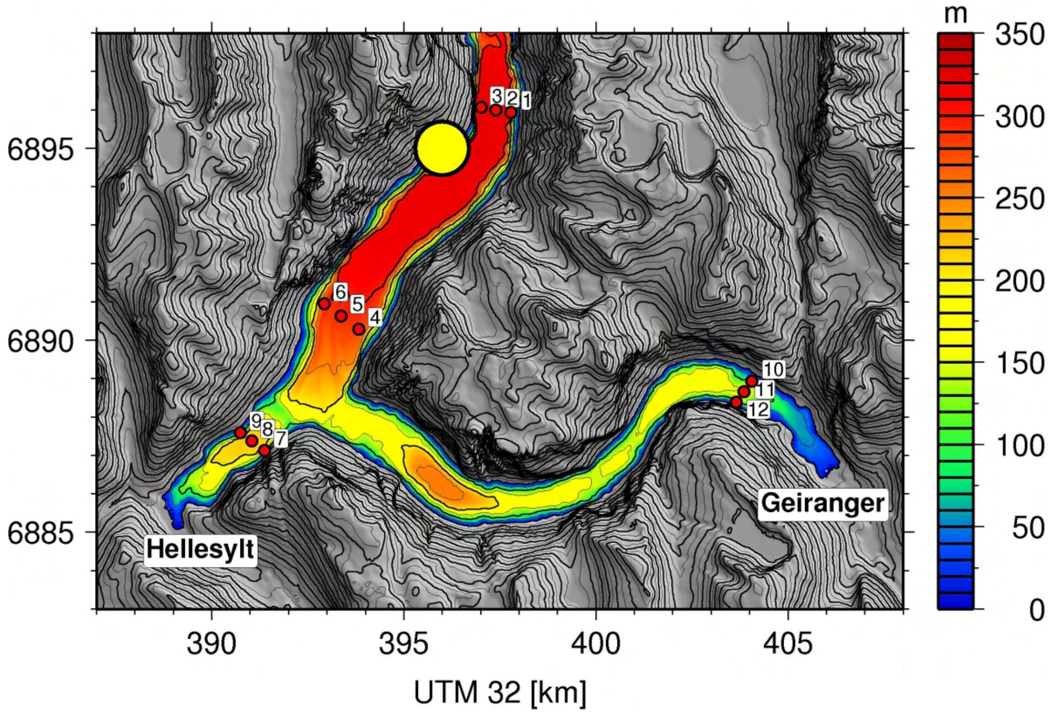

Figure 5.1. Bathymetry and topography for the laboratory experiments. The red bullets (numbered 1 to 12) are the gauges where the surface elevation is measured. The big yellow bullet indicates the location of the potential rock slide at Åknes.

5.1 Input data to numerical model conveyed from the laboratory experiments

5.1.1 Tsunami propagation

The propagation model applied for these simulations is the model called *DpWaves*, see Appendix E. This model labelled "improved model" in previous reports (NGI 2006, 2008a). *DpWaves* is capable to be initiated by forced input along a boundary and it includes the effects of both dispersion and non-linearities. The northern boundary of the model setup (where the input from the laboratory experiments is given) is identical to a line through the points 4-6, and the (coarse) input is interpolated along the line across the fjord by using linear interpolation. On the part of the line between the outermost points (4 and 6) and land, the values at these points are distributed (constant value between gauge 4 and 6 and shoreline on each side). In Appendix E more information about the laboratory experiment data are found.

Some examples of comparisons are found in Figure 5.2 and Figure 5.3 for scenarios 1C and 3A, respectively. 1C is the scenario giving the largest waves (54 Mm^3) while 3A is the smallest western flank scenario giving the lowest waves of all evaluated scenarios.

The leading waves are fairly well reproduced compared to the laboratory experiments despite a phase-shift for the leading wave for some of the solutions. It is also evident that there are larger problems with reproducing the trailing waves. However, numerical tests show that even for trailing waves larger than the leading ones, the leading waves give largest run-up. This is true especially for locations at the fjord heads (for instance Tafjord, Hellesylt, and Geiranger). The reason for this is that the trailing waves are shorter and formed by reflections that are criss-crossing the fjord in a chaotic pattern, while the longer (and therefore also larger energy) leading waves are heading directly towards the fjord heads. However, this is in contradiction to eyewitness observations at Tafjord where the third wave was the one giving the largest impact.

The non-linear solutions for the largest scenarios break down after a few minutes due to instability problems. For scenario 1C this takes place after about 4.5 minutes. As a cure for the breakdown of the solutions, data from *DpWaves* are further conveyed as initial conditions for *GloBouss* after 4 minutes and 10 s. This technique gives unphysical trailing waves, but as noted above, this has no influence on the maximum inundation.

In Figure 5.4 the relative difference between the heights of the leading waves in the numerical model and in the laboratory is plotted. By inspecting Figure 5.2 and Figure 5.3, it is clear that the best match, surprisingly enough, is found for the linear dispersive solution, and not the Boussinesq solution (both dispersion and non-linearities) as expected. The relative difference for the linear dispersive solutions are mainly ranging between -5% up to +10%. The mean values (of all scenarios) at the center gauge for these solutions outside Hellesylt (gauge 8) and Geiranger (gauge 11) is about +5% and +1%, respectively. On the other hand, the differences for the Boussinesq solutions are mainly ranging between +8% and +20%. The mean difference for gauge 8 (Hellesylt) and 11 (Geiranger) is +10% and +15%, respectively. For the leading waves, non-linearities have strongest effect on the largest scenarios, see Figure 5.2. In the upper panel, a solitary wave is presumably about to be formed, and the shape of the leading waves differ significantly compared to the laboratory experiments. In a solitary wave the dispersive and non-linear effects are balancing giving a wave with a symmetric and constant shape. However, regarding the sensitivity tests in Appendix E, the discrepancies between the numerical solutions and the results from the laboratory experiments may to a great extent be related to the effect of the threshold depth applied in the numerical model. The differences between laboratory experiments and numerical models for both dispersive and Boussinesq solutions are in this context small, seen in light of the “simple” coupling between the laboratory experiments and the numerical model.

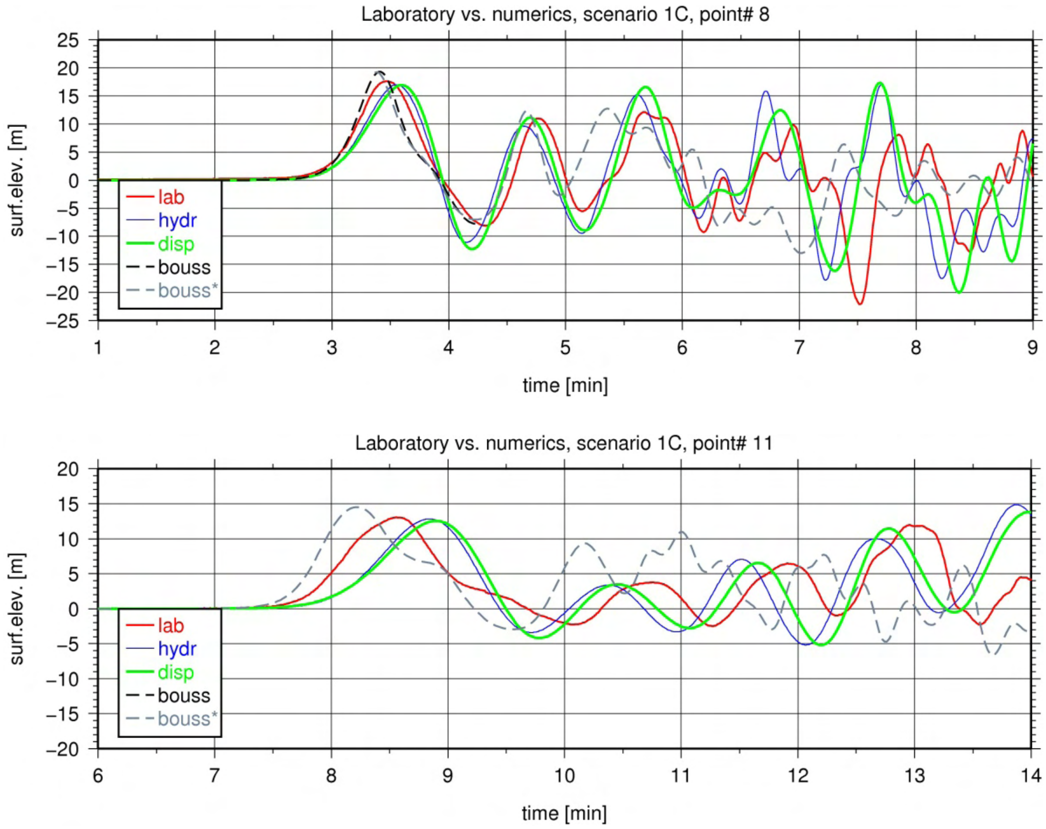

Figure 5.2. Comparison of results from lab and numerical simulations with input from lab at gauge 4-6 using scenario 1C. The figure shows results at the gauges 8 (outside Hellesylt, upper panel) and 11 (outside Geirnager, lower panel). "lab" is the surface elevation measured in the laboratory, while the other keys refer to different mathematical descriptions in the numerical model: "hydr"- linear hydrostatic, "disp"- linear dispersive, and "bouss" – non-linear and dispersive (simulation crashes after 4 min and 15 s). The label "bouss" (with an asterics) is the solution for the GloBouss model derived as explained in the text.*

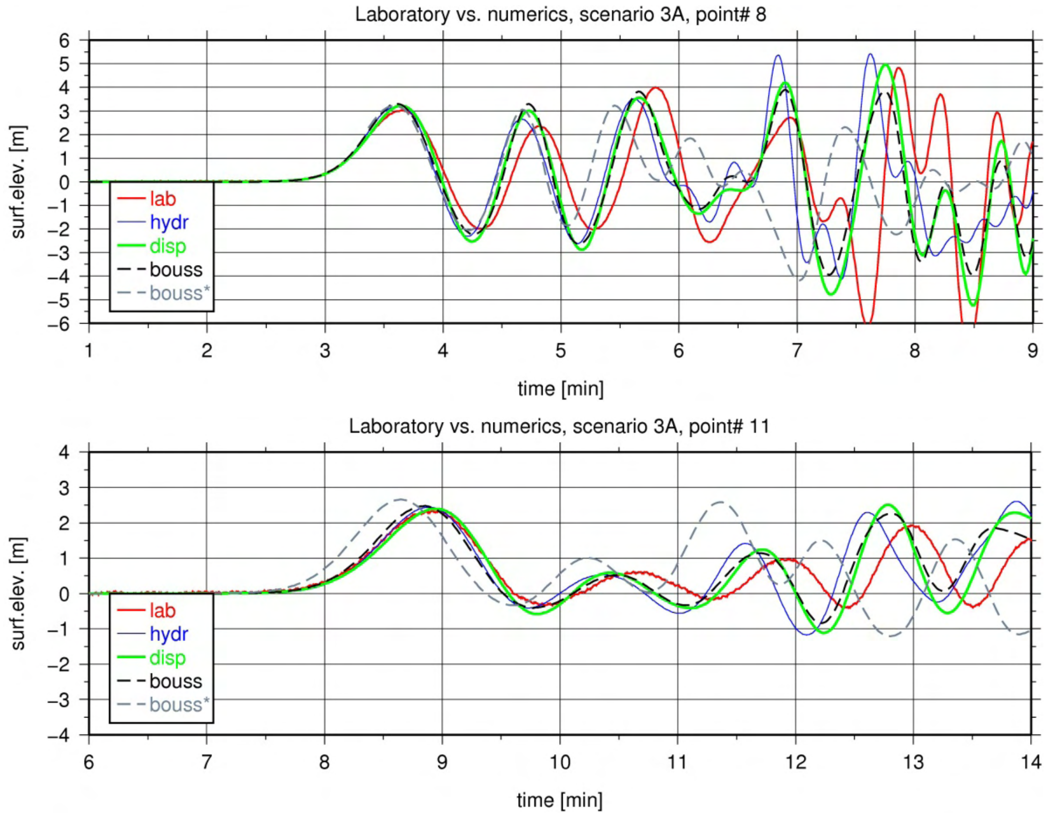

Figure 5.3. Comparison of results from lab and numerical simulations with input from lab at gauge 4-6 using scenario 3A. The figure shows results at the gauges 8 (upper panel) and 11 (lower panel). For explanation of the different keys applied in the figure, see Figure 5.2.

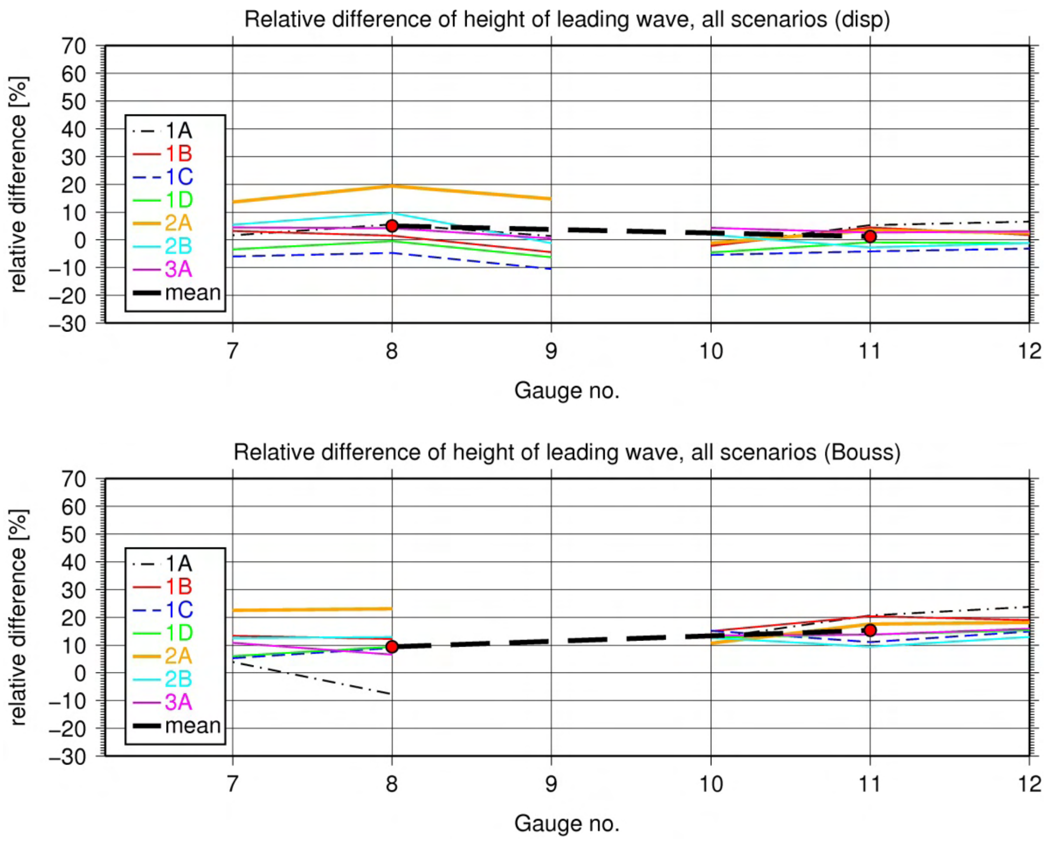

Figure 5.4. Relative difference between the surface elevation of the leading peak in the numerical model and the laboratory experiments at the gauges 7 to 12. Remember that pts. 10-12 is located at a longer distance than pts. 7-9. The legend reflects the different scenarios. The upper and lower panel shows the linear dispersive and non-linear dispersive (Boussinesq) cases, respectively. The red dots (connected with a thick dashed black line in the upper panel) are the mean difference of all scenarios at the midpoint gauges (8 and 11).

5.1.2 Run-up at Hellesylt and Geiranger

In the laboratory experiments, the inundation (flow height) is measured as a function of time at two points, one at Hellesylt and one at Geiranger given in UTM32 coordinates (389092 m, 6885273 m) and (406234 m, 6886498 m), respectively. The height above mean sea level is 3.0 m at Hellesylt and 3.9 m at Geiranger (upscaled values to full scale after measuring in the laboratory).

The 1:500 scale model at CHL is build up by linear interpolation between depth profiles with a distance of 250 m, see SINTEF (2008). To reproduce this bathymetry for the numerical run-up modelling, same procedure followed as close as possible for building up the digital bathymetry at Hellesylt and Geiranger, see Figure 5.5.

The input to the run-up model (ComMIT, see Appendix B) is surface elevations and current velocities from linear dispersive simulations in *DpWaves*. For the non-linear (Boussinesq) simulations, the input to ComMIT is taken from the GloBouss model (see previous section).

In Figure 5.6, Figure 5.7, and Figure 5.8 the run-up at Hellesylt and Geiranger (measured at the two locations specified above) is evaluated for scenario 1C, 1D, and 3A, respectively. The discrepancies between the numerical model and the laboratory experiments are remarkably small. At Hellesylt especially the largest scenarios reproduce the run-up measured in the laboratory closely. At Geiranger, the best mach is found for the dispersive solution (the input to ComMIT). The non-linear (Boussinesq) input is somewhat underestimated. This may be due to steeper front of the leading wave for the propagation phase, leading to stronger breaking and reduced surface elevation in the run-up stage. See Section 5.1.1 above where the differences between the dispersive and non-linear solution is discussed and the sensitivity tests in Appendix E where the effect of threshold depth is found. For scenario 3A larger deviations are found (for both Hellesylt and Geiranger), but this may be due to scale effects. The flow depths measured in the laboratory is only 0.2 to 0.4 cm and may be highly influenced by scale effects such as surface tension and seabed friction.

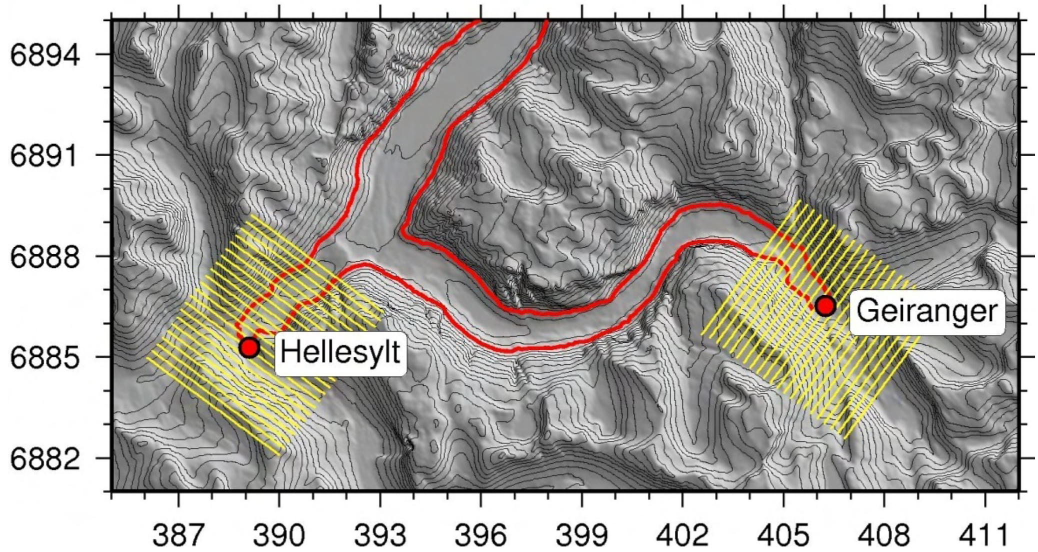

Figure 5.5. Definition map for the reconstruction of the bathymetry used in the run-up calculations at Hellesylt and Geiranger. The yellow lines are the tracks for the profiles (with a distance of 250 m between the tracks) and are identical as those used for establishing the bathymetry in the CHL 1:500 scale model. The two red dots show the location of the measurements for comparing the run-up from the laboratory experiments and the numerical modeling.

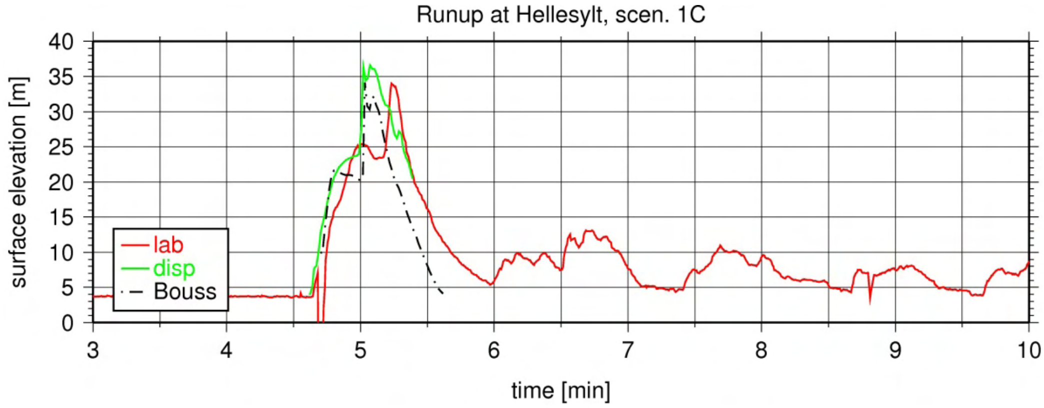

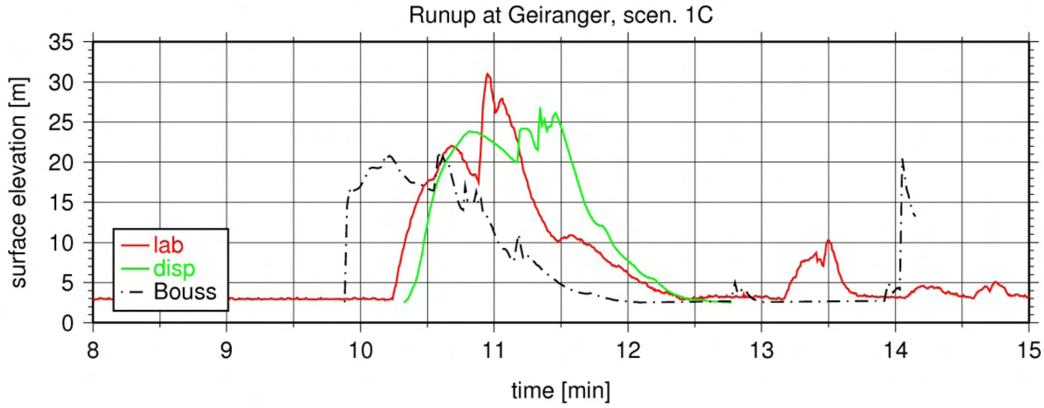

Figure 5.6. Comparison between measured run-up for scenario 1C at Hellesylt (upper panel) and Geiranger (lower) for the laboratory experiments ("lab") and numerical simulations ("disp" and "bouss") with input from the laboratory experiments.

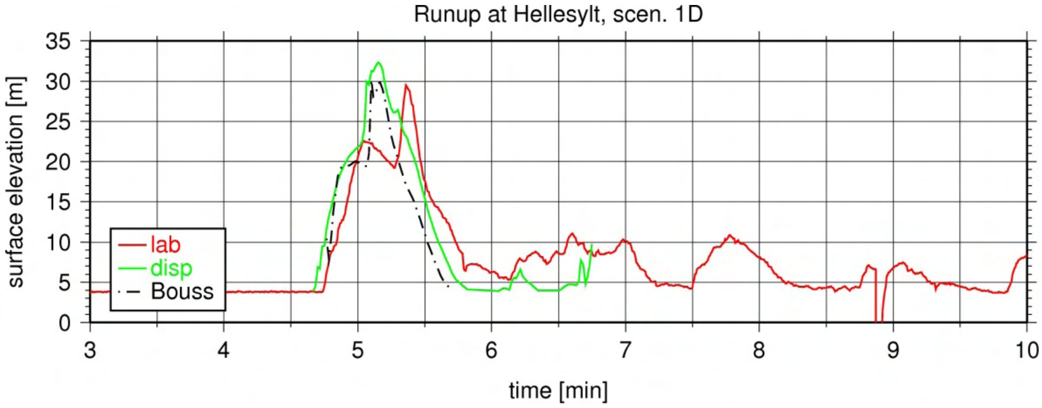

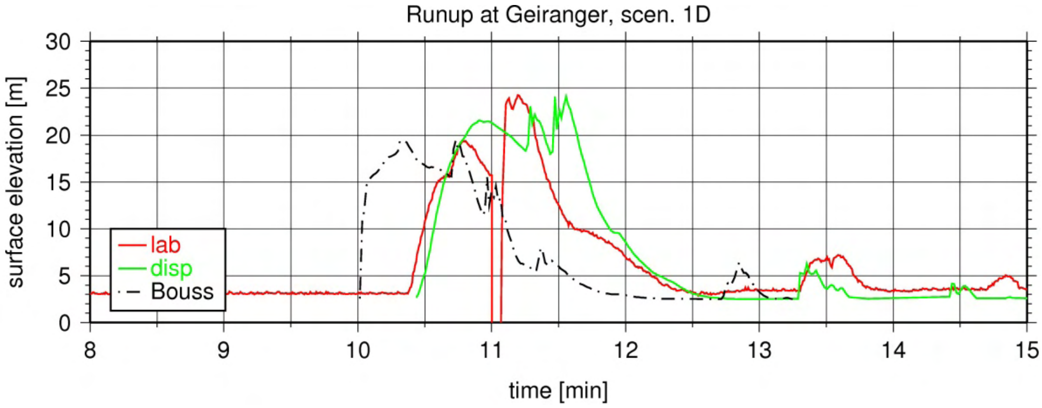

Figure 5.7. Comparison between measured run-up for scenario 1D at Hellesylt (upper panel) and Geiranger (lower) for the laboratory experiments ("lab") and numerical simulations ("disp" and "bouss") with input from the laboratory experiments.

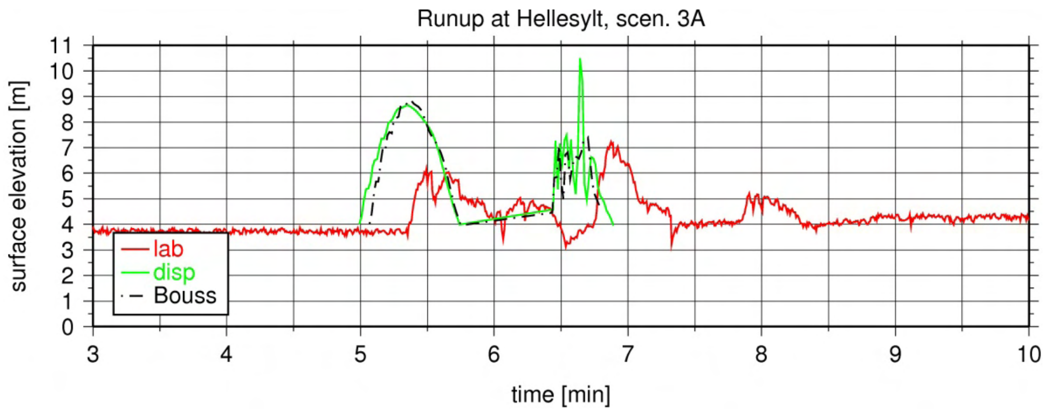

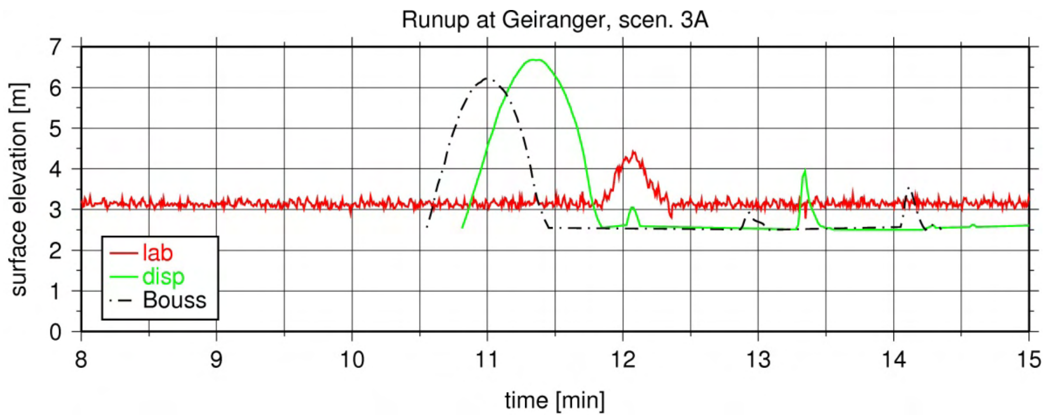

Figure 5.8. Comparison between measured run-up for scenario 3A at Hellesylt (upper panel) and Geiranger (lower) for the laboratory experiments ("lab") and numerical simulations ("disp" and "bouss") with input from the laboratory experiments.

5.2 Numerical simulation of both the tsunami generation and propagation

5.2.1 Tsunami propagation

In previous subsection the numerical model read input from the laboratory experiments through the boundary at the gauges 4 to 6. However, in this subsection, we present results where also the generation of waves are modelled numerically. The rock slide dimensions and velocity progression of the rock slide are identical to the one applied/measured in the laboratory experiments. Note that the front of the slide in the laboratory experiments was taken to be normal to the slide plane, and hence not as specified during the project (Arne Lothe, SINTEF, pers. comm.). In the numerical modelling the frontal angle is slightly below 45 degrees.

Time series at gauges 2, 5, and 11 for three scenarios are presented in Figure 5.9 - Figure 5.11. In addition to 1C and 3A we have also included time series for scenario 1D as scenario 1D best matches the results from the laboratory at gauges

4-6, and we may then easier explain the possible differences between the results from laboratory and the numerical model.

Best match (in the combination of height and shape) is given by the dispersive solution. The Boussinesq solutions overestimates the laboratory experiments with increasing differences for points at longer distances away (e.g. gauge 11): the effect of non-linearity steepens and amplifies the leading wave. The latter effect can not clearly be seen in the laboratory experiments. As described above, it seems like a solitary wave is about to be formed for the larges scenario when the waves are travelling towards Geiranger. Again, the increase of the wave height outside Geiranger is at least partly due to the use of the threshold depth, see Appendix E.

By investigating the height of the leading waves, we are able to quantify the difference between the laboratory experiments and the numerical solutions, see Figure 5.12. For the linear dispersive solutions for scenario 1D, the averaged difference at gauges 2 is +17%, 5 is +10%, 8 is +10%, and 11 is +15%. On the other hand, the Boussinesq solutions gave +18%, +30%, +38%, and +46%. As we can see, best match is found for the largest scenarios (1A, 1B, 1C, 1D) and 3A. The Boussinesq solution for scenario 1D gives a relative difference of (only) +3%, +6%, and +18%. Poorest match is given by the scenarios 2A and 2B with differences in the range +25% to +58%. The reason for the poor match for 2A and 2B is not fully understood.

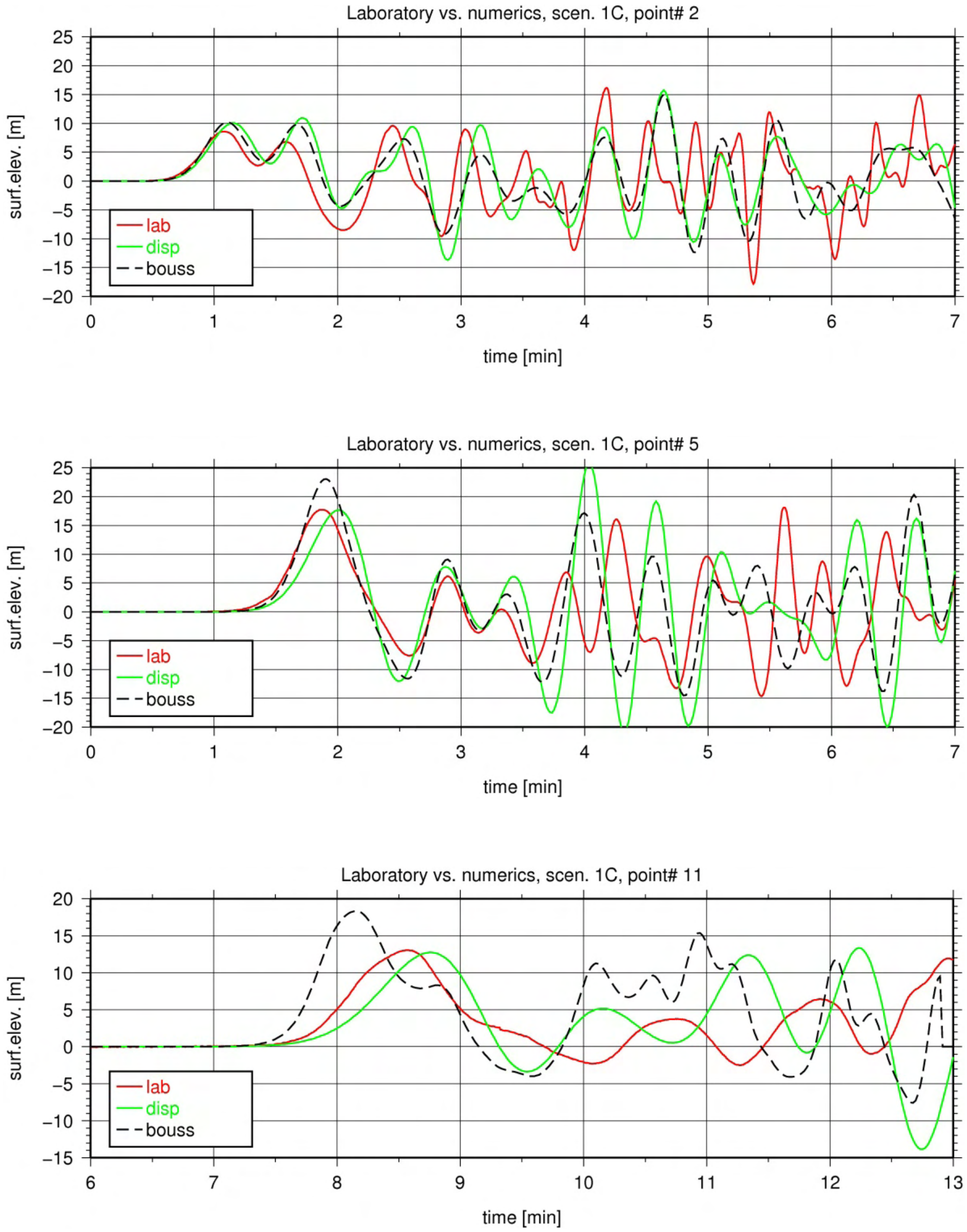

Figure 5.9. Surface elevations from laboratory experiments compared to numerical simulations. In this case the wave generation is modeled numerically. Figure shows the comparison for scenario 1C at gauge 2 (upper panel), 5 (mid), and 11 (lower). For explanation of the different keys applied in the figure, see Figure 5.2.

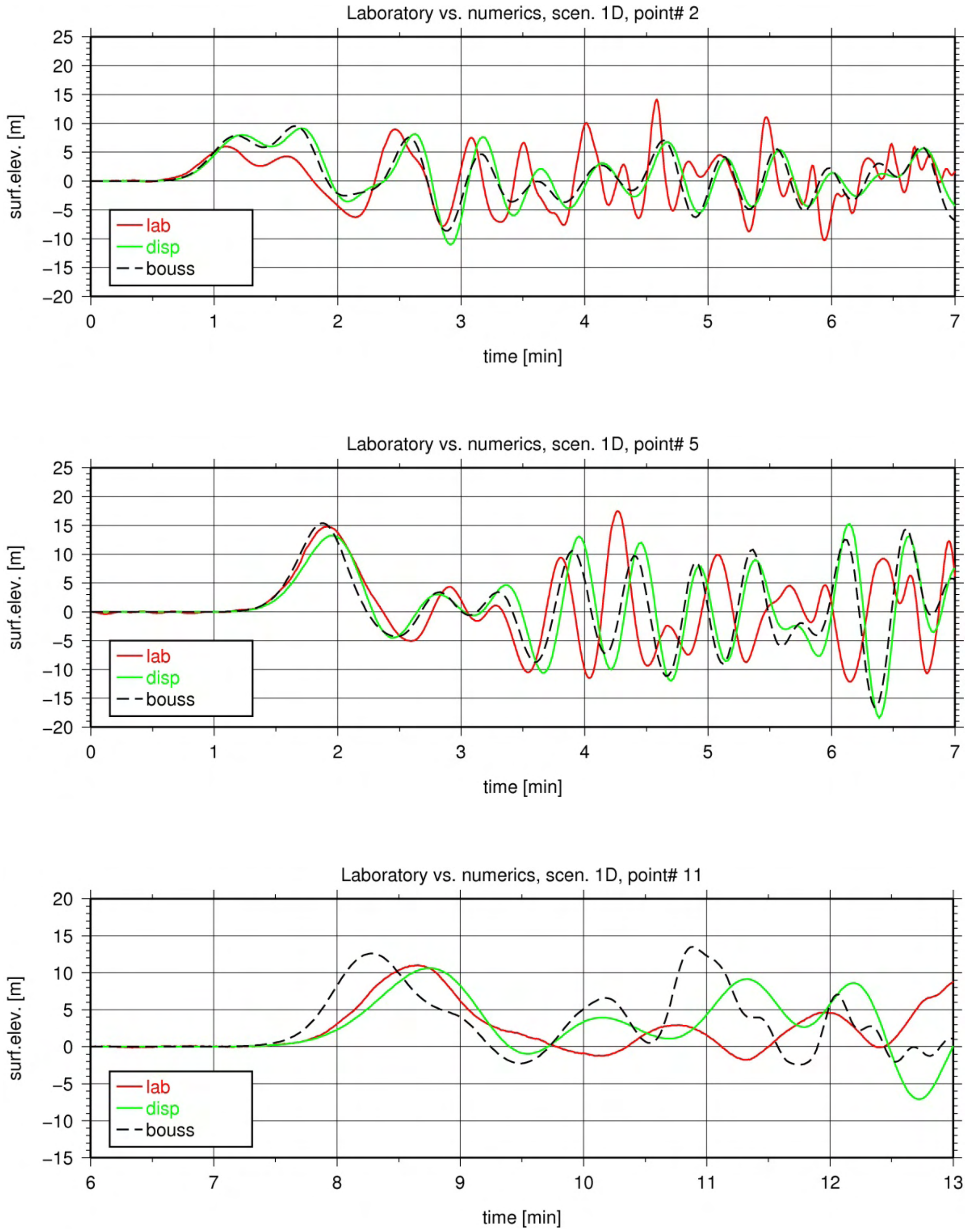

Figure 5.10. Surface elevations from laboratory experiments compared to numerical simulations. In this case the wave generation is modelled numerically. Figure shows the comparison for scenario 1D *at gauge 2 (upper panel), 5 (mid), and 11 (lower).* For explanation of the different keys applied in the figure, see Figure 5.2

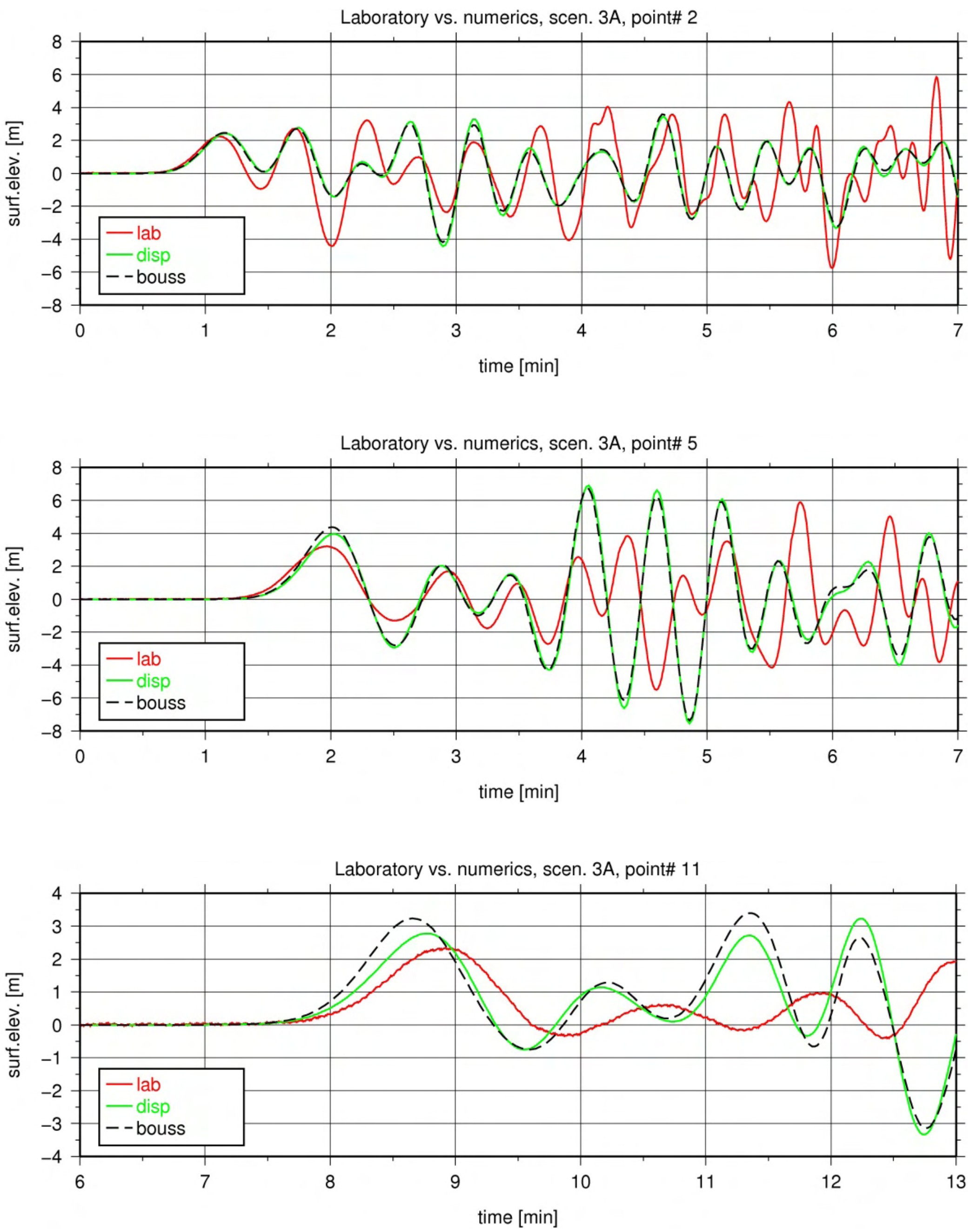

Figure 5.11. Surface elevations from laboratory experiments compared to numerical simulations (the wave generation is modeled numerically). Figure shows the comparison of scenario 3A at gauge 2 (upper panel), 5 (mid), and 11 (lower). For explanation of the different keys applied in the figure, see Figure 5.2.

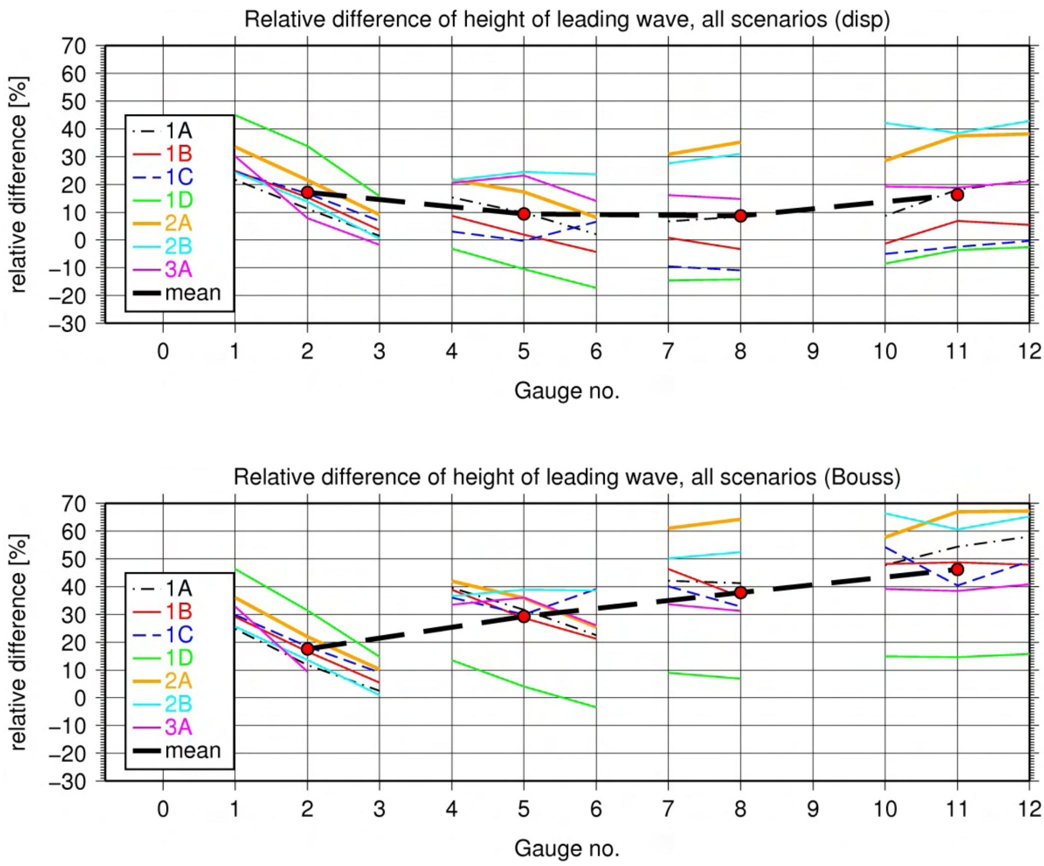

Figure 5.12. Relative difference between the surface elevation of the leading peak in the numerical model and the laboratory experiments at the gauges 1 to 12. The midpoint gauges 2 (north of Åknes), 5, 8, and 11 is located with increasing distance from the slide area. The legend reflects the different scenarios. The upper and lower panel shows the linear dispersive and non-linear dispersive (Boussinesq) case, respectively. The red dots (connected with a thick dashed black line) are the mean difference of all scenarios at the midpoint gauges.

5.2.2 Run-up at Hellesylt and Geiranger

Here the result for the run-up calculations using input from the numerical model where also the generation phase is modelled numerically is applied. Again, we evaluate the scenarios 1C (Figure 5.13), 1D (Figure 5.14), and 3A (Figure 5.15) at Hellesylt and Geiranger. By using the input from the linear dispersive simulations, the discrepancies in the run-up measured for the leading wave is ranging between -5 % to + 25 % compared to the laboratory experiments. On the other hand, for the non-linear Boussinesq solutions the discrepancies are found to be between +8 % to + 33%. The poorest mach is for scenario 3A, and again one important reason may be the scale effects evident for small flow depths (the flow depth for 3A is 0.3 cm and 0.6 cm at Geiranger and Hellesylt, respectively). Again we see remarkable good match between the numerical models and the laboratory experiments.

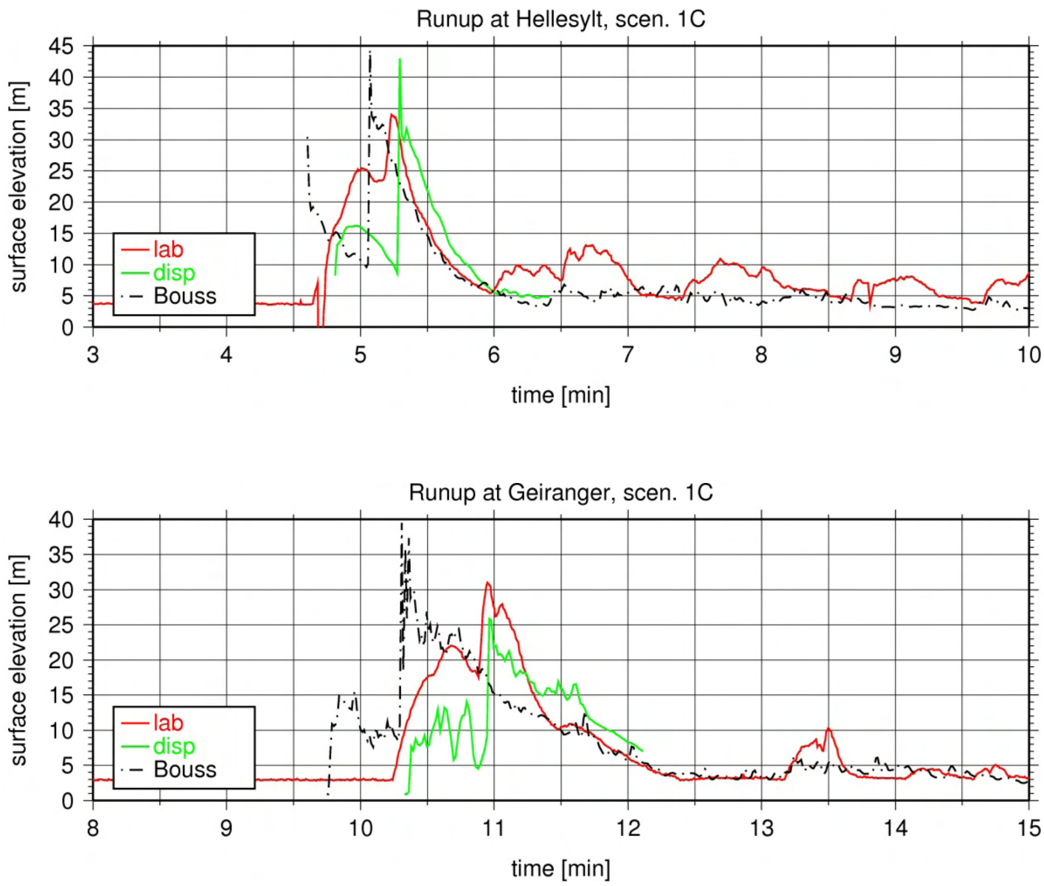

Figure 5.13. Comparison between measured run-up for scenario 1C at Hellesylt (upper panel) and Geiranger (lower) for the laboratory experiments ("lab") and numerical simulations ("disp" and "bouss"). The generation phase is modeled numerically.

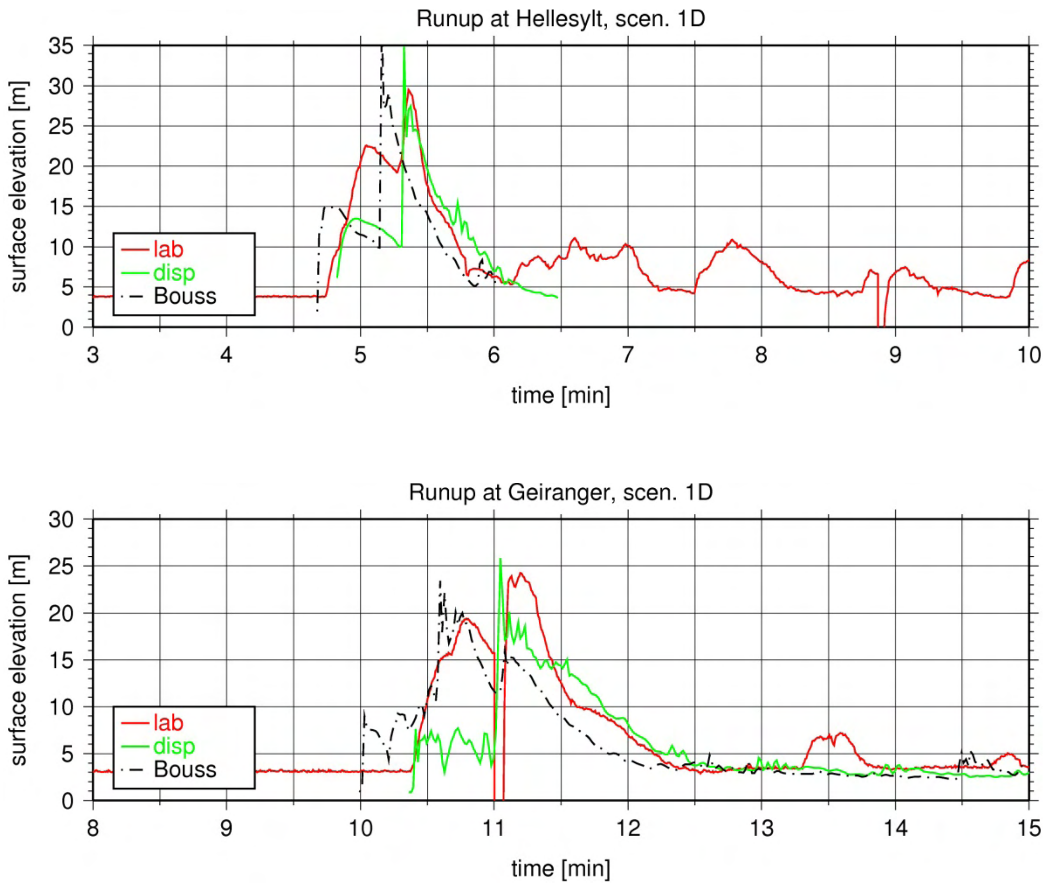

Figure 5.14. Comparison between measured run-up for scenario 1D at Hellesylt (upper panel) and Geiranger (lower) for the laboratory experiments ("lab") and numerical simulations ("disp" and "bouss"). The generation phase is modeled numerically.

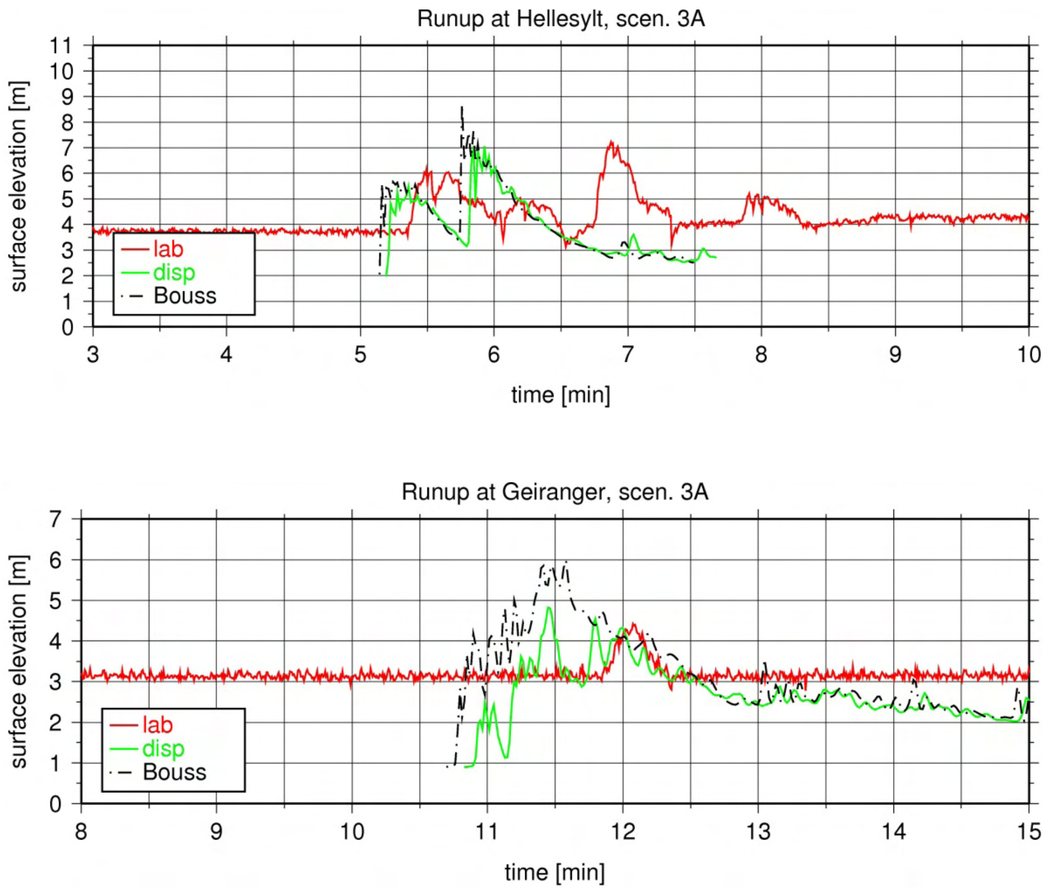

Figure 5.15. Comparison between measured run-up for scenario 3A at Hellesylt (upper panel) and Geiranger (lower) for the laboratory experiments ("lab") and numerical simulations ("disp" and "bouss"). The generation phase is modeled numerically.

5.3 Discussion

The comparison above of the both propagation and run-up between numerical modelling and laboratory experiments show that the numerical models are capable to mimic the laboratory experiments closely seen in light of the two quite different approaches. In the numerical model, the waves seem to be somewhat overestimated especially in the fjord of Geiranger. This effect is partly due to effect of the use of threshold depth (see Appendix E, sensitivity analyses. As we have seen above, the higher wave height outside Geiranger do not contribute significantly to higher run-up. In some of the cases the effect related to increased wave height in the propagation phase is reduced through more intensive wave breaking, see also Lynett et al. (2003). This is true especially at Geiranger.

6 Comparisons of run-up models

For validating the run-up model applied for the run-up calculations, ComMIT/MOST, we have performed comparisons with other independent inundation/run-up models. In Appendix B, a thorough comparison is made between ComMIT/MOST and GEOCLAW, with the corresponding convergence tests in Appendix C. One important conclusion is that the results for the two models have only minor deviations, with the ComMIT/MOST model slightly more conservative than the GEOCLAW model. Since ComMIT/MOST is a standard model and the most common model used world wide, we have applied this model for the run-up calculations in this project.

In Appendix D, ComMIT/MOST is compared to the COMCOT model. The latter comparison show clear differences in the two models, even the overall wave pattern are partly captured in both models. In addition COMCOT is much more hampered with noise. Possible sources for the discrepancies are inconsistent use of model parameters as well as different treatment of the input wave.

7 Comments on uncertainties

In this report we have described how the tsunami generation, propagation, and run-up phases are modelled. The corresponding results for potential scenarios from Åknes and Hegguraksla, back-calculation of historical events, and comparison between numerical modelling and laboratory experiments are also presented.

Throughout this project we have performed a large series of sensitivity analysis for determining the most important parameters for the generation, propagation, and run-up.

For the generation phase the physical dimensions of the rock slide (especially the cross sectional frontal area), the run-out distance, the water depth, and the velocity progression will all contribute to the height and the shape of the generated waves. However, the most important parameter is the frontal area of the rock slide. A rock slide release may consist of several minor or in the worst case one big event. In the present work the rock slide is always modelled as one block, which represents the worst cases for each individual volume. Geological findings at Åknes confirm that simultaneous releases of large blocks or even the total volumes are not unlikely.

The wave generation in the numerical model is validated against laboratory experiments by using a wave channel (NGI, 2008a) and the three dimensional laboratory experiments presented in this report. The rock slide parameters in the numerical simulations (dimension, velocity, etc.) are made as close as possible to the laboratory experiments, and the comparison confirms that the numerical wave model reproduces the laboratory experiments with only minor discrepancies.

The models for the tsunami propagation phase are previously thoroughly tested against analytical solutions, Pedersen and Løvholt (2008) and Langtangen and Pedersen (1998). In the present work the models are also tested against the laboratory experiments with a high degree of accuracy.

The run-up model, ComMIT/MOST, is a standard model and is probably the most common model world wide applied for run-up calculations. The model is extensively tested against analytical solutions as well as several (laboratory and field scale) benchmark tests. In our work, the model is also thoroughly tested at Hellesylt (for a scenario from Åknes) against an independent run-up model (GEOCLAW) with insignificant discrepancies. In addition, the comparison between ComMIT/MOST and the laboratory experiments reveal remarkably small discrepancies.

Through back-calculation of the well documented historical events (Tafjord 1934, Skafjell 1731, and Tjelle 1756), we find that the modelling using the new set of numerical models (for generation, propagation, and run-up) are able to reproduce the events fairly close. However, by tuning the rock slide parameters, it is still possible to improve the results further.

To conclude, the most uncertain part of the numerical modelling is how the rock slides will enter the water. However, the block slide applied for the calculation represents a credible worst case scenario. When the slide parameters are given, the accuracy of the numerical modelling of the generation, propagation, and run-up is ensured by numerous sensitivity tests, as well as comparison with other models, laboratory experiments, and back-calculation of historical events as presented in this report.

The estimate of the sea level rise used as basis for this report is also uncertain, see DSB (2009).

The results from the run-up calculations in this report are best estimate predictions, i.e. they are not taking any safety factors into account.

8 References

DSB (2009) Havnivåstigning: Estimater av framtidig havnivåstigning i norske kystkommuner. Revidert utgave (2009).Utgitt av: Det nasjonale klimatilpasningssekretariatet ved Direktoratet for samfunnssikkerhet og beredskap. September 2009.

Furseth, A. (2006). Skredulykker i Norge. Tun Forlag

Furseth, A. (1985). Dommedagsfjellet – Tafjord 1934. Gyldendal Norsk Forlag, Oslo. ISBN 82-05-16413-4.

Harbitz, C., Pedersen, G., and Gjevik, B. (1993) Numerical Simulations of Large Water Waves due to Landslides. Journal of Hydraulic Engineering, vol. 119, no. 12, 1325-1342.

Jørstad, F. (1968). Waves generated by landslides in Norwegian fjords and lakes. Publication 79, NGI, Oslo, Norway, 13-31.

Kaldhol, H. and Kolderup, N.-H. (1937). Skredet i Tafjord 7. april 1934. Bergens museums Årbok 1936, Naturvidenskapelig rekke, Bergen, Norway, 11.

Langtangen, H.P. and Pedersen, G. (1998). Computational models for weakly dispersive and nonlinear water waves. Comput. Methods Appl. Mech. Engrg. 160, 337-358.

Lynett, P.J., Borrero, J.C.,Liu, P. L.-F., and Synolakis, C. E. (2003). Field survey and Numerical Simulations: A review of the 1998 Papua New Guinea Tsunami, Pure appl. Geophys. Vol. 160, 2119-2146

NGI (2003). Tsunamis generated by rockslides in Geiranger- and Tafjorden – scenarios and modell comparisons. NGI report 20011622-1.

NGI (2005). Innledende numeriske analyser av flodbølger som følge av mulige skred fra Åknes. NGI rapport 20031100-2.

NGI (2006). Semi-annual report: Preliminary results using an improved tsunami model. NGI rapport 20051018-1.

NGI (2008a). Semi-annual report: Tsunami impact in the outer part of Storfjorden, testing of numerical models for rock slide and tsunami, coupling to laboratory experiments. 20051018-2.

NGI (2008b). Operational tsunami models with run-up. NGI report 20061073-1.

NGI (in prep.). Evaluation of the flow characteristics of the potential Akneset rock slide, western Norway – Contributions to the design of laboratory experiments on wave generation. NGI report.

NGU (2001).Hazard evaluation of rock avalanches; the Baraldsnes-Oterøya area, Geological Survey of Norway (NGU), Trondheim, 33 pp.

Pedersen G. and Løvholt F. (2008). Documentation of a global Boussinesq solver. Dept of Mathematics, University of Oslo, Norway. URL: http://www.math.uio.no/eprint/appl_math/2008/01-08.html

SINTEF (2008). Notat – rasmodell, dated 2008-09-12.

UNESCO-IOC (2006). Tsunami Glossary.

ÅTB (2009a). Åknes/Tafjord Beredskap IKS v/Lars Harald Blikra: Scenarios for tsunami modelling.

ÅTB (2009b). Åknes/Tafjord Beredskap IKS v/Jarle Hole: Lokalitetar og område for produksjon av detaljert oppskyllingshøgder.

Appendix A - Details for hazard zoning

Contents

Appendix A

Details for hazard zoning

A.1 Introduction

In this appendix the run-up results for scenarios from both Hegguraksla (H2, H3) and Åknes (1C, 2B) are presented. For details about the scenarios see main report. The locations and areas of interest is given by the Åknes/Tafjord project. The evaluated locations (see Figure A.1) are Dyrkorn (3), Eidsdal (11), Fjora (8), Geiranger (12), Gravaneset (5), Hellesylt (13), Hundeidvik (18), Linge (6), Magerholm[1] (1), Norddal (10), Oaldsbygda (14), Ramstadvika (17), Raudbergvika (19), Skardbøen (21), Stordal[1] (4), Stranda[1] (15), Sykkylven[1] (16), Tafjord (9), Vaksvik (20), Valldal[1] (7), Vegsundet (1), Vika (8), and Ørskog[1] (2). The scenarios from Hegguraksla are evaluated at Tafjord, Fjøra, Vika, and Valldal only. The detailed run-up heights presented through figures in this appendix refer to 0.7 m above today's mean sea level. This is in contradiction to the run-up heights given in tables in the main report which refer to the today's sea level.

[1]For the areas at Magerholm, Ørskog, Stordal, Stranda, Ikornes, and Valldal, we present maximum values for the inundation height, velocity, and flow depth as well as the time-history for surface elevation and velocity extracted at five positions at each location.

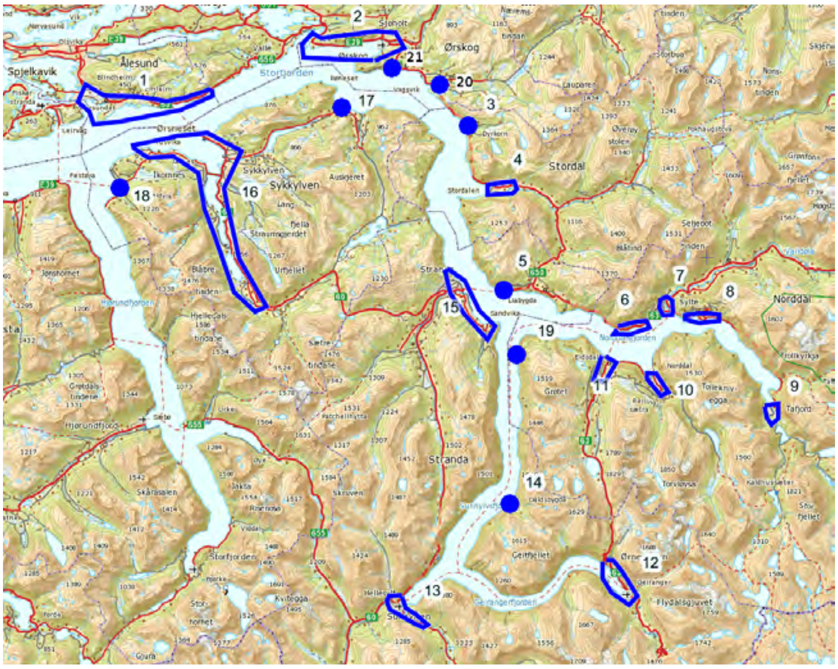

Figure A.1: Overview of the 21 locations for run-up calculations.

A.2 Maximum surface elevation

For better overview of the tsunami impact for the whole region, we present the maximum surface elevations for the four scenarios 1C, 2B, H2, and H3. The deatils for run-up are found in Section A.3.

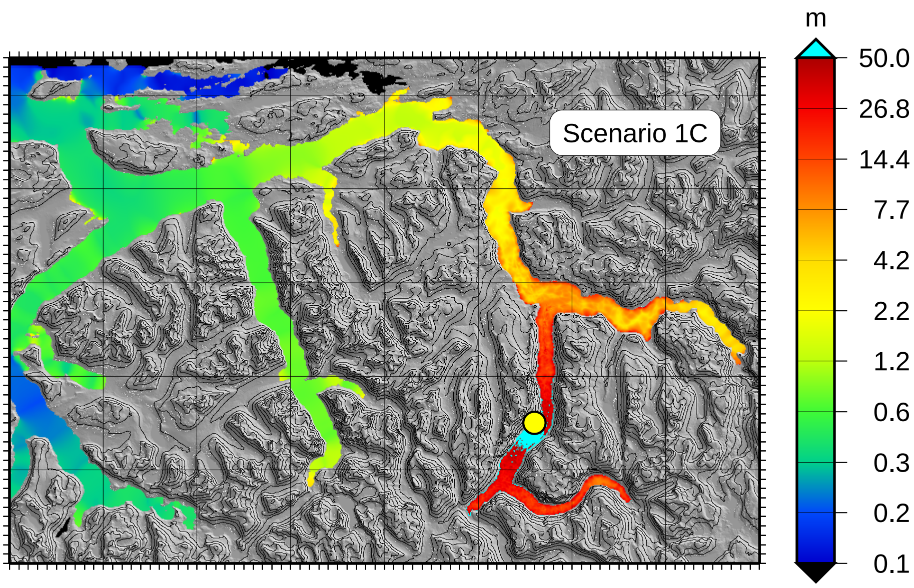

Figure A.2: Maximum surface elevation given in meters (logarithmic scale) for whole Storfjorden, scenario 1C. The distance between gridlines are 10 km.

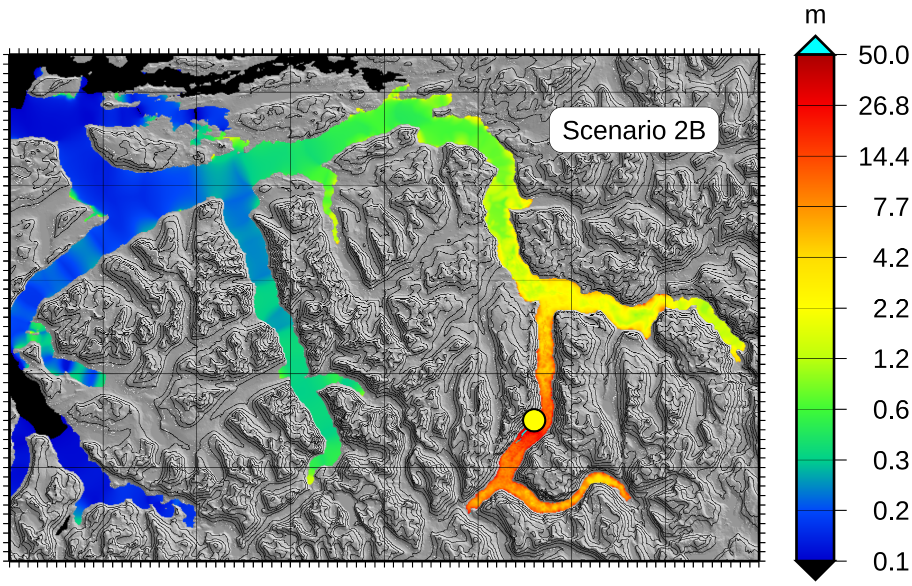

Figure A.3: Maximum surface elevation given in meters (logarithmic scale) for whole Storfjorden, scenario 2B. The distance between gridlines are 10 km.

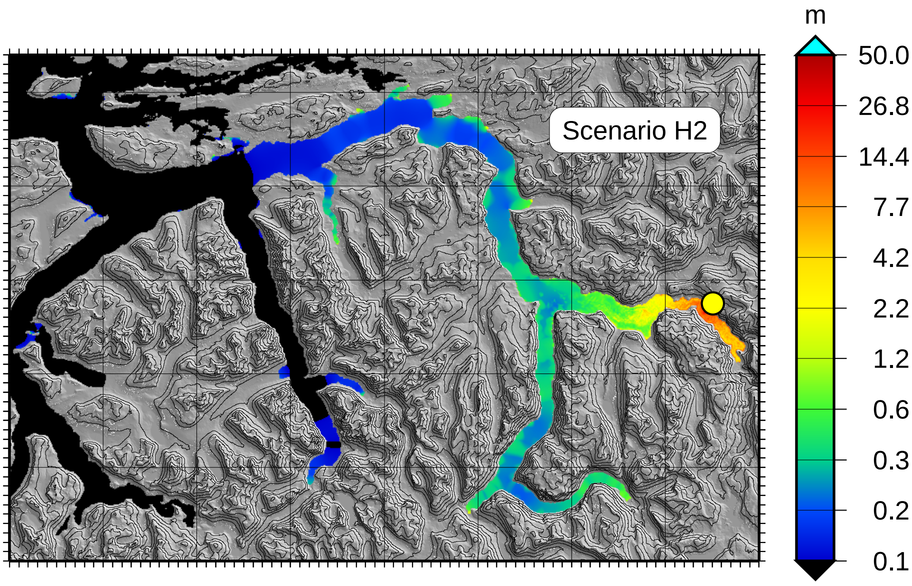

Figure A.4: Maximum surface elevation given in meters (logarithmic scale) for whole Storfjorden, scenario H2. The distance between gridlines are 10 km.

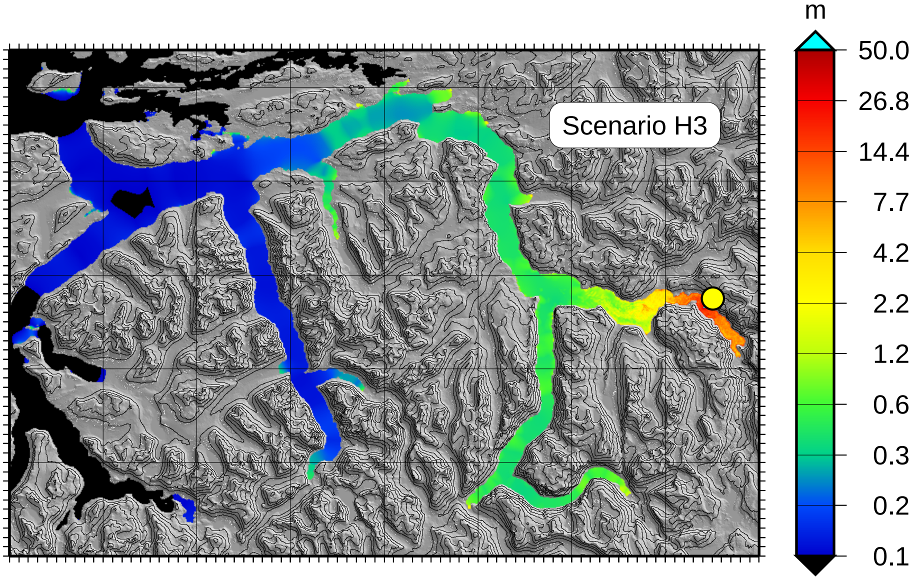

Figure A.5: Maximum surface elevation given in meters (logarithmic scale) for whole Storfjorden, scenario H3. The distance between gridlines are 10 km.

A.3 Run-up calculations

In this section the detailed run-up calculations are presented. The computations are performed for 21 locations with totally 26 grids to cover the areas of interest. The locations and the areas for run-up calculations are stated by the Åknes/Tafjord project. For the definition of the maximum water level, velocity, and flow depth see the main report. In the figures, the shoreline is marked by a cyan line. The depth contours are marked with thick dashes (equidistance 20 m) and thin lines (equidistance 5 m), while the contours on dry land are marked with a thick line (equidistance 20 m) and thin dash-dotted lines (equidistance 5 m).

A.3.1 Blakstad - Breivika

Location number 16, see Figure A.1.

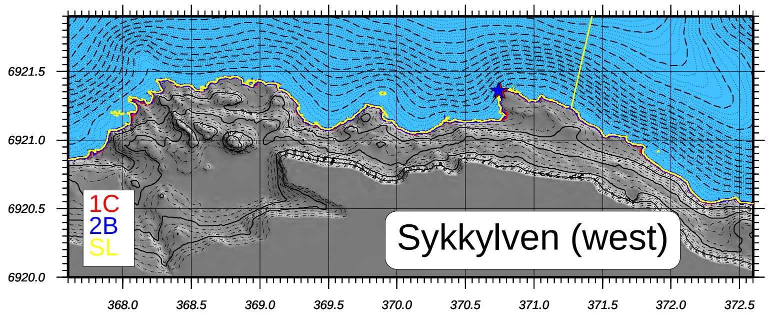

Figure A.6: Trimlines for each scenario at Blakstad - Breivika. The highest water level along the shoreline and the maximum run-up is indicated with a triangle and a star, respectively. The yellow line is the shoreline for today's mean sea level. Coordinates given in UTM32 (km) and gridlines printed every 500 m.

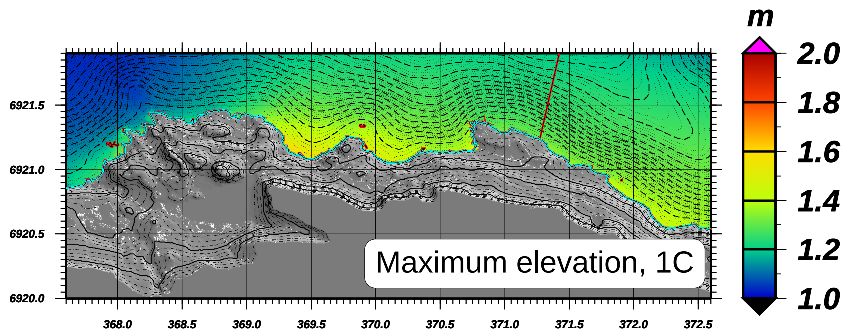

Figure A.7: Maximum water level measured from 0.7 m above today's mean sea level at Blakstad - Breivika, scenario 1C. The red line is the shoreline for today's mean sea level (MSL) while the cyan line is the shoreline including the estimated sea level rise of 0.7 m. Coordinates given in UTM32 (km) and gridlines printed every 500 m.

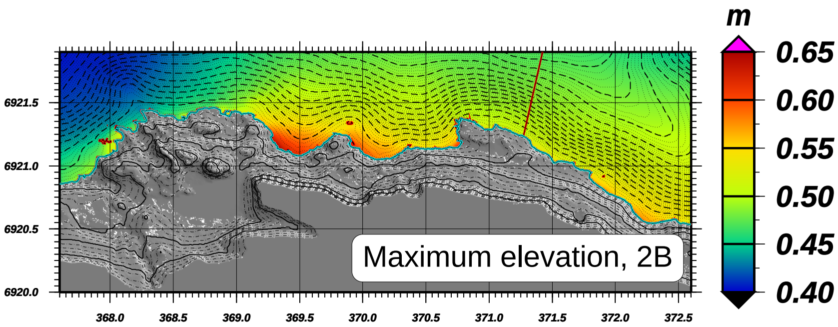

Figure A.8: Maximum water level measured from 0.7 m above today's mean sea level at Blakstad - Breivika, scenario 2B. The red line is the shoreline for today's mean sea level (MSL) while the cyan line is the shoreline including the estimated sea level rise of 0.7 m. Coordinates given in UTM32 (km) and gridlines printed every 500 m.

A.3.2 Dyrkorn

Location number 3, see Figure A.1.

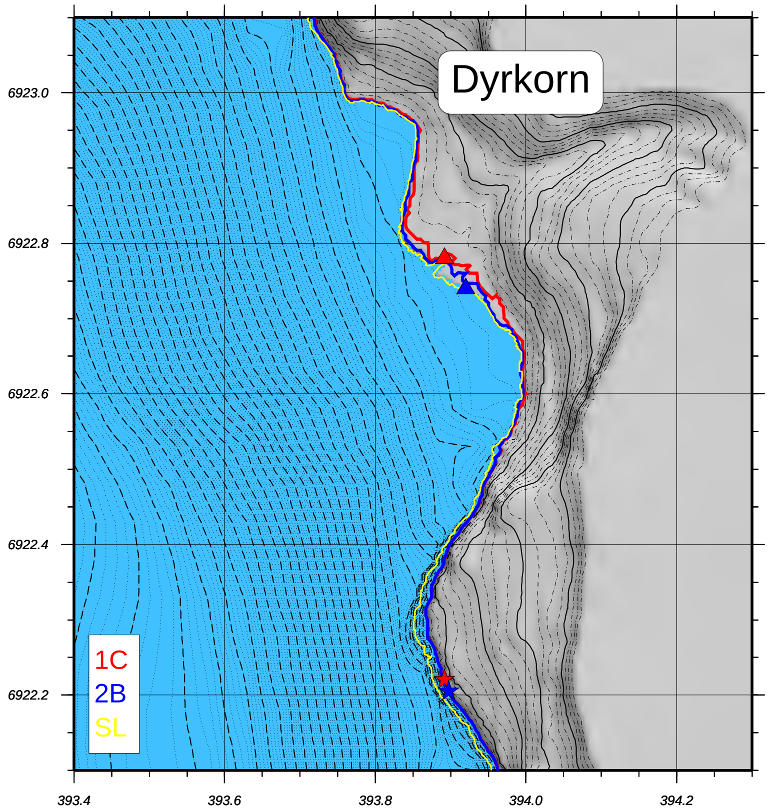

Figure A.9: Trimlines for each scenario at Dyrkorn. The highest water level along the shoreline and the maximum run-up is indicated with a triangle and a star, respectively. The yellow line is the shoreline for today's mean sea level. Coordinates given in UTM32 (km) and gridlines printed every 200 m.

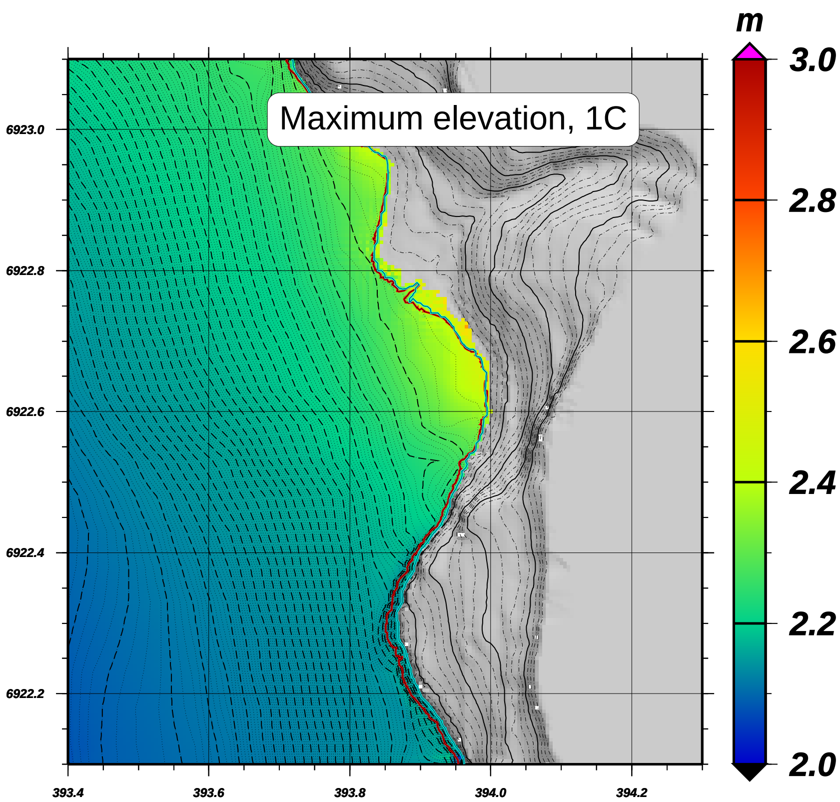

Figure A.10: Maximum water level measured from 0.7 m above today's mean sea level at Dyrkorn, scenario 1C. The red line is the shoreline for today's mean sea level (MSL) while the cyan line is the shoreline including the estimated sea level rise of 0.7 m. Coordinates given in UTM32 (km) and gridlines printed every 200 m.

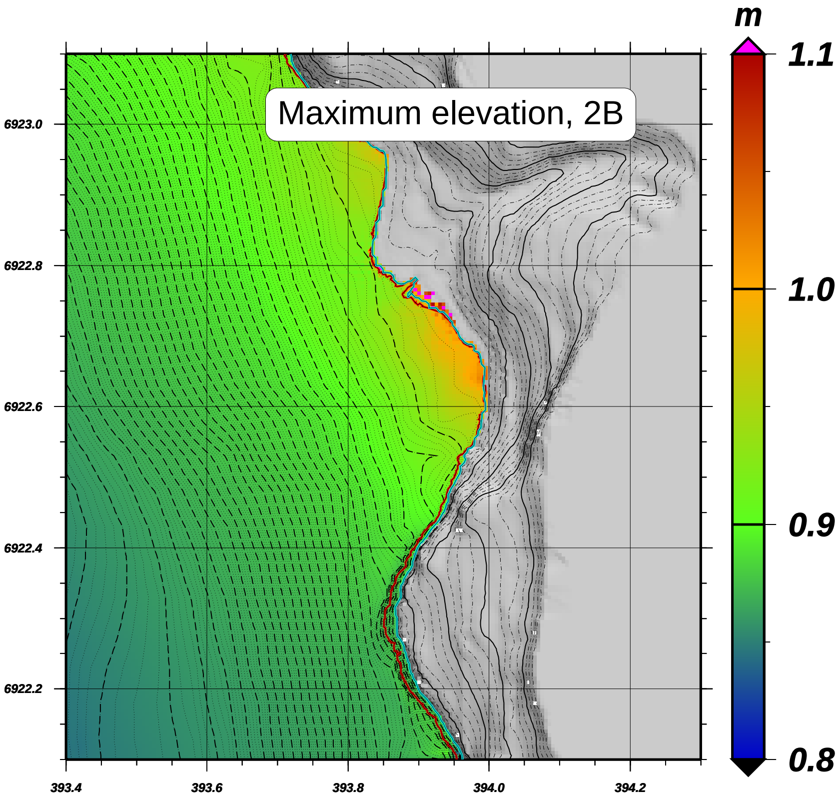

Figure A.11: Maximum water level measured from 0.7 m above today's mean sea level at Dyrkorn, scenario 2B. The red line is the shoreline for today's mean sea level (MSL) while the cyan line is the shoreline including the estimated sea level rise of 0.7 m. Coordinates given in UTM32 (km) and gridlines printed every 200 m.

A.3.3 Eidsdal

Location number 11, see Figure A.1.

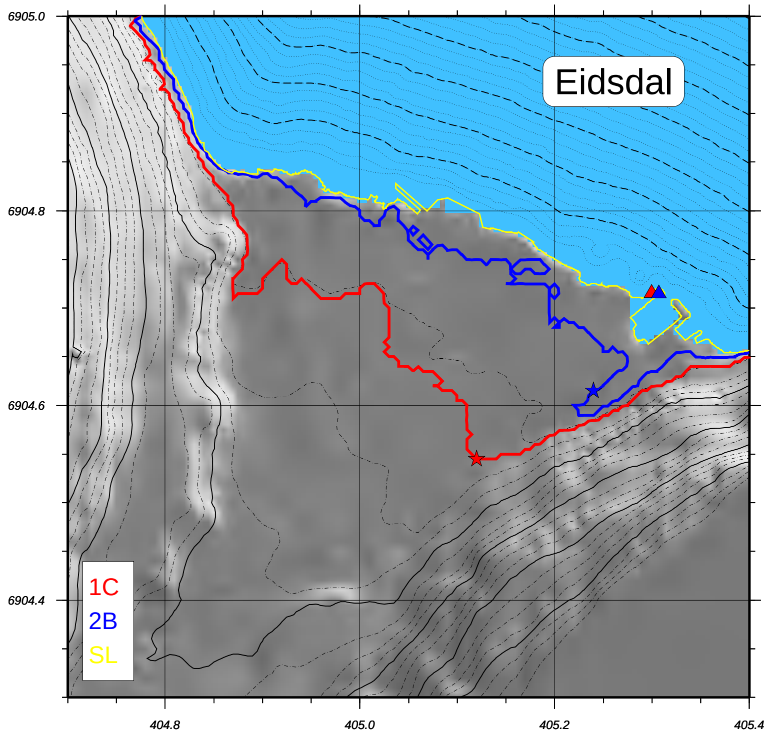

Figure A.12: Trimlines for each scenario at Eidsdal. The highest water level along the shoreline and the maximum run-up is indicated with a triangle and a star, respectively. The yellow line is the shoreline for today's mean sea level. Coordinates given in UTM32 (km) and gridlines printed every 200 m.

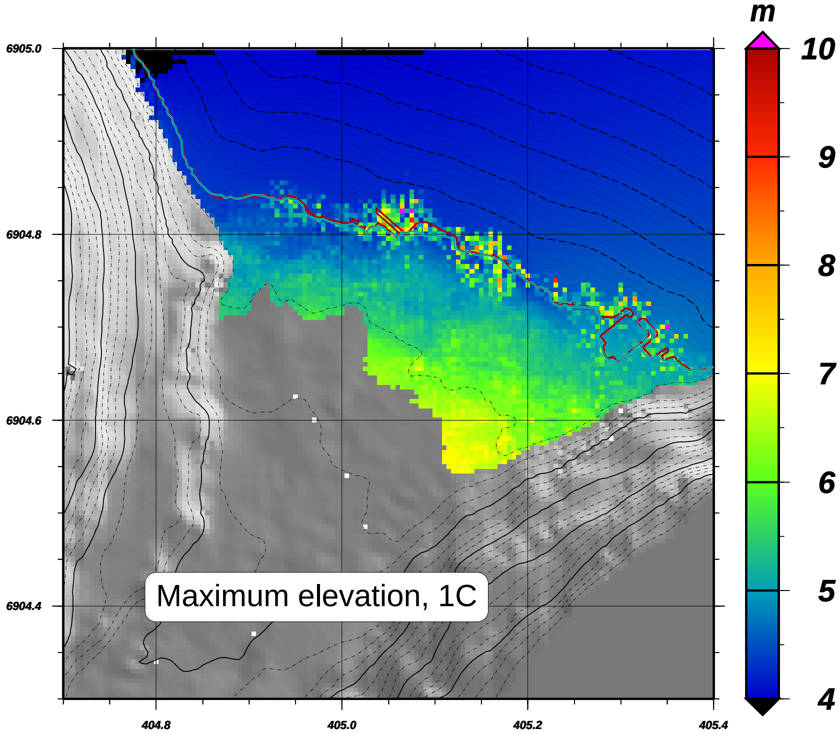

Figure A.13: Maximum water level measured from 0.7 m above today's mean sea level at Eidsdal, scenario 1C. The red line is the shoreline for today's mean sea level (MSL) while the cyan line is the shoreline including the estimated sea level rise of 0.7 m. Coordinates given in UTM32 (km) and gridlines printed every 200 m.

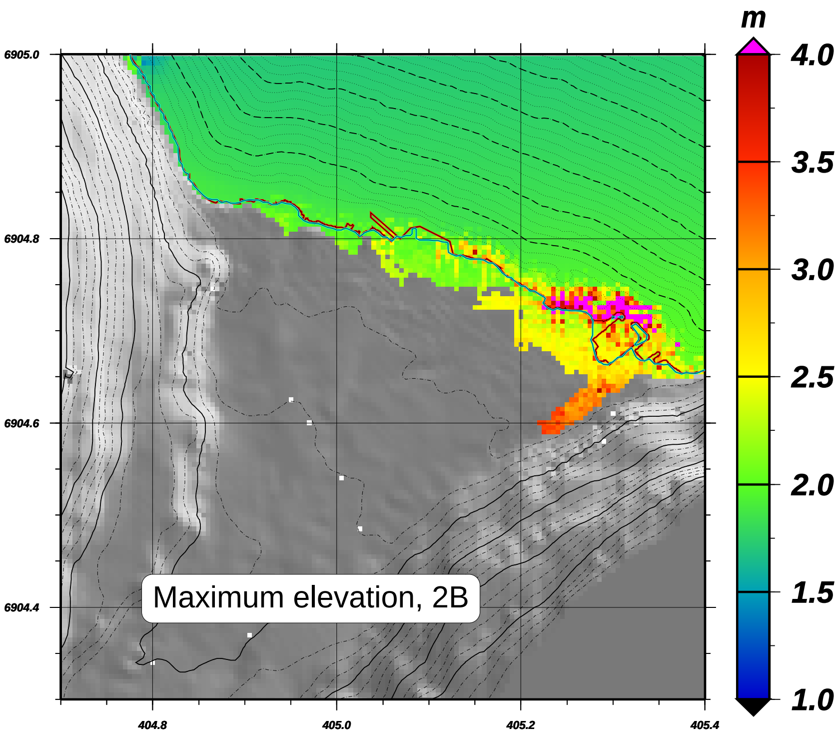

Figure A.14: Maximum water level measured from 0.7 m above today's mean sea level at Eidsdal, scenario 2B. The red line is the shoreline for today's mean sea level (MSL) while the cyan line is the shoreline including the estimated sea level rise of 0.7 m. Coordinates given in UTM32 (km) and gridlines printed every 200 m.

A.3.4 Fjora

Location number 8, see Figure A.1.

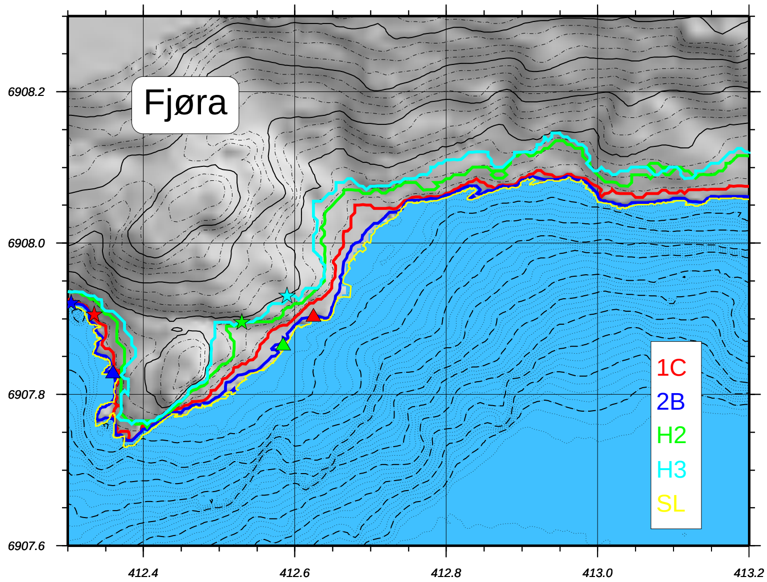

Figure A.15: Trimlines for each scenario at Fjora. The highest water level along the shoreline and the maximum run-up is indicated with a triangle and a star, respectively. The yellow line is the shoreline for today's mean sea level. Coordinates given in UTM32 (km) and gridlines printed every 200 m.

Figure A.16: Fjøra. Photo Normanns Kunstforlag A/S.

Figure A.17: Haugsbukt. Photo: NGI.

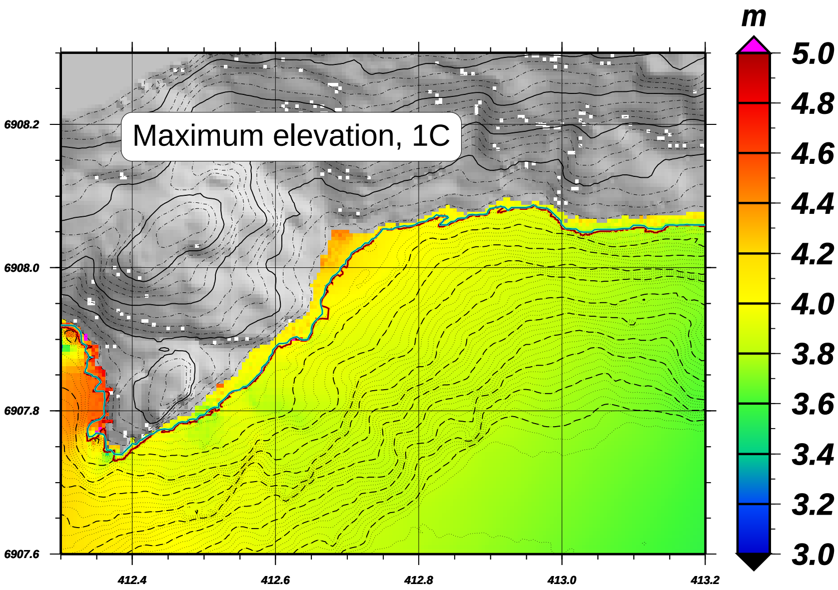

Figure A.18: Maximum water level measured from 0.7 m above today's mean sea level at Fjora, scenario 1C. The red line is the shoreline for today's mean sea level (MSL) while the cyan line is the shoreline including the estimated sea level rise of 0.7 m. Coordinates given in UTM32 (km) and gridlines printed every 200 m.

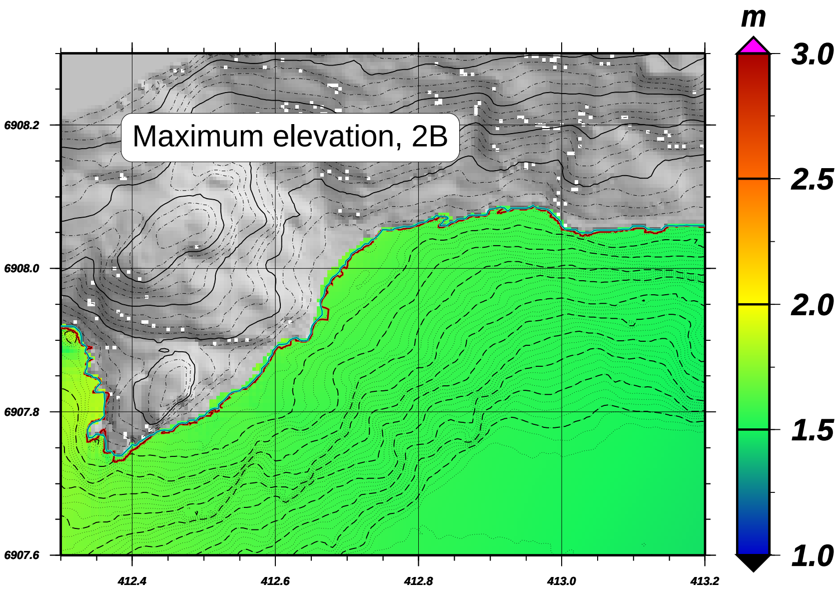

Figure A.19: Maximum water level measured from 0.7 m above today's mean sea level at Fjora, scenario 2B. The red line is the shoreline for today's mean sea level (MSL) while the cyan line is the shoreline including the estimated sea level rise of 0.7 m. Coordinates given in UTM32 (km) and gridlines printed every 200 m.

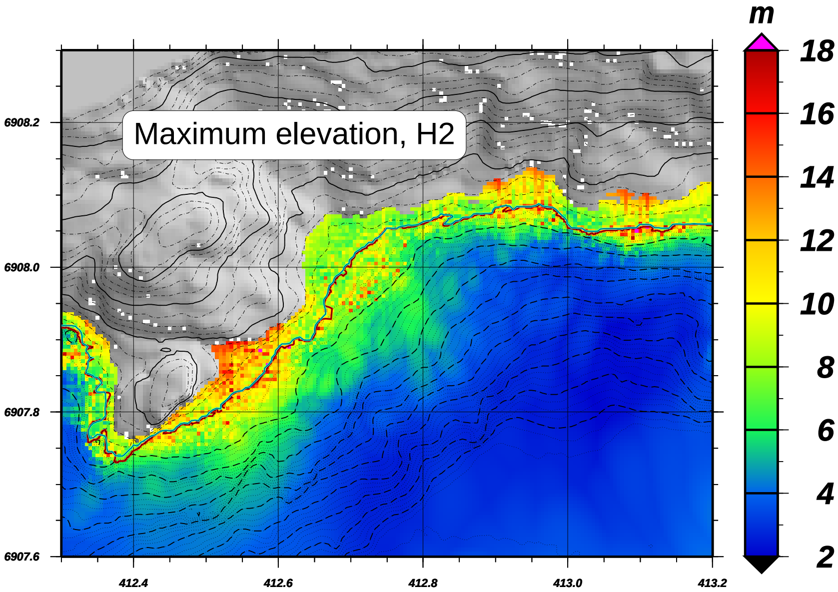

Figure A.20: Maximum water level measured from 0.7 m above today's mean sea level at Fjora, scenario H2. The red line is the shoreline for today's mean sea level (MSL) while the cyan line is the shoreline including the estimated sea level rise of 0.7 m. Coordinates given in UTM32 (km) and gridlines printed every 200 m.

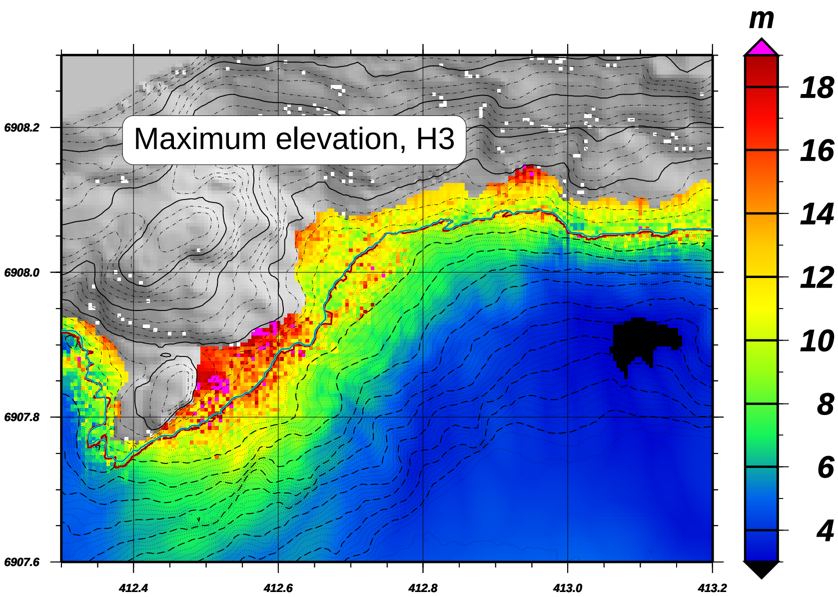

Figure A.21: Maximum water level measured from 0.7 m above today's mean sea level at Fjora, scenario H3. The red line is the shoreline for today's mean sea level (MSL) while the cyan line is the shoreline including the estimated sea level rise of 0.7 m. Coordinates given in UTM32 (km) and gridlines printed every 200 m.

A.3.5 Geiranger

Location number 12, see Figure A.1.

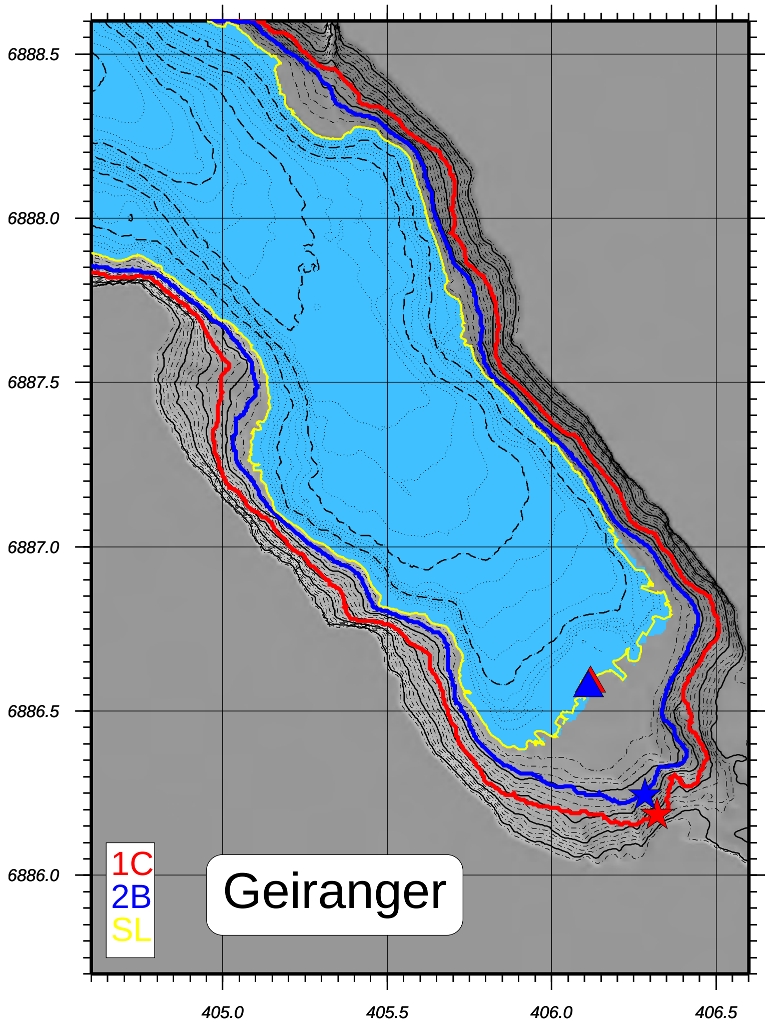

Figure A.22: Trimlines for each scenario at Geiranger. The highest water level along the shoreline and the maximum run-up is indicated with a triangle and a star, respectively. The yellow line is the shoreline for today's mean sea level. Coordinates given in UTM32 (km) and gridlines printed every 500 m.

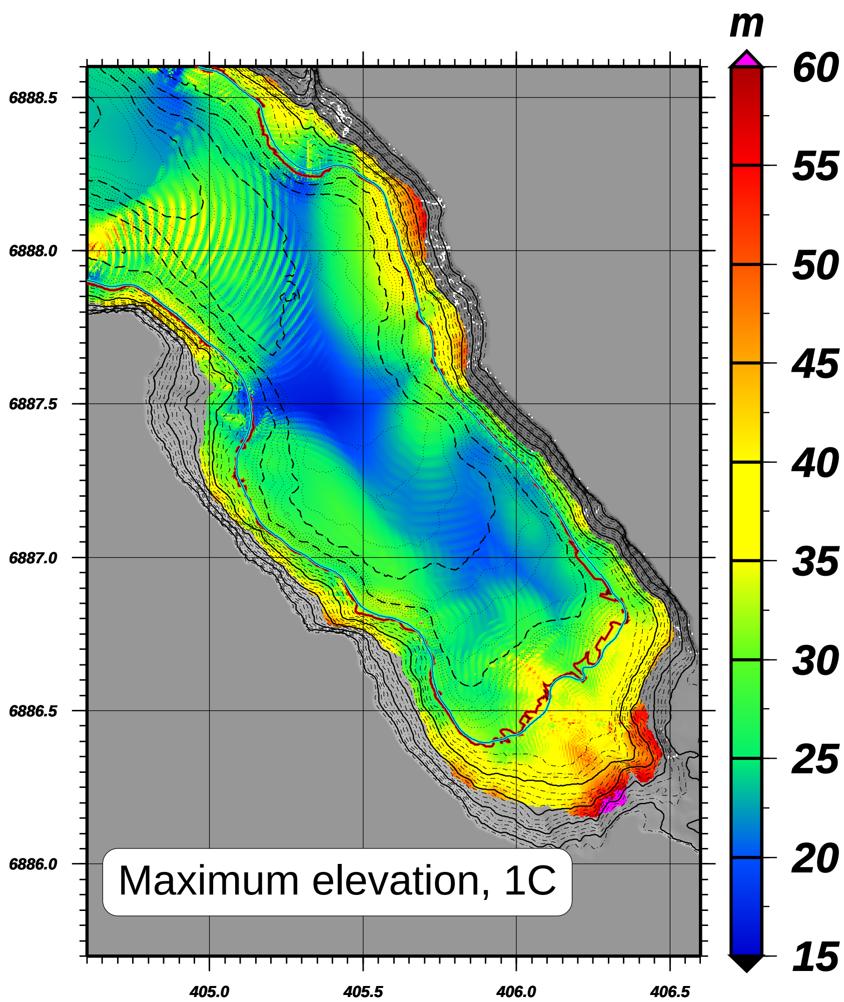

Figure A.23: Maximum water level measured from 0.7 m above today's mean sea level at Geiranger, scenario 1C. The red line is the shoreline for today's mean sea level (MSL) while the cyan line is the shoreline including the estimated sea level rise of 0.7 m. Coordinates given in UTM32 (km) and gridlines printed every 500 m.

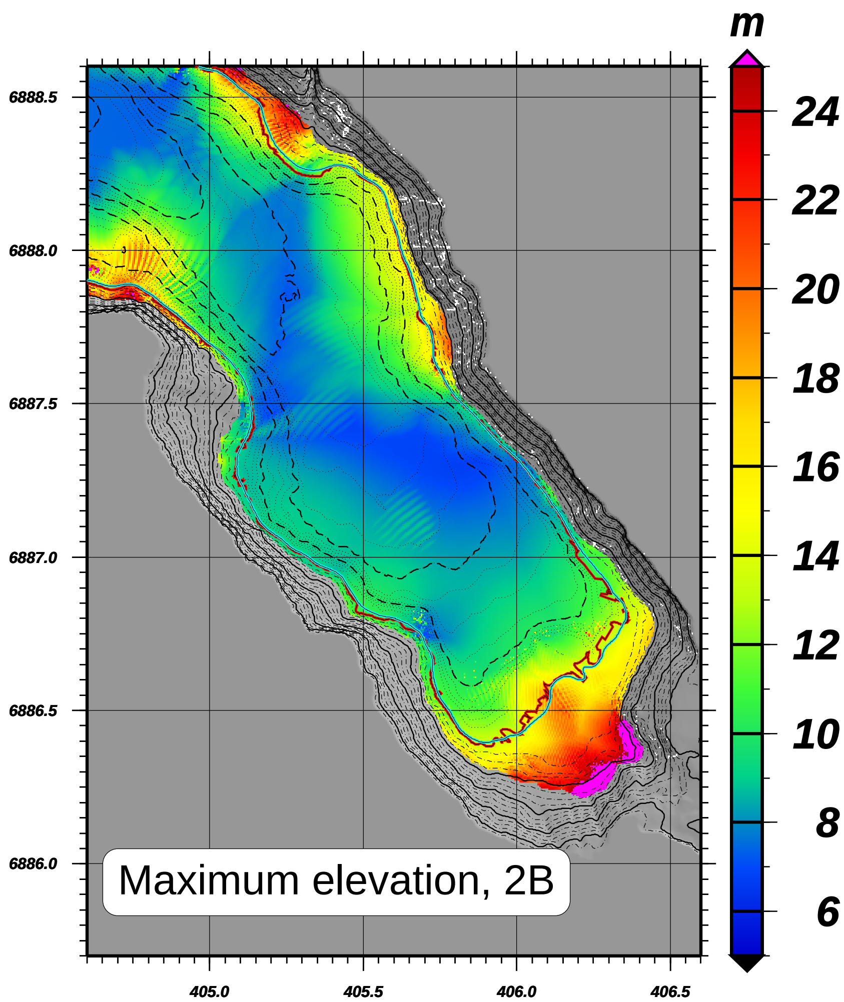

Figure A.24: Maximum water level measured from 0.7 m above today's mean sea level at Geiranger, scenario 2B. The red line is the shoreline for today's mean sea level (MSL) while the cyan line is the shoreline including the estimated sea level rise of 0.7 m. Coordinates given in UTM32 (km) and gridlines printed every 500 m.

A.3.6 Gravaneset

Location number 5, see Figure A.1.

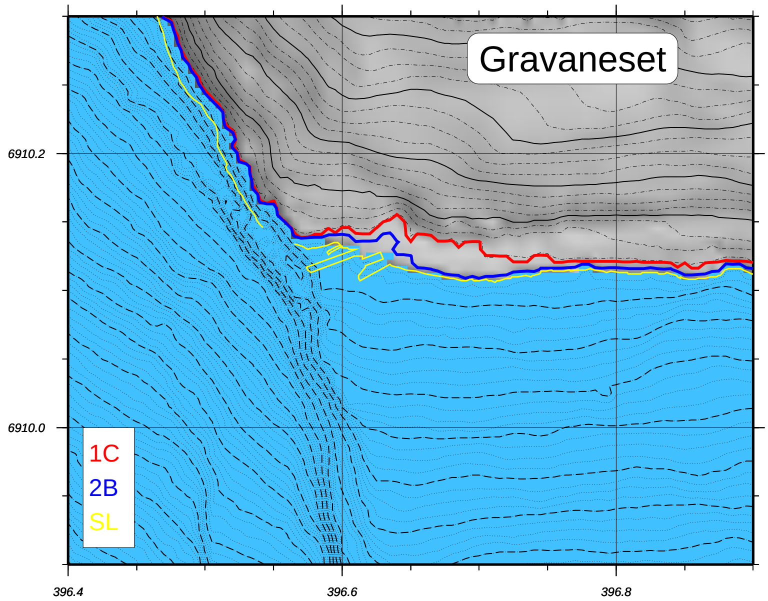

Figure A.25: Trimlines for each scenario at Gravaneset. The highest water level along the shoreline and the maximum run-up is indicated with a triangle and a star, respectively. The yellow line is the shoreline for today's mean sea level. Coordinates given in UTM32 (km) and gridlines printed every 200 m.

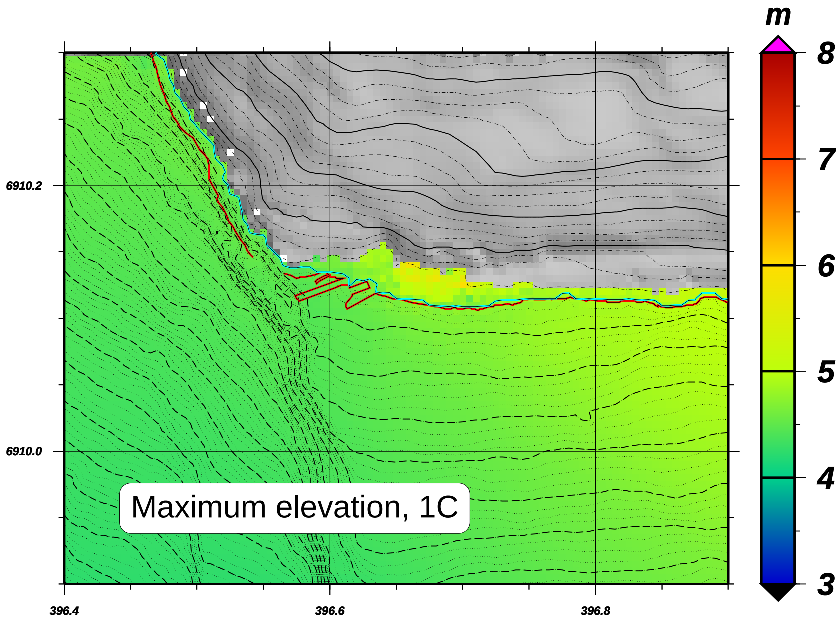

Figure A.26: Maximum water level measured from 0.7 m above today's mean sea level at Gravaneset, scenario 1C. The red line is the shoreline for today's mean sea level (MSL) while the cyan line is the shoreline including the estimated sea level rise of 0.7 m. Coordinates given in UTM32 (km) and gridlines printed every 200 m.

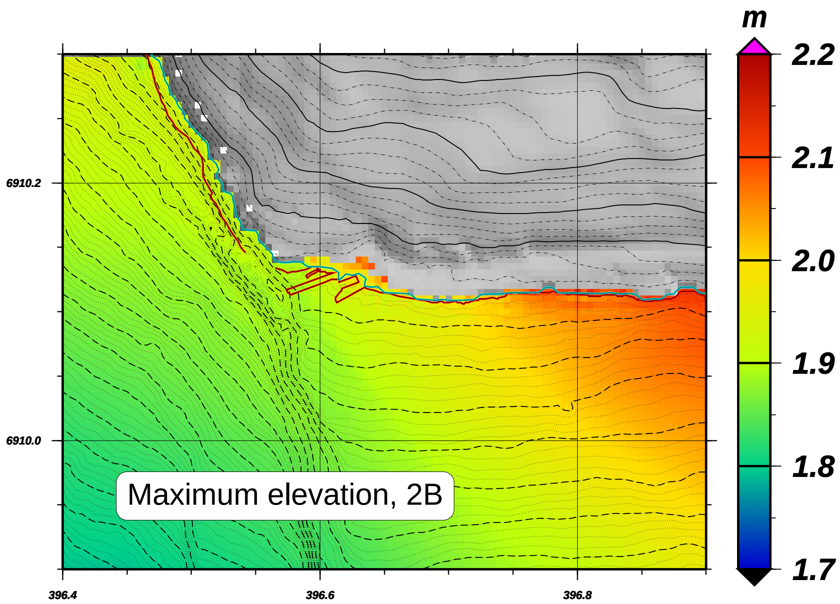

Figure A.27: Maximum water level measured from 0.7 m above today's mean sea level at Gravaneset, scenario 2B. The red line is the shoreline for today's mean sea level (MSL) while the cyan line is the shoreline including the estimated sea level rise of 0.7 m. Coordinates given in UTM32 (km) and gridlines printed every 200 m.

A.3.7 Hellesylt

Location number 13, see Figure A.1.

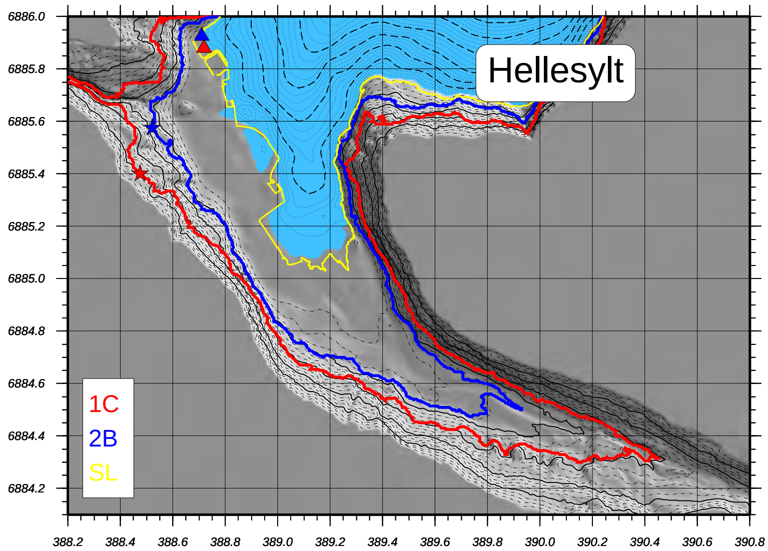

Figure A.28: Trimlines for each scenario at Hellesylt. The highest water level along the shoreline and the maximum run-up is indicated with a triangle and a star, respectively. The yellow line is the shoreline for today's mean sea level. Coordinates given in UTM32 (km) and gridlines printed every 200 m.

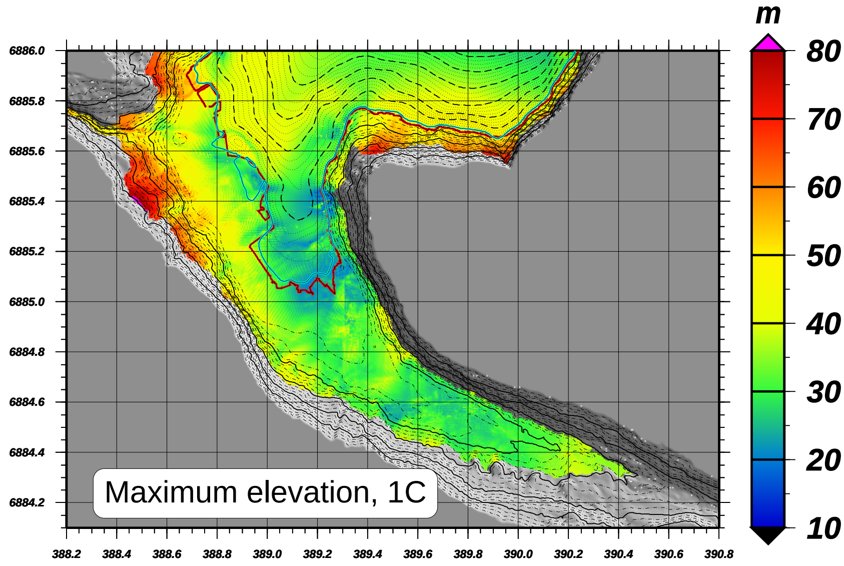

Figure A.29: Maximum water level measured from 0.7 m above today's mean sea level at Hellesylt, scenario 1C. The red line is the shoreline for today's mean sea level (MSL) while the cyan line is the shoreline including the estimated sea level rise of 0.7 m. Coordinates given in UTM32 (km) and gridlines printed every 200 m.

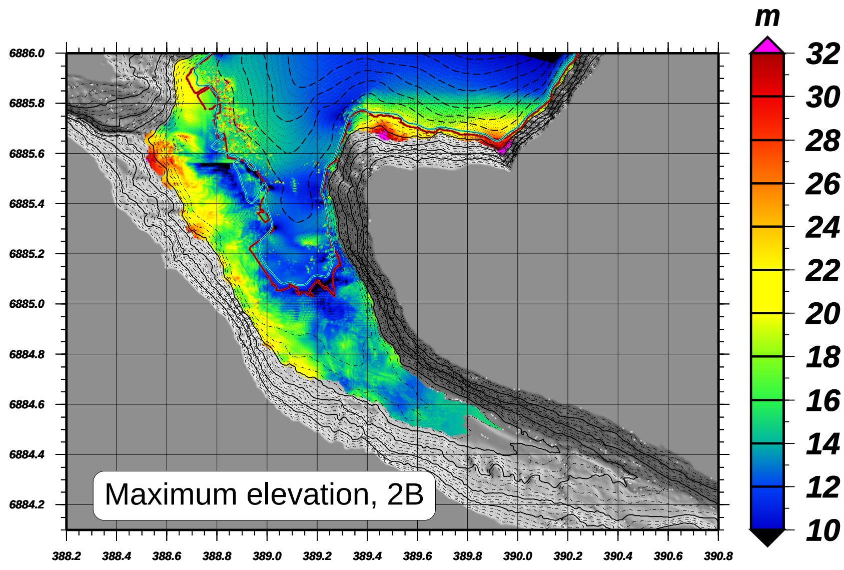

Figure A.30: Maximum water level measured from 0.7 m above today's mean sea level at Hellesylt, scenario 2B. The red line is the shoreline for today's mean sea level (MSL) while the cyan line is the shoreline including the estimated sea level rise of 0.7 m. Coordinates given in UTM32 (km) and gridlines printed every 200 m.

A.3.8 Hundeidvik

Location number 18, see Figure A.1.

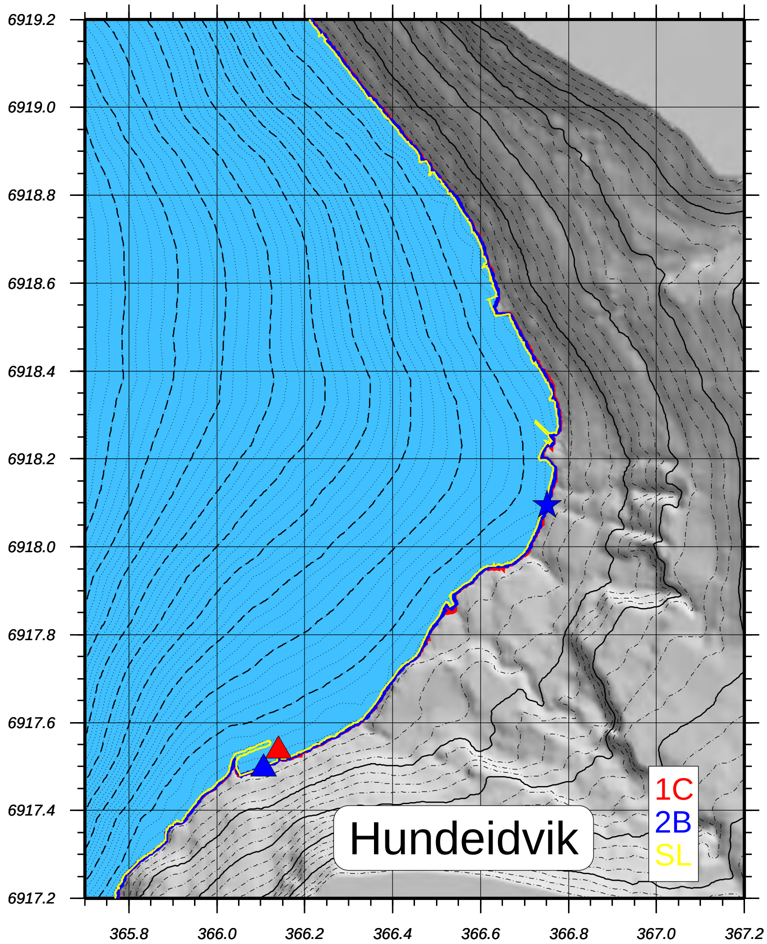

Figure A.31: Trimlines for each scenario at Hundeidvik. The highest water level along the shoreline and the maximum run-up is indicated with a triangle and a star, respectively. The yellow line is the shoreline for today's mean sea level. Coordinates given in UTM32 (km) and gridlines printed every 200 m.

Figure A.32: Hundeidvik. Photo: NGI.

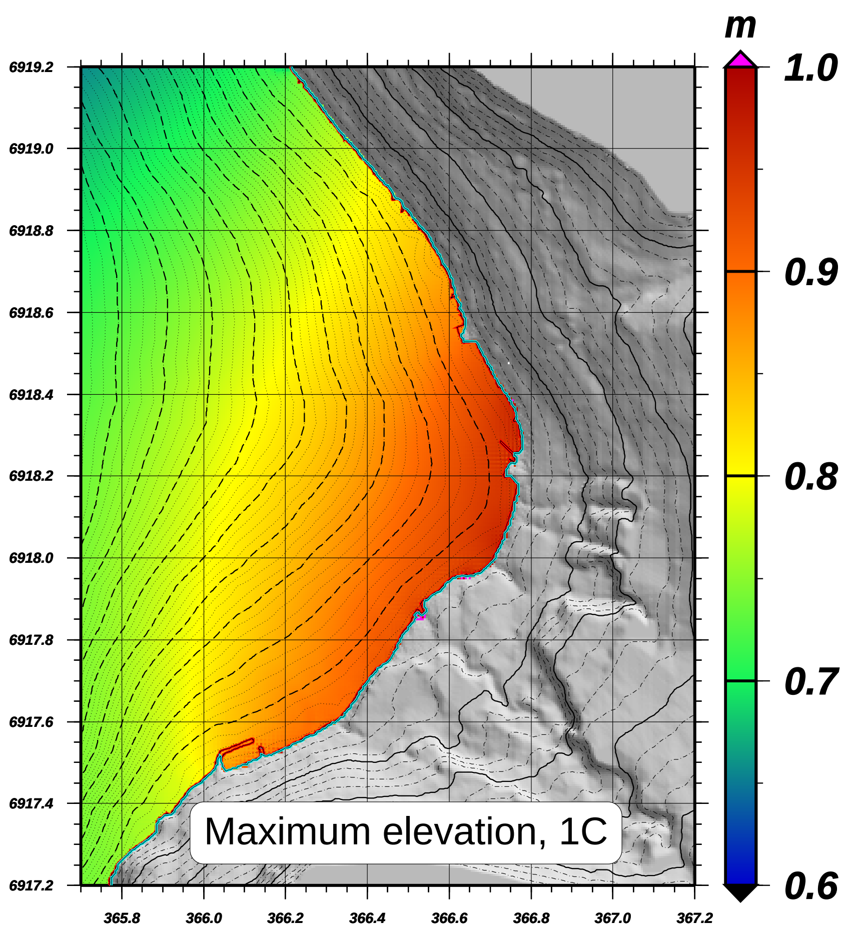

Figure A.33: Maximum water level measured from 0.7 m above today's mean sea level at Hundeidvik, scenario 1C. The red line is the shoreline for today's mean sea level (MSL) while the cyan line is the shoreline including the estimated sea level rise of 0.7 m. Coordinates given in UTM32 (km) and gridlines printed every 200 m.

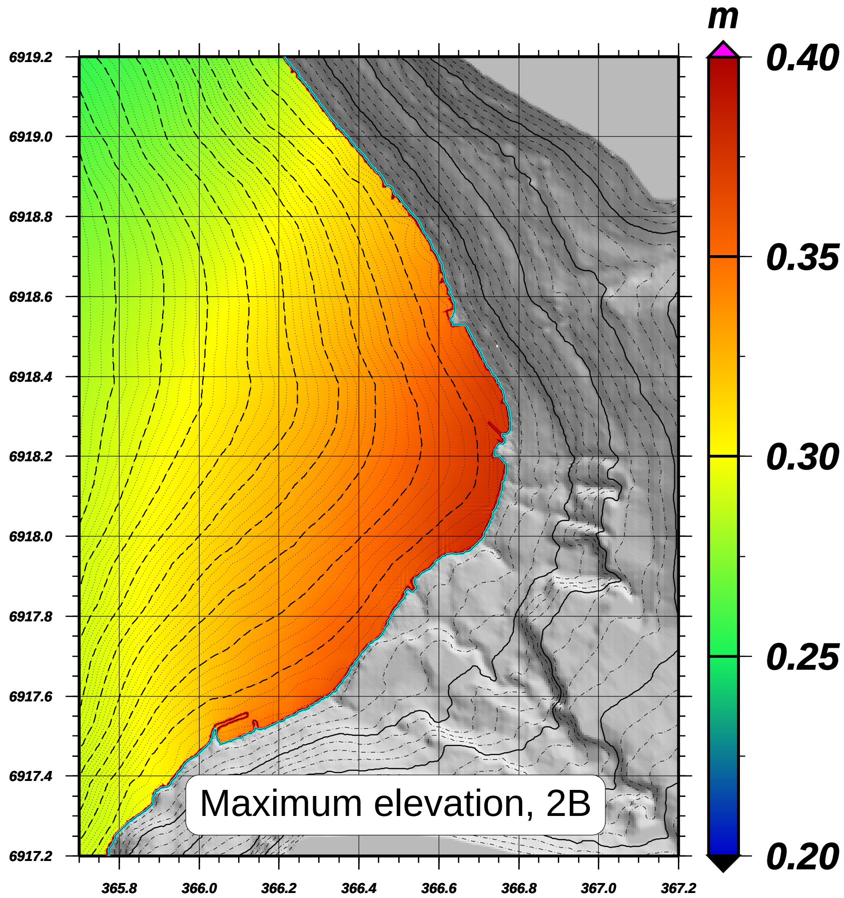

Figure A.34: Maximum water level measured from 0.7 m above today's mean sea level at Hundeidvik, scenario 2B. The red line is the shoreline for today's mean sea level (MSL) while the cyan line is the shoreline including the estimated sea level rise of 0.7 m. Coordinates given in UTM32 (km) and gridlines printed every 200 m.

A.3.9 Linge

Location number 6, see Figure A.1.

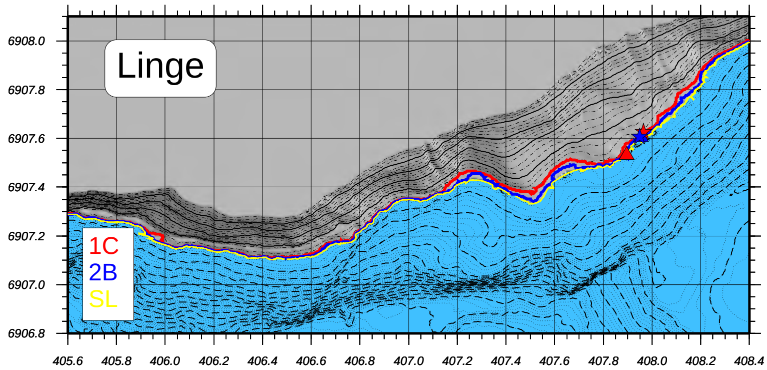

Figure A.35: Trimlines for each scenario at Linge. The highest water level along the shoreline and the maximum run-up is indicated with a triangle and a star, respectively. The yellow line is the shoreline for today's mean sea level. Coordinates given in UTM32 (km) and gridlines printed every 200 m.

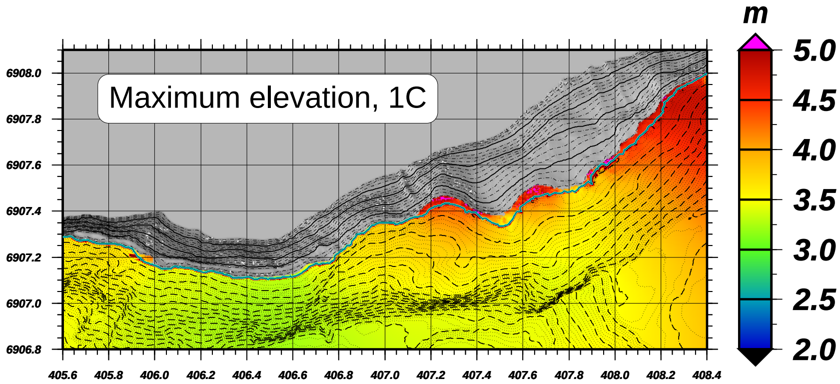

Figure A.36: Maximum water level measured from 0.7 m above today's mean sea level at Linge, scenario 1C. The red line is the shoreline for today's mean sea level (MSL) while the cyan line is the shoreline including the estimated sea level rise of 0.7 m. Coordinates given in UTM32 (km) and gridlines printed every 200 m.

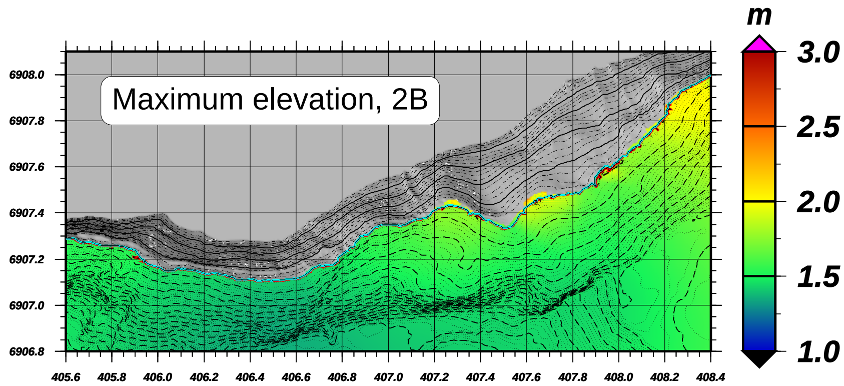

Figure A.37: Maximum water level measured from 0.7 m above today's mean sea level at Linge, scenario 2B. The red line is the shoreline for today's mean sea level (MSL) while the cyan line is the shoreline including the estimated sea level rise of 0.7 m. Coordinates given in UTM32 (km) and gridlines printed every 200 m.

A.3.10 Magerholm

Location number 1, see Figure A.1.

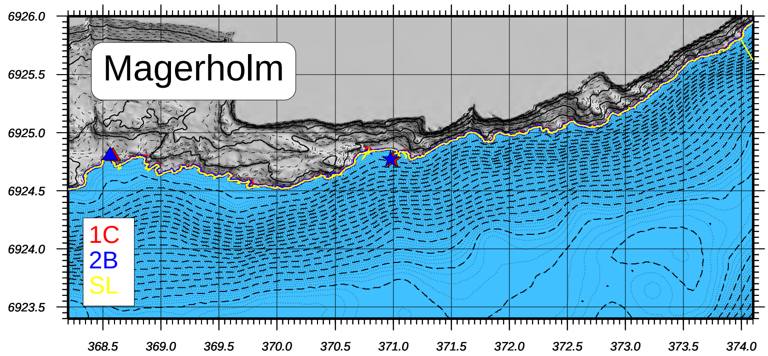

Figure A.38: Trimlines for each scenario at Magerholm. The highest water level along the shoreline and the maximum run-up is indicated with a triangle and a star, respectively. The yellow line is the shoreline for today's mean sea level. Coordinates given in UTM32 (km) and gridlines printed every 500 m.

Figure A.39: Magerholm. Photo: NGI.

Magerholm, scenario 1C.

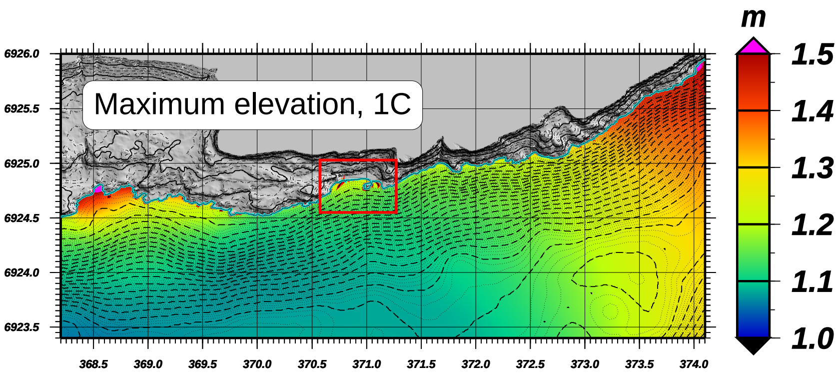

Figure A.40: Maximum water level at Magerholm, scenario 1C. The red line is the shoreline for today's mean sea level (MSL) while the cyan line is the shoreline including the estimated sea level rise of 0.7 m. Coordinates given in UTM32 (km) and gridlines printed every 500 m.

Details at Magerholm for scenario 1C.

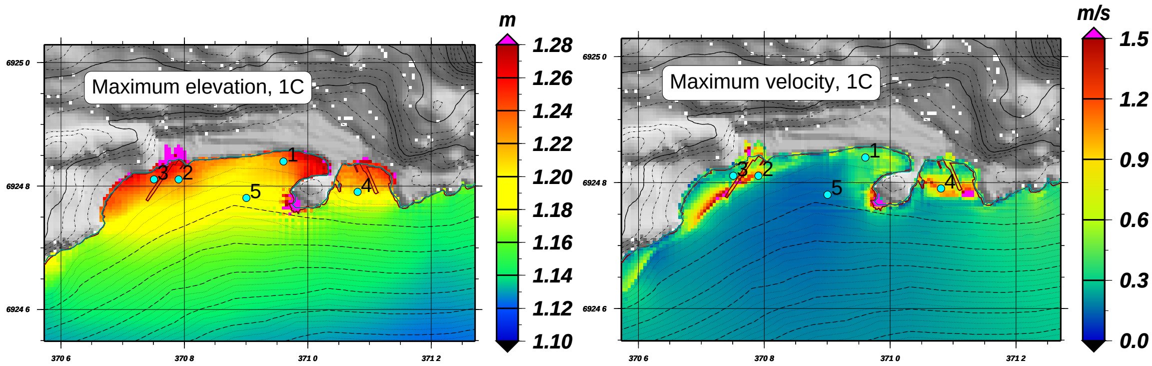

Figure A.41: Maximum water level measured from 0.7 m above today's mean sea level (left) and velocity (right) at Magerholm, scenario 1C. The red line is the shoreline for today's mean sea level (MSL) while the cyan line is the shoreline including the estimated sea level rise of 0.7 m. Coordinates given in UTM32 (km) and gridlines printed every 500 m.

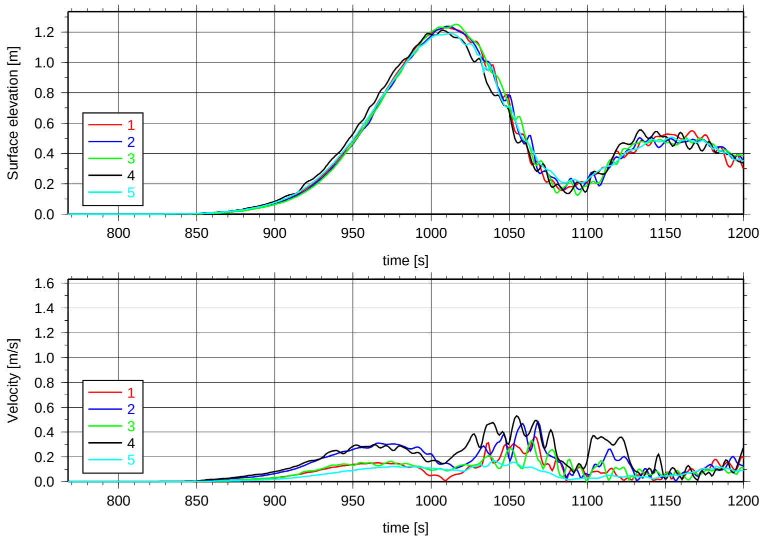

Figure A.42: Time history of the water level (upper panel) and velocity (lower panel - absolute values) measured at gauges 1-5 (see Figure A.41) at Magerholm for scenario 1C. The surface elevation is given in meters, while the velocity is given in meters per second.

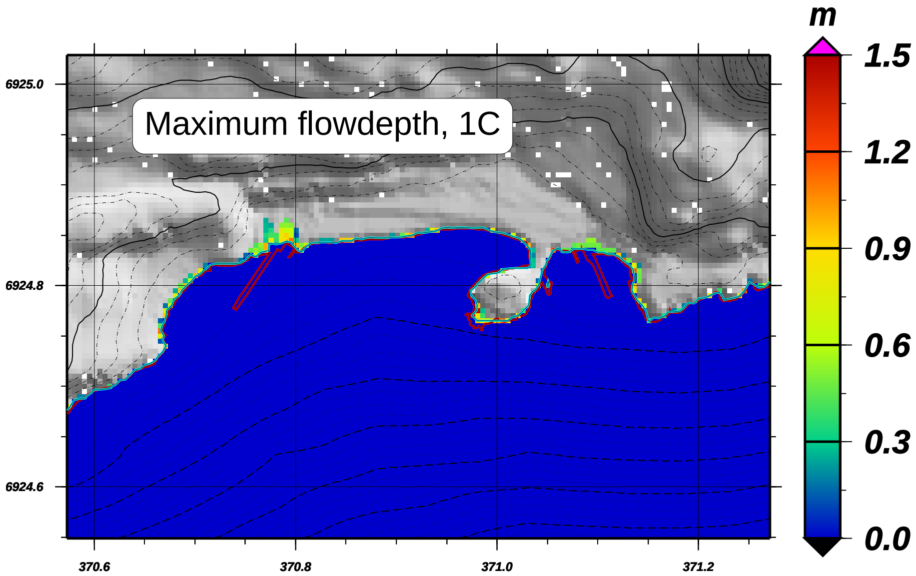

Figure A.43: Maximum flow depth at Magerholm for scenario 1C given in meters. The red line is the shoreline for today's mean sea level (MSL) while the cyan line is the shoreline including the estimated sea level rise of 0.7 m.

Magerholm, scenario 2B.

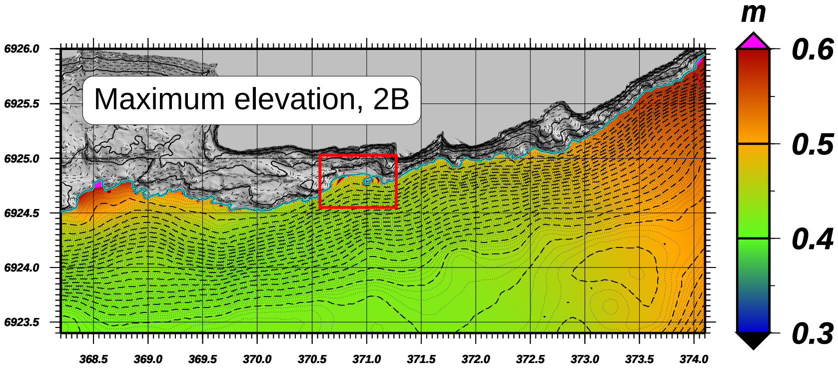

Figure A.44: Maximum water level at Magerholm, scenario 2B. The red line is the shoreline for today's mean sea level (MSL) while the cyan line is the shoreline including the estimated sea level rise of 0.7 m. Coordinates given in UTM32 (km) and gridlines printed every 500 m.

Details at Magerholm for scenario 2B.

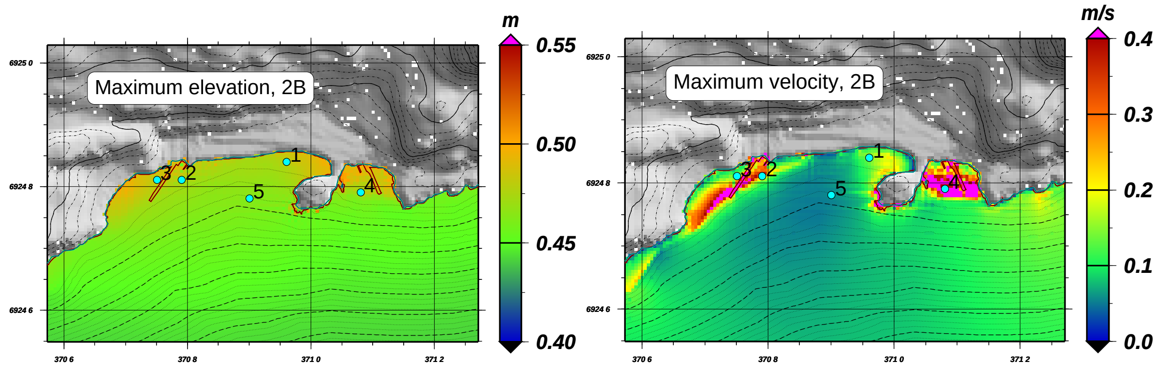

Figure A.45: Maximum water level measured from 0.7 m above today's mean sea level (left) and velocity (right) at Magerholm, scenario 2B. The red line is the shoreline for today's mean sea level (MSL) while the cyan line is the shoreline including the estimated sea level rise of 0.7 m. Coordinates given in UTM32 (km) and gridlines printed every 500 m.

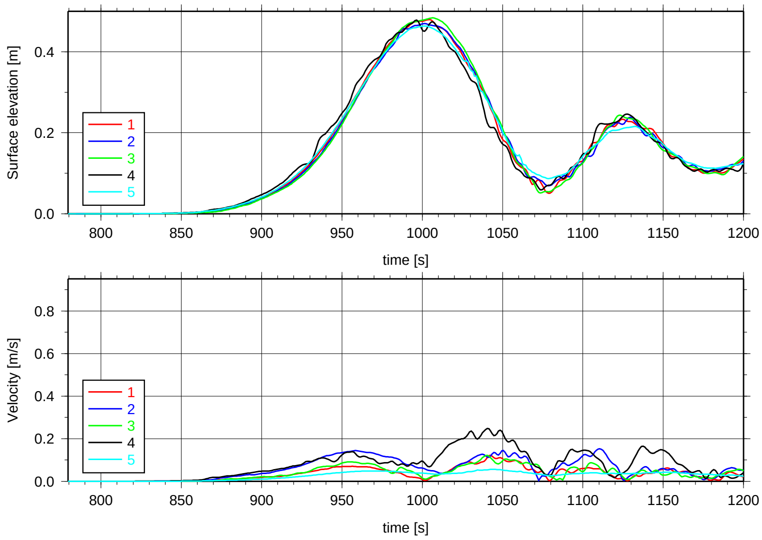

Figure A.46: Time history of the water level (upper panel) and velocity (lower panel - absolute values) measured at gauges 1-5 (see Figure A.45) at Magerholm for scenario 2B. The surface elevation is given in meters, while the velocity is given in meters per second.

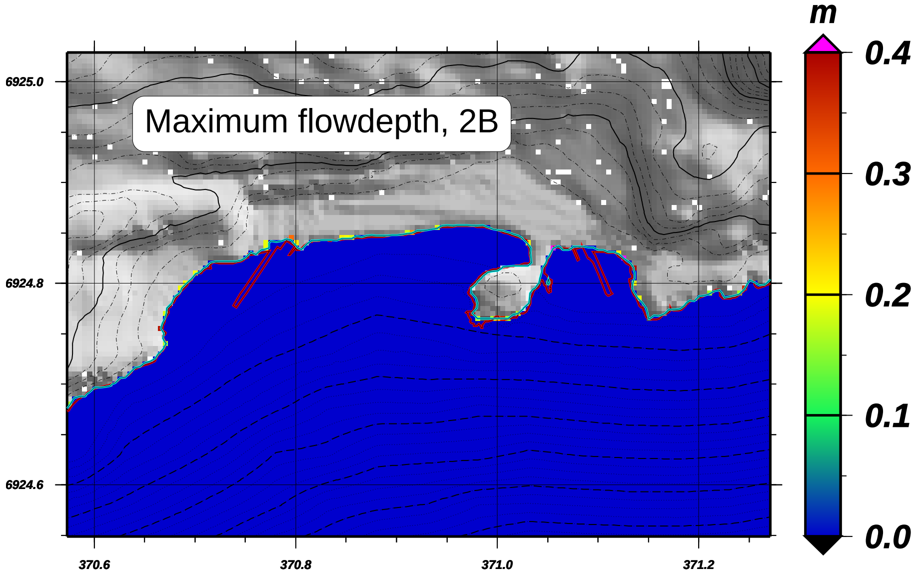

Figure A.47: Maximum flow depth at Magerholm for scenario 2B given in meters. The red line is the shoreline for today's mean sea level (MSL) while the cyan line is the shoreline including the estimated sea level rise of 0.7 m.

A.3.11 Norddal

Location number 10, see Figure A.1.

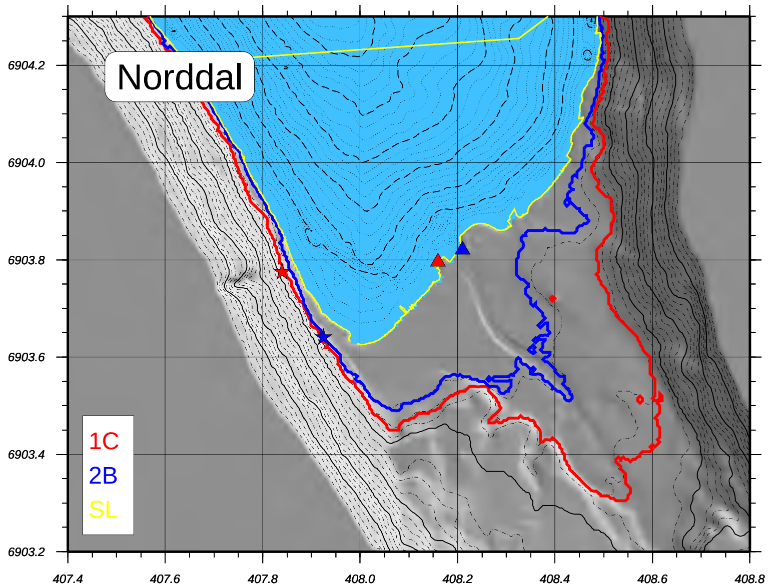

Figure A.48: Trimlines for each scenario at Norddal. The highest water level along the shoreline and the maximum run-up is indicated with a triangle and a star, respectively. The yellow line is the shoreline for today's mean sea level. Coordinates given in UTM32 (km) and gridlines printed every 200 m.

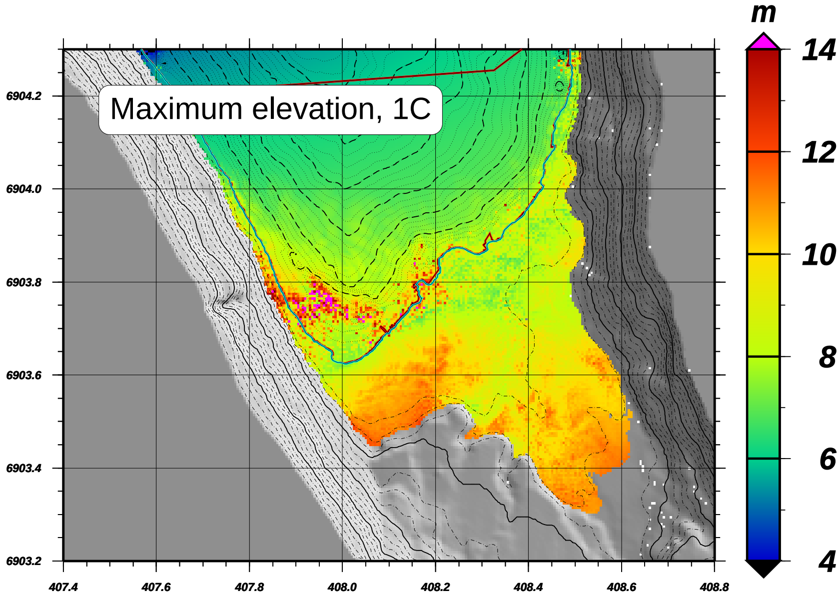

Figure A.49: Maximum water level measured from 0.7 m above today's mean sea level at Norddal, scenario 1C. The red line is the shoreline for today's mean sea level (MSL) while the cyan line is the shoreline including the estimated sea level rise of 0.7 m. Coordinates given in UTM32 (km) and gridlines printed every 200 m.

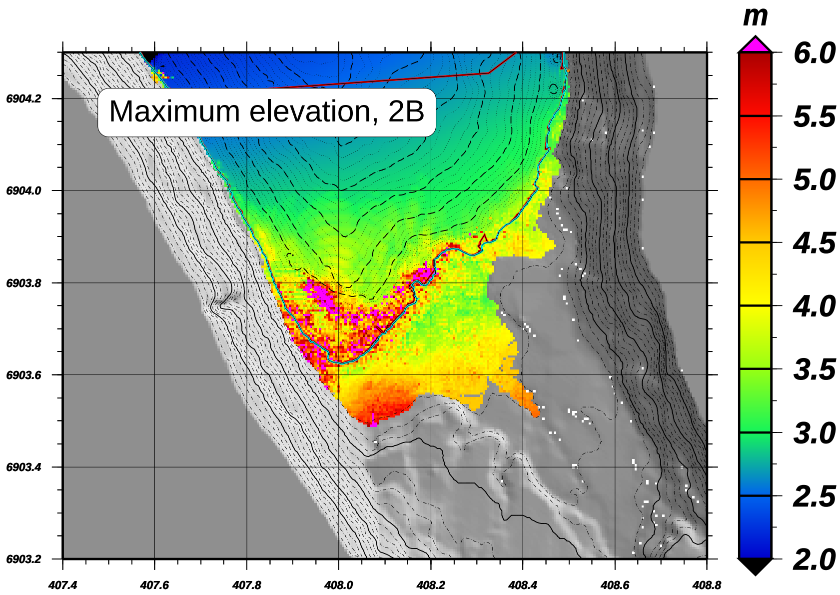

Figure A.50: Maximum water level measured from 0.7 m above today's mean sea level at Norddal, scenario 2B. The red line is the shoreline for today's mean sea level (MSL) while the cyan line is the shoreline including the estimated sea level rise of 0.7 m. Coordinates given in UTM32 (km) and gridlines printed every 200 m.

A.3.12 Oaldsbygda

Location number 14, see Figure A.1.

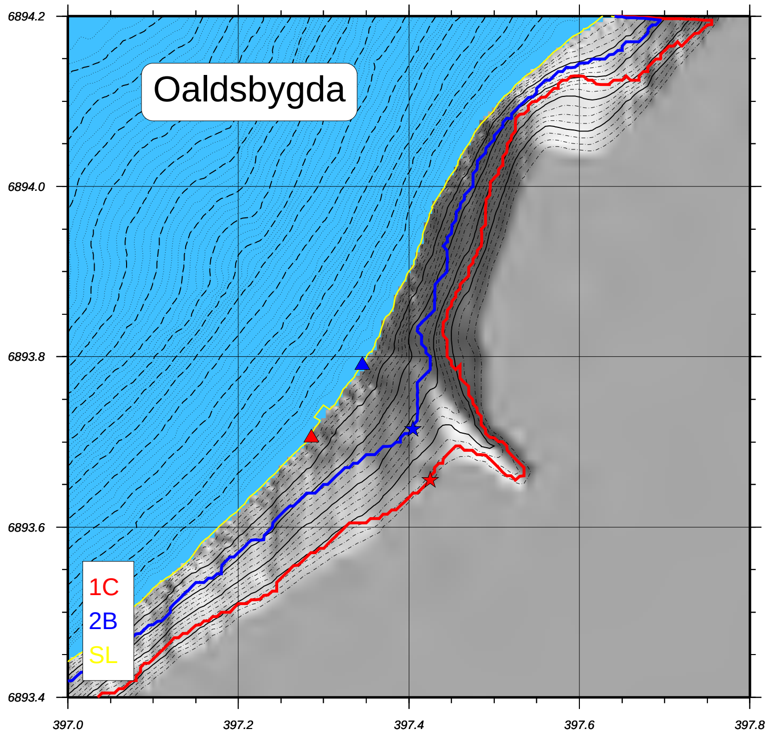

Figure A.51: Trimlines for each scenario at Oaldsbygda. The highest water level along the shoreline and the maximum run-up is indicated with a triangle and a star, respectively. The yellow line is the shoreline for today's mean sea level. Coordinates given in UTM32 (km) and gridlines printed every 200 m.

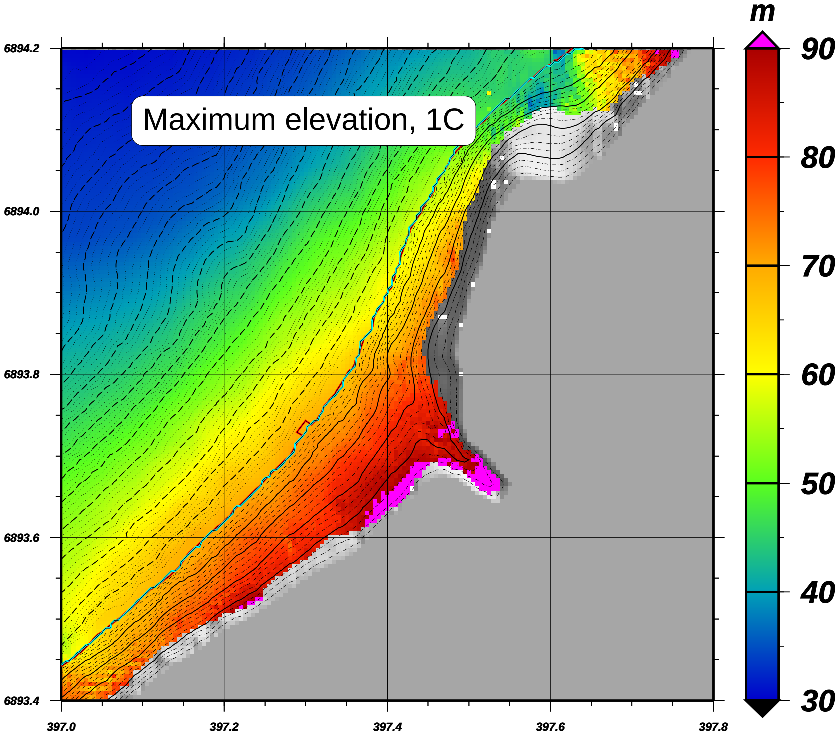

Figure A.52: Maximum water level measured from 0.7 m above today's mean sea level at Oaldsbygda, scenario 1C. The red line is the shoreline for today's mean sea level (MSL) while the cyan line is the shoreline including the estimated sea level rise of 0.7 m. Coordinates given in UTM32 (km) and gridlines printed every 200 m.

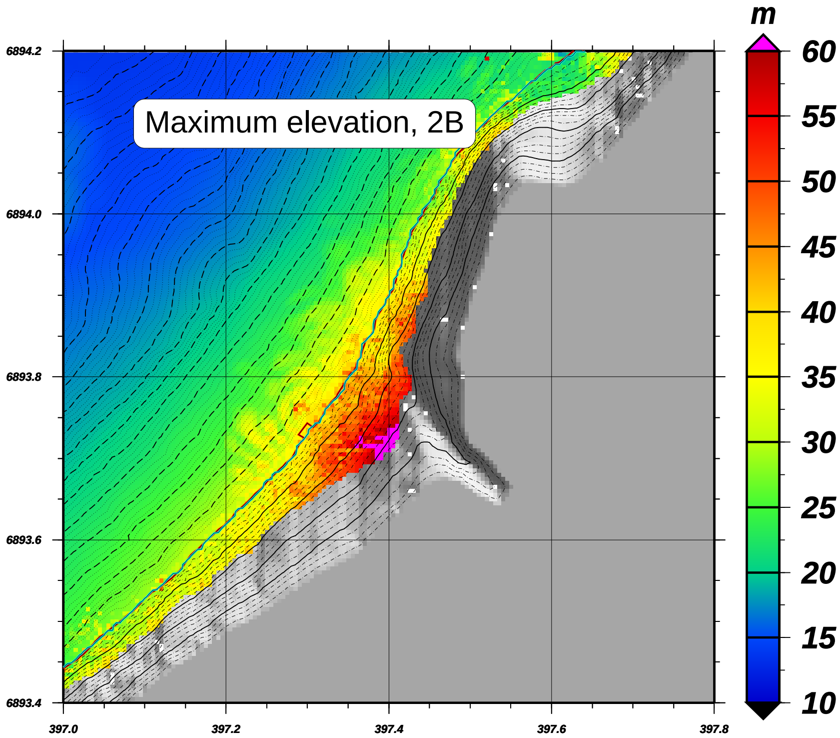

Figure A.53: Maximum water level measured from 0.7 m above today's mean sea level at Oaldsbygda, scenario 2B. The red line is the shoreline for today's mean sea level (MSL) while the cyan line is the shoreline including the estimated sea level rise of 0.7 m. Coordinates given in UTM32 (km) and gridlines printed every 200 m.

A.3.13 Ramstadvika

Location number 17, see Figure A.1.

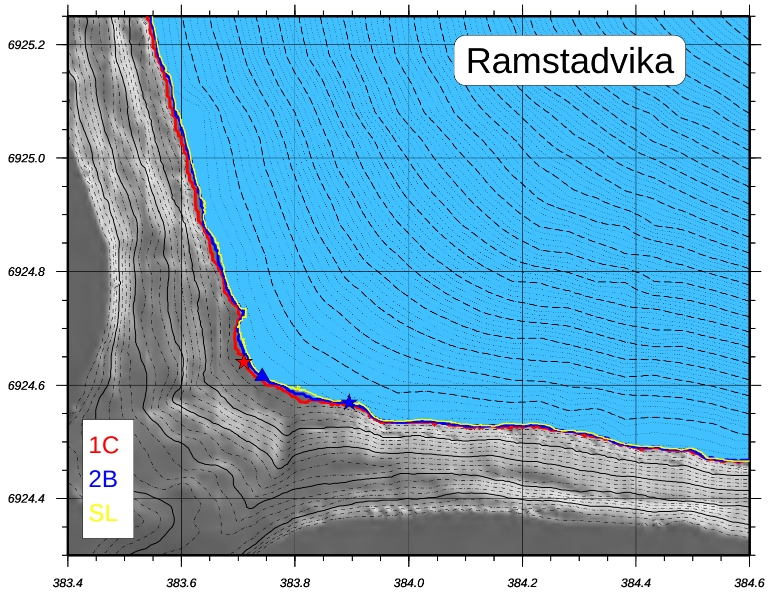

Figure A.54: Trimlines for each scenario at Ramstadvika. The highest water level along the shoreline and the maximum run-up is indicated with a triangle and a star, respectively. The yellow line is the shoreline for today's mean sea level. Coordinates given in UTM32 (km) and gridlines printed every 200 m.

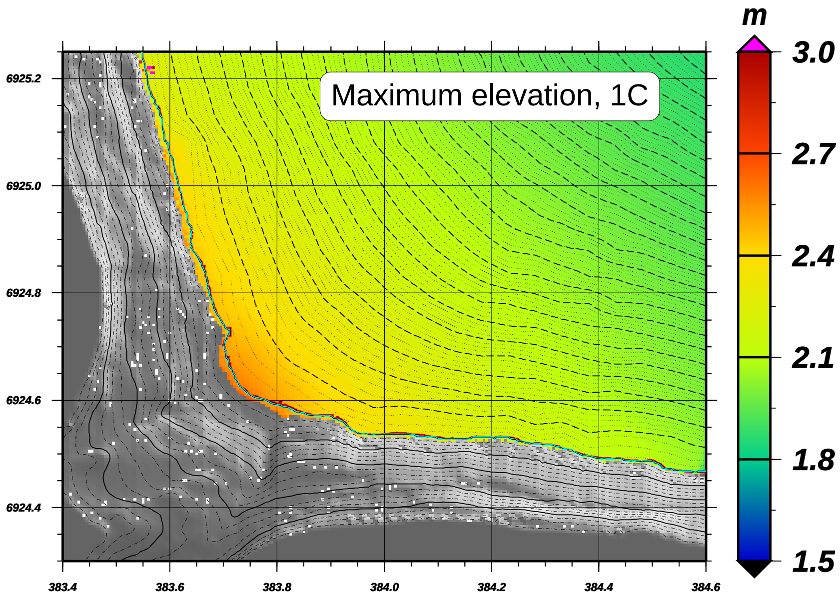

Figure A.55: Maximum water level measured from 0.7 m above today's mean sea level at Ramstadvika, scenario 1C. The red line is the shoreline for today's mean sea level (MSL) while the cyan line is the shoreline including the estimated sea level rise of 0.7 m. Coordinates given in UTM32 (km) and gridlines printed every 200 m.

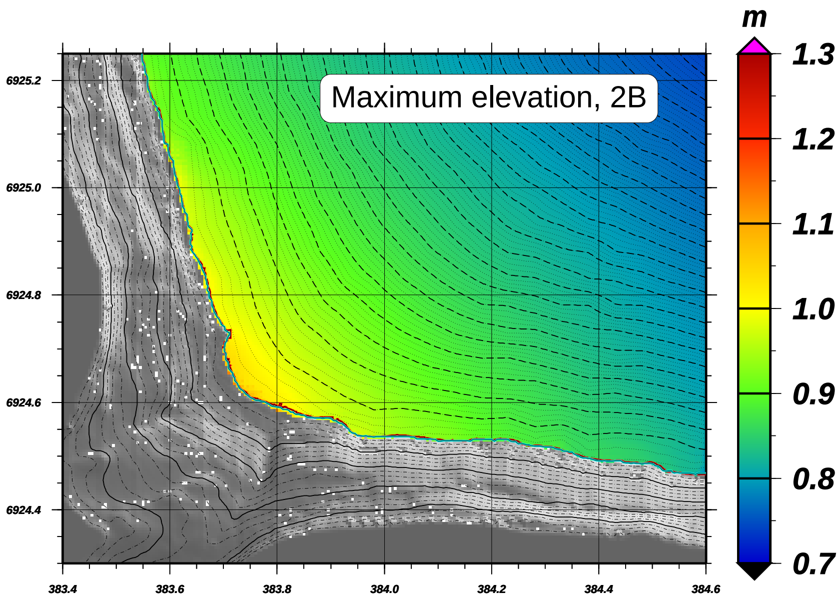

Figure A.56: Maximum water level measured from 0.7 m above today's mean sea level at Ramstadvika, scenario 2B. The red line is the shoreline for today's mean sea level (MSL) while the cyan line is the shoreline including the estimated sea level rise of 0.7 m. Coordinates given in UTM32 (km) and gridlines printed every 200 m.

A.3.14 Raudbergvika

Location number 19, see Figure A.1.

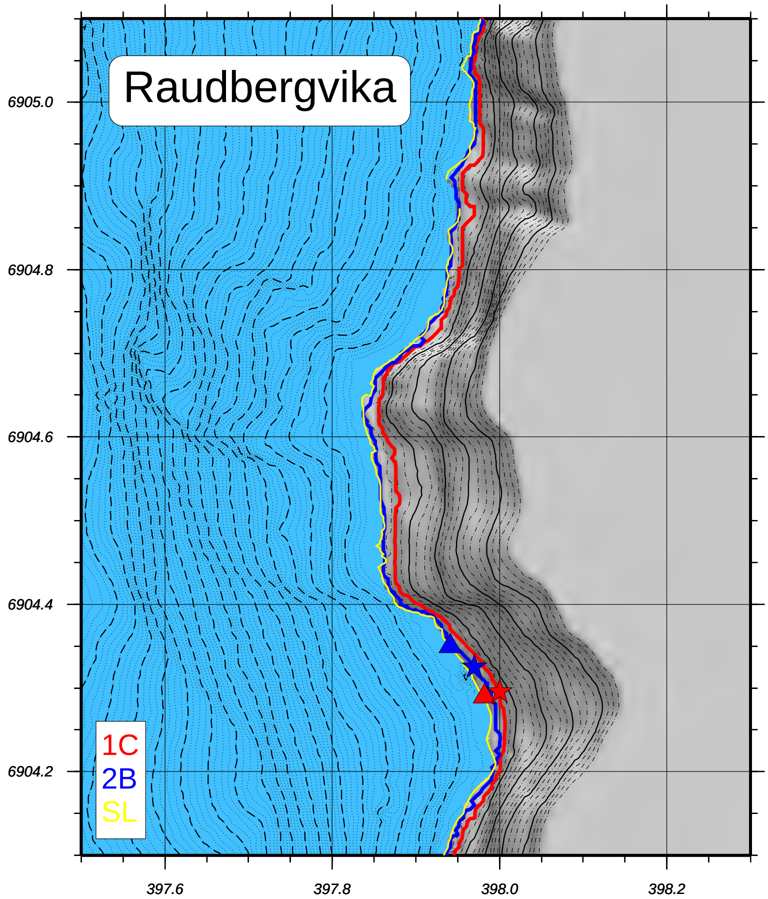

Figure A.57: Trimlines for each scenario at Raudbergvika. The highest water level along the shoreline and the maximum run-up is indicated with a triangle and a star, respectively. The yellow line is the shoreline for today's mean sea level. Coordinates given in UTM32 (km) and gridlines printed every 200 m.

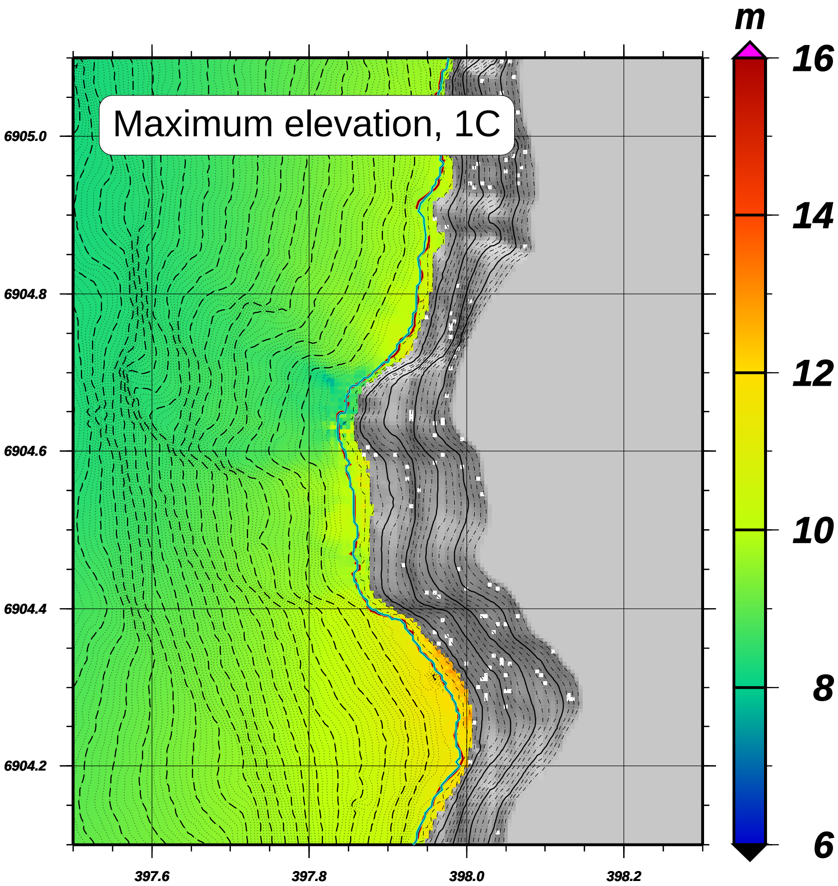

Figure A.58: Maximum water level measured from 0.7 m above today's mean sea level at Raudbergvika, scenario 1C. The red line is the shoreline for today's mean sea level (MSL) while the cyan line is the shoreline including the estimated sea level rise of 0.7 m. Coordinates given in UTM32 (km) and gridlines printed every 200 m.

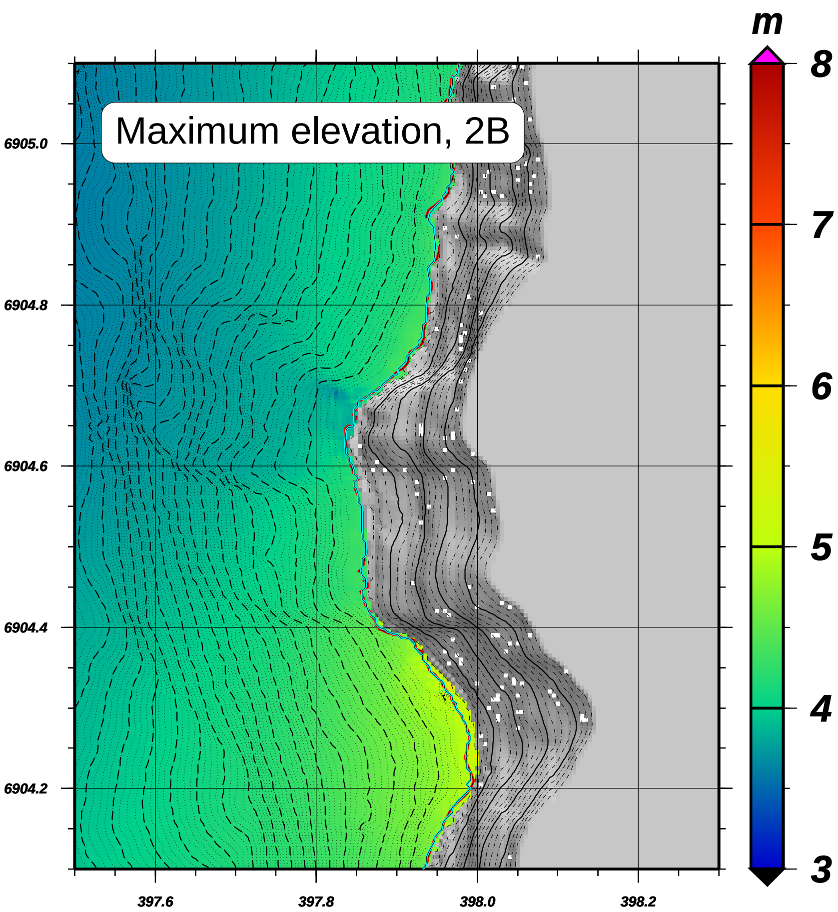

Figure A.59: Maximum water level measured from 0.7 m above today's mean sea level at Raudbergvika, scenario 2B. The red line is the shoreline for today's mean sea level (MSL) while the cyan line is the shoreline including the estimated sea level rise of 0.7 m. Coordinates given in UTM32 (km) and gridlines printed every 200 m.

A.3.15 Skardbøen

Location number 21, see Figure A.1.

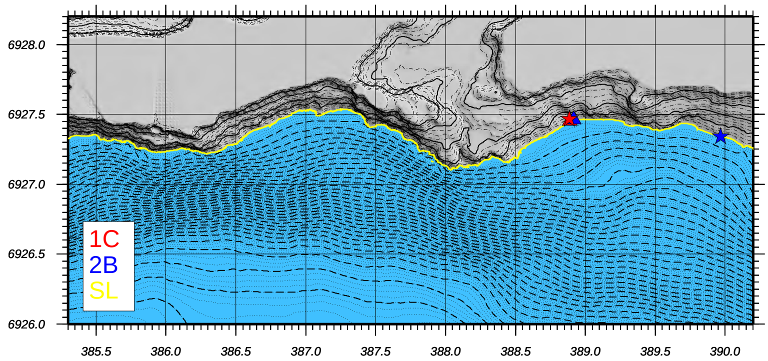

Figure A.60: Trimlines for each scenario at Skardbøen. The highest water level along the shoreline and the maximum run-up is indicated with a triangle and a star, respectively. The yellow line is the shoreline for today's mean sea level. Coordinates given in UTM32 (km) and gridlines printed every 200 m.

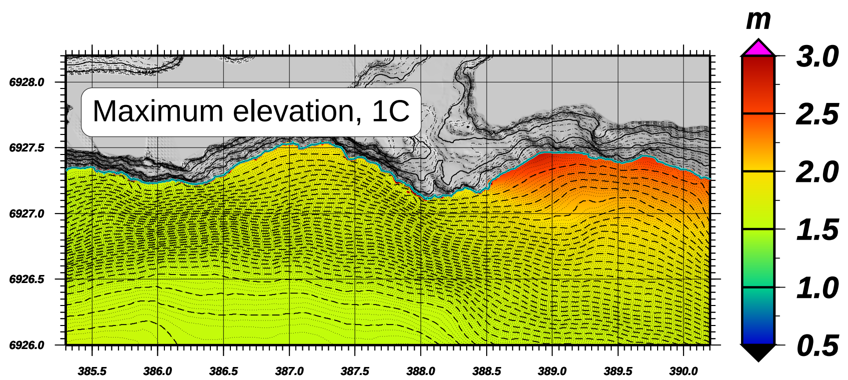

Figure A.61: Maximum water level measured from 0.7 m above today's mean sea level at Skardbøen, scenario 1C. The red line is the shoreline for today's mean sea level (MSL) while the cyan line is the shoreline including the estimated sea level rise of 0.7 m. Coordinates given in UTM32 (km) and gridlines printed every 200 m.

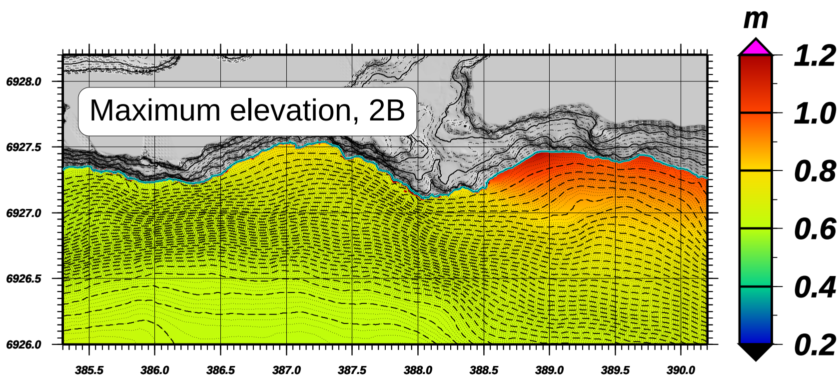

Figure A.62: Maximum water level measured from 0.7 m above today's mean sea level at Skardbøen, scenario 2B. The red line is the shoreline for today's mean sea level (MSL) while the cyan line is the shoreline including the estimated sea level rise of 0.7 m. Coordinates given in UTM32 (km) and gridlines printed every 200 m.

A.3.16 Stordal

Location number 4, see Figure A.1.

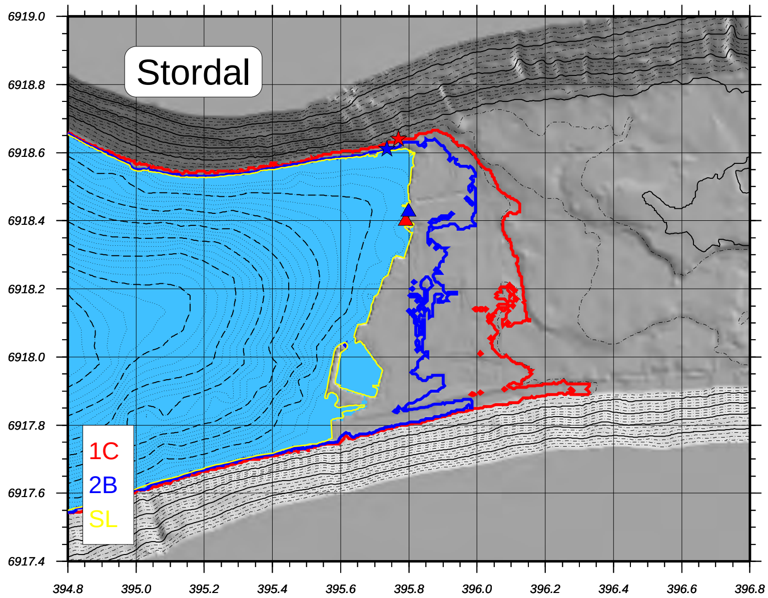

Figure A.63: Trimlines for each scenario at Stordal. The highest water level along the shoreline and the maximum run-up is indicated with a triangle and a star, respectively. The yellow line is the shoreline for today's mean sea level. Coordinates given in UTM32 (km) and gridlines printed every 200 m.

Details at Stordal for scenario 1C.

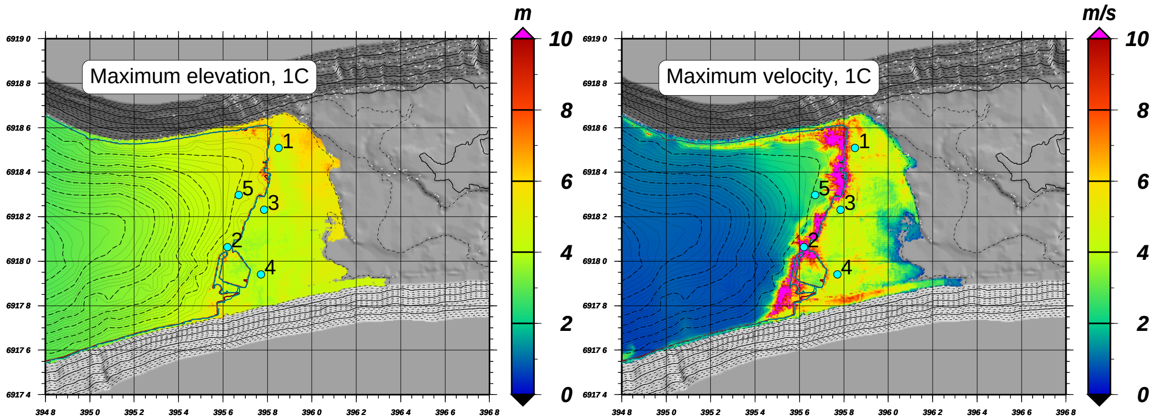

Figure A.64: Maximum water level measured from 0.7 m above today's mean sea level (left) and velocity (right) at Stordal, scenario 1C. The red line is the shoreline for today's mean sea level (MSL) while the cyan line is the shoreline including the estimated sea level rise of 0.7 m. Coordinates given in UTM32 (km) and gridlines printed every 200 m.

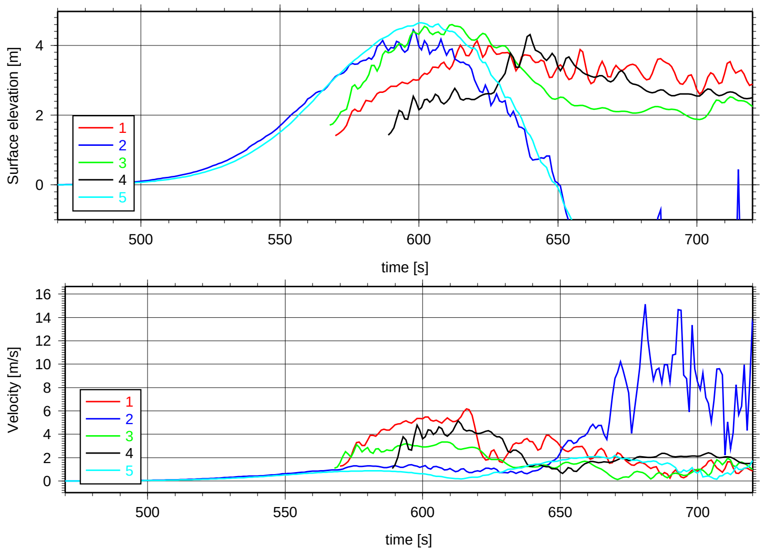

Figure A.65: Time history of the water level (upper panel) and velocity (lower panel - absolute values) measured at gauges 1-5 (see Figure A.64) at Stordal for scenario 1C. The surface elevation is given in meters, while the velocity is given in meters per second.

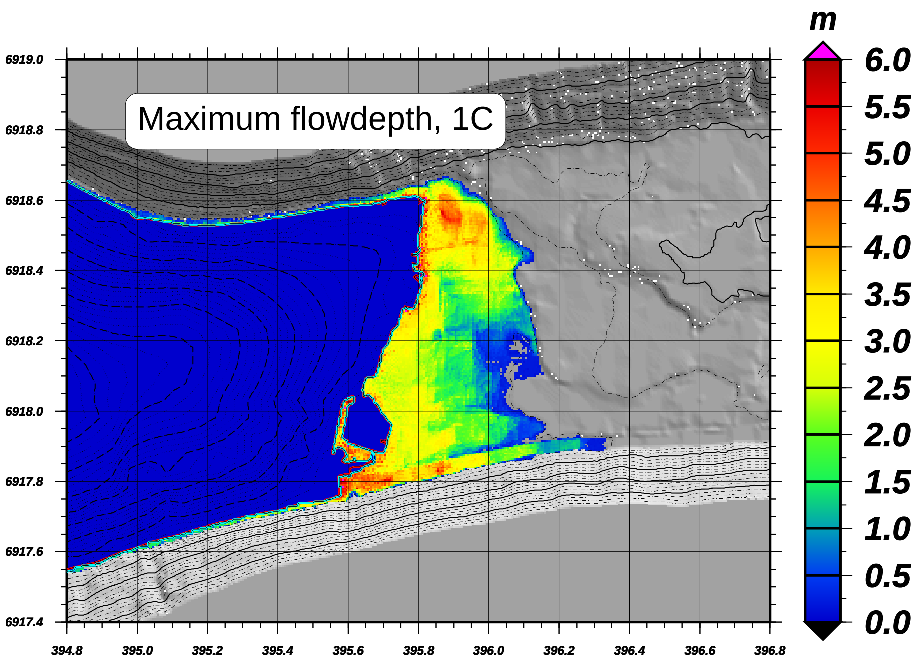

Figure A.66: Maximum flow depth at Stordal for scenario 1C given in meters. The red line is the shoreline for today's mean sea level (MSL) while the cyan line is the shoreline including the estimated sea level rise of 0.7 m.

Details at Stordal for scenario 2B.

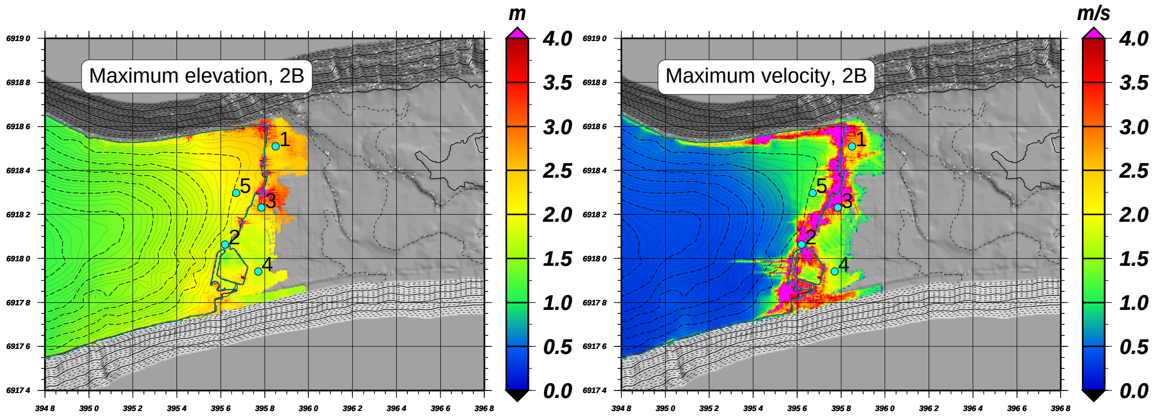

Figure A.67: Maximum water level measured from 0.7 m above today's mean sea level (left) and velocity (right) at Stordal, scenario 2B. The red line is the shoreline for today's mean sea level (MSL) while the cyan line is the shoreline including the estimated sea level rise of 0.7 m. Coordinates given in UTM32 (km) and gridlines printed every 200 m.

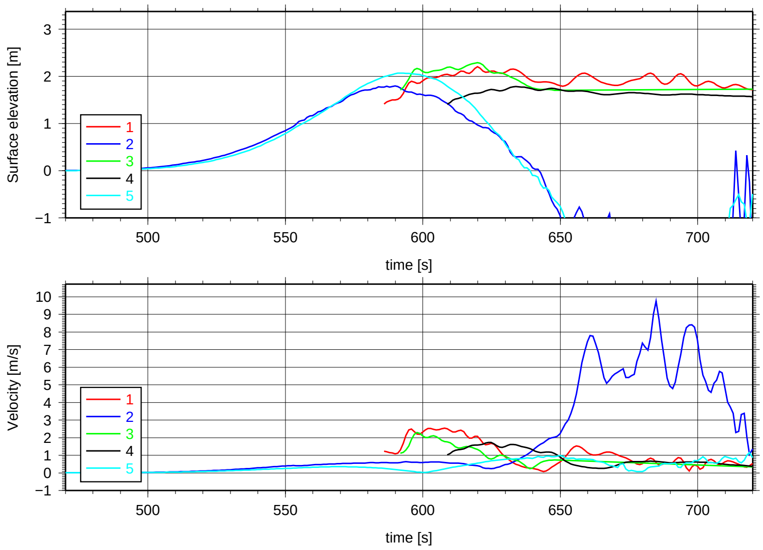

Figure A.68: Time history of the water level (upper panel) and velocity (lower panel - absolute values) measured at gauges 1-5 (see Figure A.67) at Stordal for scenario 2B. The surface elevation is given in meters, while the velocity is given in meters per second.

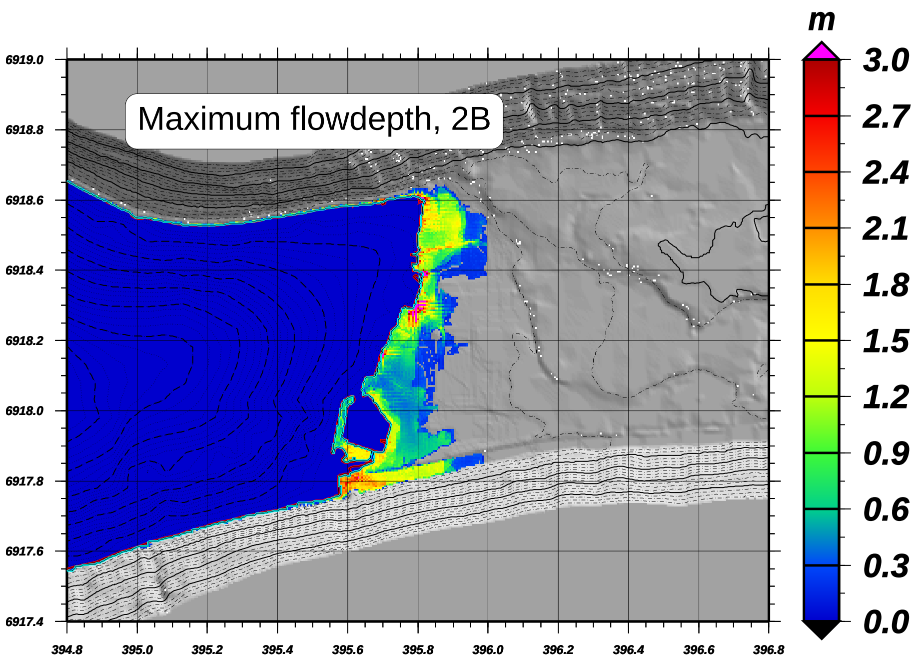

Figure A.69: Maximum flow depth at Stordal for scenario 2B given in meters. The red line is the shoreline for today's mean sea level (MSL) while the cyan line is the shoreline including the estimated sea level rise of 0.7 m.

A.3.17 Stranda

Location number 15, see Figure A.1.

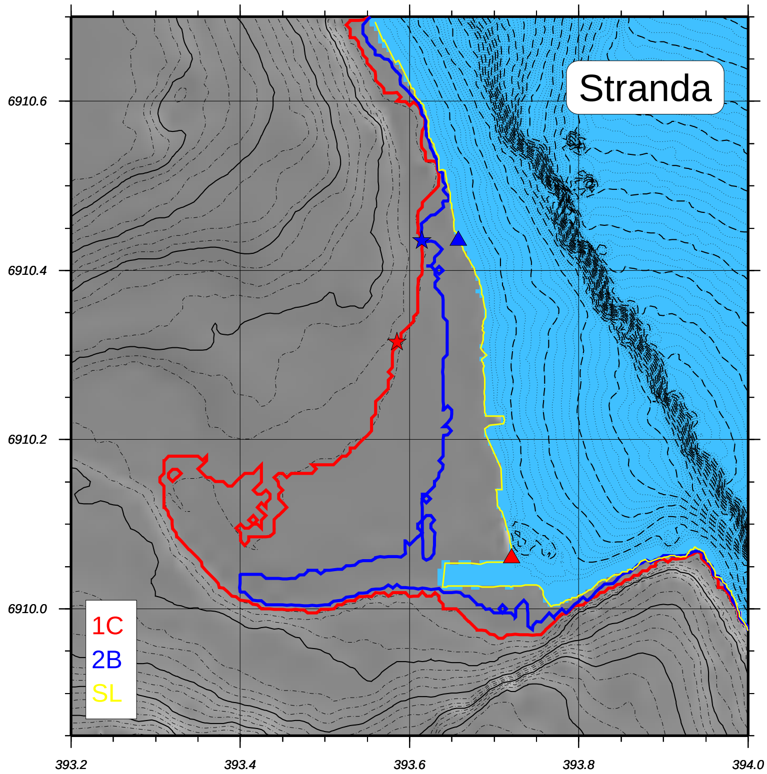

Figure A.70: Trimlines for each scenario at Stranda. The highest water level along the shoreline and the maximum run-up is indicated with a triangle and a star, respectively. The yellow line is the shoreline for today's mean sea level. Coordinates given in UTM32 (km) and gridlines printed every 200 m.

Details at Stranda for scenario 1C.

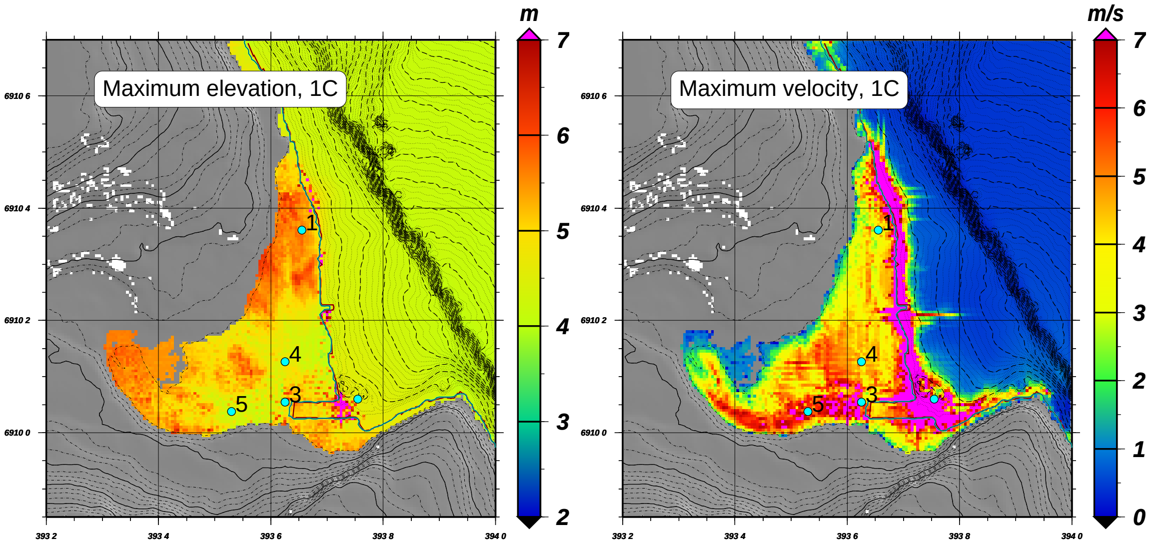

Figure A.71: Maximum water level measured from 0.7 m above today's mean sea level (left) and velocity (right) at Stranda, scenario 1C. The red line is the shoreline for today's mean sea level (MSL) while the cyan line is the shoreline including the estimated sea level rise of 0.7 m. Coordinates given in UTM32 (km) and gridlines printed every 200 m.

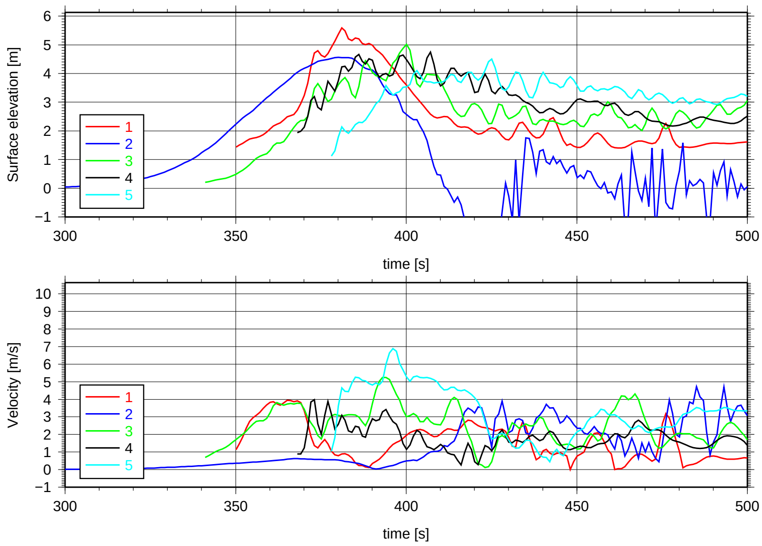

Figure A.72: Time history of the water level (upper panel) and velocity (lower panel - absolute values) measured at gauges 1-5 (see Figure A.71) at Stranda for scenario 1C. The surface elevation is given in meters, while the velocity is given in meters per second.

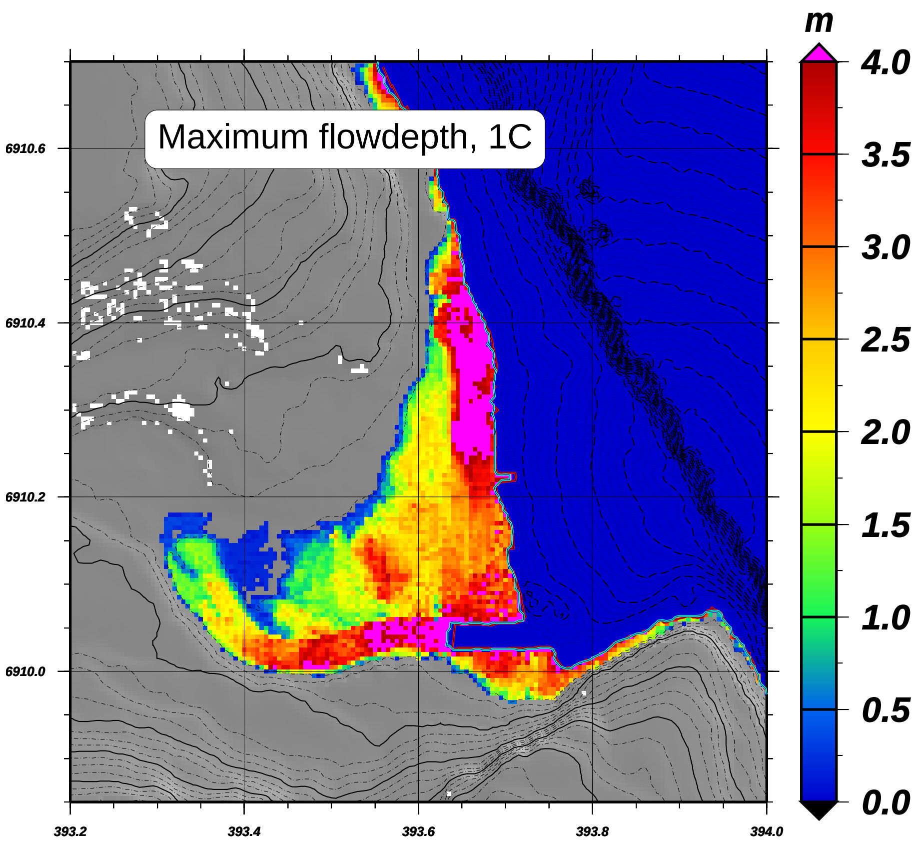

Figure A.73: Maximum flow depth at Stranda for scenario 1C given in meters. The red line is the shoreline for today's mean sea level (MSL) while the cyan line is the shoreline including the estimated sea level rise of 0.7 m.

Details at Stranda for scenario 2B.

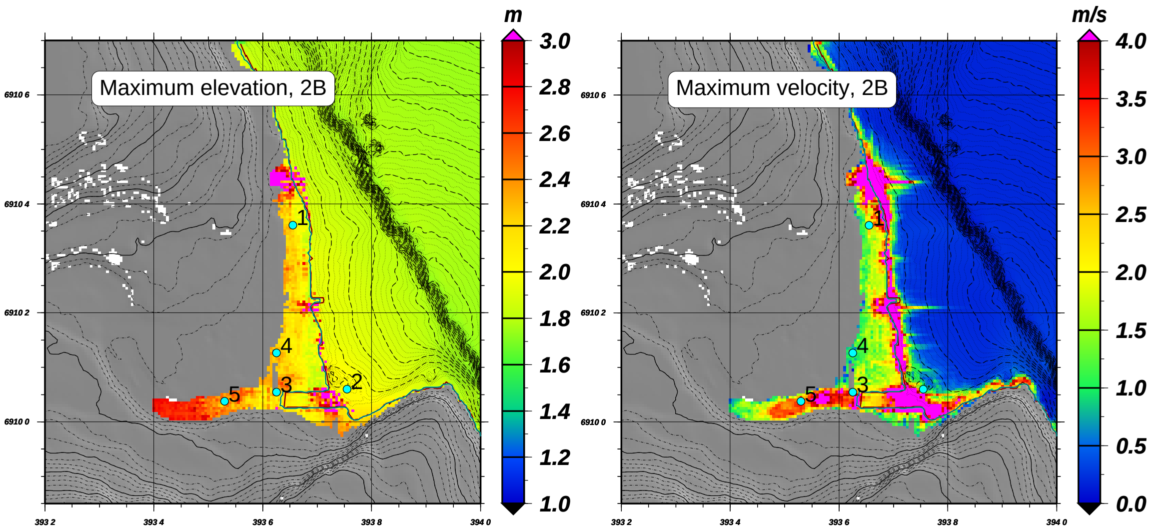

Figure A.74: Maximum water level measured from 0.7 m above today's mean sea level (left) and velocity (right) at Stranda, scenario 2B. The red line is the shoreline for today's mean sea level (MSL) while the cyan line is the shoreline including the estimated sea level rise of 0.7 m. Coordinates given in UTM32 (km) and gridlines printed every 200 m.

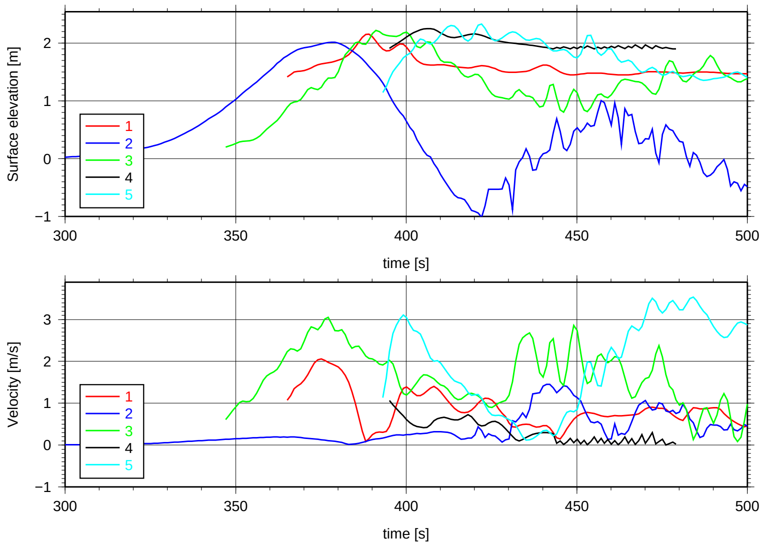

Figure A.75: Time history of the water level (upper panel) and velocity (lower panel - absolute values) measured at gauges 1-5 (see Figure A.74) at Stranda for scenario 2B. The surface elevation is given in meters, while the velocity is given in meters per second.

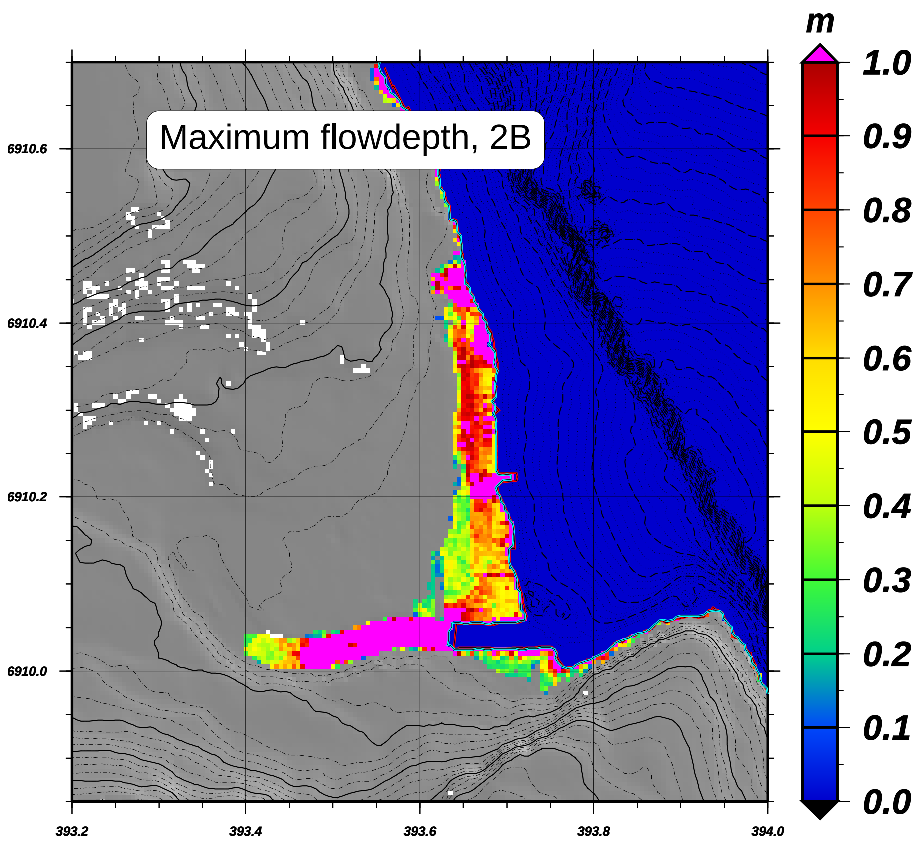

Figure A.76: Maximum flow depth at Stranda for scenario 2B given in meters. The red line is the shoreline for today's mean sea level (MSL) while the cyan line is the shoreline including the estimated sea level rise of 0.7 m.

A.3.18 Stranda (south)

Location number 15, see Figure A.1.

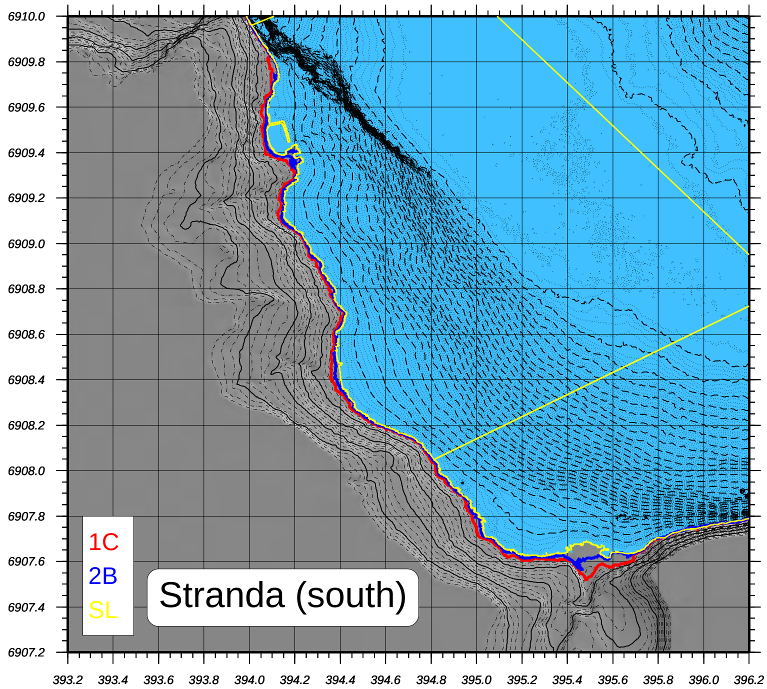

Figure A.77: Trimlines for each scenario at Stranda (south). The highest water level along the shoreline and the maximum run-up is indicated with a triangle and a star, respectively. The yellow line is the shoreline for today's mean sea level. Coordinates given in UTM32 (km) and gridlines printed every 200 m.

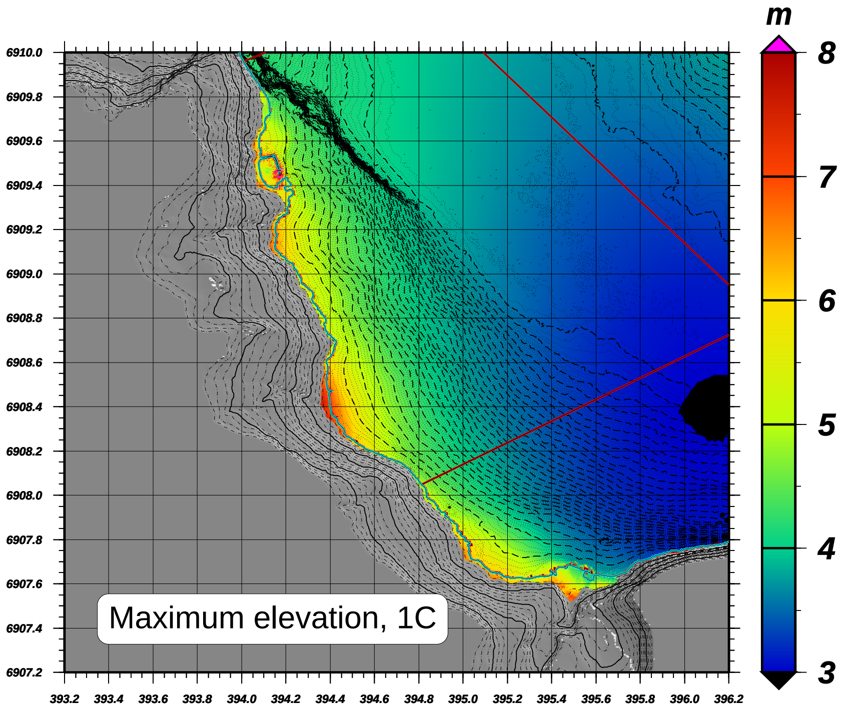

Figure A.78: Maximum water level measured from 0.7 m above today's mean sea level at Stranda (south), scenario 1C. The red line is the shoreline for today's mean sea level (MSL) while the cyan line is the shoreline including the estimated sea level rise of 0.7 m. Coordinates given in UTM32 (km) and gridlines printed every 200 m.

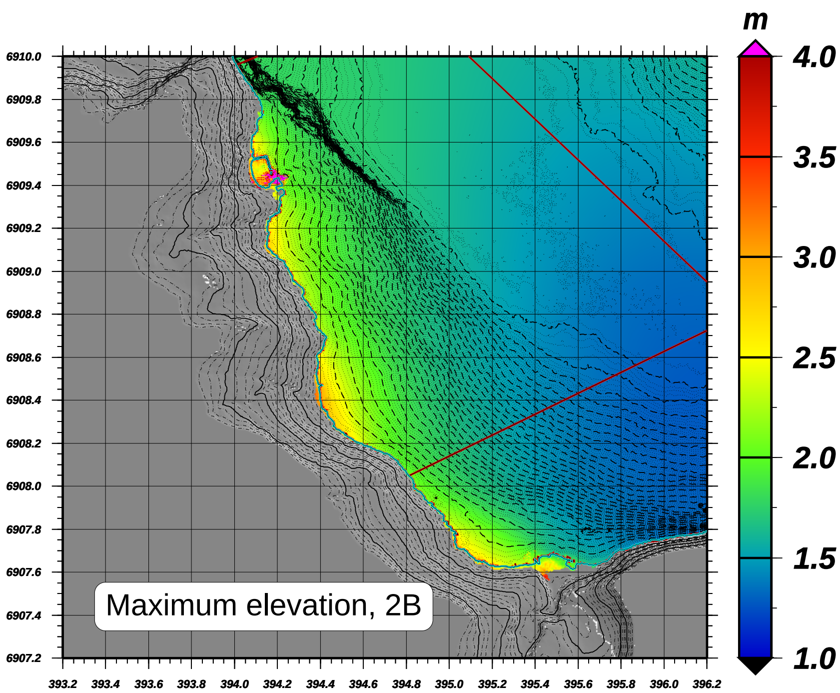

Figure A.79: Maximum water level measured from 0.7 m above today's mean sea level at Stranda (south), scenario 2B. The red line is the shoreline for today's mean sea level (MSL) while the cyan line is the shoreline including the estimated sea level rise of 0.7 m. Coordinates given in UTM32 (km) and gridlines printed every 200 m.

A.3.19 Straumgjerde

Location number 16, see Figure A.1.

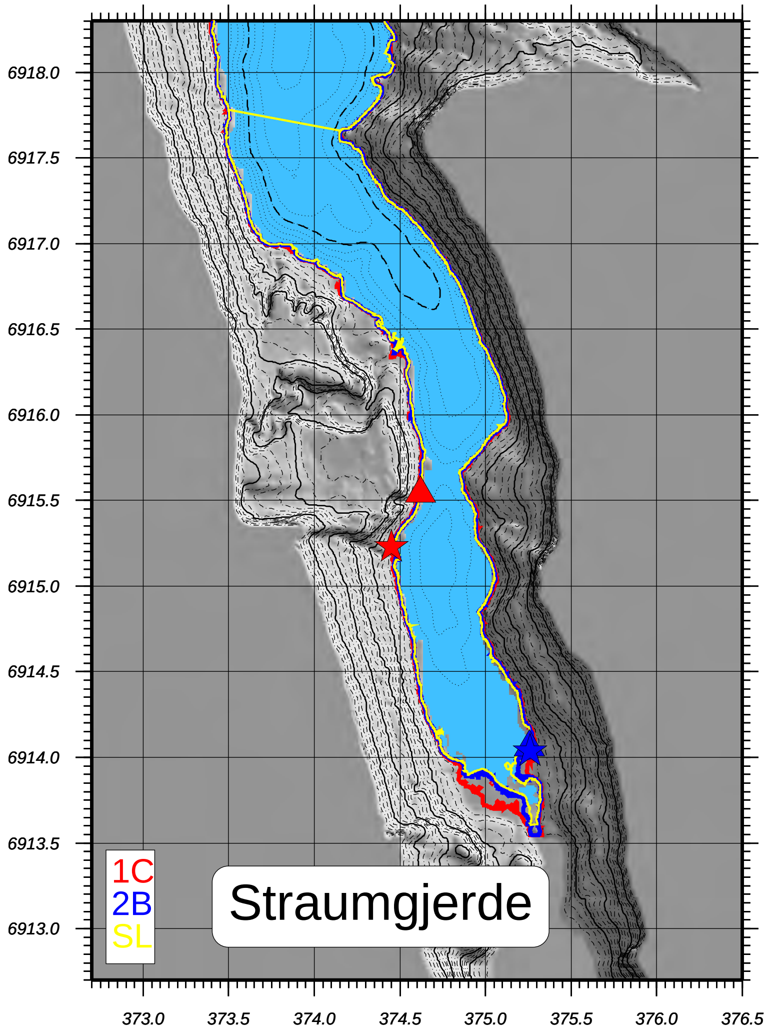

Figure A.80: Trimlines for each scenario at Straumgjerde. The highest water level along the shoreline and the maximum run-up is indicated with a triangle and a star, respectively. The yellow line is the shoreline for today's mean sea level. Coordinates given in UTM32 (km) and gridlines printed every 500 m.

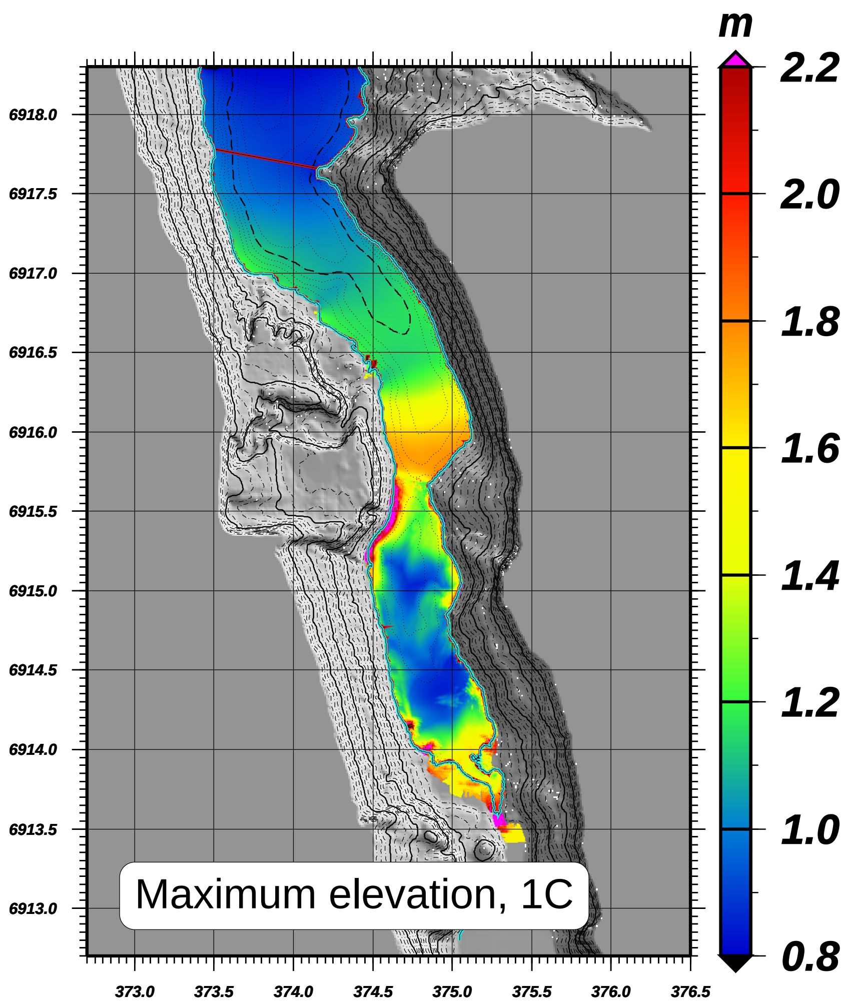

Figure A.81: Maximum water level measured from 0.7 m above today's mean sea level at Straumgjerde, scenario 1C. The red line is the shoreline for today's mean sea level (MSL) while the cyan line is the shoreline including the estimated sea level rise of 0.7 m. Coordinates given in UTM32 (km) and gridlines printed every 500 m.

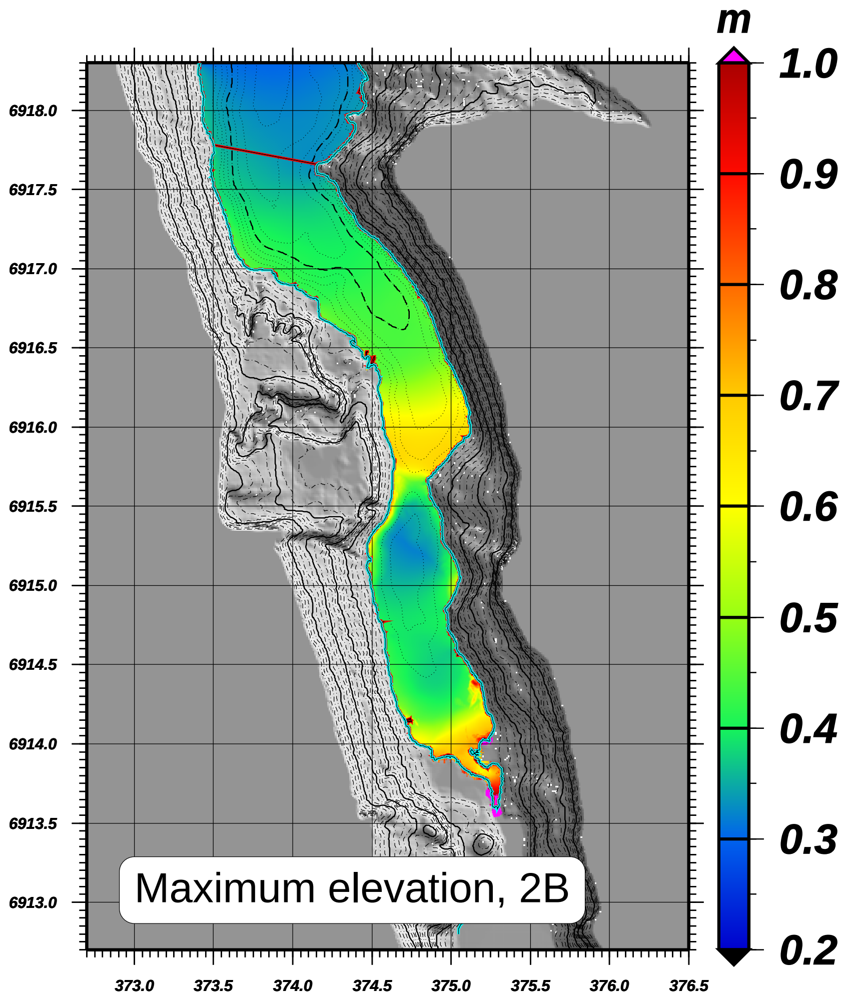

Figure A.82: Maximum water level measured from 0.7 m above today's mean sea level at Straumgjerde, scenario 2B. The red line is the shoreline for today's mean sea level (MSL) while the cyan line is the shoreline including the estimated sea level rise of 0.7 m. Coordinates given in UTM32 (km) and gridlines printed every 500 m.

A.3.20 Sykkylven and Ikornes

Location number 16, see Figure A.1.

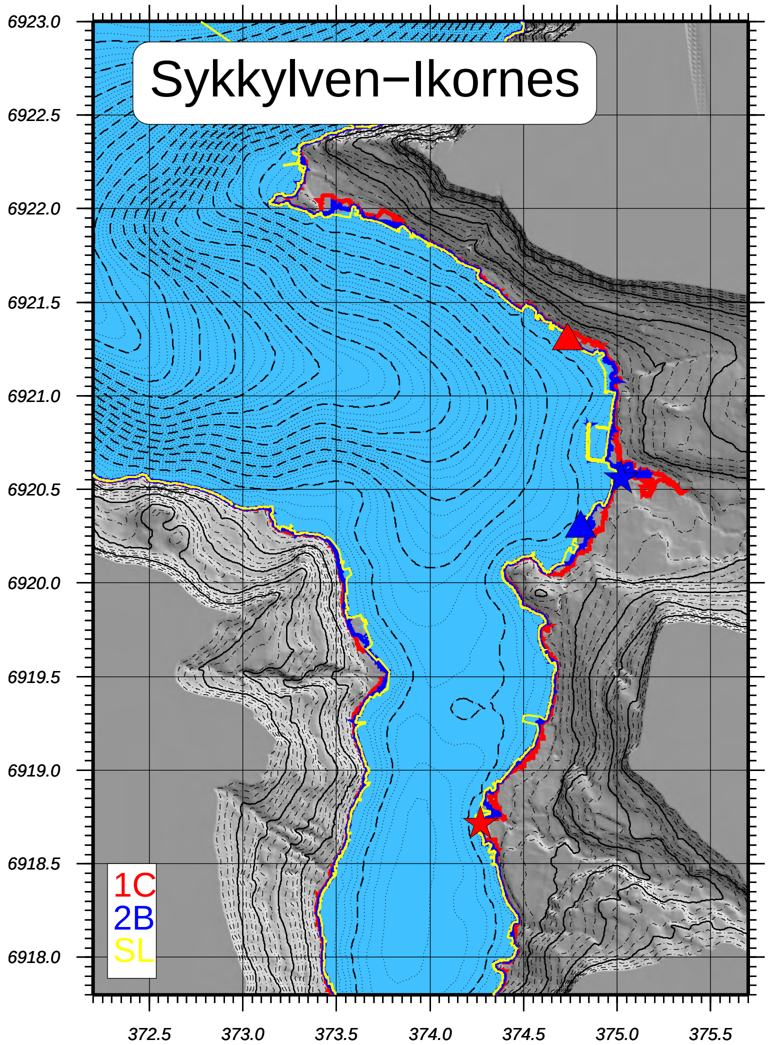

Figure A.83: Trimlines for each scenario at Sykkylven and Ikornes. The highest water level along the shoreline and the maximum run-up is indicated with a triangle and a star, respectively. The yellow line is the shoreline for today's mean sea level. Coordinates given in UTM32 (km) and gridlines printed every 500 m.

Figure A.84: Ikornes. Photo: NGI.

Figure A.85: Ørsnes. Photo: NGI.

Figure A.86: Sykkylven. Photo: NGI.

Sykkylven and Ikornes, scenario 1C.

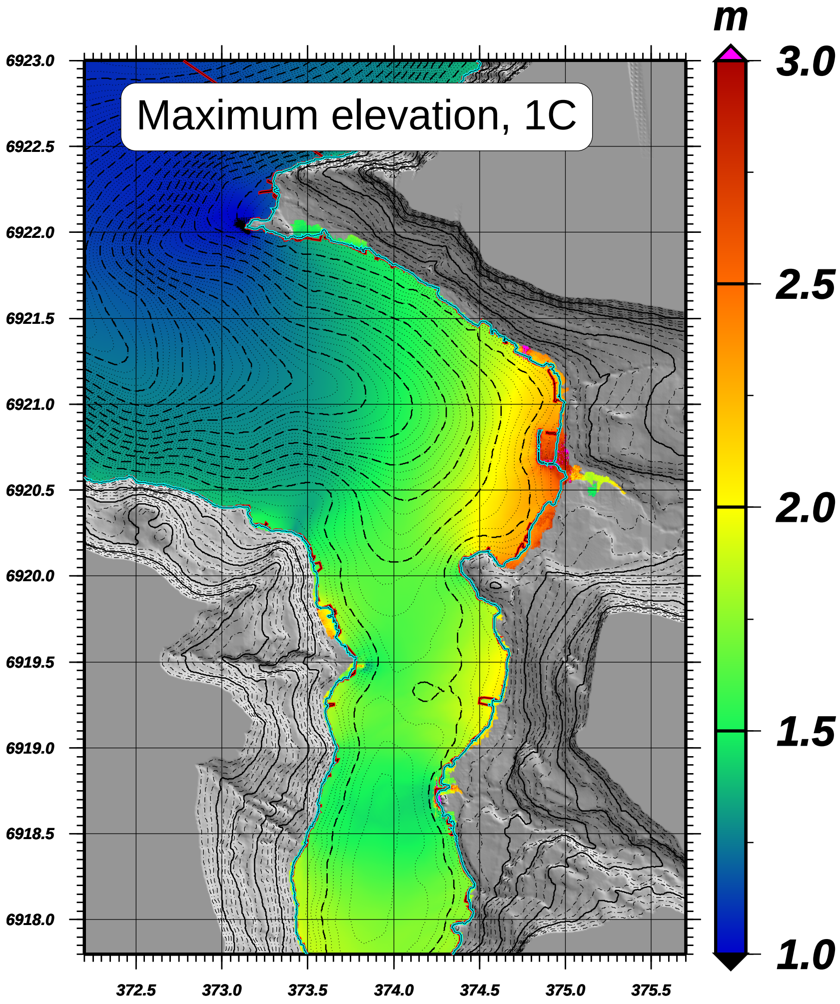

Figure A.87: Maximum water level at Sykkylven and Ikornes, scenario 1C. The red line is the shoreline for today's mean sea level (MSL) while the cyan line is the shoreline including the estimated sea level rise of 0.7 m. Coordinates given in UTM32 (km) and gridlines printed every 500 m.

Details at Ikornes for scenario 1C.

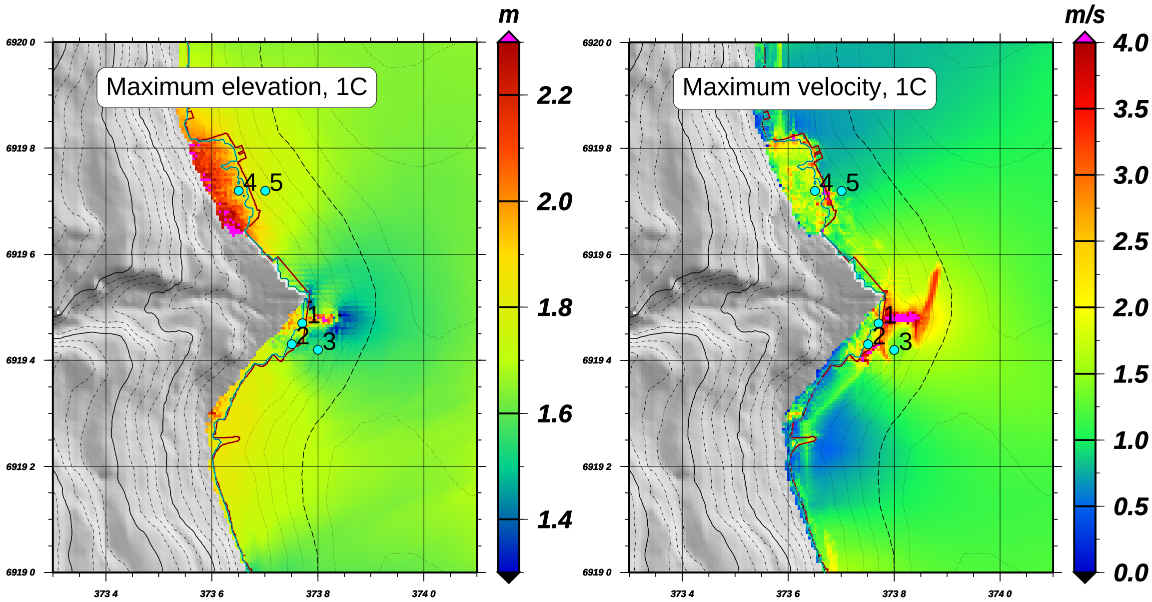

Figure A.88: Maximum water level measured from 0.7 m above today's mean sea level (left) and velocity (right) at Ikornes, scenario 1C. The red line is the shoreline for today's mean sea level (MSL) while the cyan line is the shoreline including the estimated sea level rise of 0.7 m. Coordinates given in UTM32 (km) and gridlines printed every 500 m.

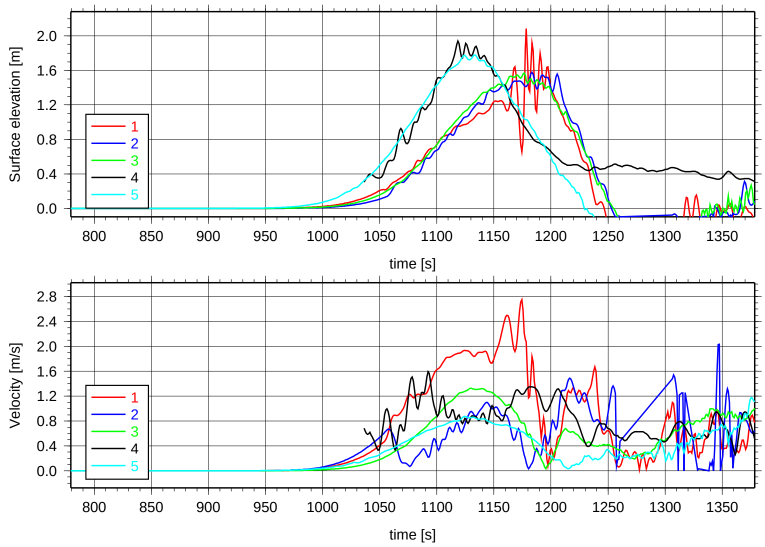

Figure A.89: Time history of the water level (upper panel) and velocity (lower panel - absolute values) measured at gauges 1-5 (see Figure A.88) at Ikornes for scenario 1C. The surface elevation is given in meters, while the velocity is given in meters per second.

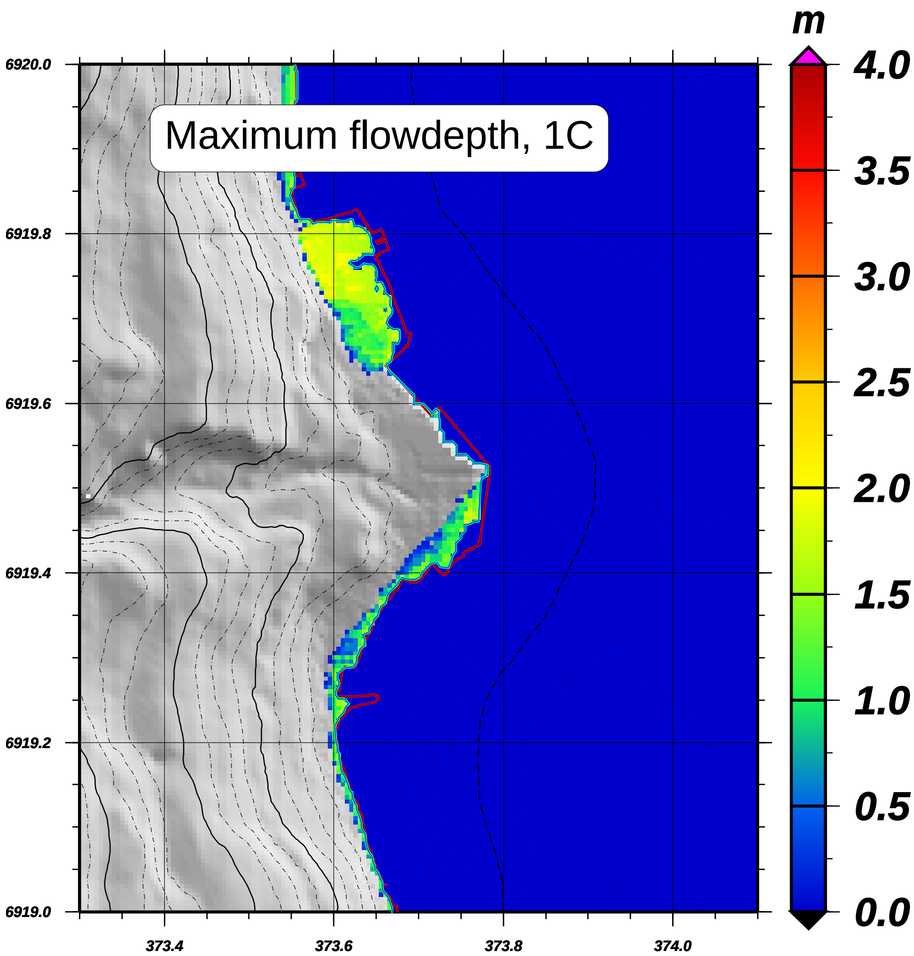

Figure A.90: Maximum flow depth at Ikornes for scenario 1C given in meters. The red line is the shoreline for today's mean sea level (MSL) while the cyan line is the shoreline including the estimated sea level rise of 0.7 m.

Ikornes, scenario 2B.

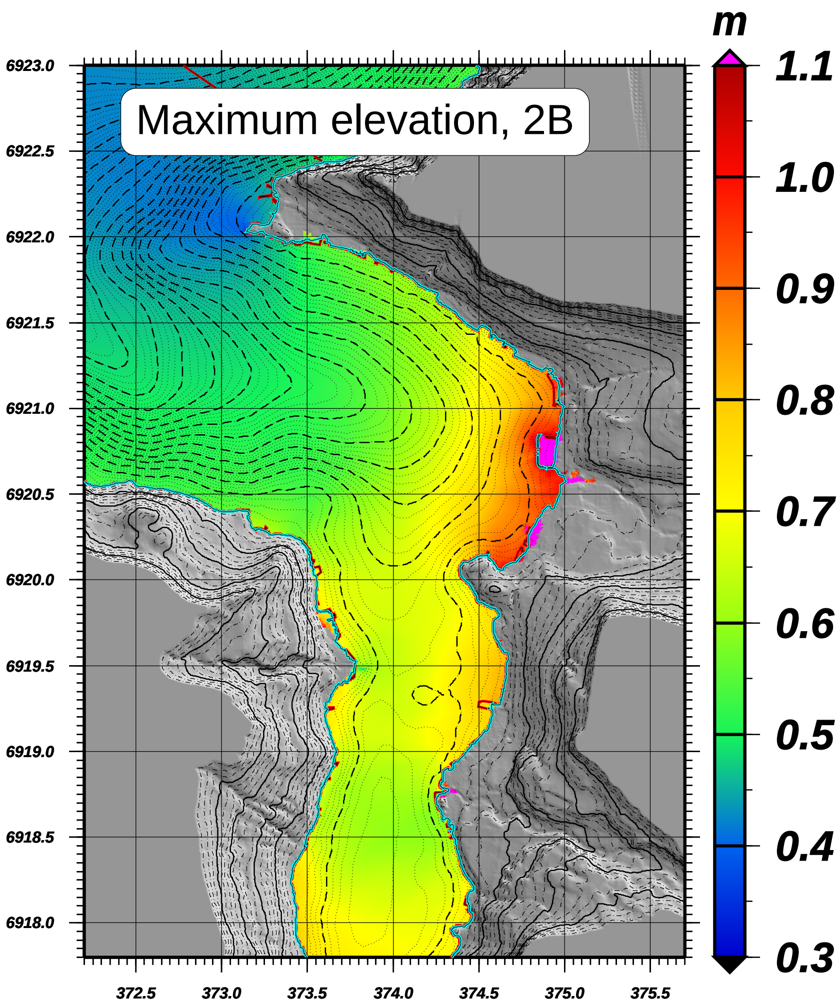

Figure A.91: Maximum water level at Ikornes, scenario 2B. The red line is the shoreline for today's mean sea level (MSL) while the cyan line is the shoreline including the estimated sea level rise of 0.7 m. Coordinates given in UTM32 (km) and gridlines printed every 500 m.

Details at Ikornes for scenario 2B.

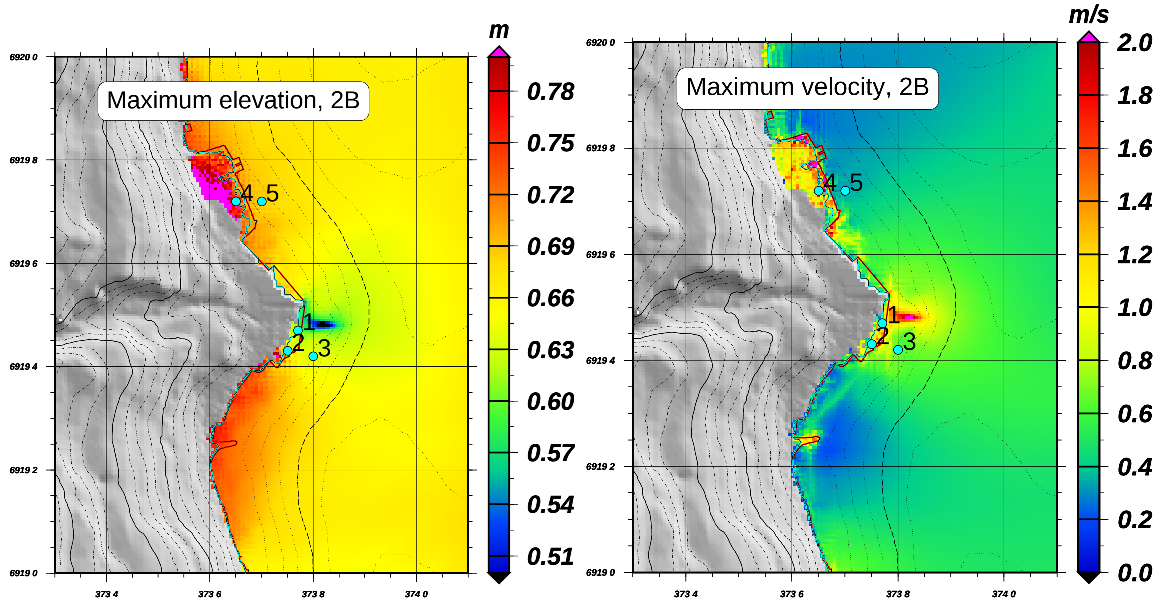

Figure A.92: Maximum water level measured from 0.7 m above today's mean sea level (left) and velocity (right) at Ikornes, scenario 2B. The red line is the shoreline for today's mean sea level (MSL) while the cyan line is the shoreline including the estimated sea level rise of 0.7 m. Coordinates given in UTM32 (km) and gridlines printed every 500 m.

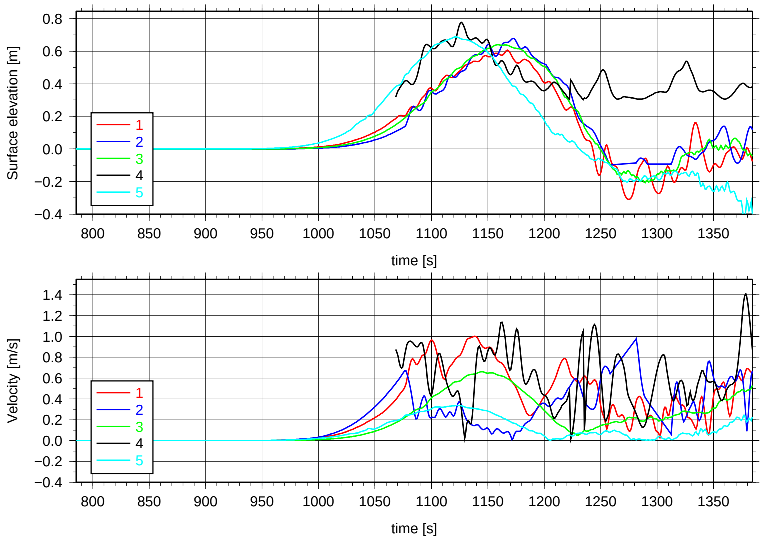

Figure A.93: Time history of the water level (upper panel) and velocity (lower panel - absolute values) measured at gauges 1-5 (see Figure A.92) at Ikornes for scenario 2B. The surface elevation is given in meters, while the velocity is given in meters per second.

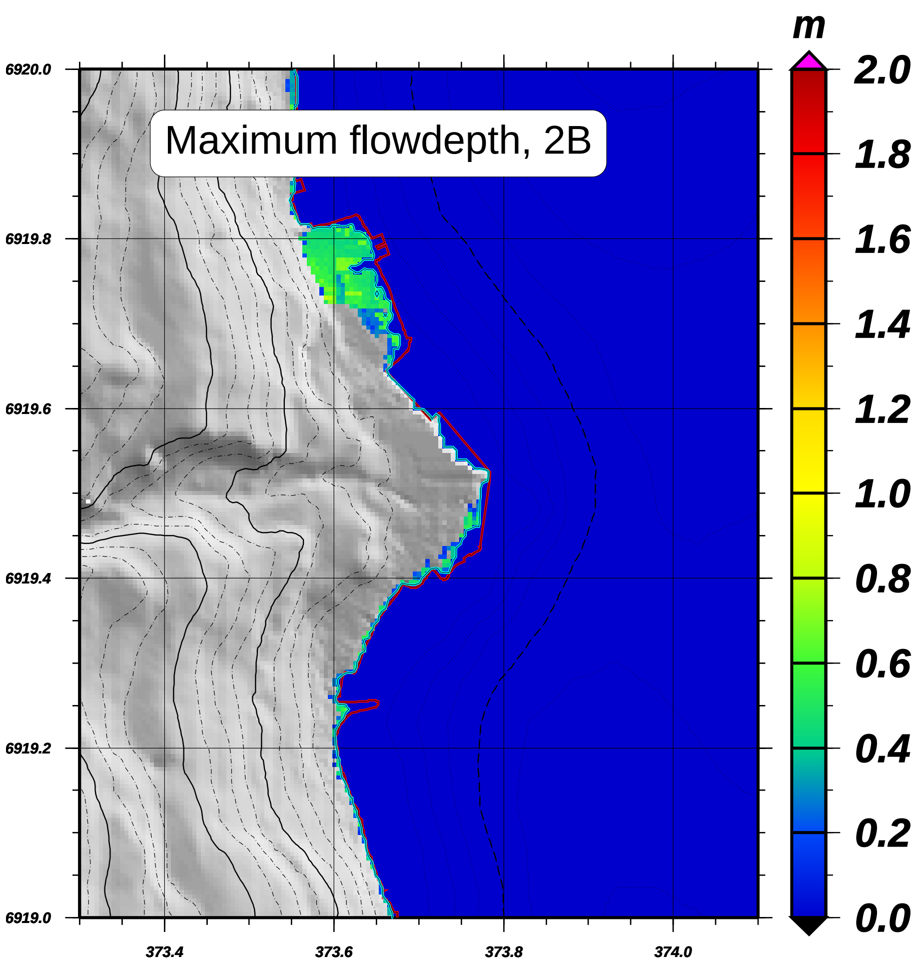

Figure A.94: Maximum flow depth at Ikornes for scenario 2B given in meters. The red line is the shoreline for today's mean sea level (MSL) while the cyan line is the shoreline including the estimated sea level rise of 0.7 m.

A.3.21 Tafjord

Location number 9, see Figure A.1.

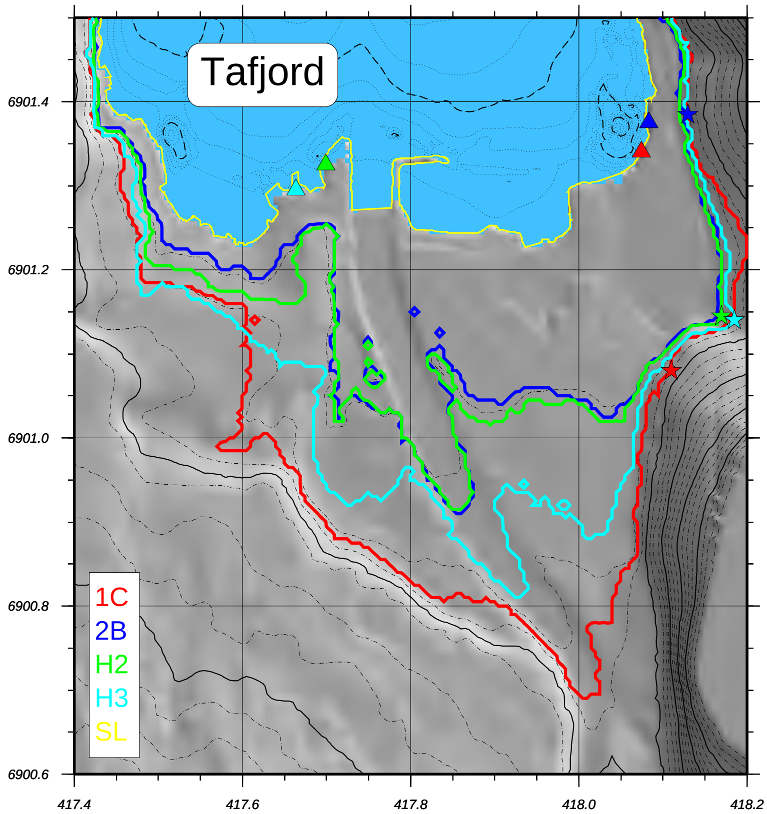

Figure A.95: Trimlines for each scenario at Tafjord. The highest water level along the shoreline and the maximum run-up is indicated with a triangle and a star, respectively. The yellow line is the shoreline for today's mean sea level. Coordinates given in UTM32 (km) and gridlines printed every 200 m.

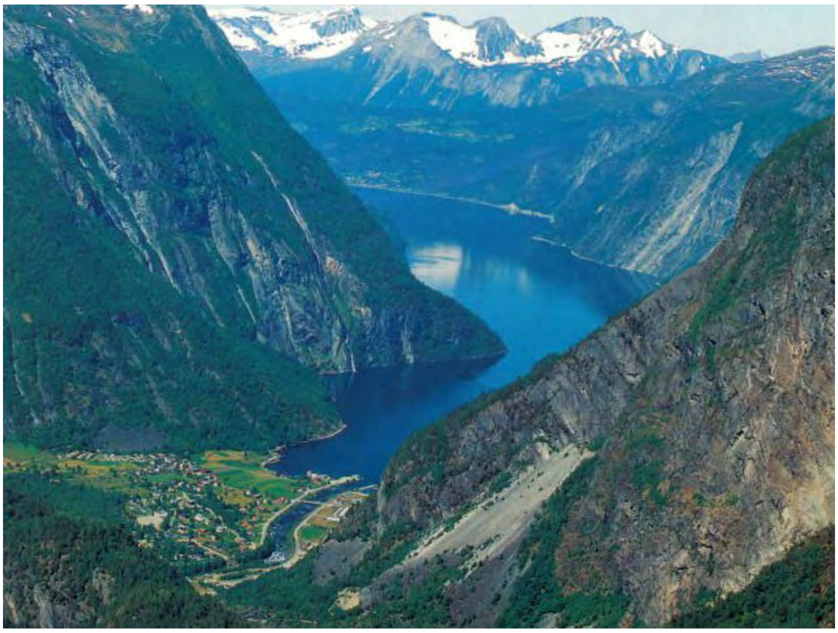

Figure A.96: Tafjord. Slide scar can be seen at the fjordside in the upper right part of the photo. Photo: Normann Kunstforlag A/S.

Details at Tafjord for scenario 1C.

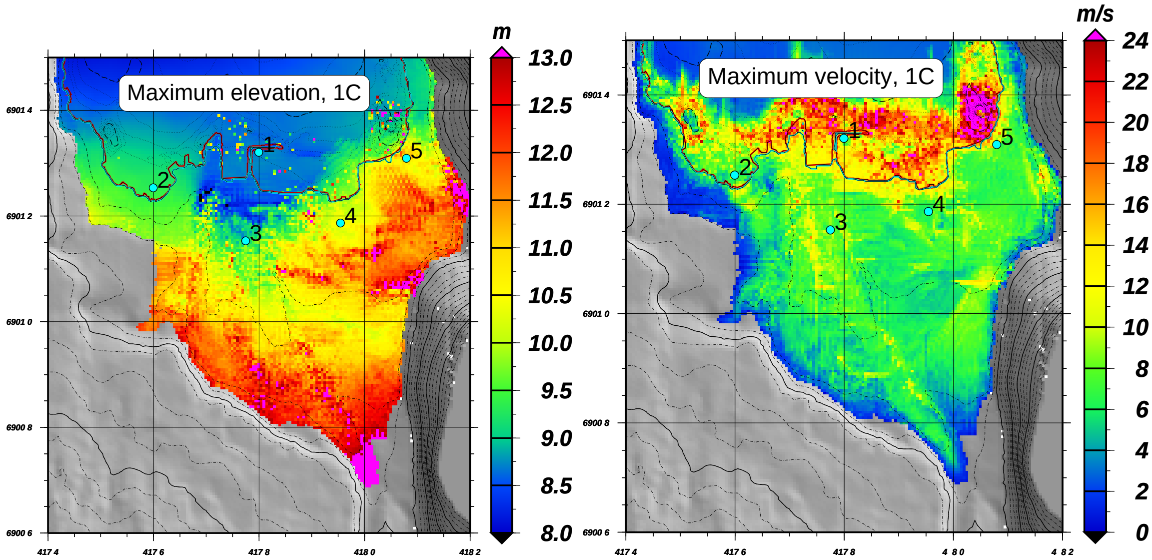

Figure A.97: Maximum water level measured from 0.7 m above today's mean sea level (left) and velocity (right) at Tafjord, scenario 1C. The red line is the shoreline for today's mean sea level (MSL) while the cyan line is the shoreline including the estimated sea level rise of 0.7 m. Coordinates given in UTM32 (km) and gridlines printed every 200 m.

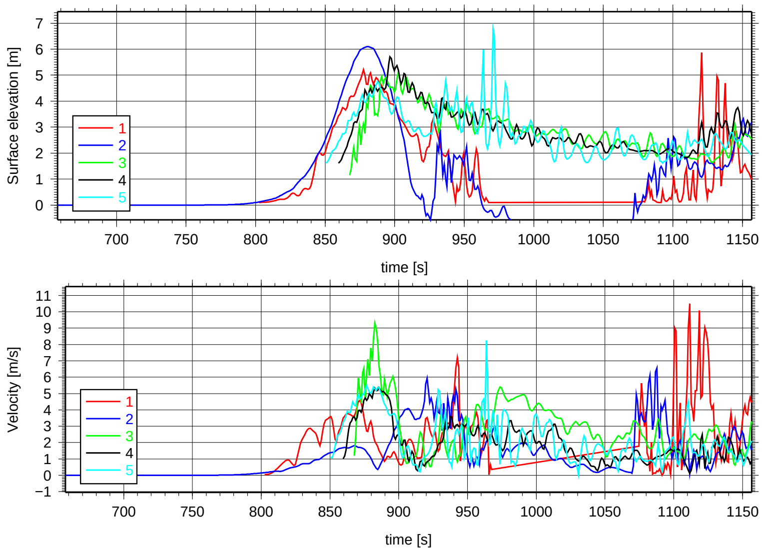

Figure A.98: Time history of the water level (upper panel) and velocity (lower panel - absolute values) measured at gauges 1-5 (see Figure A.97) at Tafjord for scenario 1C. The surface elevation is given in meters, while the velocity is given in meters per second.

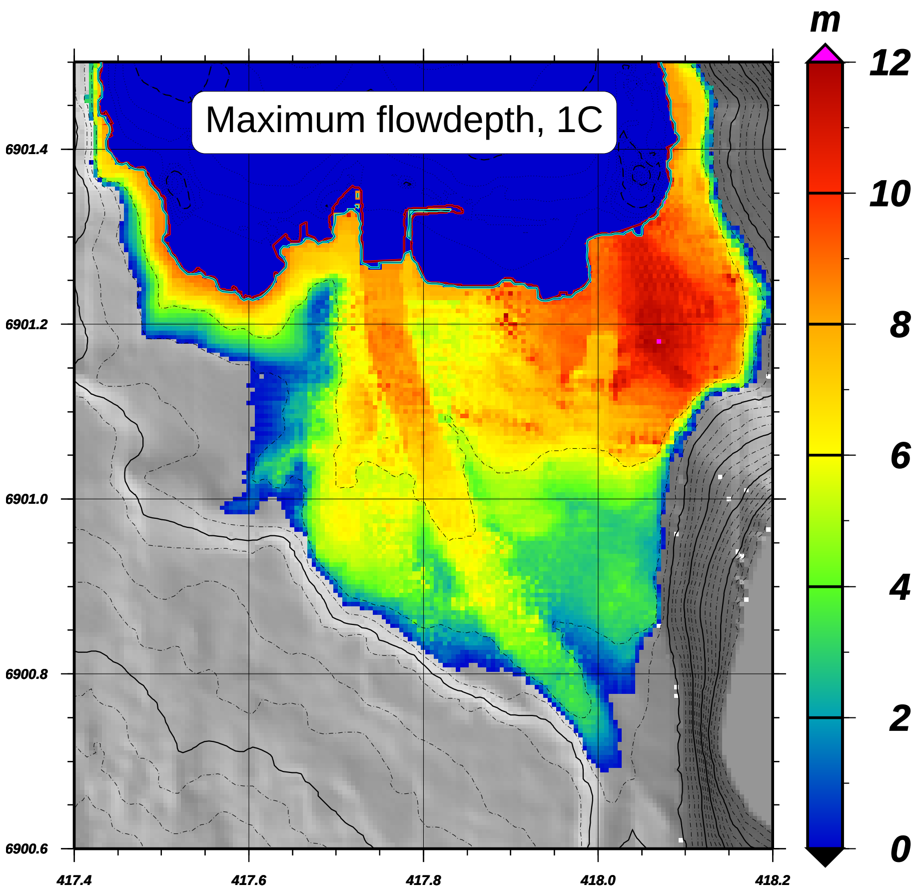

Figure A.99: Maximum flow depth at Tafjord for scenario 1C given in meters. The red line is the shoreline for today's mean sea level (MSL) while the cyan line is the shoreline including the estimated sea level rise of 0.7 m.

Details at Tafjord for scenario 2B.

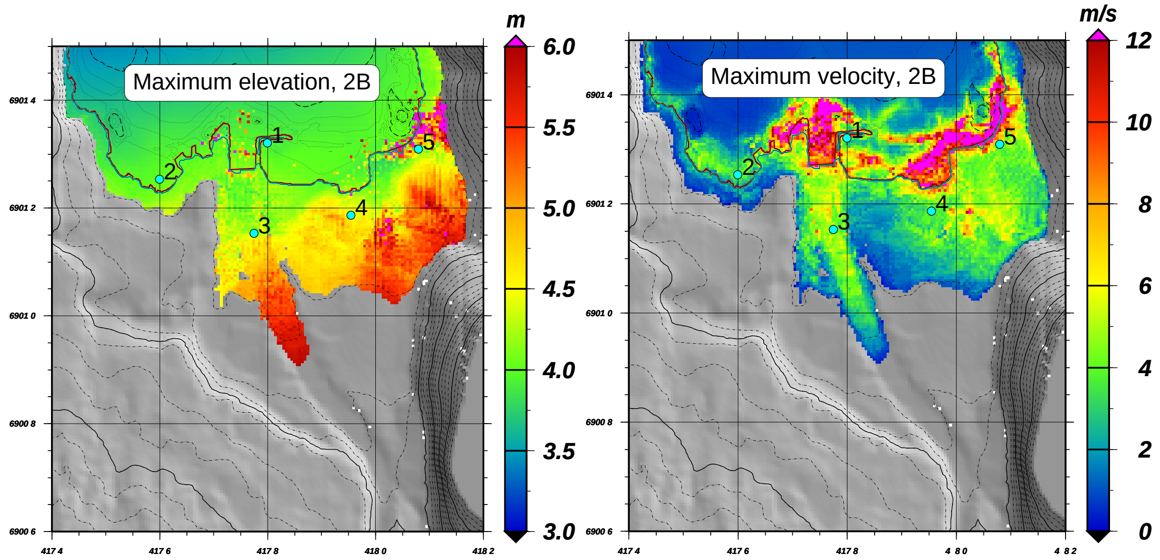

Figure A.100: Maximum water level measured from 0.7 m above today's mean sea level (left) and velocity (right) at Tafjord, scenario 2B. The red line is the shoreline for today's mean sea level (MSL) while the cyan line is the shoreline including the estimated sea level rise of 0.7 m. Coordinates given in UTM32 (km) and gridlines printed every 200 m.

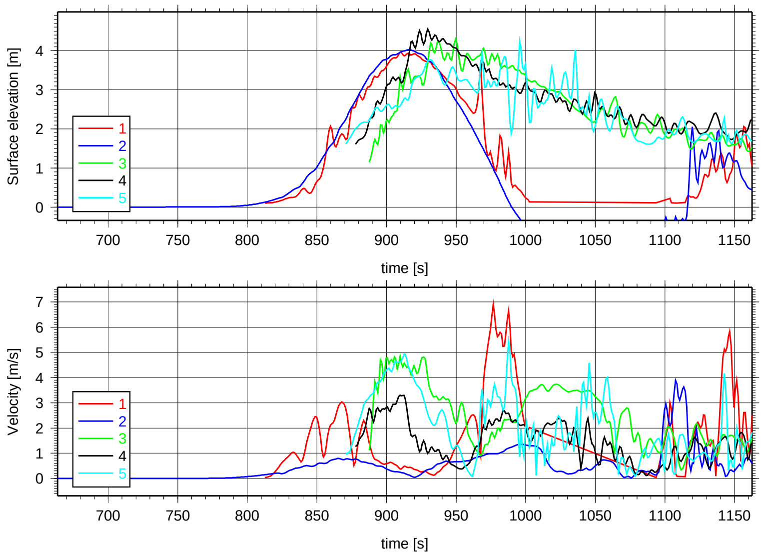

Figure A.101: Time history of the water level (upper panel) and velocity (lower panel - absolute values) measured at gauges 1-5 (see Figure A.100) at Tafjord for scenario 2B. The surface elevation is given in meters, while the velocity is given in meters per second.

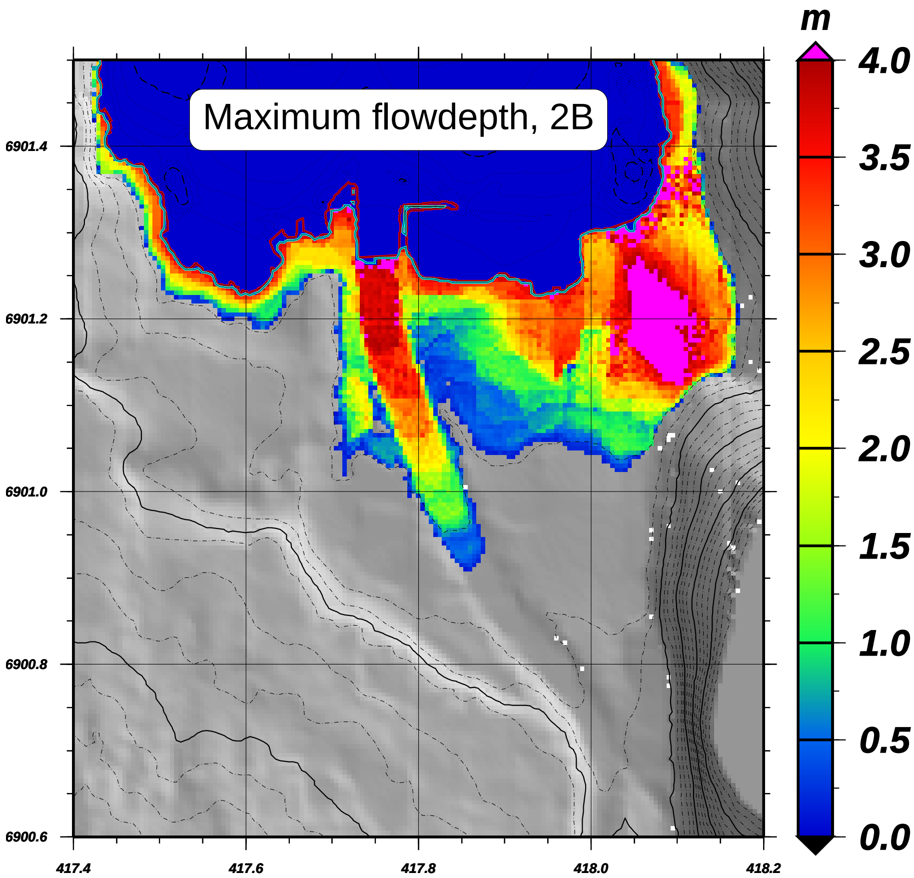

Figure A.102: Maximum flow depth at Tafjord for scenario 2B given in meters. The red line is the shoreline for today's mean sea level (MSL) while the cyan line is the shoreline including the estimated sea level rise of 0.7 m.

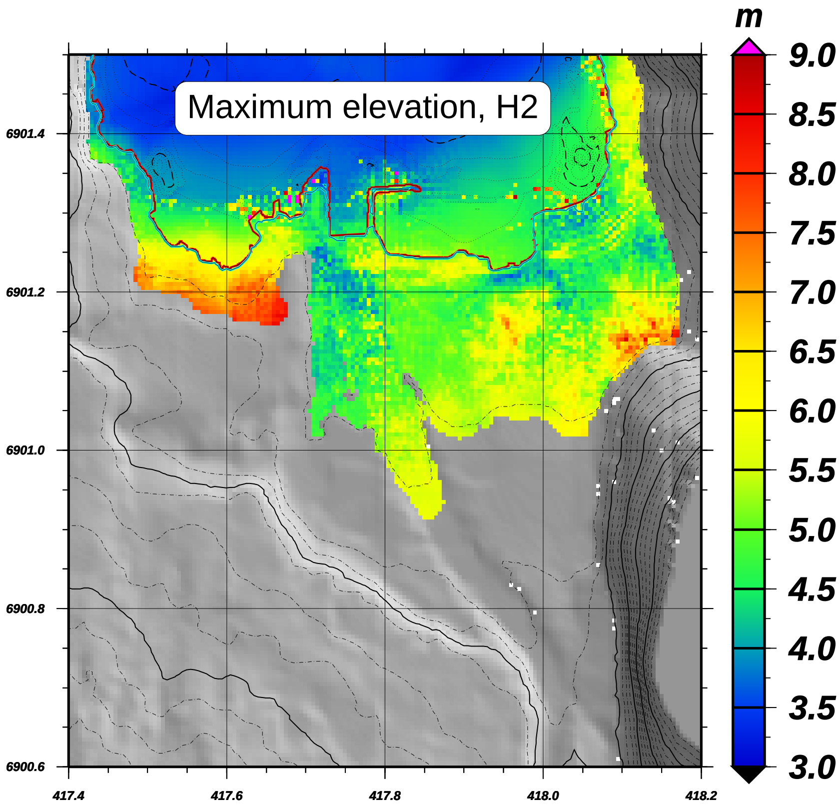

Figure A.103: Maximum water level measured from 0.7 m above today's mean sea level at Tafjord, scenario H2. The red line is the shoreline for today's mean sea level (MSL) while the cyan line is the shoreline including the estimated sea level rise of 0.7 m. Coordinates given in UTM32 (km) and gridlines printed every 200 m.

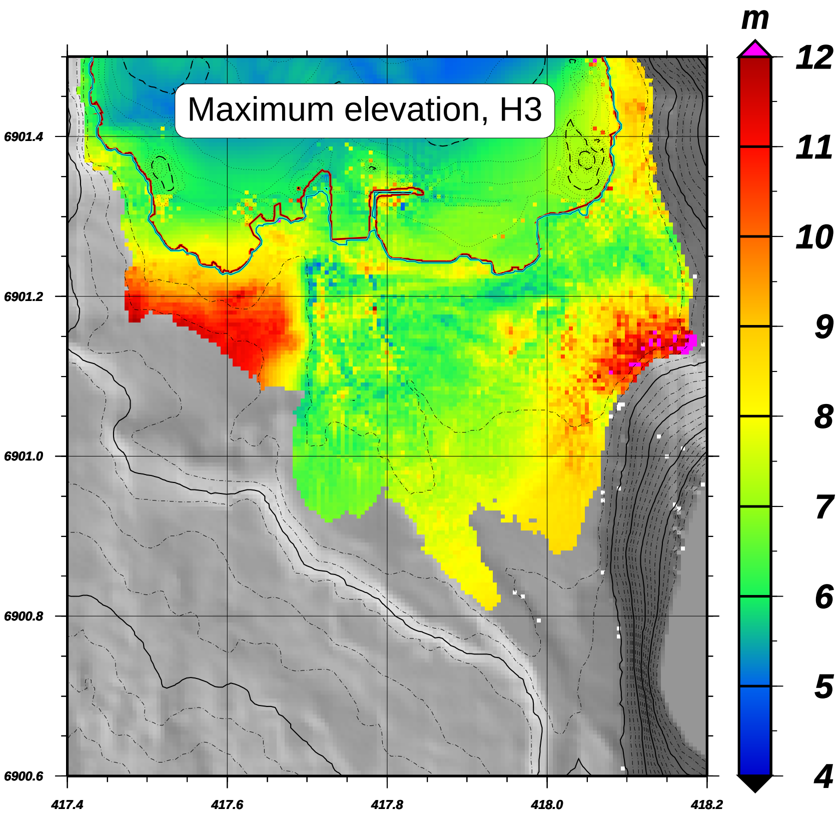

Figure A.104: Maximum water level measured from 0.7 m above today's mean sea level at Tafjord, scenario H3. The red line is the shoreline for today's mean sea level (MSL) while the cyan line is the shoreline including the estimated sea level rise of 0.7 m. Coordinates given in UTM32 (km) and gridlines printed every 200 m.

A.3.22 Vaksvik

Location number 20, see Figure A.1.

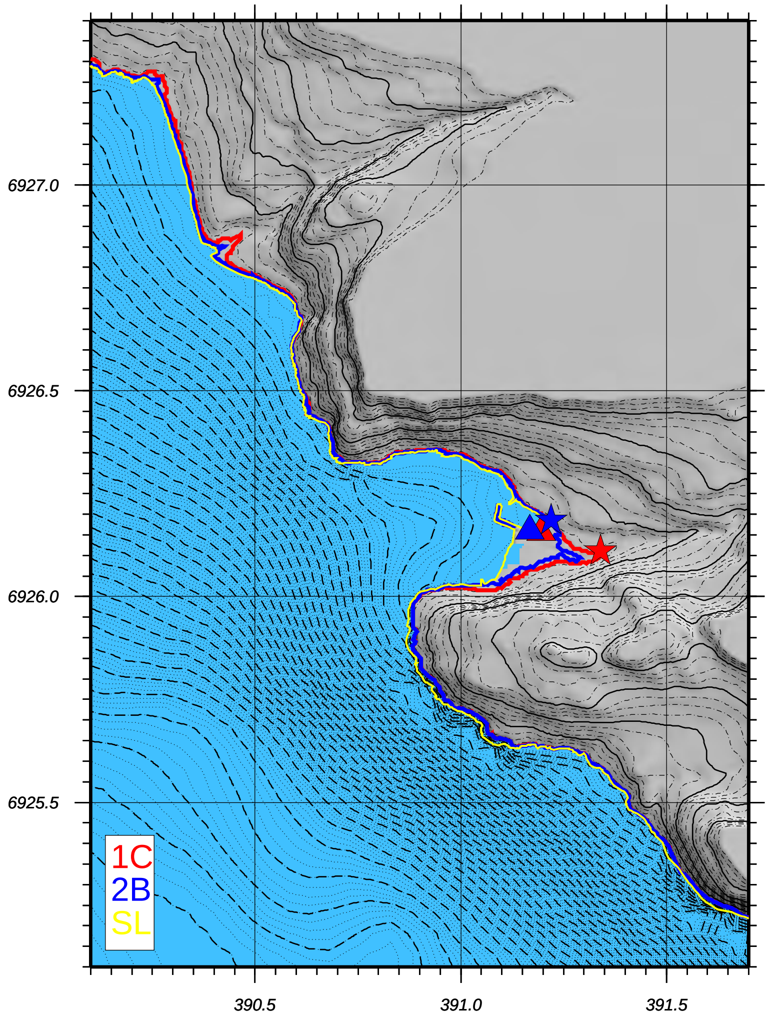

Figure A.105: Trimlines for each scenario at Vaksvik. The highest water level along the shoreline and the maximum run-up is indicated with a triangle and a star, respectively. The yellow line is the shoreline for today's mean sea level. Coordinates given in UTM32 (km) and gridlines printed every 200 m.

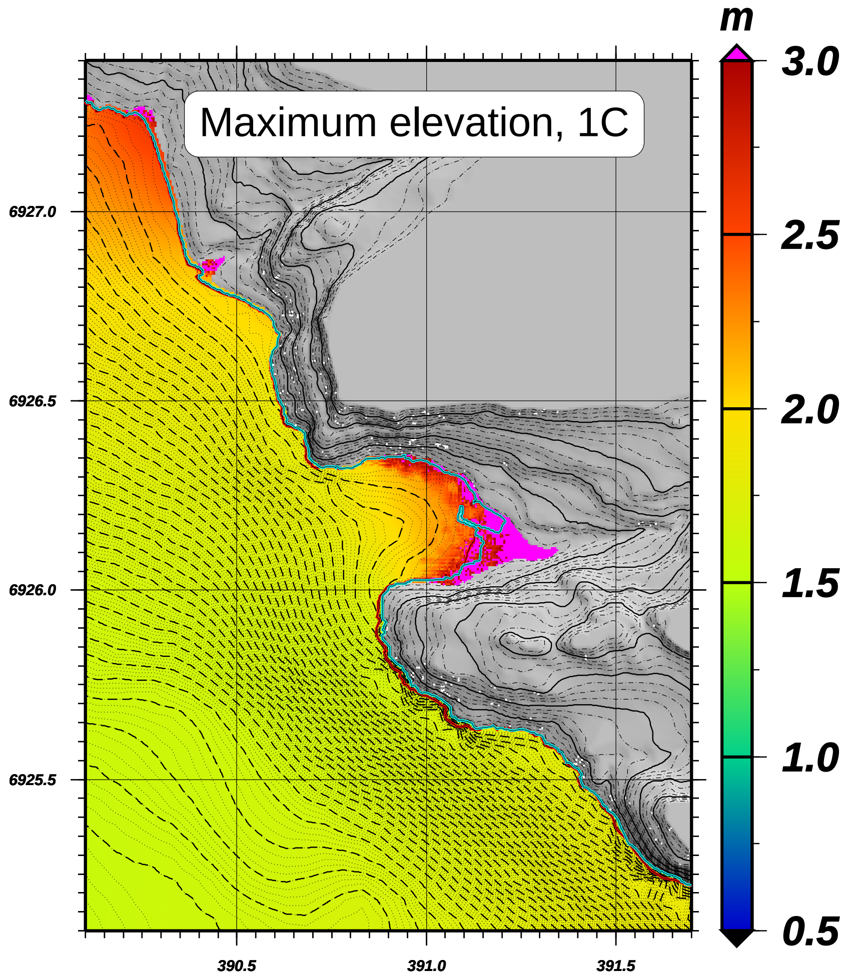

Figure A.106: Maximum water level measured from 0.7 m above today's mean sea level at Vaksvik, scenario 1C. The red line is the shoreline for today's mean sea level (MSL) while the cyan line is the shoreline including the estimated sea level rise of 0.7 m. Coordinates given in UTM32 (km) and gridlines printed every 200 m.

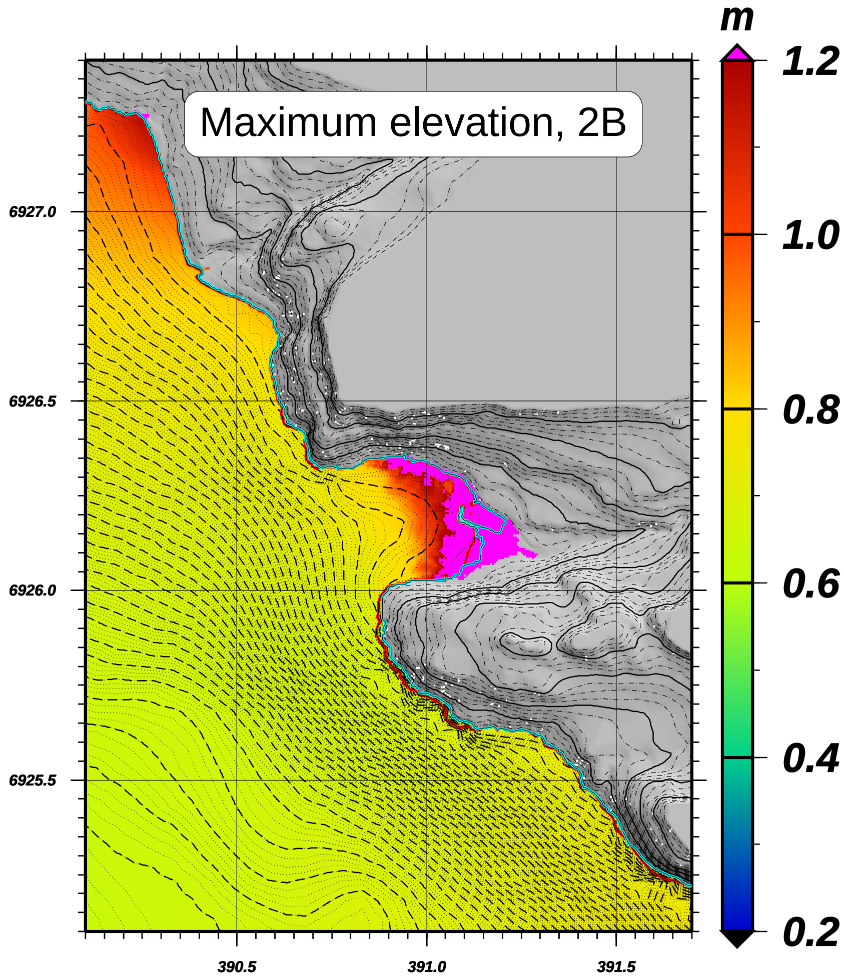

Figure A.107: Maximum water level measured from 0.7 m above today's mean sea level at Vaksvik, scenario 2B. The red line is the shoreline for today's mean sea level (MSL) while the cyan line is the shoreline including the estimated sea level rise of 0.7 m. Coordinates given in UTM32 (km) and gridlines printed every 200 m.

A.3.23 Valldal

Location number 7, see Figure A.1.

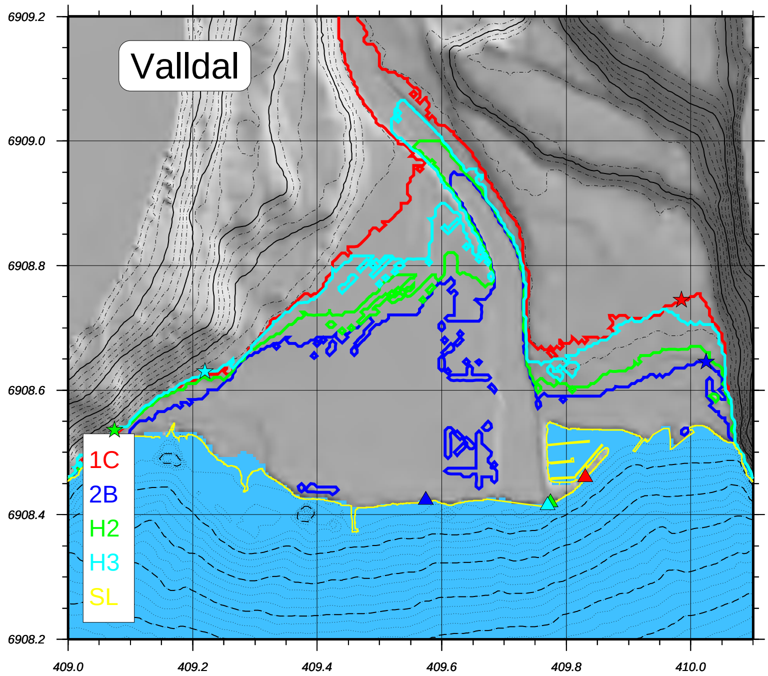

Figure A.108: Trimlines for each scenario at Valldal. The highest water level along the shoreline and the maximum run-up is indicated with a triangle and a star, respectively. The yellow line is the shoreline for today's mean sea level. Coordinates given in UTM32 (km) and gridlines printed every 200 m.

Figure A.109: Valldal. Photo: Normann Kunstforlag A/S.

Details at Valldal for scenario 1C.

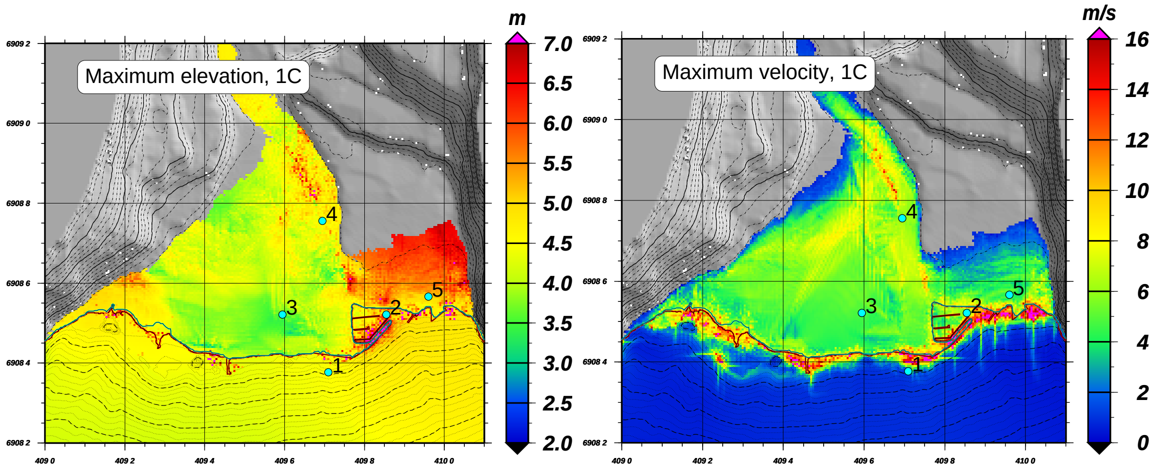

Figure A.110: Maximum water level measured from 0.7 m above today's mean sea level (left) and velocity (right) at Valldal, scenario 1C. The red line is the shoreline for today's mean sea level (MSL) while the cyan line is the shoreline including the estimated sea level rise of 0.7 m. Coordinates given in UTM32 (km) and gridlines printed every 200 m.

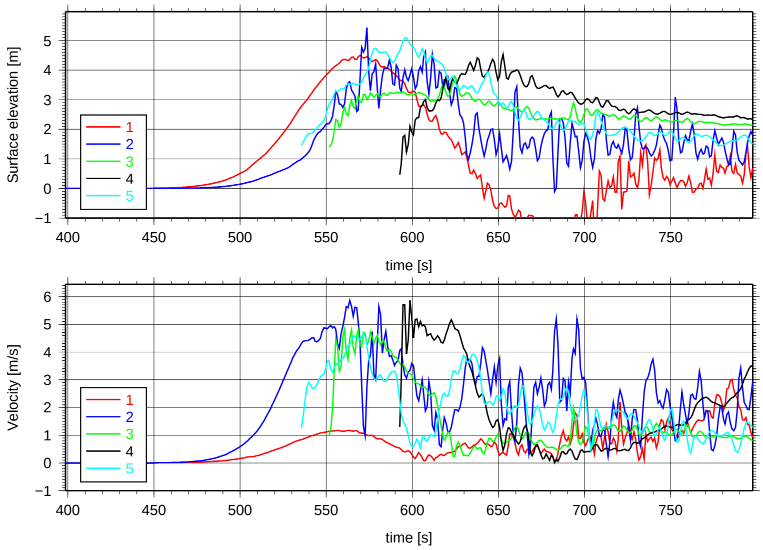

Figure A.111: Time history of the water level (upper panel) and velocity (lower panel - absolute values) measured at gauges 1-5 (see Figure A.110) at Valldal for scenario 1C. The surface elevation is given in meters, while the velocity is given in meters per second.

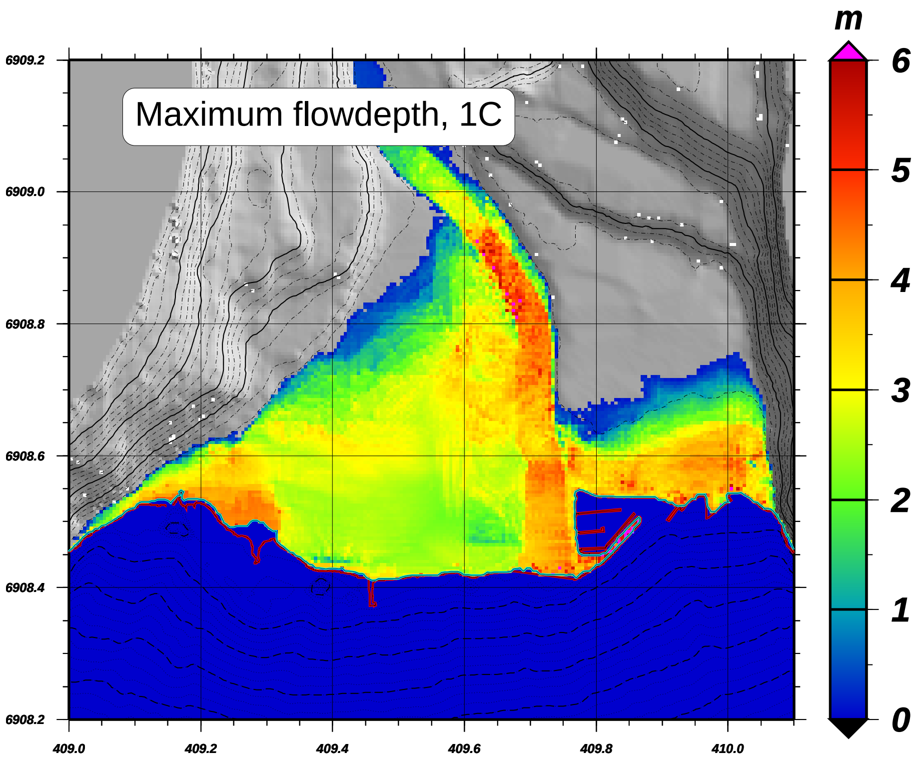

Figure A.112: Maximum flow depth at Valldal for scenario 1C given in meters. The red line is the shoreline for today's mean sea level (MSL) while the cyan line is the shoreline including the estimated sea level rise of 0.7 m.

Details at Valldal for scenario 2B.

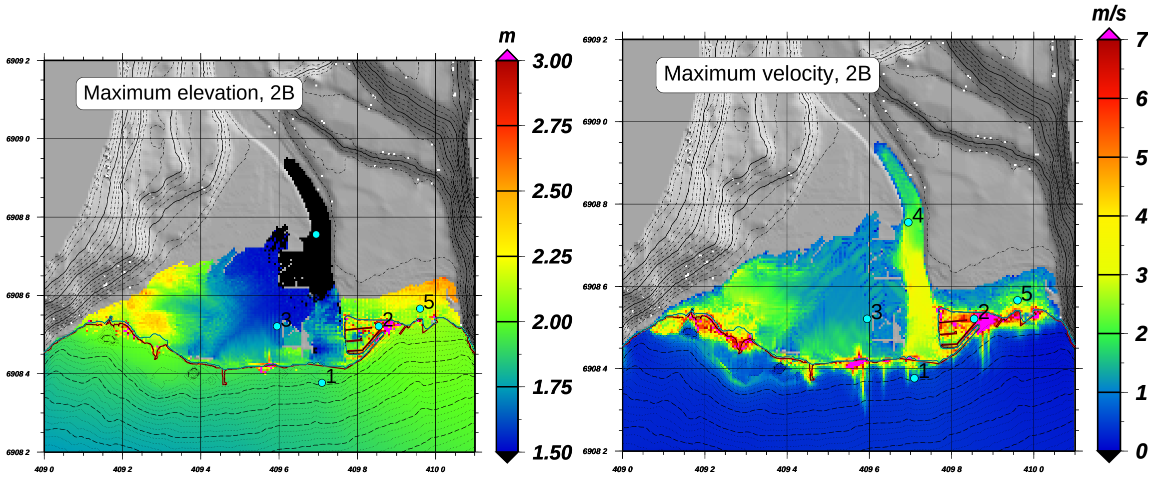

Figure A.113: Maximum water level measured from 0.7 m above today's mean sea level (left) and velocity (right) at Valldal, scenario 2B. The red line is the shoreline for today's mean sea level (MSL) while the cyan line is the shoreline including the estimated sea level rise of 0.7 m. Coordinates given in UTM32 (km) and gridlines printed every 200 m.

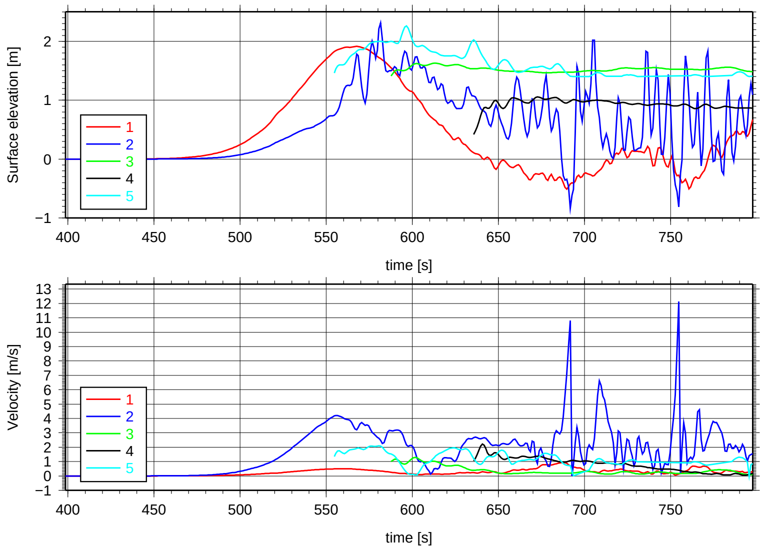

Figure A.114: Time history of the water level (upper panel) and velocity (lower panel - absolute values) measured at gauges 1-5 (see Figure A.113) at Valldal for scenario 2B. The surface elevation is given in meters, while the velocity is given in meters per second.

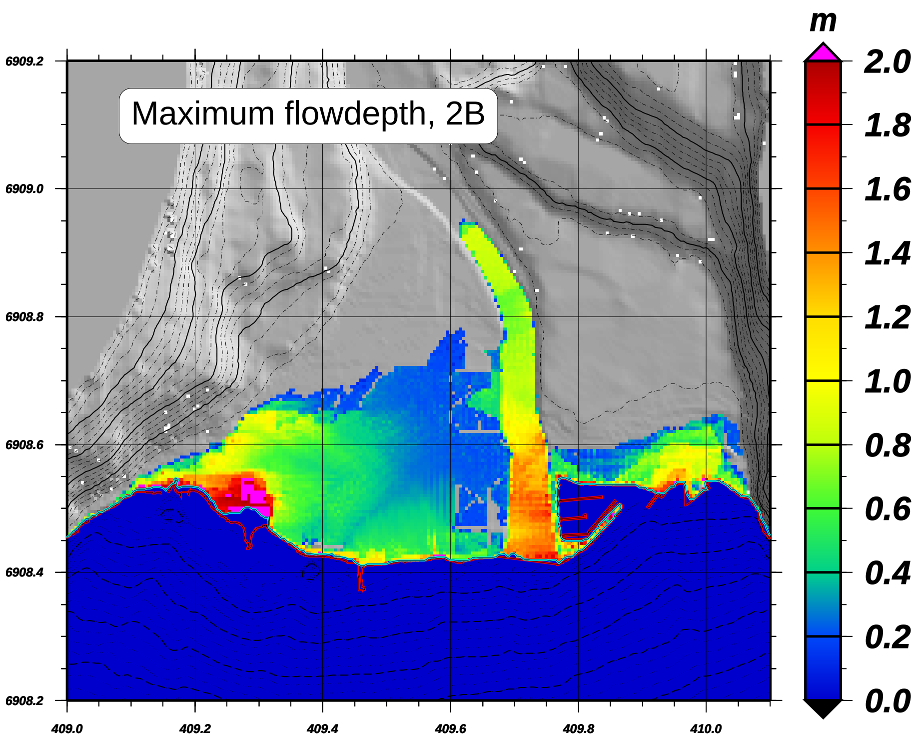

Figure A.115: Maximum flow depth at Valldal for scenario 2B given in meters. The red line is the shoreline for today's mean sea level (MSL) while the cyan line is the shoreline including the estimated sea level rise of 0.7 m.

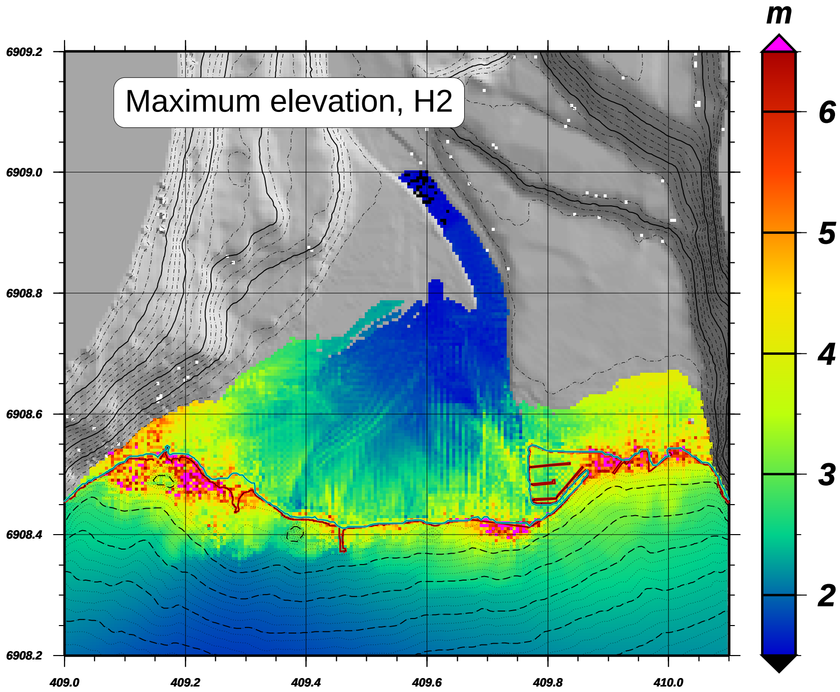

Figure A.116: Maximum water level measured from 0.7 m above today's mean sea level at Valldal, scenario H2. The red line is the shoreline for today's mean sea level (MSL) while the cyan line is the shoreline including the estimated sea level rise of 0.7 m. Coordinates given in UTM32 (km) and gridlines printed every 200 m.

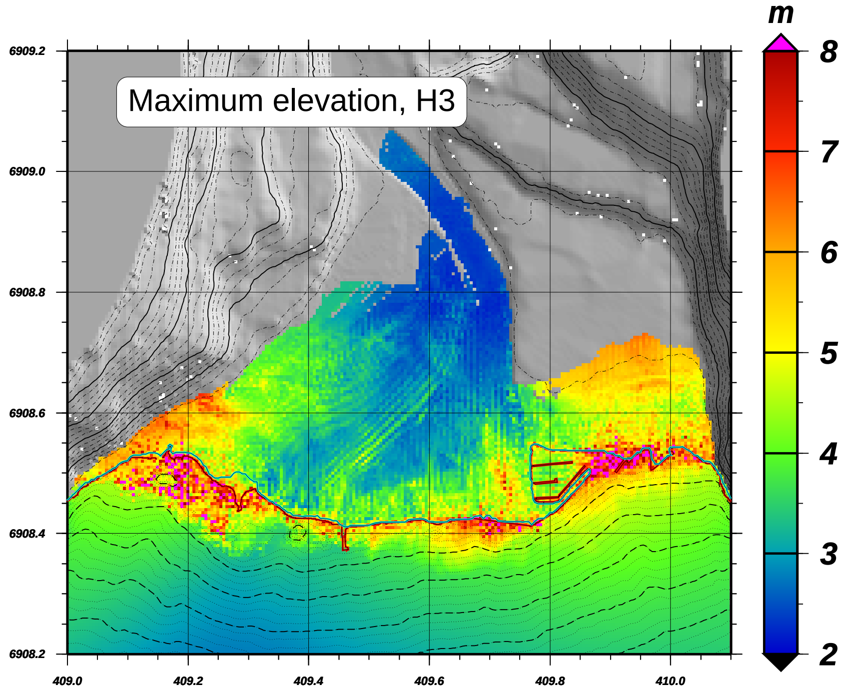

Figure A.117: Maximum water level measured from 0.7 m above today's mean sea level at Valldal, scenario H3. The red line is the shoreline for today's mean sea level (MSL) while the cyan line is the shoreline including the estimated sea level rise of 0.7 m. Coordinates given in UTM32 (km) and gridlines printed every 200 m.

A.3.24 Vegsundet

Location number 1, see Figure A.1.

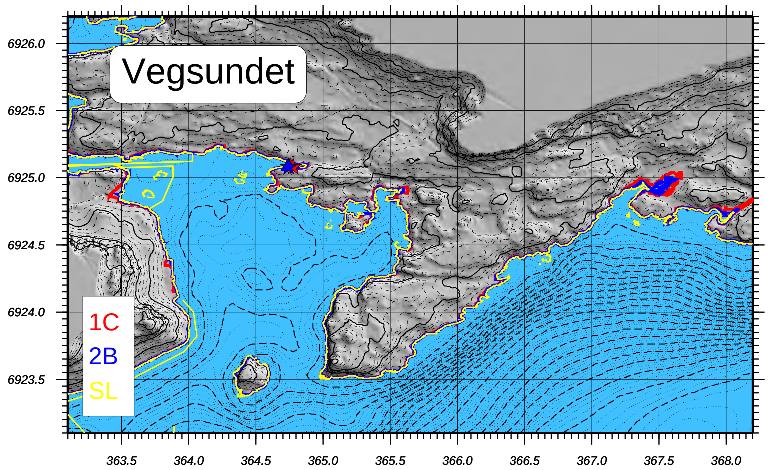

Figure A.118: Trimlines for each scenario at Vegsundet. The highest water level along the shoreline and the maximum run-up is indicated with a triangle and a star, respectively. The yellow line is the shoreline for today's mean sea level. Coordinates given in UTM32 (km) and gridlines printed every 500 m.

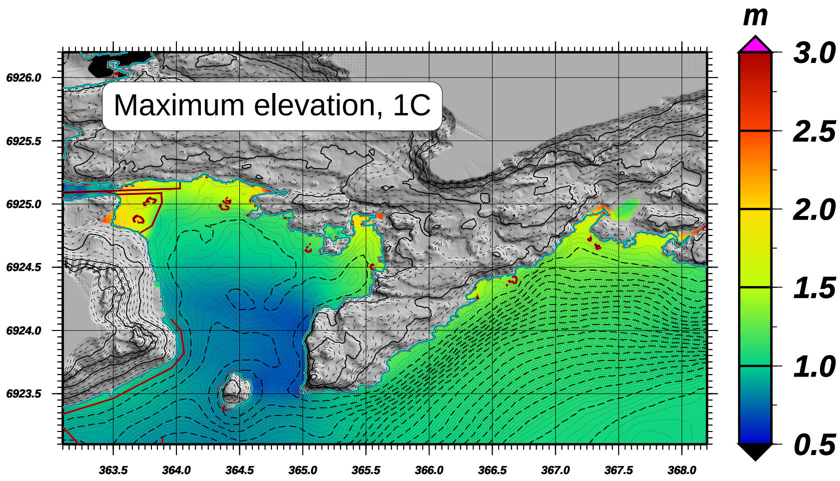

Figure A.119: Maximum water level measured from 0.7 m above today's mean sea level at Vegsundet, scenario 1C. The red line is the shoreline for today's mean sea level (MSL) while the cyan line is the shoreline including the estimated sea level rise of 0.7 m. Coordinates given in UTM32 (km) and gridlines printed every 500 m.

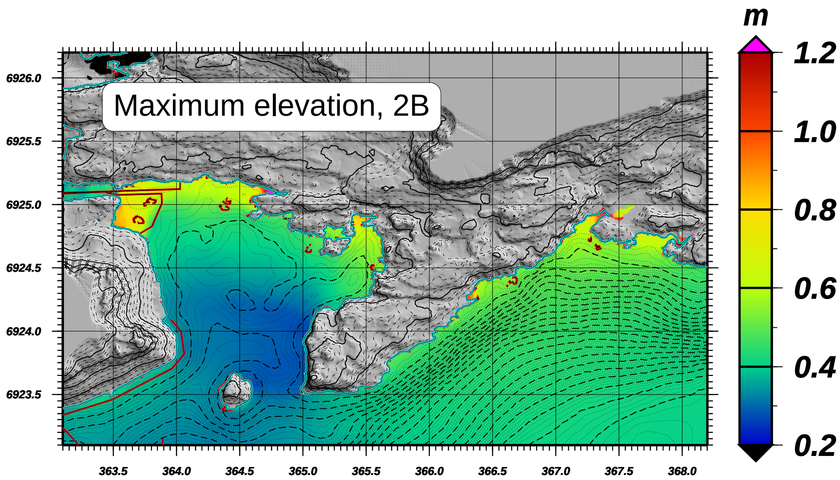

Figure A.120: Maximum water level measured from 0.7 m above today's mean sea level at Vegsundet, scenario 2B. The red line is the shoreline for today's mean sea level (MSL) while the cyan line is the shoreline including the estimated sea level rise of 0.7 m. Coordinates given in UTM32 (km) and gridlines printed every 500 m.

A.3.25 Vika

Location number 8, see Figure A.1.

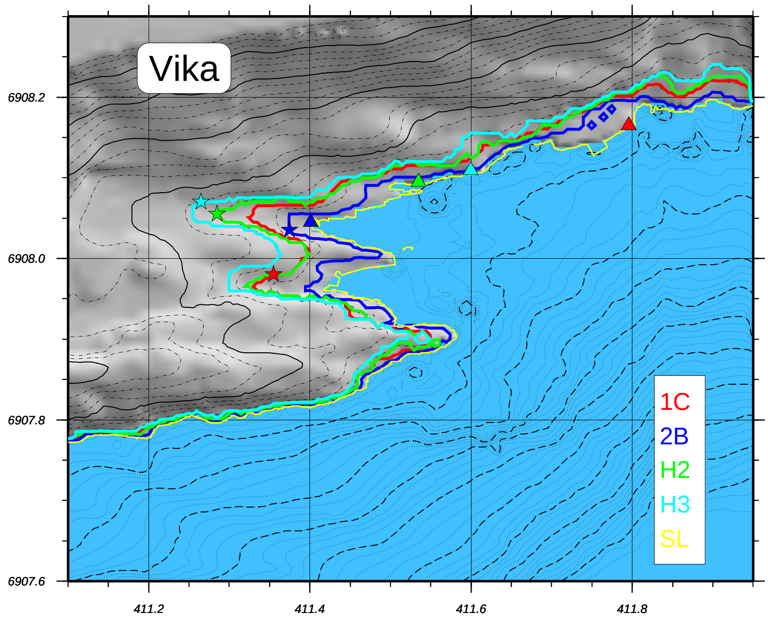

Figure A.121: Trimlines for each scenario at Vika. The highest water level along the shoreline and the maximum run-up is indicated with a triangle and a star, respectively. The yellow line is the shoreline for today's mean sea level. Coordinates given in UTM32 (km) and gridlines printed every 200 m.

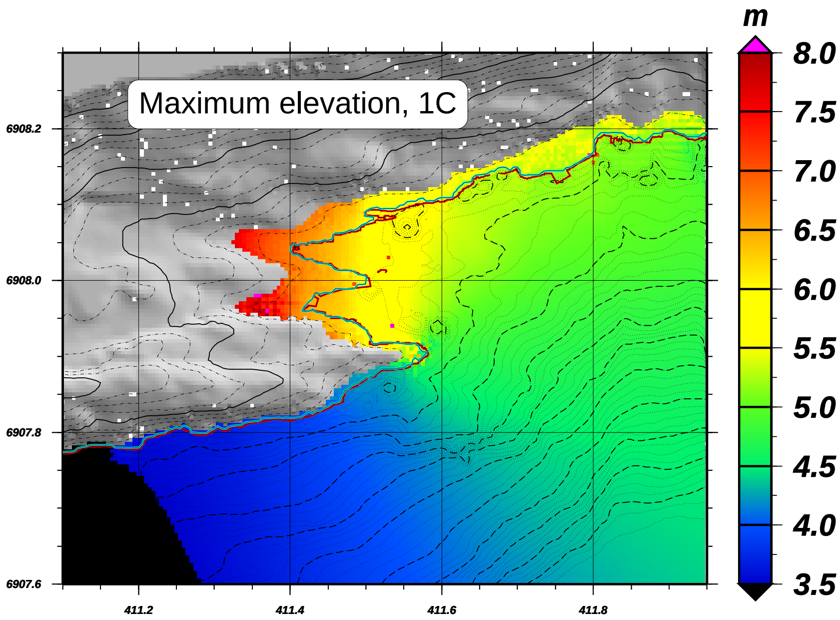

Figure A.122: Maximum water level measured from 0.7 m above today's mean sea level at Vika, scenario 1C. The red line is the shoreline for today's mean sea level (MSL) while the cyan line is the shoreline including the estimated sea level rise of 0.7 m. Coordinates given in UTM32 (km) and gridlines printed every 200 m.

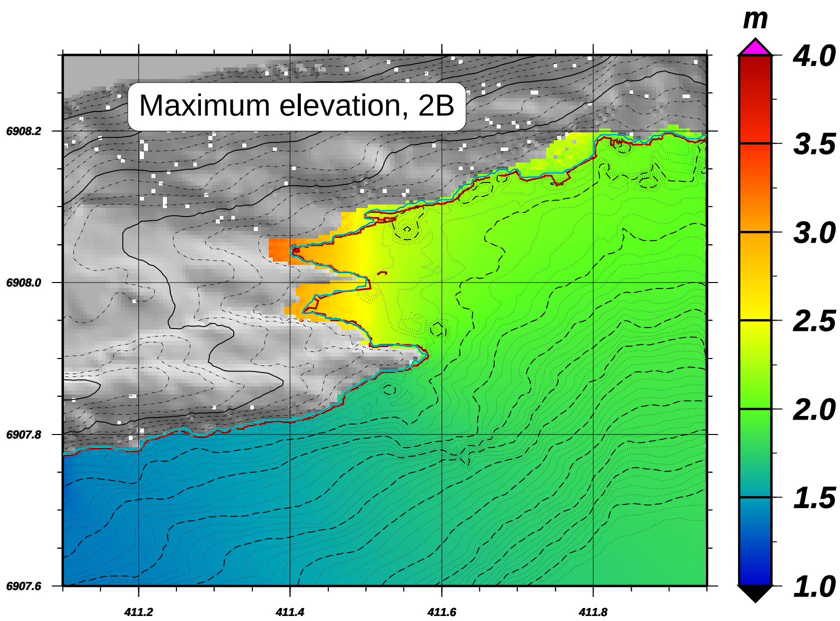

Figure A.123: Maximum water level measured from 0.7 m above today's mean sea level at Vika, scenario 2B. The red line is the shoreline for today's mean sea level (MSL) while the cyan line is the shoreline including the estimated sea level rise of 0.7 m. Coordinates given in UTM32 (km) and gridlines printed every 200 m.

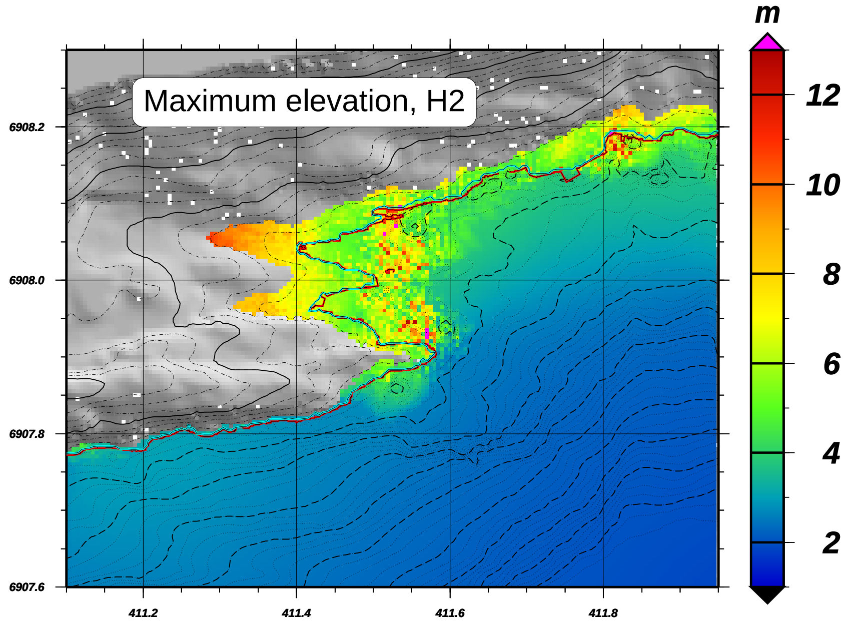

Figure A.124: Maximum water level measured from 0.7 m above today's mean sea level at Vika, scenario H2. The red line is the shoreline for today's mean sea level (MSL) while the cyan line is the shoreline including the estimated sea level rise of 0.7 m. Coordinates given in UTM32 (km) and gridlines printed every 200 m.

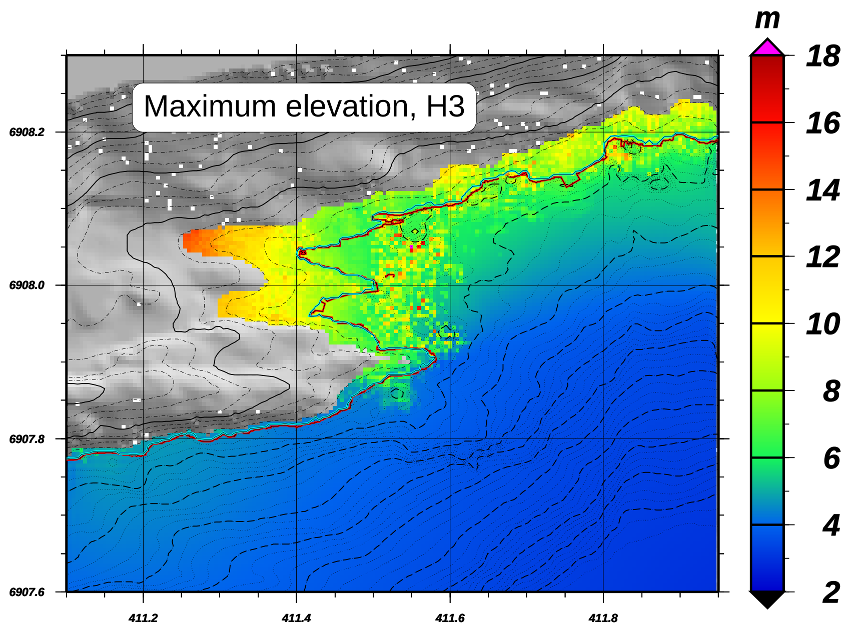

Figure A.125: Maximum water level measured from 0.7 m above today's mean sea level at Vika, scenario H3. The red line is the shoreline for today's mean sea level (MSL) while the cyan line is the shoreline including the estimated sea level rise of 0.7 m. Coordinates given in UTM32 (km) and gridlines printed every 200 m.

A.3.26 Ørskog

Location number 2, see Figure A.1.

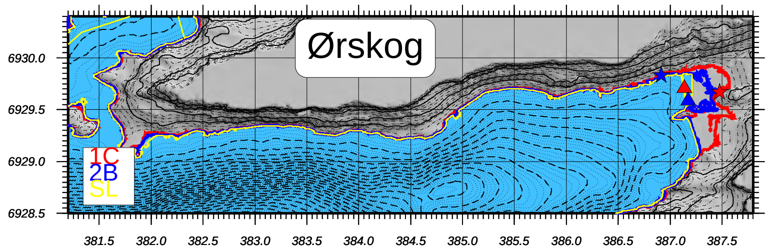

Figure A.126: Trimlines for each scenario at Ørskog. The highest water level along the shoreline and the maximum run-up is indicated with a triangle and a star, respectively. The yellow line is the shoreline for today's mean sea level. Coordinates given in UTM32 (km) and gridlines printed every 500 m.

Ørskog, scenario 1C.

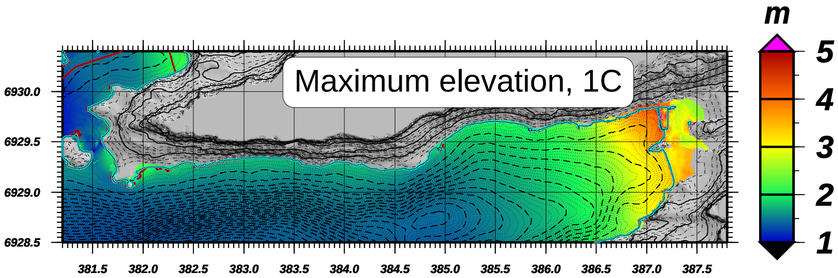

Figure A.127: Maximum water level at Ørskog, scenario 1C. The red line is the shoreline for today's mean sea level (MSL) while the cyan line is the shoreline including the estimated sea level rise of 0.7 m. Coordinates given in UTM32 (km) and gridlines printed every 500 m.

Details at Ørskog for scenario 1C.

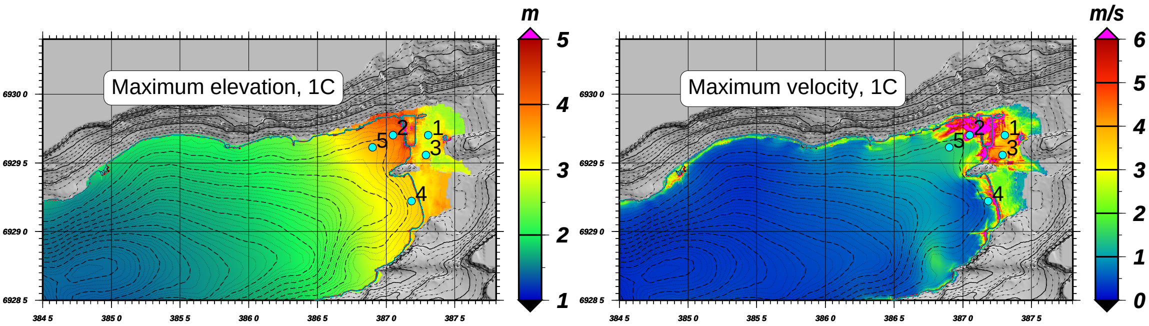

Figure A.128: Maximum water level measured from 0.7 m above today's mean sea level (left) and velocity (right) at Ørskog, scenario 1C. The red line is the shoreline for today's mean sea level (MSL) while the cyan line is the shoreline including the estimated sea level rise of 0.7 m. Coordinates given in UTM32 (km) and gridlines printed every 500 m.

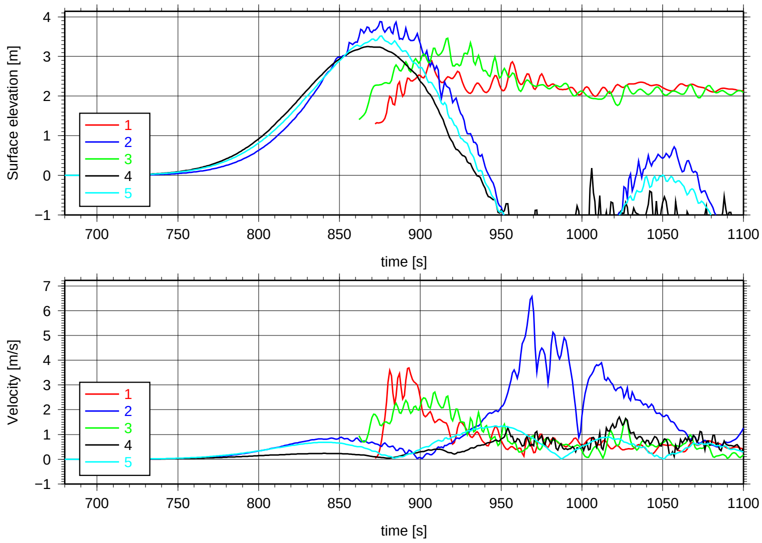

Figure A.129: Time history of the water level (upper panel) and velocity (lower panel - absolute values) measured at gauges 1-5 (see Figure A.128) at Ørskog for scenario 1C. The surface elevation is given in meters, while the velocity is given in meters per second.

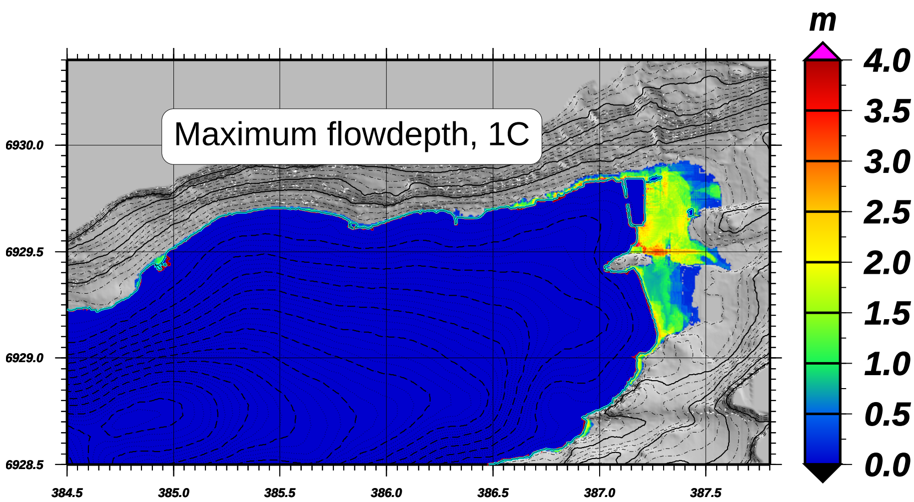

Figure A.130: Maximum flow depth at Ørskog for scenario 1C given in meters. The red line is the shoreline for today's mean sea level (MSL) while the cyan line is the shoreline including the estimated sea level rise of 0.7 m.

Ørskog, scenario 2B.

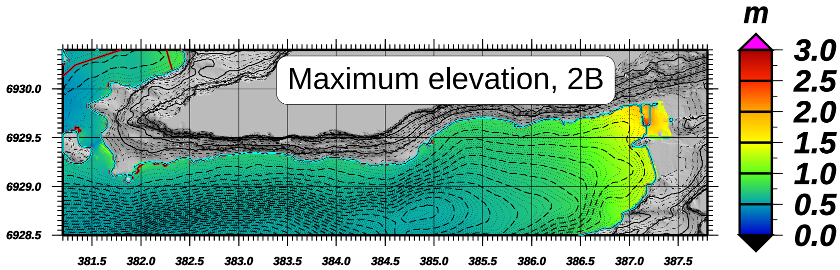

Figure A.131: Maximum water level at Ørskog, scenario 2B. The red line is the shoreline for today's mean sea level (MSL) while the cyan line is the shoreline including the estimated sea level rise of 0.7 m. Coordinates given in UTM32 (km) and gridlines printed every 500 m.

Details at Ørskog for scenario 2B.

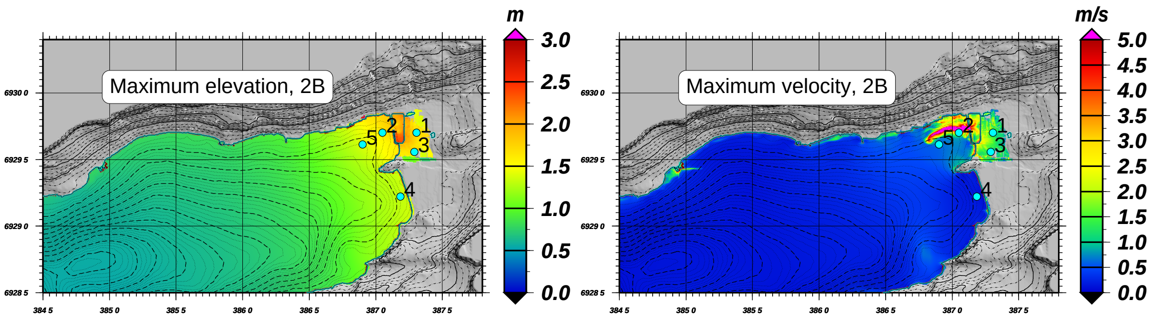

Figure A.132: Maximum water level measured from 0.7 m above today's mean sea level (left) and velocity (right) at Ørskog, scenario 2B. The red line is the shoreline for today's mean sea level (MSL) while the cyan line is the shoreline including the estimated sea level rise of 0.7 m. Coordinates given in UTM32 (km) and gridlines printed every 500 m.

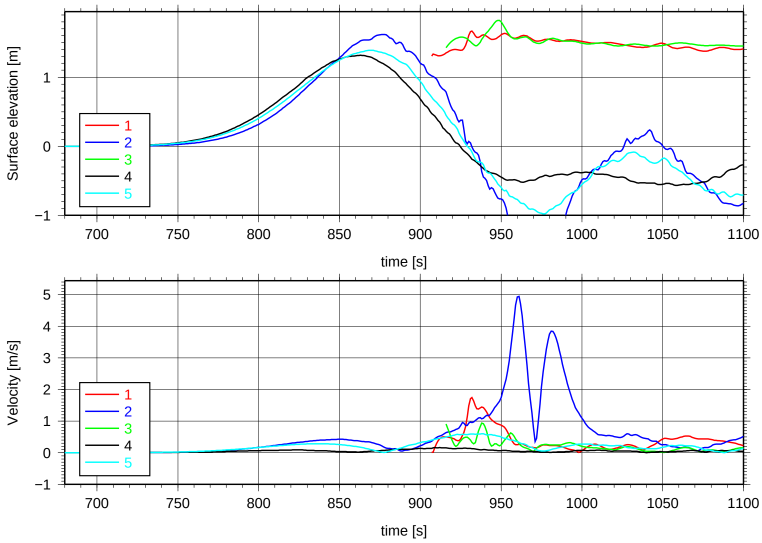

Figure A.133: Time history of the water level (upper panel) and velocity (lower panel - absolute values) measured at gauges 1-5 (see Figure A.132) at Ørskog for scenario 2B. The surface elevation is given in meters, while the velocity is given in meters per second.

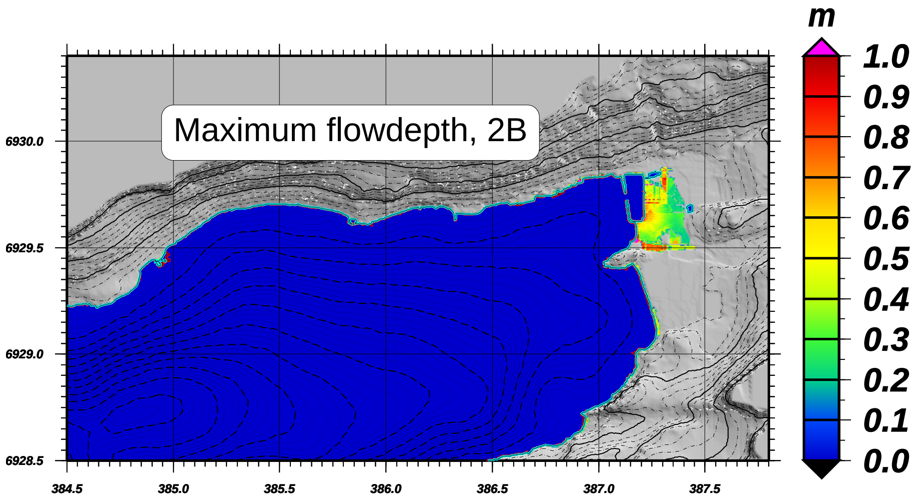

Figure A.134: Maximum flow depth at Ørskog for scenario 2B given in meters. The red line is the shoreline for today's mean sea level (MSL) while the cyan line is the shoreline including the estimated sea level rise of 0.7 m.

Appendix B - Comparisons between the runup-models MOST and GEOCLAW in 2HD

Contents

Abstract

In this report two tsunami inundation models, GEOCLAW and MOST, are compared. Convergence tests for maximum runup in 1HD is performed before we analyze the 2HD inundation heights computed by the two models for a rock slide tsunami in a Norwegian fjord.

For the 1HD test, the models produce similar results for maximum runup. In the tsunami rock slide scenario the leading wave is comparable during runup, but limitations in the MOST model due to water loss and unphysical oscillations associated with high draw-down speeds along steep slopes reduce the confidence in the MOST model with time. The GEOCLAW model handles bores in a better way than the MOST model as the MOST model also introduces unphysical ripples near steep gradients in the surface elevation.

Appendix B

Comparisons between the runup-models MOST and GEOCLAW in 2HD

B.1 Introduction

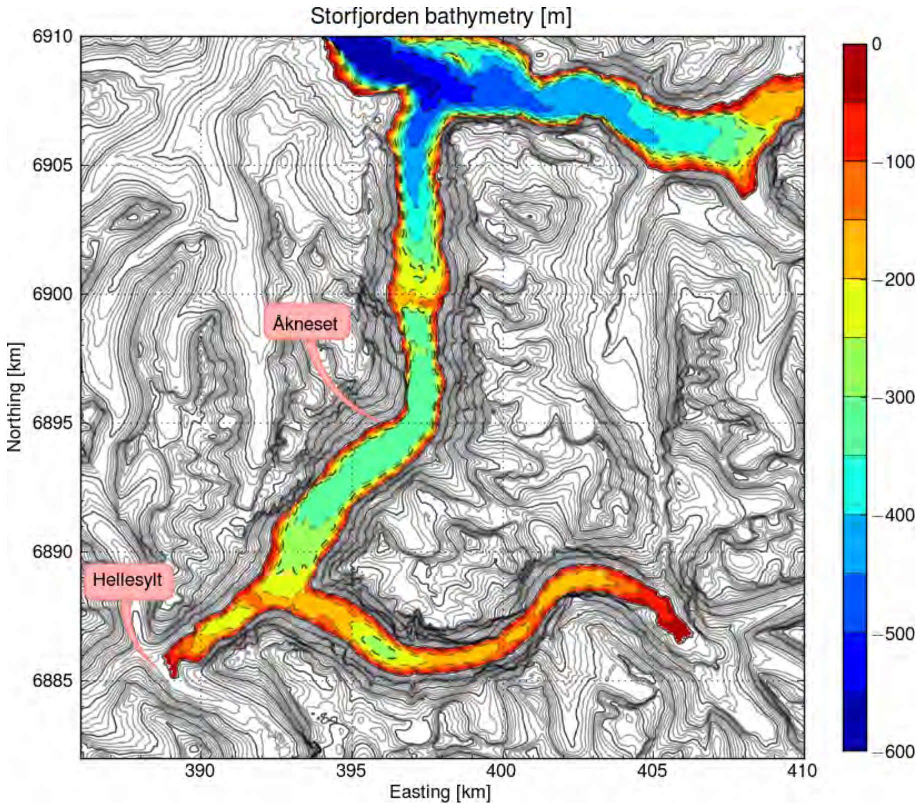

Figure B.1: The topography in the Storfjorden area with a contour line interval of 250 m for the thick lines and 50 m for the thin lines. The bathymetry [m] is colored showing the water depth for the fjord.

The main purpose of this appendix is to compare the tsunami runup models GEOCLAW and MOST. A convergence test is performed in Section C.1 while we compare how the models handle runup in a Norwegian fjord rock slide tsunami in Section B.2.

The tsunami, created by a 42 M m^3 rock slide at Åkneset (see Figure B.1), will propagate and reach Hellesylt after approximately 4 minutes. The comparison in done at Hellesylt. Hellesylt, is a small village of about 250 people, where a school, elder center, and several homes are located very close to the shoreline.

The specific topography at Hellesylt makes it a challenging task to uniquely determine runup. As seen in Figure B.2, the terrain at Hellesylt is like a shelf. Following Transect A there is first a steep slope, then flat terrain at Hellesylt before the steep terrain continues uphill. With this terrain there are several numerical difficulties: First, waves can rapidly amplify and form steep waves in the steep region right outside Hellesylt. Second, even small waves will swiftly flood the whole swash zone (flat area). Third, water will run up the steep slope above the relatively flat swash zone. Small variations in the different flow phases at Hellesylt will influence the calculation of the tsunami making it a challenging task to accurately predict runup heights. Differences in how the tsunami models handle runup can easily be inspected using this scenario.

For this rock slide tsunami scenario the computation is split into several parts. A dispersive and nonlinear long-wave (Boussinesq) model is applied for the generation and propagation stage of the tsunami. Since this particular long-wave model cannot handle runup, the output from this model will be used as input for the two non-linear shallow water (NLSW) models GEOCLAW and MOST, which are both capable of calculating runup.

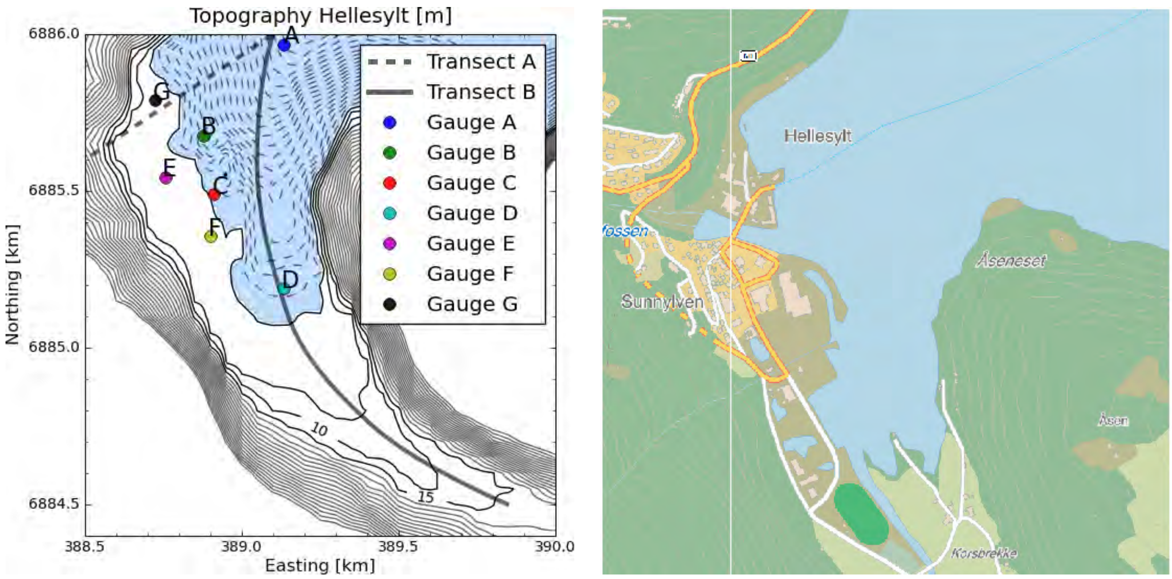

Figure B.2: Left: Topography at Hellesylt with the location of transects and gauges. Contour line interval is 5 m. Right: Map showing Hellesylt and the river valley south of Hellesylt. The populated area is shown as yellow.

B.1.1 Method of Splitting Tsunamis (MOST)

The MOST model [9, 10, 11], developed by Titov and Synolakis, uses an explicit finite-difference scheme, based on the method of undetermined coefficients of the characteristic form of the NLSW equations. The MOST model is known to produce good results and is freely distributed in the ComMIT package [4]. To track the shoreline, Titov and Synolakis [10] introduced a moving shoreline algorithm for non-uniform grids. The velocity of the fluid in the shoreline is extrapolated to determine the movement and the position of the shoreline at the next time step. Grid points are then added or removed so that the computational grid still covers the wet domain, with the moving shoreline being the end point. The model also incorporates handling of bores and wave breaking.

B.1.2 GEOCLAW

The software package GEOCLAW, formerly known as TSUNAMICLAW, and written by George, was an extension of the widely used conservation law package CLAWPACK [3], developed by LeVeque. Now, GEOCLAW can be found as an integrated part of the development version of CLAWPACK 5.0. An early version of GEOCLAW, from October 2008, is applied in this report. Both CLAWPACK and GEOCLAW are written in Fortran 77, they are easy to use and integrate with other software, and the packages are freely available for research use.

GEOCLAW is based on the NLSW equations, and is discretized using a finite volume method with an approximative Riemann solver. The model may handle bores and wave breaking and can apply adaptive grids established by a method for dynamically choosing the most appropriate resolution during the simulation. However the latter facility is not used herein. The numerical method behind GEOCLAW is presented by George and LeVeque [5], while a more complete description can be found in Chapter 6 of George's PhD thesis [6].

The model has been applied to simulate the Indian Ocean Tsunami [5]. Additionally, the TSUNAMICLAW model was bench-marked against the Catalina 04 benchmark # 1 [2] with good results for runup [1, 7] .

In GEOCLAW, a moving bathymetry can be supported by the specification of a time-varying perturbation of the initial bathymetry. In this way, waves emerging from both earthquakes and landslides can be investigated. The model supports both Cartesian and spherical coordinates and bottom friction is incorporated by specifying a Manning friction coefficient.

A front-end script, written in Python, is used to control the GEOCLAW model. Features such as forced boundary conditions and initialization with both velocity and surface data are added to support communication with other models (Boussinesq).

B.2 Runup at Hellesylt in 2HD

B.2.1 The rock slide scenario

The test case used in this simulation corresponds to a modified version of the slide scenario 1A (see main text). The dimensions of the 1A rock slide scenario is: length x width x height = 1000 m x 450 m x 80 m = 36 M m^3. Because of the rounding of the block slide, the applied scenario has a little higher volume of 42 M m^3. The applied scenario also has a slightly changed slide direction and progression, with slightly less run-out than what is defined for the 1A case. The maximum velocity of the slide is 45 m/s with a run-out of 800 m. The direction of the slide was 315° relative to east.

B.2.2 The spatial and temporal computational domain

The computational domain, consisting of 385 by 349 points, is shown in Figure B.3. The results from the shaded region (inspection area) is saved and used in the comparison. We

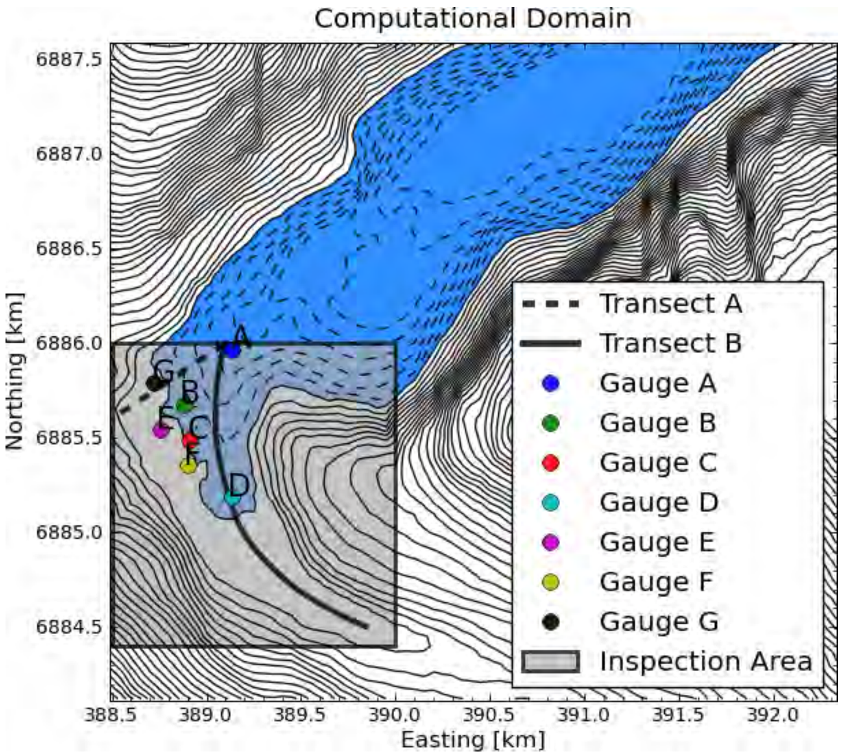

Figure B.3: The extent of the computational domain and the inspection area.

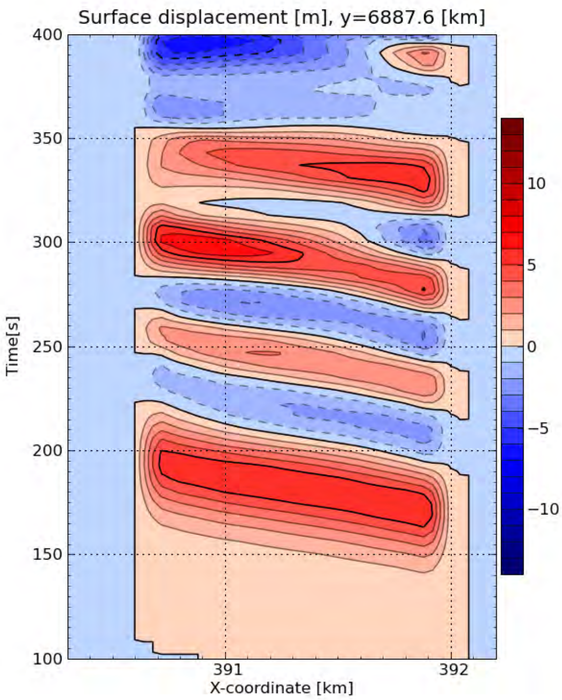

Figure B.4: Surface displacement across the fjord at the northern boundary of the computational domain (y=6887.6) as a function of time.

have used a fixed grid resolution of 10 m for both models. The grid refinement test in Section C.1 suggests that this is a reasonable resolution to use in the comparison of the models. The applied bathymetry has a resolution of 50 m. Nesting was avoided for the MOST model by specifying the same sub-grid at each level. This coarse resolution will give some interpolation effects, but overall it will produce a smoother surface which is essential for the stability of the MOST model (GEOCLAW seems to be less sensitive to this problem). Both models applies exactly the same bathymetry.

At the northern boundary, the surface elevation and the horizontal velocity components are specified as boundary conditions. The surface displacement at the northern boundary as a function of time is shown in Figure B.4. The time is given in seconds after the release of the rock slide. The input signal consists of a series of 5 waves between 3 and 8 meters high and with a period of about 50 seconds.

The simulation covers the full evolution of the wide leading wave as well as the runup of the steeper third incident wave, which enters the computational domain at $t = 300$ s. The simulation is carried out until $t = 460$ s.

B.2.3 Model setup

The results from GEOCLAW and MOST is expected to vary depending on how key parameters are set. We have therefore created an ensemble of cases where the key parameters have been tuned in a parameter sensitivity analysis. The parameters used for the most interesting GEOCLAW cases: GC 1, GC 2, GC 3, GC 4, as well as the MOST cases: MOST 1, MOST 2, and MOST 3 are listed in Table B.1. The parameters will be described in the following subsections while the results are presented in Section B.2.4.

Riemann solvers, time step and CPU time

For the GEOCLAW runs we first used both a first and a second order Riemann solver in time in conjunction with a fixed time step of 0.01 s. The combination of a short time step and a first order Riemann solver is mainly chosen to prevent instabilities caused by draw-down in steep slopes. For very short time steps one can expect much more diffusion (smoothing) when using a first order compared with a second order Riemann solver. This is because second order Riemann solvers are better at capturing the shape of, e.g., shock fronts (here bores). An inspection showed that both Riemann solvers gave very similar and equally smooth results, but they differed in the shape of the primary bore as the first order runs had a dampened and somewhat flattened bore. To better compare against the second order MOST model, we used a second order Riemann solver in GC 1, GC 2 and GC 3, while we used a first order Riemann solver for GC 4 which has the other parameters set equal to GC 2 (see Table B.1). Due to stability issues, the GC 2 run presented here was run with an adaptive time step of maximum 0.01 s, constrained by a given maximum Courant number of 0.1. The other GC runs used a fixed time step of 0.01 s.

The MOST models are run at the default time step of 0.1 s. Although it is possible to run the model with lower time step, it should be avoided since we experienced instabilities at this grid resolution.

If we correct the used CPU time (computer execution time) by the difference in time step we note that the MOST model is about 50 % faster than the GEOCLAW model (for second order and fixed time step).

Shoreline representation

How the shoreline is handled differs between the two models. GEOCLAW consistently includes the dry grid cells in the computation while MOST tracks the shoreline.

The *dry tolerance* parameter in GEOCLAW is used to determine whether a cell is dry or not. If a cell has a depth below the *dry tolerance* value it is considered dry and the water depth is set to zero. This will result in waterloss, and it is therefore important to set a low value, since the drying is done at every time step. Inspections have shown that this value should be set as low as 1 mm, while values lower than this will give stability problems. In the ensemble, GC 1 will suffer from waterloss because of this effect (see Figure B.23).

The *cutoff* parameter in MOST, corresponding to the *dry tolerance* in GEOCLAW, specifies at what depth the last wet point used in the numerical scheme is located. If this value is set too low it will destabilize the numerical scheme since the numerical equations are solved in too shallow regions. In the MOST model, the depth of the last wet point is used to position the shoreline point. How this shoreline point is positioned is well defined for runup [11, 10], but it is not described for the draw-down beyond saying it is done in an analogous manner. Note that draw-down is much more unstable.

Manning friction coefficient

In GEOCLAW, a Manning friction coefficient is applied in cells with depths less than *friction depth*. The default friction coefficient is used in runs GC 1 and GC 3, while the friction is (effectively) turned off in GC 2 and GC 4. The friction coefficient is kept constant in the presented ensemble since the results differed more when changing the above parameters (*dry tolerance* and *friction depth*).

The Manning friction coefficient, n^2, used in MOST is described as a roughness coefficient squared. It is reasonable to believe that the GEOCLAW friction coefficient should be comparable to the roughness coefficient, since the default value (n) is only about 20% larger in MOST (see Table B.1). We have used default friction for MOST 3, while we have tried to reduce the friction n^2 by a factor 0.1 for MOST 1. The Manning friction should be thought of as a stabilizing term with a physical pretext since it is very important for damping unphysical waves in the MOST runs. In MOST 2 the friction value has been set corresponding to the friction value used in the GC runs.

At the web page "Manning's n Pictorial" [8], one can compare the different terrain and conditions for a Manning roughness coefficient in the range of $n = 0.024$ to 0.075. The default parameters in GEOCLAW and MOST seems reasonable.

			GEOCLAW Parameters				
		CPU [min]	dx [m]	dt [s]	dry tolerance [m]	friction depth [m]	friction coefficient n
GC 1	$\mathcal{O}(2)$	165	10	0.01	0.01	20	0.025 ($0.025^2 = 0.000625$)
GC 2	$\mathcal{O}(2)$	250	10	0.01*	0.001	0.1	0.025
GC 3	$\mathcal{O}(2)$	165	10	0.01	0.001	20	0.025
GC 4	$\mathcal{O}(1)$	135	10	0.01	0.001	0.1	0.025

			MOST Parameters				
					cutoff [m]		roughness coeff squared n^2
MOST 1	$\mathcal{O}(2)$	11	10	0.1	0.05		0.0001 ($n = 0.010$)
MOST 2	$\mathcal{O}(2)$	11	10	0.1	0.05		0.000625 ($n = 0.025$)
MOST 3	$\mathcal{O}(2)$	11	10	0.1	0.05		0.0009 ($n = 0.030$)

Table B.1: Simulation parameter values. (GC 1: waterloss, GC 2: no friction, GC 3: most physical, GC 4: GC 2 with first order Riemann solver, MOST 1: heavily reduced friction, MOST 2: GC friction, MOST 3: default friction). The asterisk, *, means that adaptive time stepping was used, the maximum time step is indicated.

B.2.4 Results

In the following subsections we will present the maximum surface elevation and inundation height of the tsunami from the MOST and GEOCLAW runs. The parameters for the runs are the ones specified in Table B.1. The surface elevation is presented as time-series at Gauges A, B, C, D, E, F, and G. To better visualize the effect of the topography, we also present the results along two transects: one across the shelf (A) and one along the southern river valley (B), as snapshots in time. The extent and inundation height of the tsunami is presented using surface maps for the inundated regions at given times. We also present the maximum inundation heights, extent, and velocities that occurred. The unphysical waterloss is presented as time-series.

Surface elevations along transects A and B

In this subsection we will present the surface elevation and inundation height along Transect A and Transect B. The most important topics discussed will be wave shape, bore propagation (including wave speeds), ripples in the MOST runs, and instabilities due to draw-down. In Figures B.5-B.8 the surface elevation is presented for the given times while the maximum and minimum surface elevation that occurred during the simulation is presented in Figure B.9.

For the transect plots, the bathymetry of the underwater slope is not plotted for the whole transect. But by inspecting Figures B.2 and B.3 we see that the slope for the underwater section of Transect A has the same steepness all the way while it steepens inside the depth of 25 m for Transect B.

Until the leading wave climbs the shelf of Transect A, at $t = 240$ s, the surface elevations are close for all the runs (similar to Transect B at $t = 270$ s in Figure B.5).

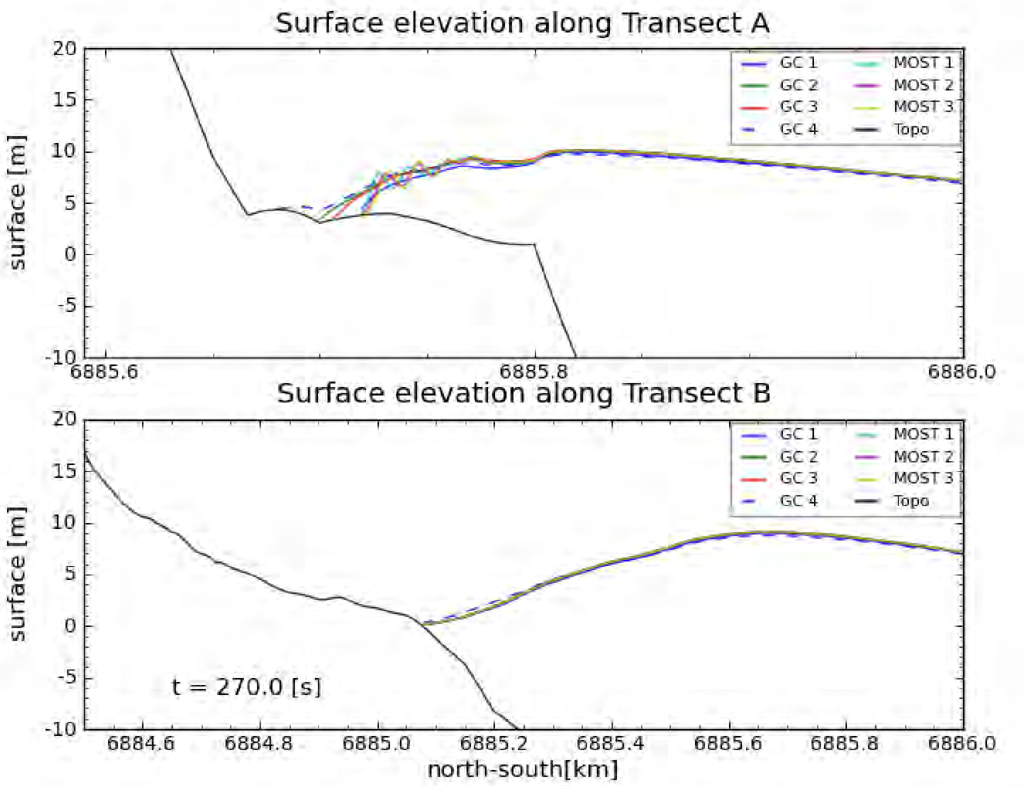

Figure B.5: Transect plots at $t = 270$ s. The topography along the transects is plotted as black line, while the each model run is plotted by the color shown in the legend. Note the difference in the horizontal scale as the range in the north-south coordinate is 400 m along Transect A and 1500 m along Transect B.

From Figure B.5 we see, for Transect A, that the GEOCLAW runs are preceding the MOST runs with the exception of GC 1, which already has lost a lot of water. The MOST runs are steeper and have at this time ripples with a wave length corresponding to the width of two grid cells (20 m). The ripples appear at the tip of the bore and propagate seaward away from the bore with time. GC 4, the first order version of GC 2, have a smooth wave front ahead of all the second order runs. For Transect B all runs are close to identical.

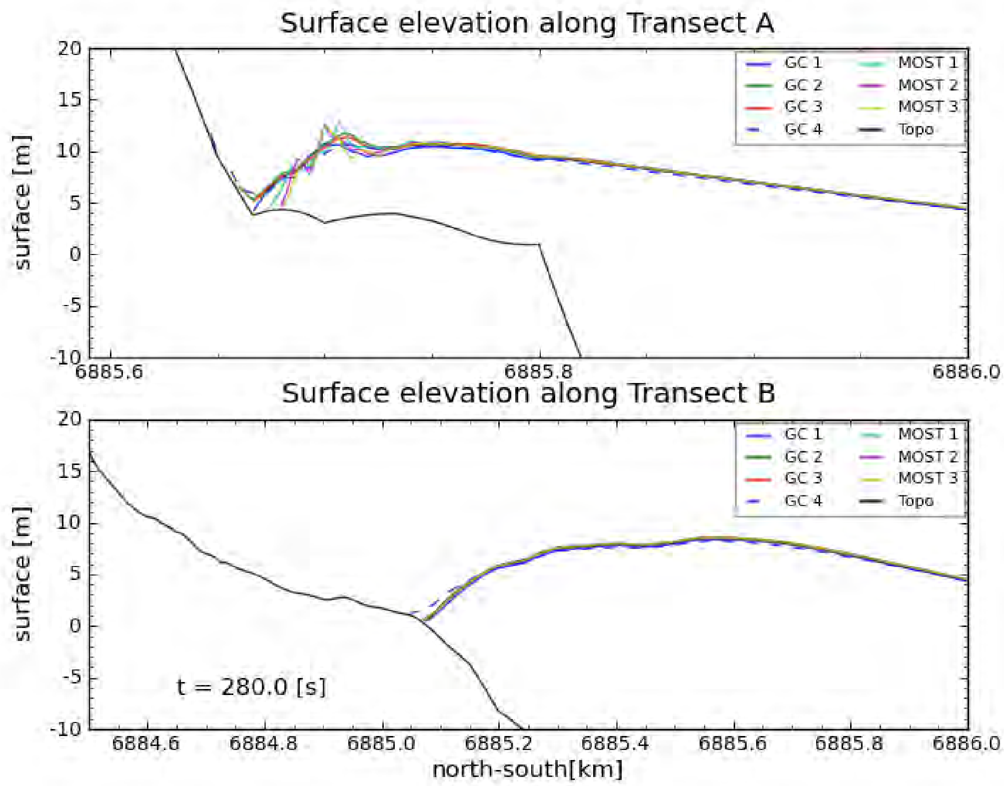

Figure B.6: Transect plots at $t = 280$ s. See Figure B.5 for further explanation.

Along Transect A in Figure B.6 we see that the GC runs are leading. All MOST runs have ripples which are about 2 meters higher than the smoother GC 2 and GC 3 surface elevations. Additionally, the MOST runs have a steeper front with more water contained in a smaller region. This can partly explain maximum inundation differences at later stages (see Figure B.9). Along Transect B the results are still very similar, with the exception of the leading first order run (GC 4). Here, runup is just starting.

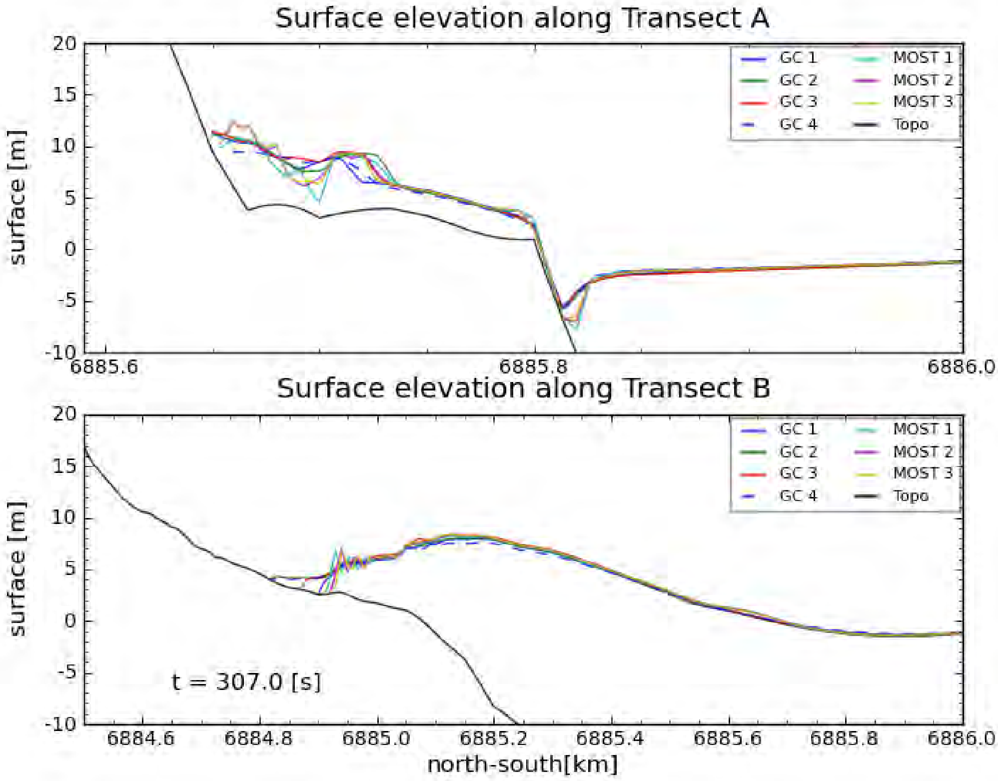

Figure B.7: Transect plots at $t = 307$ s. See Figure B.5 for further explanation.

In Figure B.7, most runs along Transect A are withdrawing from their maximum runup heights. A transect plot with maximum surface elevations and inundation heights, Figure B.9, are presented later because the wave will reach its highest point at different times for the different runs. However, the interesting part of Figure B.7 is the draw-down at the north-south coordinate of 6885.8 km. Here the GEOCLAW runs and MOST runs are clustered at separate troughs, which indicates that the MOST model has higher draw-down velocities, leading to a stability problem at later times, because of the high velocities in the very thin water layer. Spurious oscillations in the water surface will later appear for the MOST runs because of the violation of the Courant Friedrich Levy-stability criterion (CFL). The stability problem for MOST can also be linked to the bore formation at draw-down. The location of maximum draw-down will be at about the same location for all runs at a later time with the exception of MOST 3 (see Figure B.9).

Along Transect B we again see that the wave front is travelling faster in the GC runs with the exception of GC 1 (presumably related to volume loss). GC 2 and GC 4 are ahead of GC 3 (similar wave form, but with a broken wave tip), this is most likely due to friction differences.

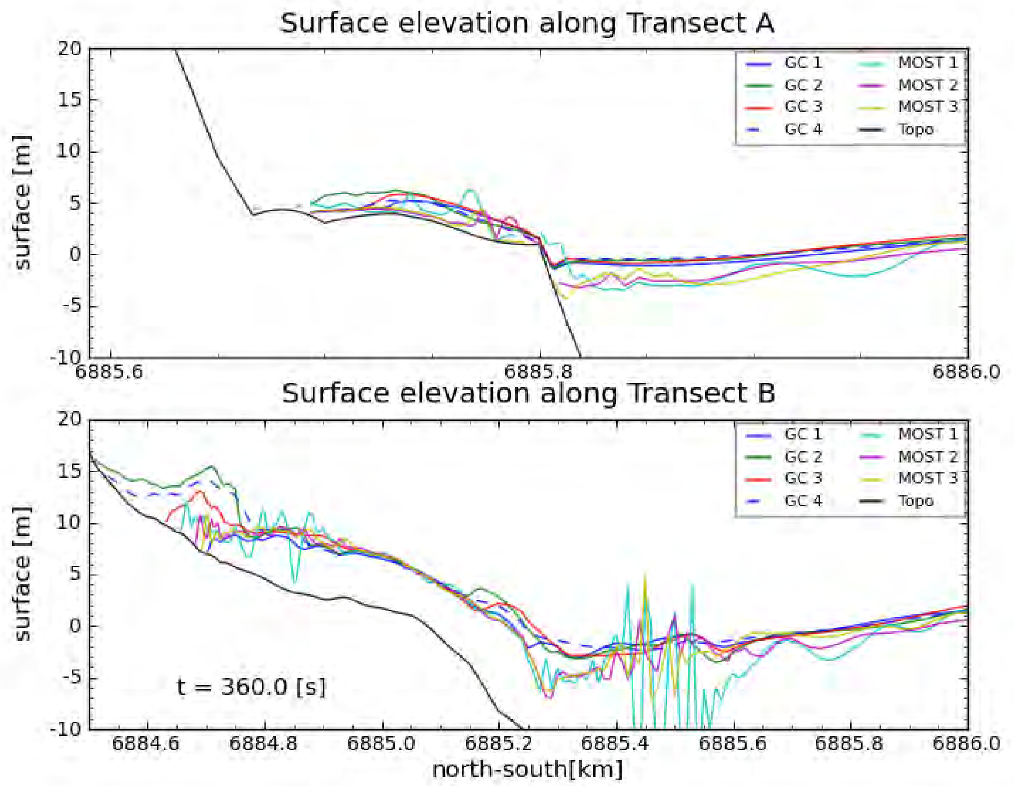

Figure B.8: Transect plots at $t = 360$ s. See Figure B.5 for further explanation.

Along Transect B in Figure B.8 it should be noted that MOST 1 has followed GC 3 remarkably well. GC 2 and GC 4, which are run effectively without friction will continue to runup for some time, while the others will soon stop.The peak in the GC runs (y=6884.7), especially evident at this time step, is caused by the combination of the narrowing channel effect (focusing) and the interference with the reflections from the first wave along Transect A.

Stability issues can be seen as oscillating waves in the MOST model. At the time step of Figure B.8, MOST 1 (with the lowered Manning friction) is close to blowing up. This part of the transect is located very close to the steep slope outside Gauge C (see Figure B.2).

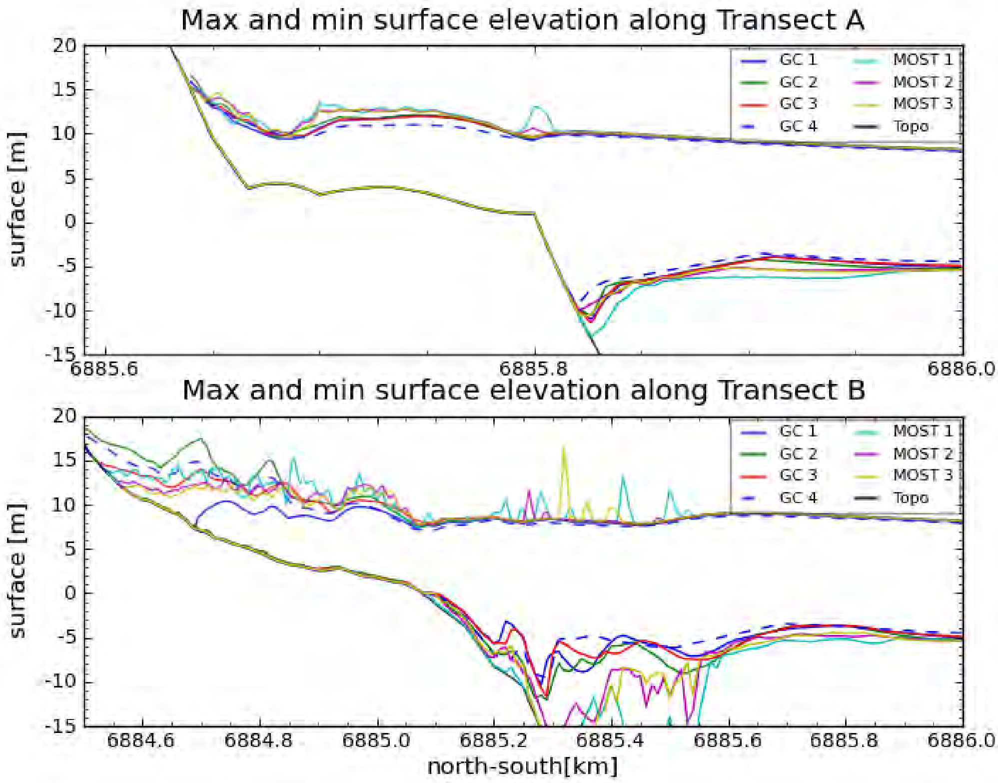

Figure B.9: The maximum and minimum surface elevation and inundation height along transects A and B that occurred over the time interval. See Figure B.5 for further explanation.

In Figure B.9, the temporal extreme values are presented ($\eta_{max}(x) \equiv {}^{max}_{0\leq t\leq T}\eta(x,t)$). If we inspect maximum runup (shoreline edge in plot) along transect A, we realize that the runup results are very similar for all runs. The inundation height for GC 4 is lower than the others since the wave height was lower. The higher maximum inundation values along Transect A can be prescribed to the effect of the ripples in the MOST runs.

For all runs the maximum draw-down location along Transect A is identical with the exception of MOST 1 (low friction), that probably had higher draw-down velocities. It is clear that friction is necessary to stabilize the MOST model. For the GC 2 and GC 4 runs, friction was only applied in cells with depths less than 10 cm. This was evidently enough to dampen the increasing draw-down velocities, giving the same maximum draw-down location as GC 1 and GC 3.

For longer inundation distances, effects such as friction and waterloss is more important. The relatively gentle inclination along Transect B compared to the steep part of Transect A and the longer inundation distances could be the reason why the GC runs (except GC 1) have higher runup than the MOST runs along transect B. The low runup heights for GC 1 along Transect B are likely due to waterloss, as will be shown in Figure B.23.

The peaks along the upper parts of Transect B, especially evident for the GC runs, appear simultaneously with the interference from the reflected waves, while the high runup heights can be an effect of focusing due to the narrowing of the valley.

Lower draw-down velocities, associated with the gentler slope reduces the drying of the seabed along Transect B for all runs except MOST 1. The oscillations linked to the minimum surface elevation for all the MOST runs in transect B are artificial since the solutions are contaminated by the unphysical oscillations further north. It should be noted that this part of Transect B is located below a steep draw-down area for flow in the transverse direction.

Gauges A, B, C, D, E, F and G

In this subsection we present the surface elevation as time-series at given locations (synthetic gauges). In this way the characteristics and magnitude of especially the leading (largest) wave and reflected wave can be inspected. The location of the gauges can be seen in Figure B.2 while the time-series are shown in Figure B.10.

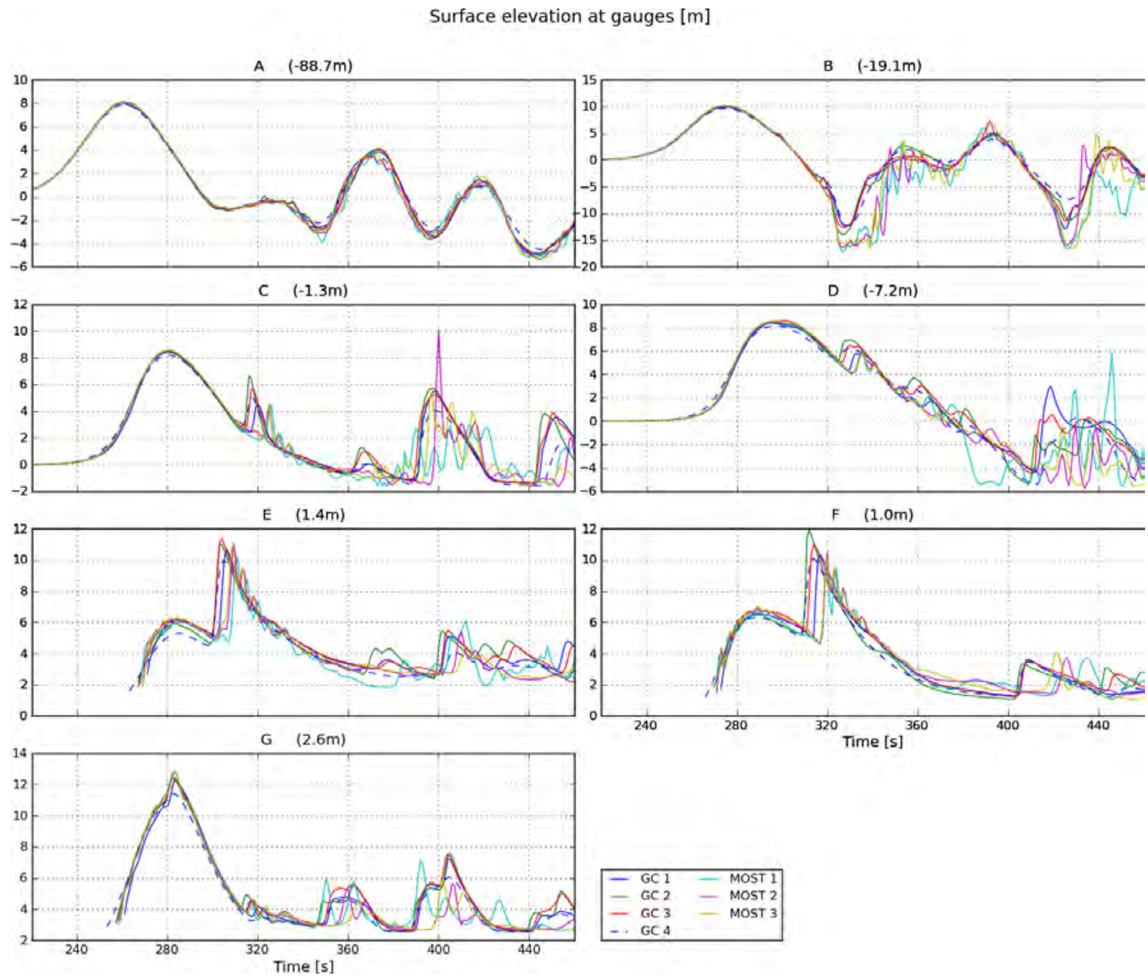

Figure B.10: Computed time-series at the gauge locations. The water depths at the gauges are given next to the gauge names in the plot titles.

Gauge A, located offshore at a depth of 90 m near the start of both transects, has very similar results for all runs. The amplitudes for the most pronounced waves are 8, 4, and 2 m, respectively. At the end of the time-series the MOST runs differ slightly at the third wave crest. We believe this is due to the numerical noise generated from the draw-down of the reflected first wave.

At Gauge G, located just north of Transect A, the incident wave approaches along a direct line, parallel to the topography gradient, from Gauge A. The leading wave has here steepened and the wave amplitude has increased to almost 13 m (overestimated due to overriding ripples) for the MOST runs and 12.5 m for the second order GC runs. GC 4 has a maximum amplitude of only 11.5 m as the bore shape is more diffused for this first order run. GC 1 is delayed, probably due to waterloss.

Inspecting Gauges E and F, one can clearly see that the initial wave is steeper in the second order runs compared to GC 4 (which is a first order version of GC 2). The waves in the MOST runs appear almost as a bore and one can clearly see the ripples on the sea surface that appears right after the initial wave at $t = 270$ s. It should also be noted that these gauges are located very close to the initial shore and on an almost horizontal surface. Hence, the reflected (almost vertical) wave is clearly steeper and higher than the incident wave, and we can assume that the reflected bore is formed from propagation in the relatively flat swash zone. An inspection using a movie supports this assertion. The reflection waves for GC 2, GC 3, and GC 4 are leading with about 10 s, but the shape is very similar to MOST 1, 2, and 3.

At Gauge C, the solutions appear to be quite similar until the reflections of the first wave passes just before $t = 320$ s. The lower amplitude of the reflection wave may indicate waterloss for GC 1 and the MOST runs. There is also a time shift between the MOST and the GC runs.

For Gauge B, located close to the draw-down area for Transect A, we see that the MOST runs are much closer to running dry (at $t = 325$ s), and that oscillations appear afterwards.

We will now discuss the amplification of the incoming waves due to shoaling. Comparing the leading wave at gauges A and C, we see that the leading wave (8 m) has steepened but not increased in height as the bore is not yet formed. The third and fourth incident wave at gauge A, with respective wave heights of 4 and 2 m, will form a steep wave (bore) before entering gauge C, where the wave height has increased to 6 and 4 m, respectively, for the GC 3 run.

We note that the simulation stops when the fourth incident wave from Gauge A enters Gauge C.

Comparison of surface data

In this subsection we will present surface plots showing the inundated region from time $t = 270$ s until $t = 440$ s (see Figures B.11-B.17). The MOST 2 run is omitted since the result was very similar to MOST 3 (see Figure B.19).

At $t = 270$ s (Figure B.11) it appears that the wave right outside the shoreline is slightly lower for GC 4. By inspecting Figure B.10 for Gauge A and B one can see that the difference is small, but still noticeable. GC 4 also inundates a larger area.

At time $t = 280$ s (Figure B.12) GC 4 has slightly lower wave amplitudes north of Transect A. Just south of Transect A both GC 2 and GC 4 are already climbing up to the 10 m contour in the slope west of the flat area, and more of the flat area is inundated. GC 4 has a slightly more advanced wave front along Transect B. For the MOST runs one can start to see ripples (high frequency signal) on the flat area that are about 4-5 grid cells wide. These ripples are not caused by draw-down since that happens later.

Around time $t = 290$ s (Figure B.13) the maximum runup heights occur for all the runs. The GC 4 run has climbed to 15 m.a.s.l. (meters above sea level) while the others have climbed to 20 m.a.s.l. south of Transect A in the western slope. It appears that second order numerical schemes are required to adequately describe the climbing of the wave onto steeper hill sides.The results for GC 3 and MOST 1 are very similar, despite the difference in friction. The ripples in MOST seem to be a little damped compared to the previous figure.

At time $t = 320$ s (Figure B.14) the MOST runs are comparable to the default friction GC runs (GC 3 and GC 1). GC 2 and GC 4 are far ahead along Transect B, while GC 1 seems to have lost some momentum due to volume loss (Figure B.23). The ripples in the MOST runs are now evident with a wavelength of about 50 m. There are also dry regions just outside Gauge C for all MOST runs, but the surface still looks smooth.

Around time $t = 360$ s (Figure B.15) the GC runs hit the slope east of Transect B. This can be seen by the peak in the inundation heights in the reflected wave located along the steeper slope in the southern river valley. MOST 1 and MOST 3 now have oscillations near Gauge C. GC 2 and GC 4 have the highest runup along the southern river valley, while the MOST runs have a surface inundation lying between GC 1 and GC 3. It should be noted that GC 3 has a slightly more advanced wave front and a larger flow depth than MOST 1.

10 seconds later (Figure B.16), the wave is reflected back from the east slope in the GC runs. The third incident wave can be seen near the start of the transects. At $t = 440$ s (Figure B.17) all runs are at or beyond the time of maximum runup heights. In the GC 1 run the water loss is evident. The third incident wave has reached the runup height of 10 m in the GC runs.

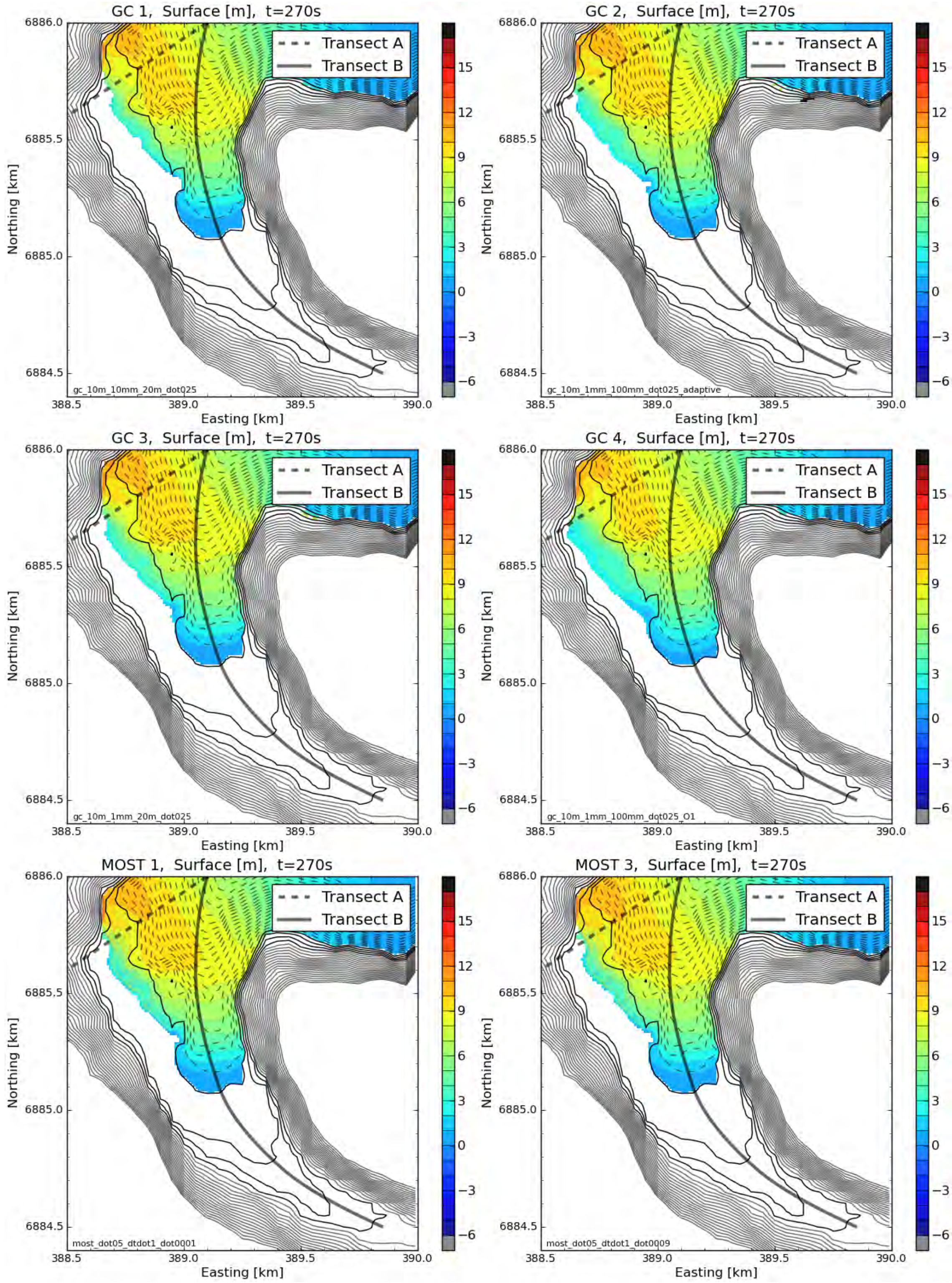

Figure B.11: Surface elevation and inundation height at t = 270 s, plotted in the wet region (color bar in meters). Data outside the color map range is plotted with black for overshooting and grey for undershooting values. The topography is plotted using 5 m contour lines. Dashed lines show negative depths while the 0, 5, 10, and 15 m level is plotted with a thicker line. The title gives the run name and the model time.

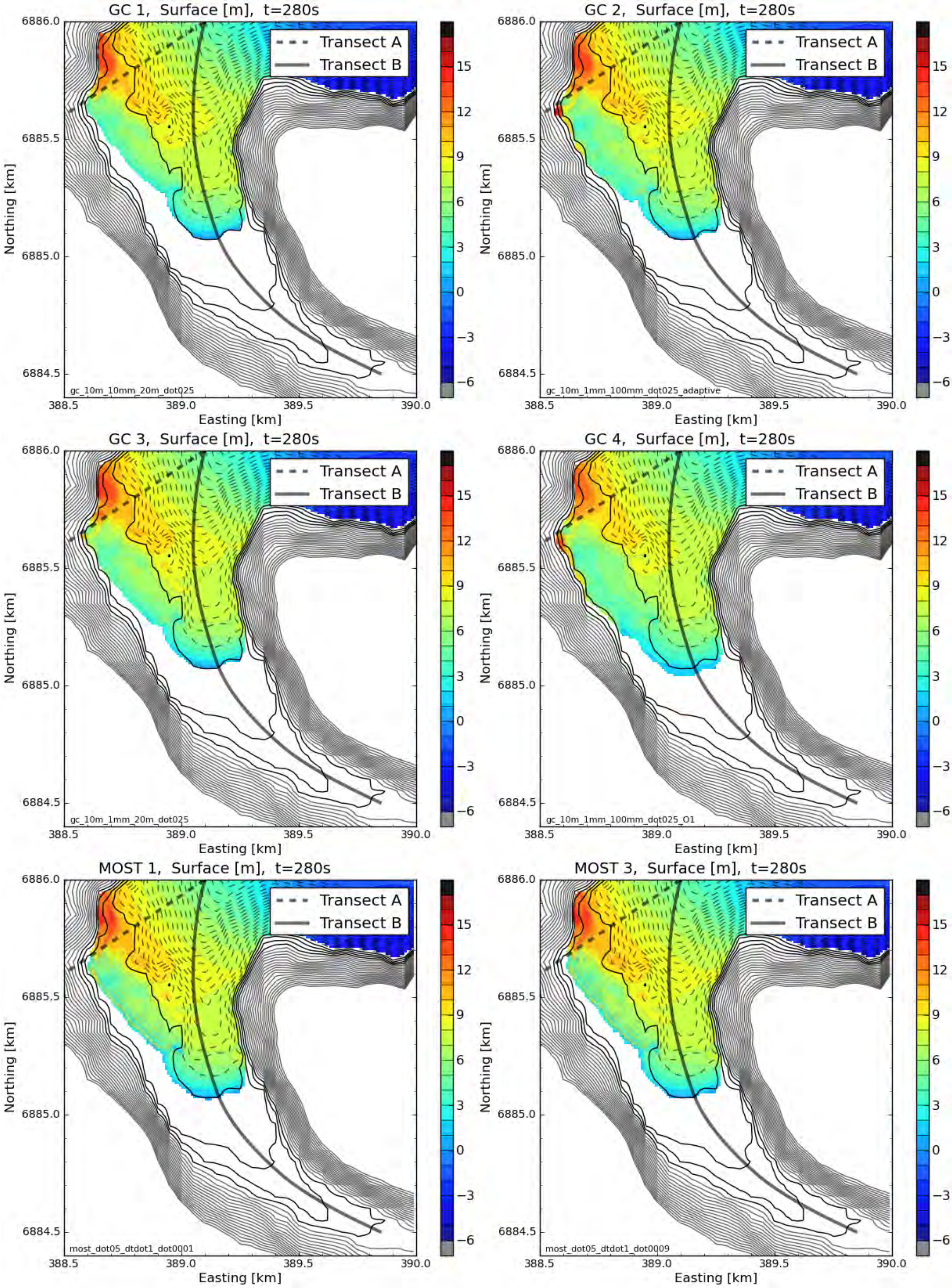

Figure B.12: Surface elevation and inundation height at $t = 280$ s. See Figure B.11 for further description.

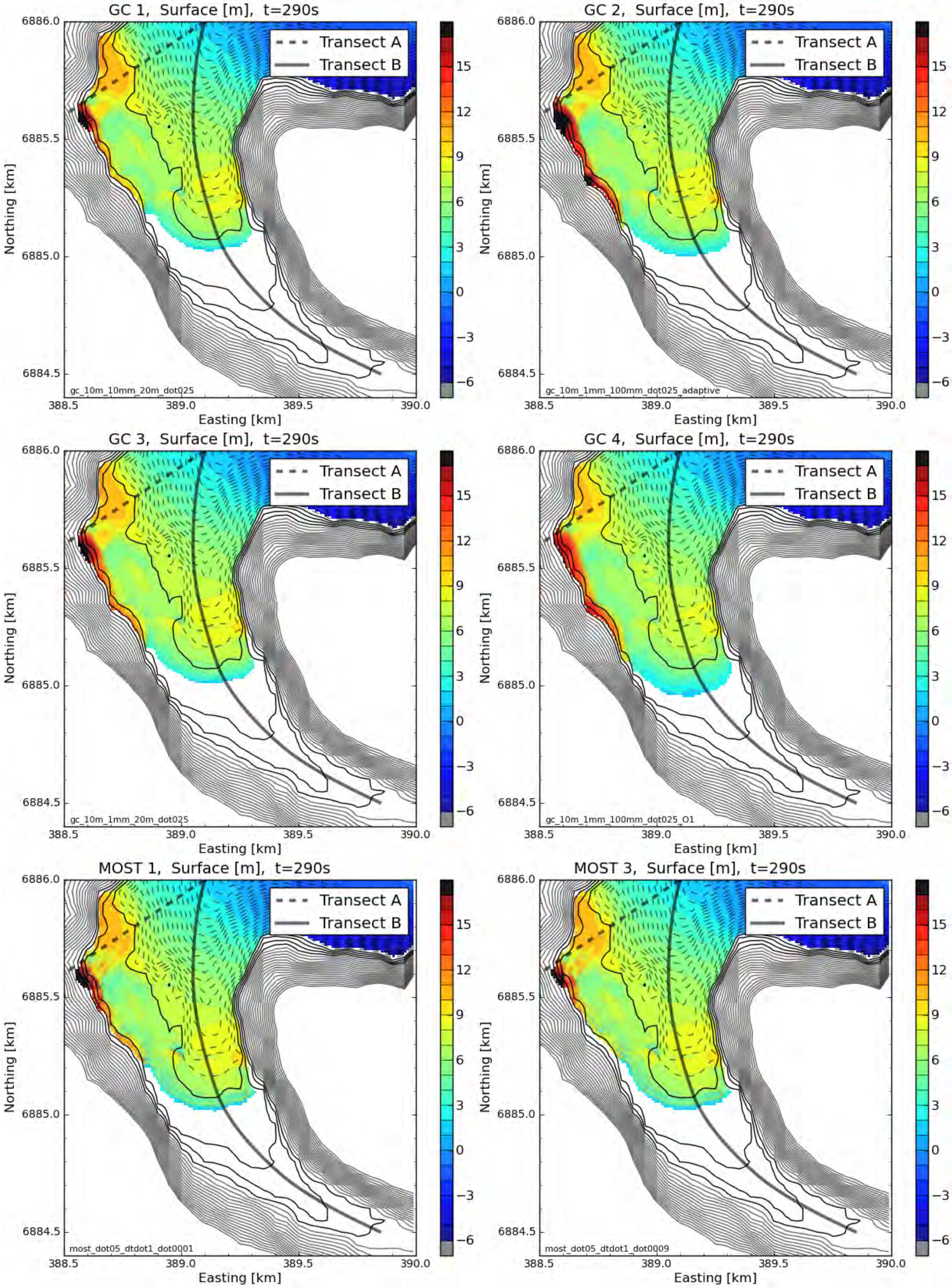

Figure B.13: Surface elevation and inundation height at $t = 290$ s. See Figure B.11 for further description.

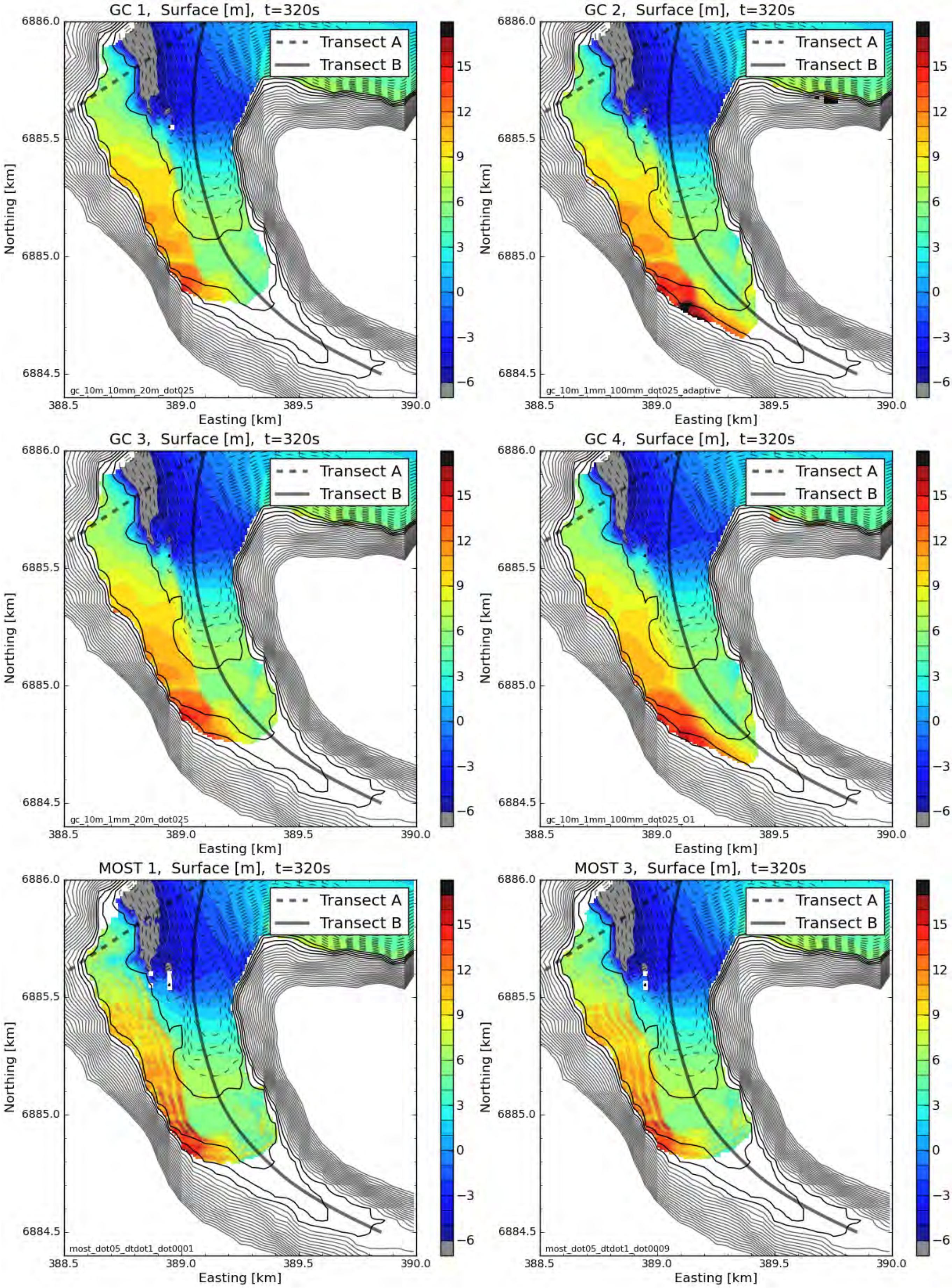

Figure B.14: Surface elevation and inundation height at $t = 320$ s. See Figure B.11 for further description.

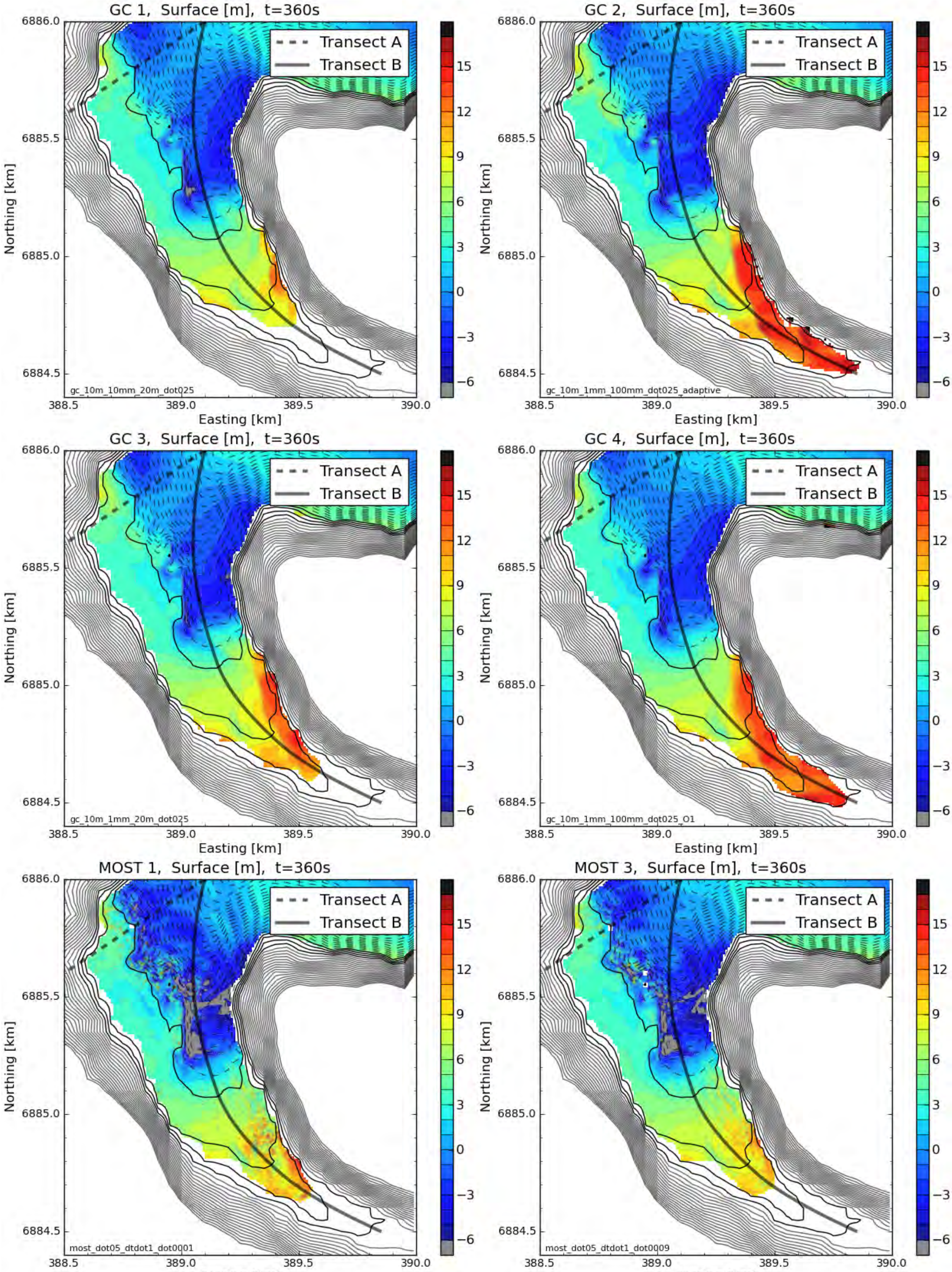

Figure B.15: Surface elevation and inundation height at $t = 360$ s. See Figure B.11 for further description.

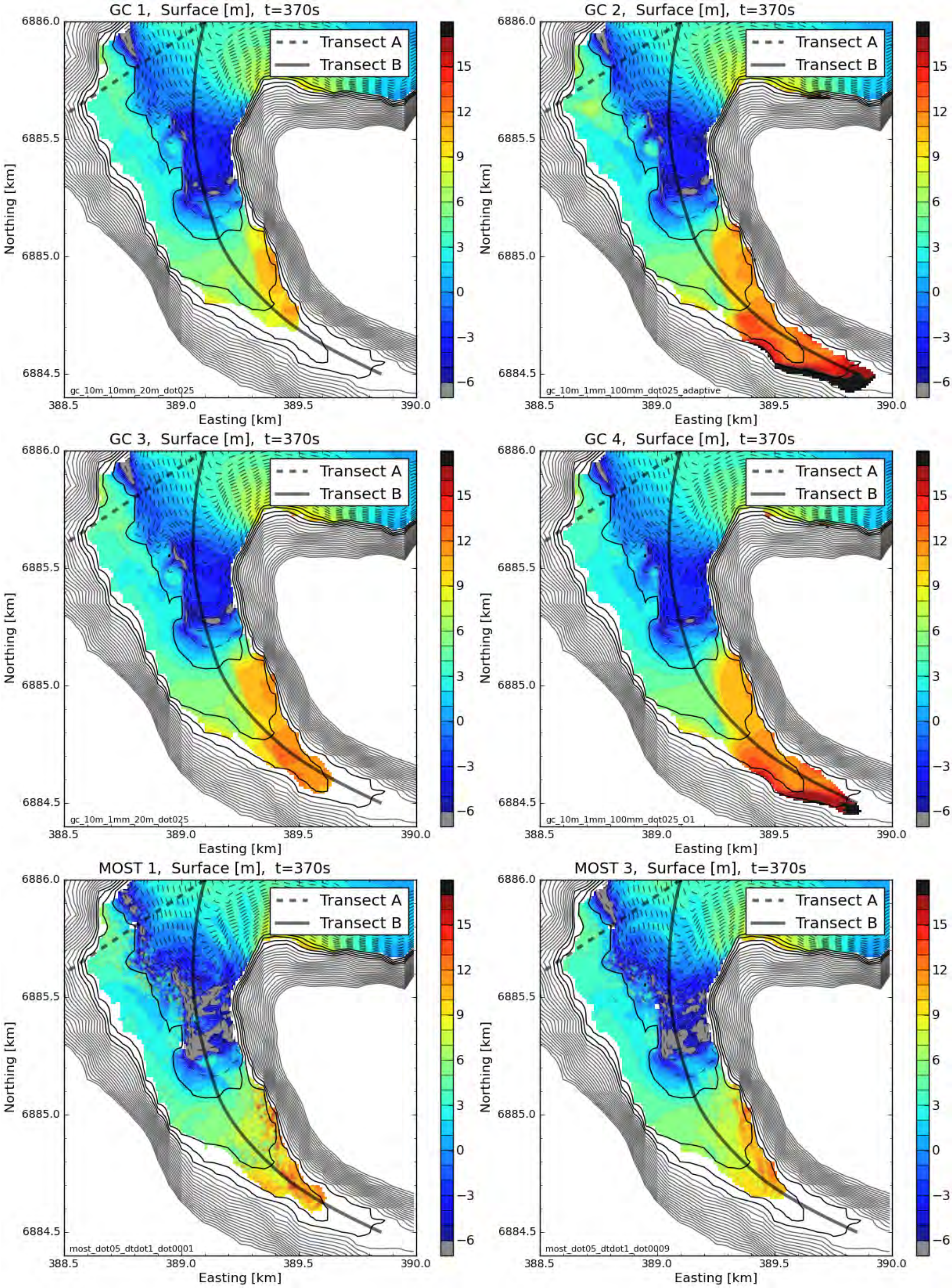

Figure B.16: Surface elevation and inundation height at $t = 370$ s. See Figure B.11 for further description.

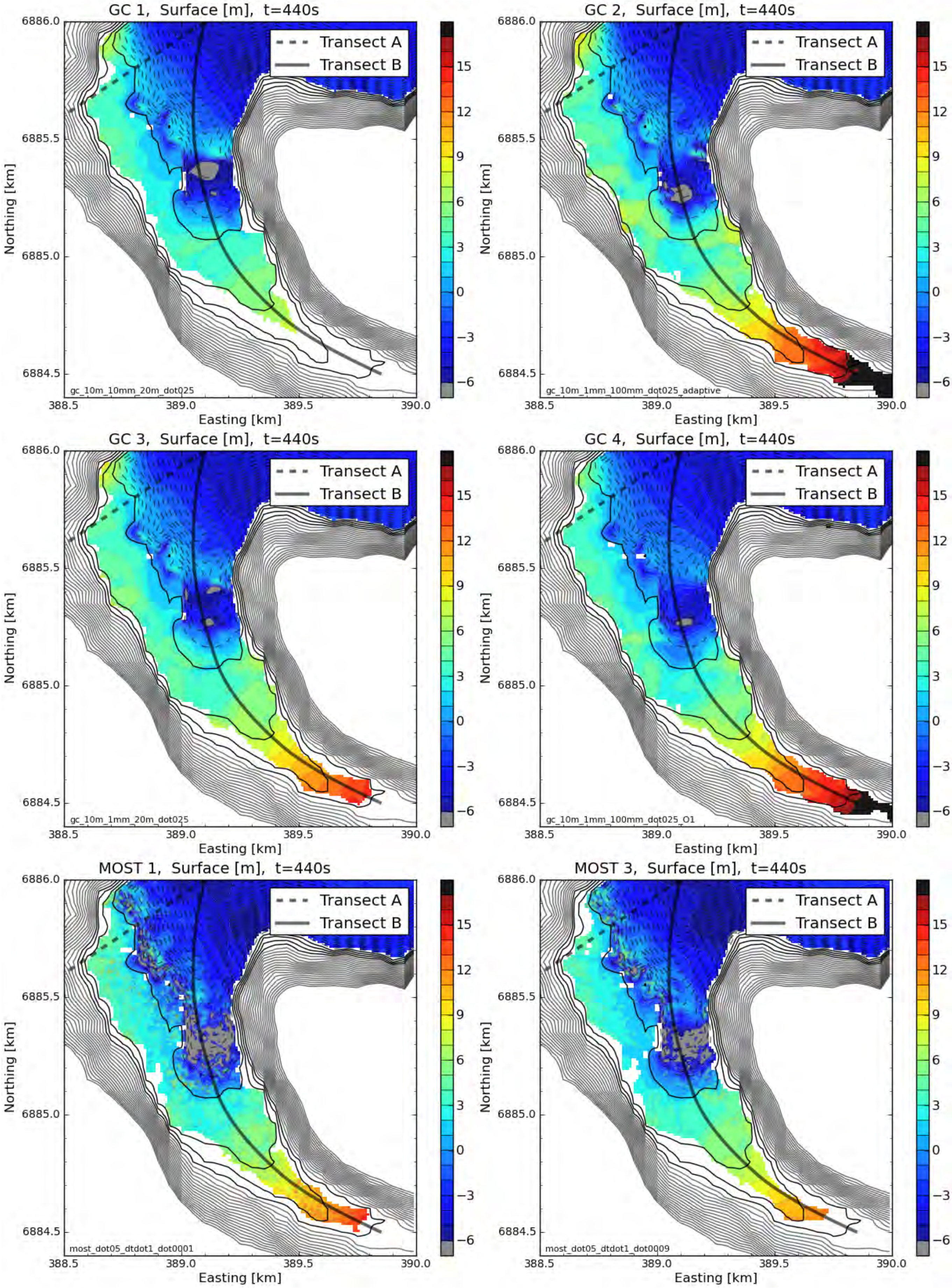

Figure B.17: Surface elevation and inundation height at $t = 440$ s. See Figure B.11 for further description.

Maximum runup and inundation

In this subsection we will present plots for maximum surface elevation and inundation height (Figure B.18) as well as maximum inundation line (Figure B.19) over the full simulation time of 460 s.

In the previous subsections we saw that MOST created ripples during runup, and this is one of the reasons for the higher inundation in Figure B.9.

GC 2 and 4 have the highest inundation along the southern river and as the tsunami propagates through the boundary of the inspection area (south-east corner) the runup heights are already 20 m. Compared to e.g. GC 3, it is clear that the gently sloping areas such as the southern river valley (Transect B), where the tsunami is channeled, will have much higher runup in the limit of no friction as the tsunami rapidly swashes forward.

MOST 1 has runup heights close to 25 m (above 20 m is colored black in the color map) just south of Transect A, while the other runs have an upper limit of 20 m. The ripples in MOST can partly explain why the inundation heights are higher compared to e.g. GC 3, (also second order). Comparing MOST 1 to MOST 3, it is clear that radically lowered friction will give higher runup. The number of unphysical peaks outside Gauge C are very evident for MOST 1, but almost nonexistent for MOST 3. The stability problem is probably the reason for choosing a slightly higher default friction coefficient in MOST compared to GEOCLAW.

Comparing GC 4 to GC 2, it is clear that the steeper waves, which were only resolved on the second order runs, would give higher inundation and slightly higher runup. It is only at the tip of Transect B that GC 4 has runup above 15 meters.

Some of the stability difficulties of second order schemes, low dry tolerance and low friction can be seen as the most likely unphysical 40 m runup, from the third incident wave, in the north-east part of Figure B.19 for GC 2. Since friction only was applied at vanishing depths this runup feature is probably a nonphysical artifact.

The interesting part of the figure is the location of maximum runup in the southern river valley. Here all GC runs have slightly higher runup, with the exception of GC 1. The difference between MOST 2 and MOST 3 is minimal, but the slightly different runup along Transect B is due to the 20 % difference in the roughness coefficient used. GC 3 and MOST 2, which are run with the same friction parameter, show very similar results. GC 2 has slightly higher runup than the first order GC 4 run, along the southern river valley. Maximum runup for GC 2 and GC 4 is not shown since the tsunami propagates out of the inspection area. It is remarkable how close GC 3 and MOST 1 are near the upper parts of Transect B.

It should be noted that it is difficult to differentiate the runup heights between the models as the sawtooth-like maximum inundation lines mostly overlap in Figure B.19. If we shift the focus from comparing the models to use them to accurately predict the runup heights along the steep western slope in Hellesylt, we need to run the models at a finer resolution than 10 m. At the resolution used, the differences between the models are barely visible.

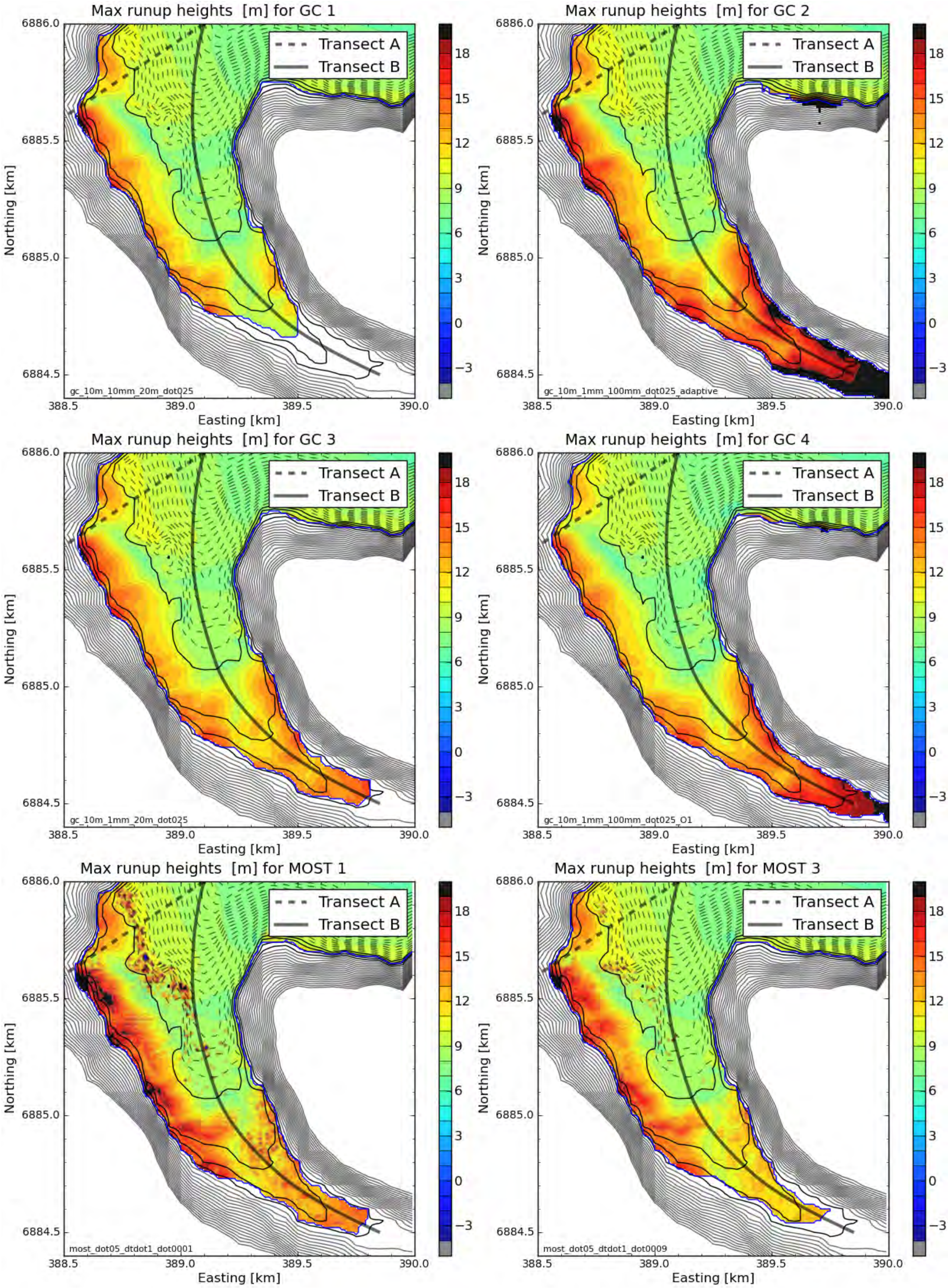

Figure B.18: Maximum surface elevation and inundation height until $t = 460$ s. See Figure B.11 for further explanation.

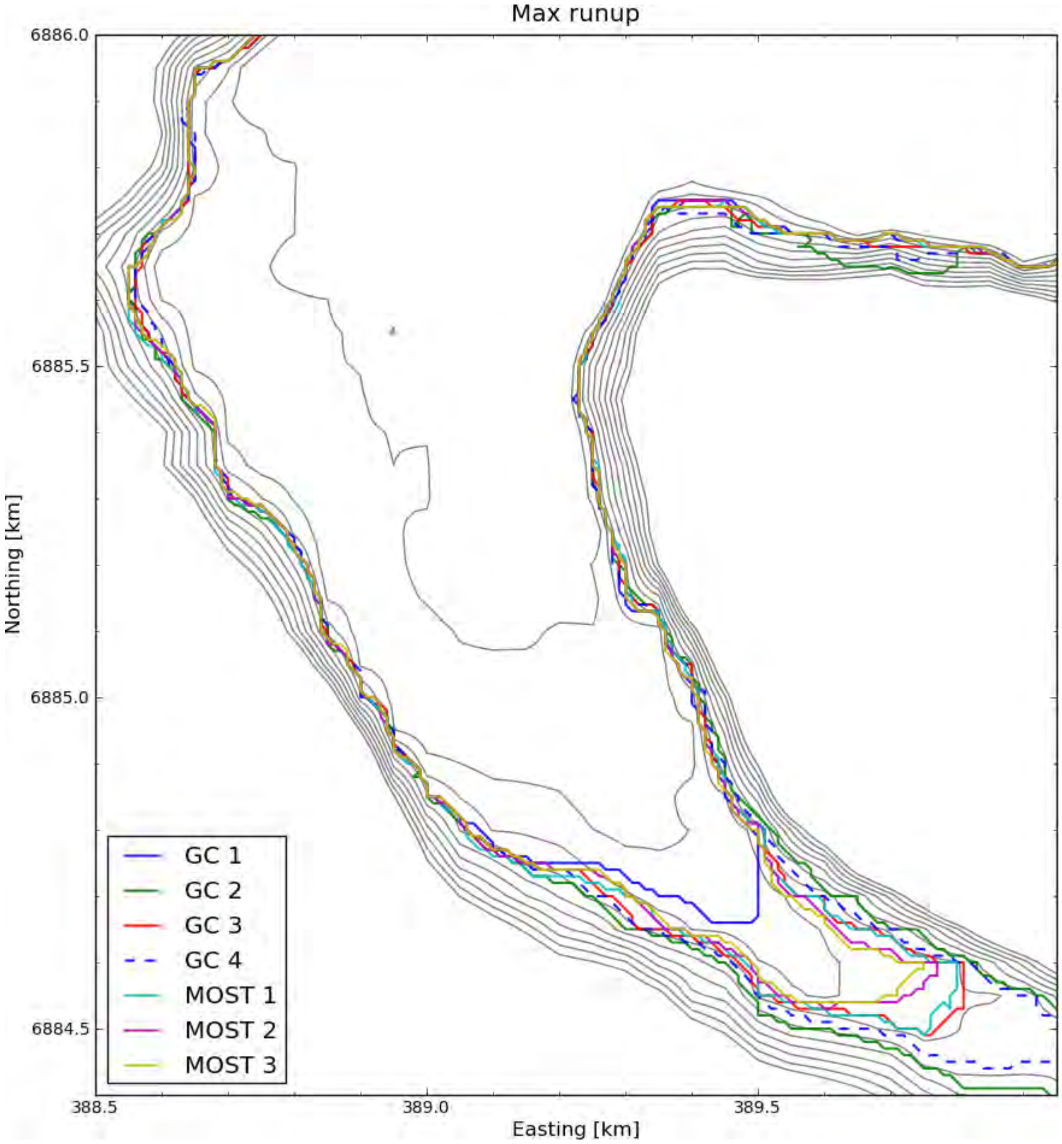

Figure B.19: Maximum inundation line. Topography is plotted every 5 meters from the equilibrium shoreline.

Maximum velocity

In this subsection we will discuss the maximum velocity and the effect of friction for damping unphysically high speeds during runup and draw-down.

The slope of the terrain, defined as $\tan(\alpha)$, where α is the slope angle, is plotted in Figure B.20. Since the topography is derived from interpolating a dataset given at 50 m resolution onto a 10 m grid, we can see blocks of 5 x 5 cells with the same slope index.

In Figures B.21 and B.22, the left subplot shows the maximum surface elevation and inundation height while the right subplot shows the maximum velocity for the simulation, with arrows to identify the direction. MOST 2 and MOST 3 show similar results, especially with respect to the surface elevation. The difference in maximum draw-down velocities is only visible near instabilities. Maximum draw-down velocities are bounded by $\sqrt{2gh}$ since that is the maximum velocity gained with a fall height h without friction. With maximum runup heights of 20 and 25 meters this corresponds to velocities of 20 and 22.4 m/s. We note that the draw-down velocities are higher in the MOST runs than in the GC runs, and highest for MOST 1. The draw-down velocities seem realistic for both GEOCLAW and MOST.

The maximum runup velocities north-east in the map for the GC runs show that one way to dampen unphysical velocities is to reduce the *dry tolerance*, but this comes at the cost of increased waterloss.

Manning friction has limitations in shallow depths since the depth dependence is weak, proportional to $h^{-\frac{1}{3}}$. Going from a depth of 1 m to 20 cm the friction effect will be only 4 times larger, this inclination is too weak to dampen the draw-down velocities. There is an asymptotic behavior in the depth dependence for depths below 20 cm.

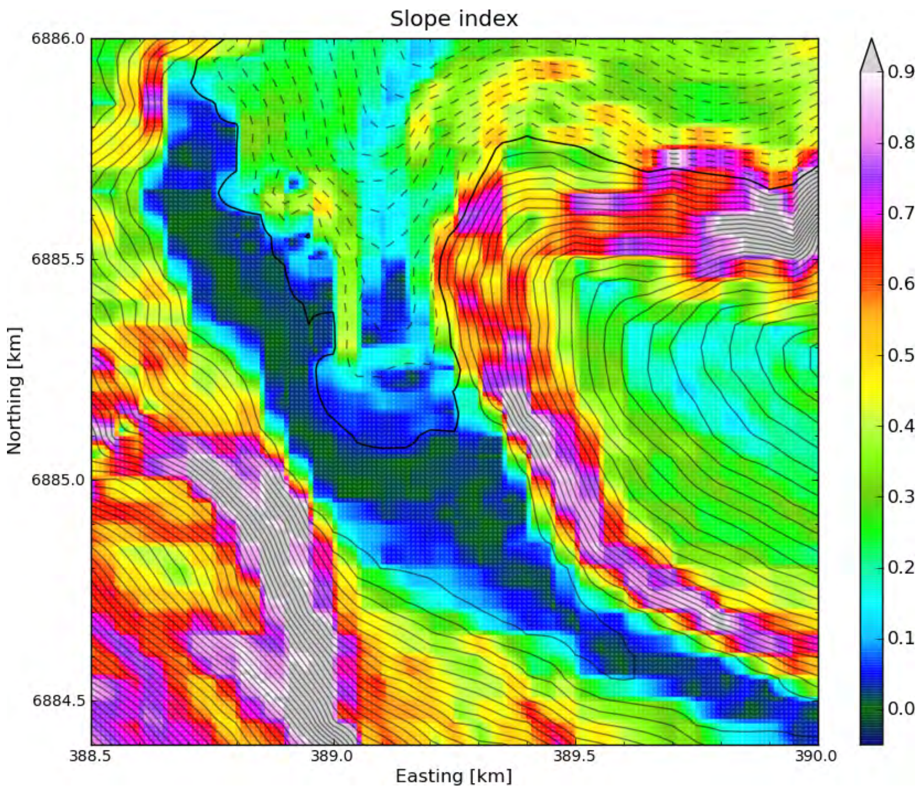

Figure B.20: Slope at Hellesylt.

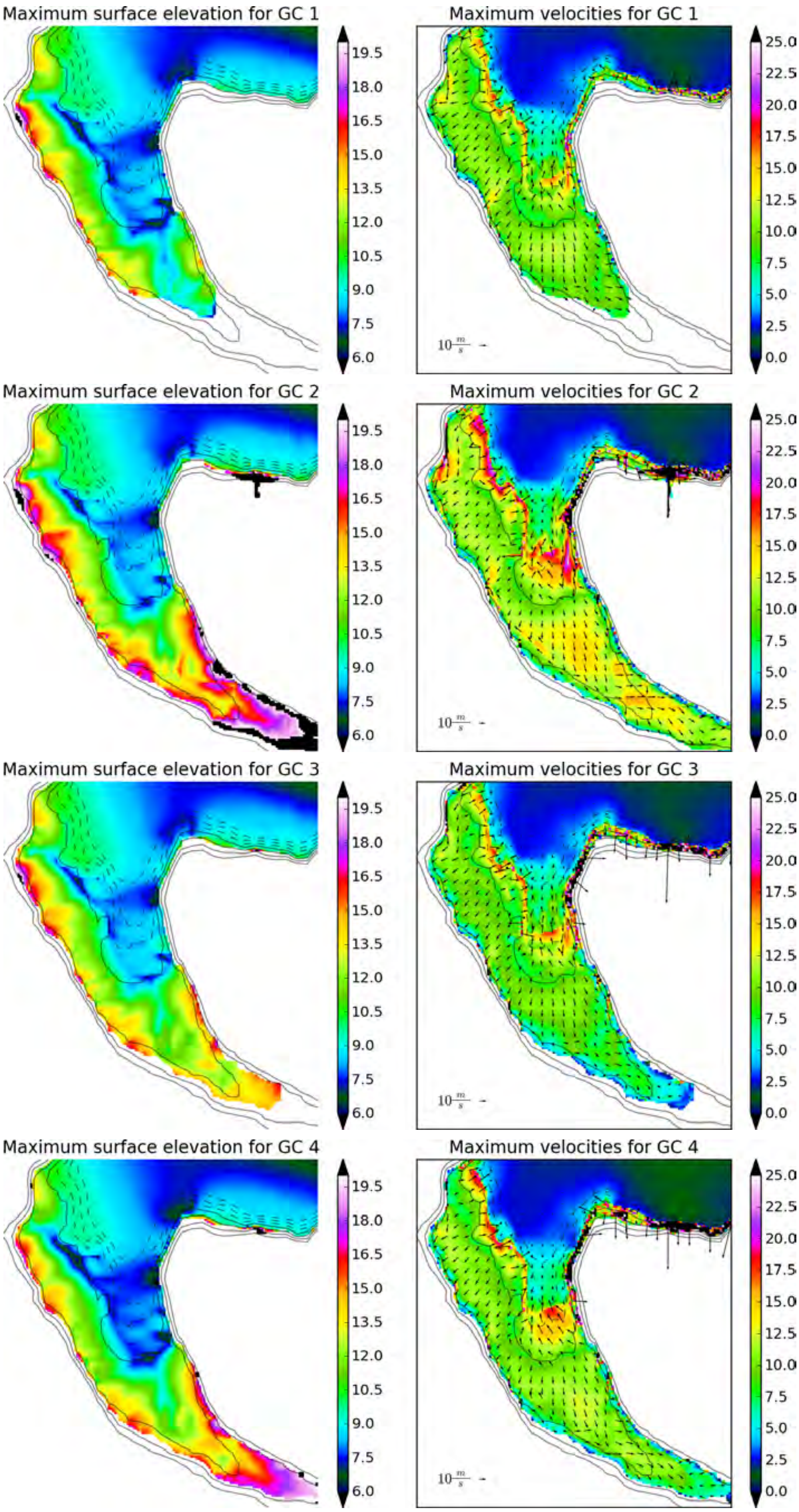

Figure B.21: Maximum surface elevation and inundation height (left) and velocity (right) for each grid point that occurred during the GEOCLAW runs. Arrows are placed with the base in the grid cell they are representing, and placed with an interval of 5 points. The topography is plotted with contour lines at 0, 10, 20, and 30 m.a.s.l.

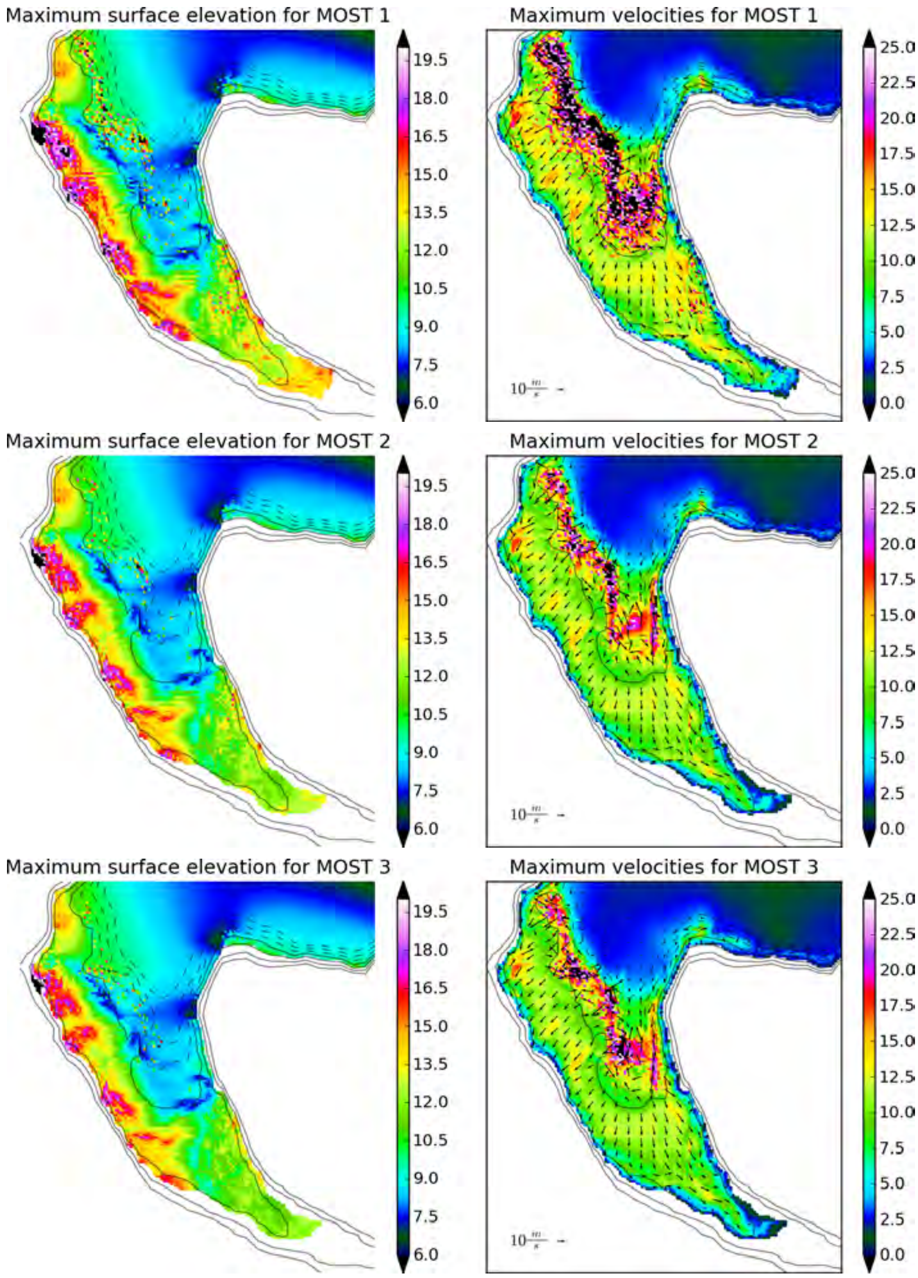

Figure B.22: Maximum surface elevation and inundation height (left) and velocity (right) for each grid point that occurred during the MOST runs. See Figure B.21 for further explanation.

Conservation of water volume

In this subsection we will compute the waterloss at the moving shoreline. The volume change per unit time in all cells within a bounded region should be balanced with the volume flux across the boundaries of the same region, here the inspection area. The imbalance can be used as an estimate for the water volume which is lost at the moving shoreline.

In Figure B.23 an estimate of the unphysical volume loss is presented for the region visible in the surface plots (same region as the inspection area in Figure B.3). The results are computed as a post process using model output from every second until $t = 460$ s. The volume loss is scaled by V_0 ($\approx 20M$ m^3), which is the initial water volume for the inspected area ($t = 0$ s). In comparison the total influx for the leading wave is 3 M m^3 and the absolute value of all fluxes combined over the time interval is 12 M m^3.

For GC 1 there is significant volume loss as soon as the tsunami starts to climb the initial shoreline. This is because all cells with depths below 1 cm will have the water removed at every time step (0.01 s). By lowering the *dry tolerance* to 1 mm, it is clear that very little water is removed for the other GC runs. For the MOST runs it appears that water is added to the simulation during the initial runup (for corresponding runs with *cutoff depths* set to the default value 0.1 m, instead of 0.05 m used here, this early accumulation of water would be slightly higher). This is due to the horizontal wet projection in the shoreline algorithm.

As soon as draw-down starts (around time 280 s), the thinning of the water layers will result in water removal for MOST when the depth gets below *cutoff*, but the amount seen in Figure B.23 seems to be much more than expected. At time 330 s, there is lost more water in the MOST simulations than in even GC 1. The endpoint for the MOST runs are not shown, but the values of the waterloss will drop below 0.92 by the time of 460 s. That means almost 10% of the initial water volume is lost.

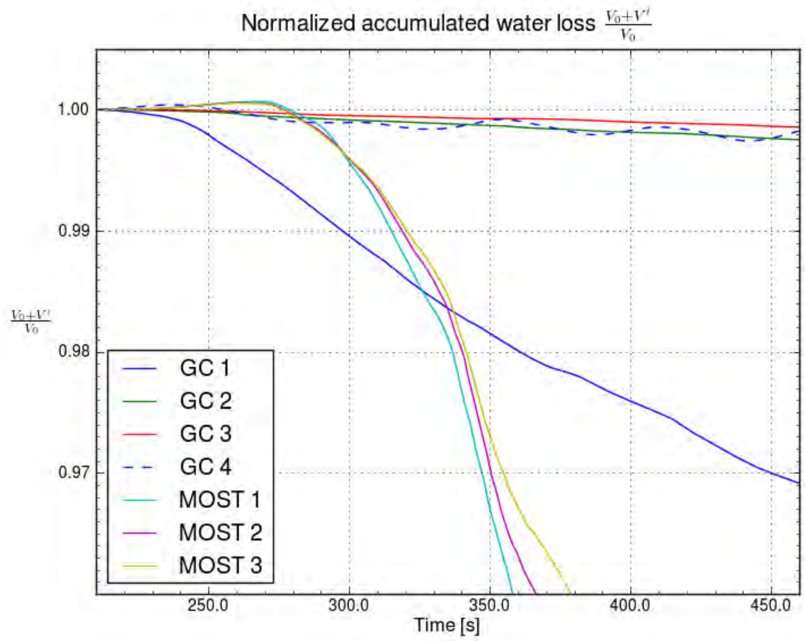

Figure B.23: Accumulated waterloss normalized by the initial water volume for the inspection area ($V_0 \approx 20M$ m^3.)

B.2.5 Discussion of results

The main difference between first and second order schemes is that a second order scheme can describe a steeper wave, with the same height, in the swash zone. The steeper wave will splash higher when entering the steep slope. The leading wave for the GC run using the first order method was diffused, wider, flatter, and smoother compared with the second order counterparts. As long as a second order Riemann solver was used in GEOCLAW, the leading wave maintained the bore shape, and this gave higher runup and inundation along transect A compared with a first order method.

The ripples in the MOST runs are numerical artifacts that appeared right behind the very steep bore in the MOST runs. The initial ripples were a few grid cells wide, but widened as they propagated backwards from the (source) bore with time. The second order GC runs, which also had a steep bore, did not have ripples as the MOST runs had. It is possible that the lower time step in the GC runs (0.01 s) compared to the MOST runs (0.1 s) are part of the reason for the lack of the ripples, but the explanation is probably that GEOCLAW applies approximative Riemann solvers that handle bores and hydraulic jumps (shocks) more accurately.

The gentle sloping along Transect B would not give the same splash effect we saw for the steep upper parts of transect A.

Due to waterloss in the MOST model the reflected wave was faster in the GEOCLAW runs. During runup the MOST model introduced water to the simulation while water was removed at an increasing rate during draw-down.

The seven runs can be briefly summarized and evaluated:

- GC 1: Higher *dry tolerance*. Loses water.
- GC 2: Highest runup along transect B due to no friction.
- GC 3: Default friction, second order. Most confident simulation.
- GC 4: Parameters as in GC 2, but with a first order scheme that did not capture the bore shape.
- MOST 1: Heavily reduced friction. Highest runup near Transect A, but also the least stable. Reduced friction compensated for waterloss along Transect B.
- MOST 2: Slightly lowered friction. Unphysical oscillations and ripples.
- MOST 3: Default MOST friction. Ripples, but relatively little oscillations.

The inundation modeling presented in the main report is similar to MOST 3 with the exception of a coarser *dry tolerance* (0.1 m), and a finer grid resolution (5 m).

A previous benchmark [1] (Catalina 04 Benchmark # 1 [2]) of the GEOCLAW model, where friction was turned completely off and the model was compared to an analytical solution (slope 1:10), showed that GEOCLAW captured the position of the moving shoreline accurately when the 10 m resolution was used. Shoreline velocities were well captured at the lower resolution of 1 m (the *dry tolerance* in those runs was 0.1 mm). This indicates that the shoreline velocities in the Hellesylt test case is not represented sufficiently with the resolution we used.

B.3 Conclusion

The parameters in the Hellesylt case (*friction coefficient, dry tolerance* etc.) were primarily chosen to inspect the differences between the GEOCLAW and the MOST model. Since the parameters were chosen for comparison purposes, some improvements can be recommended if one wants to better capture, e.g., the maximum runup heights. A further inspection of maximum runup heights could use nested grids with a finer resolution (such as 1 m) in the steep slope west of the fjord.

In the comparison, the runup models GEOCLAW and MOST produced relatively similar solutions to the runup case at Hellesylt. Especially the results for the leading wave were good. After the leading wave was reflected and draw-down started, waterloss in the MOST model would decrease the confidence in the model with time. Maximum draw-down was too deep in the MOST model and this could give a stability problem.

For both models lowering the friction coefficient would give higher runup, but the runup was very similar for similar friction coefficients. The run with the highest runup is not necessarily the most reliable, but here the runs with reduced friction (GC 2, GC 4, and MOST 1) can be used as an upper limit of what we can expect of runup at Hellesylt. Along the southern river valley (Transect B) the GEOCLAW runs had the highest runup.

MOST suffered from much waterloss during draw-down, as the water layers thinned, while the GEOCLAW model had no problems with waterloss as long as the *dry tolerance* parameter was set sufficiently low. Draw-down velocities in the MOST models were so high that the CFL stability criterion was probably violated giving unphysical oscillations, that had to be dampened using Manning friction. If the value of the friction coefficient was too low the solution in the MOST model could blow up. During initial runup, the MOST model accumulated water, this should be taken into account when the MOST model has the most runup, since added water gives higher runup.

From Section C.1 we can conclude that a grid resolution of 10 m resolution is sufficient in the flat areas of Hellesylt and in the southern river valley. We also note that both models gave similar results for the convergence test case and that the runup along the southern river valley would be more equal if waterloss in the MOST model could be avoided.

For a further inspection of runup heights a finer grid is required to accurately position maximum runup along the west hill side of Hellesylt. In the present study the maximum runup position for the various runs was within a few grid cells (10 m grid resolution). In the steep terrain where the slope is 1:3, corresponding to a vertical spacing of 3.33 m, the applied grid resolution is considered too coarse for accurate runup predictions. It is also necessary to use a second order scheme to avoid diffusion of the shape of the bore that appears when the tsunami swashes the flat areas in Hellesylt.

Although the results were quite similar for the leading wave along transect A, we are most confident in the GC 3 results.

Bibliography

[1] Rolv Erlend Bredesen, Hans Petter Langtangen, and Geir Pedersen. Benchmark of a tsunami run-up code. In B. Skallerud and H. I. Anderson, editors, MekIT'07, pages 127–134. Tapir Academic Press 2007, 2007.

[2] Third international workshop on long-wave runup models. http://isec.nacse.org/workshop/2004_cornell, 2004.

[3] *CLAWPACK* software. http://www.clawpack.org.

[4] *ComMIT* package. http://nctr.pmel.noaa.gov/ComMIT/.

[5] D. L. George and R. J. LeVeque. Finite volume methods and adaptive refinement for global tsunami propagation and local inundation. Science of Tsunami Hazards, 24:319–328, 2006.

[6] David L. George. Finite Volume Methods and Adaptive Refinement for Tsunami Propagation and Inundation. PhD thesis, University of Washington, 2006.

[7] R. J. LeVeque and D. L. George. High-resolution finite volume methods for the shallow water equations with bathymetry and dry states. In C. Synolakis P. L-F. Liu, H. Yeh, editor, Advanced Numerical Models for Simulating Tsunami Waves and Runup, pages 43–74, 2008. http://www.amath.washington.edu/~rjl/pubs/catalina04/.

[8] Mannings Roughness Pictorial. (USGS Water Supply Paper No. 1849) http://manningsn.sdsu.edu/.

[9] Vasily V. Titov. Numerical modeling of long wave runup. PhD thesis, University of Southern California, 1997.

[10] Vasily Vladimirovitch Titov and Costas Emmanuel Synolakis. Modeling of breaking and nonbreaking long-wave evolution and runup using VTCS-2. Journal of waterway, port, coastal, and ocean engineering, 121(6, November/Desember):308–316, 1995.

[11] Vasily Vladimirovitch Titov and Costas Emmanuel Synolakis. Numerical modeling of tital wave runup. Journal of waterway, port, coastal, and ocean engineering, 124(4, July/August):157–171, 1995.

Appendix C - Comparisons between the runup-models MOST and GEOCLAW in 1HD

Appendix C

Comparisons between the runup-models MOST and GEOCLAW in 1HD

C.1 Convergence test in 1HD

This study was originally done to inspect stochastic variation of runup, but here we use it to check for convergence in the standard inundation models, MOST and GEOCLAW. The idea behind this test is to run both models with model default parameters (defined below) and check for convergence for a synthesized 1HD geometry (strictly the models are run in 2HD). An idealized topography is used. We performed the tests on an ensemble of 49 slightly different cases for both models.

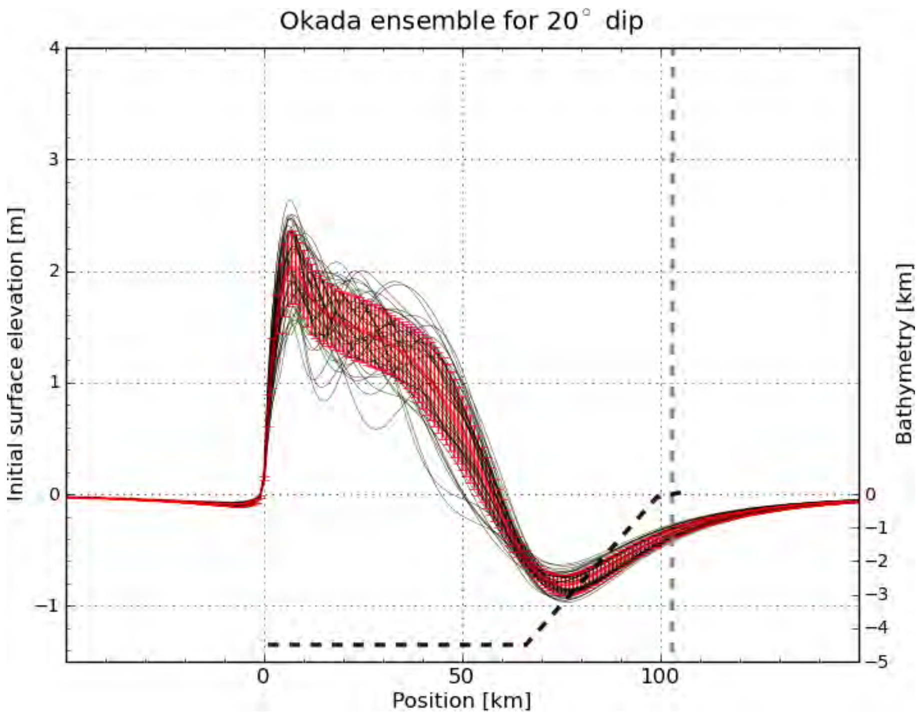

Figure C.1: Initial surface elevations for each of the test cases in a 100 km domain. The mean and standard deviations of the ensemble is plotted using a solid red line and the red error bars, respectively. The applied bathymetry is plotted as a dashed line.

C.1.1 Model setup

The 49 initial surface elevations (Figure C.1) are generated by the generalized Okada (1985) model for seabed displacement due to random earthquake slip along a fault with a 20° dip angle (mean slip is constant). The near-shore slope used is similar to Transect B (southern river valley) in the Hellesylt case (slope is 1:7.5 until the depth of 100 m, then the slope is 1:39.5). However, the maximum depth of 4.5 km is certainly deeper than in Storfjorden.

For the GEOCLAW runs we used a second order Riemann solver with an adaptive time step of maximum 0.1 s (bounded by a Courant number of 0.5). The *dry tolerance* was set to 0.1 mm with default Manning friction ($n = 0.025$) applied in regions with depths below 20 m. 1HD GEOCLAW simulations were synthesized by specifying no-flux boundary conditions in the transverse directions. In the convergence test we ran the model with constant grid resolutions of 120, 60, 30, and 10 m. For the 10 m run the CPU time was typically around 100 minutes for the GEOCLAW model (1500 s simulation with 11448 cells in the x direction).

For the MOST model, a 1HD geometry was synthesized by lateral walls with height 50 m.a.s.l., to prevent motion in the transverse direction. We verified that no significant transverse motion (10^{-5} m/s) occurred in the data presented here. The Manning friction coefficient was set to the default ($n = 0.030$), whereas the *cutoff* depth was 0.1 m. Since the MOST model uses geographical coordinates we created a grid with propagation in the meridional direction to give a fixed conversion between latitude and distance. The MOST model has a grid limit of 2000 points in each direction so nested sub-grids (3 levels) were applied near the shoreline. For all runs the grid resolution for the coarsest sub-grid was 120 m. For the nested sub-grids, we kept the ratio between the space and time step constant. We ran the model with the grid resolutions 120, 60, 30, and 7.5 m for the finest sub-grid. The time step for the finest sub-grid was 0.00156 s, giving a CPU time of 40 minutes.

C.1.2 Results

A series of the surface elevations of the tsunami at 30 s intervals, from the GEOCLAW run with 10 m resolution, is shown in Figure C.2. We note that a bore is formed after 12 minutes due to high draw-down velocities.

In Figure C.3 we see that both models give similar maximum runup heights. The maximum draw-down location seems to be similar for the finest resolutions. In GEOCLAW the hydraulic jump (bore) seaward maximum draw-down is well defined (most distinct at 10 m resolution) and without artificial oscillations at all resolutions. This is not the case for the MOST model runs where there is a lower surface elevation at the bore and seaward (probably due to ripples at maximum draw-down time) and the bore is diffused. Unphysical ripples are visible in the minimum surface elevations.

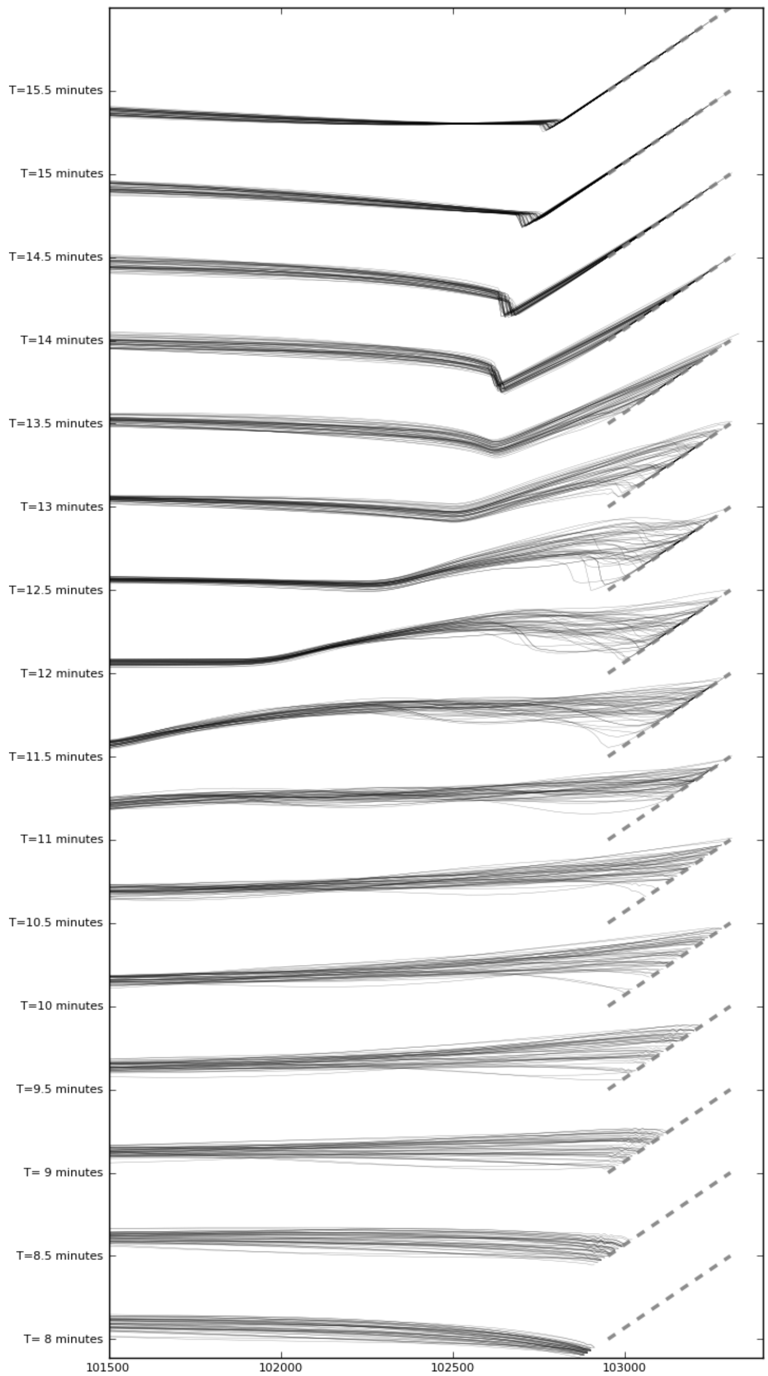

Figure C.2: Snapshots in time for the 49 different realizations in the 10 m GEOCLAW run. The time is given in minutes after the seabed displacement. The surface elevation is plotted as a thin line corresponding to the model time given on the left. The unit on the x-axis is the horizontal position in m for the computational domain. The applied topography is plotted as a grey dashed line from 0 to 9 m.a.s.l. The tick-marks for each time is also placed at mean sea level.

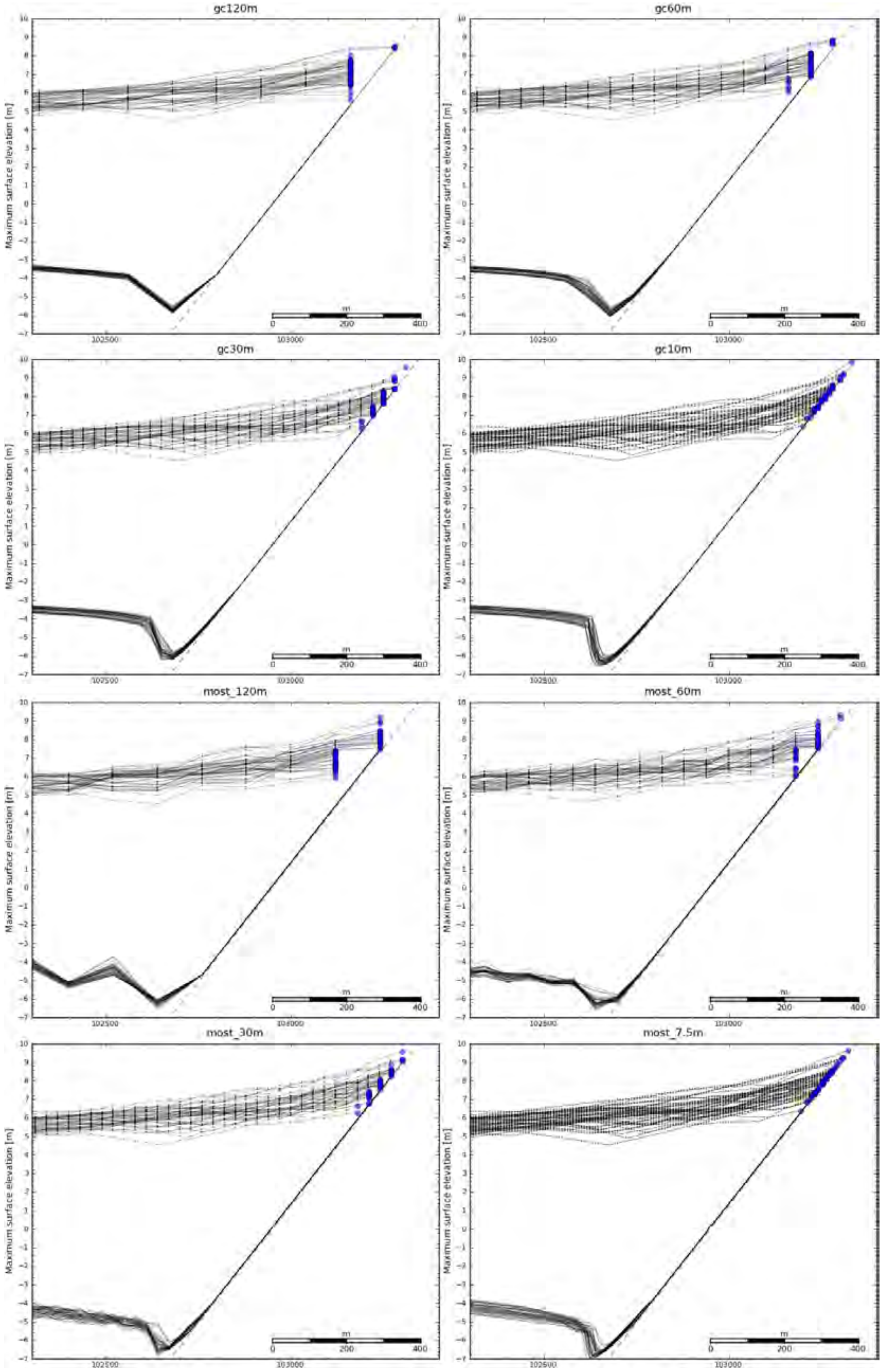

Figure C.3: The maximum (and minimum) surface elevation that occurred at each computed point along the transect is plotted using a line for every realization. The filled blue markers show maximum runup height for each realization and the scale bar is placed with the left edge corresponding to the equilibrium water shoreline and can be used to measure inundation distance. Model name and grid resolution is given in each title.

In Figure C.4 we observe a close to linear convergence for the maximum runup heights with respect to spatial grid resolutions. 10 m is a reasonable resolution to use for gentle slopes (i.e., flat areas in Hellesylt) as both models agree in the results. At 30 m grid resolution the difference between maximum runup in the models is approximately 12 cm, and at 10 m resolution the difference between the models is 4 cm. If we assume linear convergence we get an extrapolated (mean) runup height of 8.04 m at resolution $\Delta x \rightarrow 0$ m. The accuracy of the maximum runup height mean value relative to the mean at $\Delta x \rightarrow 0$ m for the GEOCLAW and MOST models are are respectively 1.0% and 0.5% at the 10 m resolution and 3.3% and 1.9% at the 30 m resolution.

If we inspect the relative difference in the maximum runup height in each realization separately (plot omitted) at resolution $\Delta x \rightarrow 0$ m, we note that the models differed with a maximum of +2.6% (MOST relative to GEOCLAW) and minimum −1.8%, while the mean difference with standard deviation was $0.03 \pm 1.02\%$. It should also be noted that for several cases the MOST model has close to the same maximum runup height at all resolutions. This is the main reason for the flatter mean convergence line for MOST in Figure C.4.

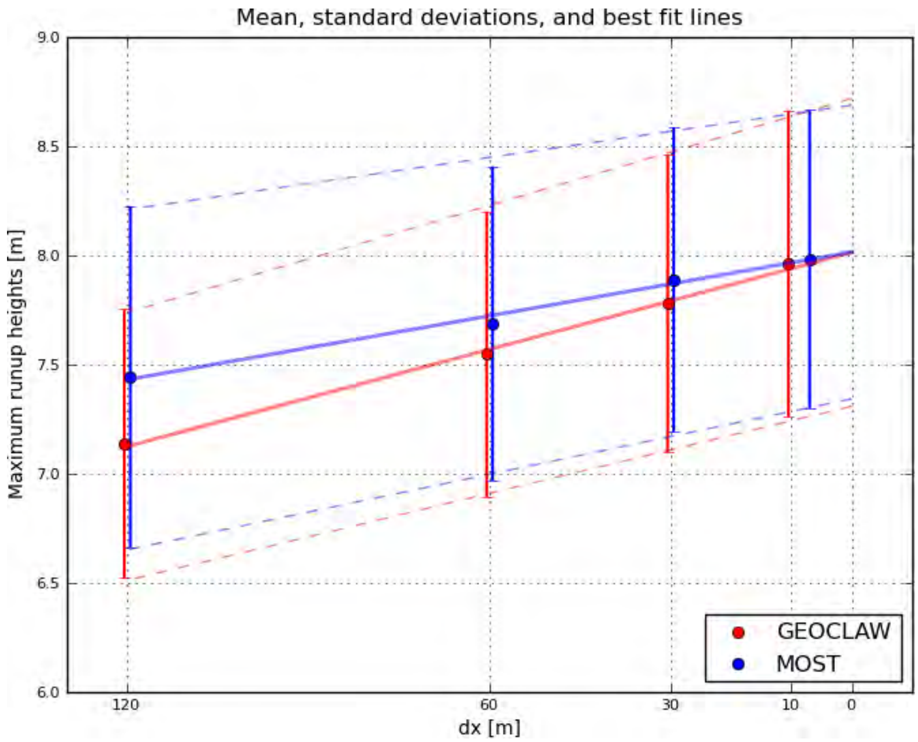

Figure C.4: The mean and standard deviations of maximum runup for each ensemble. The grid resolution is given on the x axis and best fit lines are produced based on the mean and standard deviation.

Appendix D - Comparison of the runup-models ComMIT and COMCOT

Contents

1 Comparison of the run-up models ComMIT and COMCOT

The COMCOT model (Cornell Multi-grid Coupled Tsunami Model) is originated from the work of S.N. Sea based on Shuto's model and Yongsik Cho first version from 1993. Later the model was thoroughly improved by Seung-Buhm Woo in 1999. For more information of the model, see NGI (2008b) and Cornell (2009).

The comparison between ComMIT and COMCOT is done by calculating the run-up in the village Hellesylt a few kilometres south of Åknes using the 35Mm^3 scenario from Åknes as described in NGI (2005). The tsunami propagation stage was calculated by using the DpWaves model. The latest version of COMCOT at the time of the comparison was 1.6. This version had no possibility of reading forced input along a boundary. To import the wave data into COMCOT we had to use the *"wave-maker"*. Since the waves are entering the fjord outside Hellesylt with an angle, the wave-maker option for an oblique wave was applied. The input data for the wave-maker was a mariogram of the surface elevation extracted from the simulation using the DpWaves model. In other words the input is an oblique plane wave which is a good estimate for the leading part of the waves but not for the trailing ones, where waves are criss-crossing the fjord and hence is less influence on the tsunami impact during the run-up. When comparing different models, we must reduce all possible uncertainties, such as slightly different input. Therefore, the input to the ComMIT model is also an oblique plane wave generated from the same mariogram as for the COMCOT model. In addition, the velocities are calculated from the surface elevation using a linear hydrostatic relation.

The COMCOT results show marked differences in the overall wave pattern and are more hampered with noise. Another clear difference is probably that the wave in the COMCOT solutions propagates slower on dry land than in the ComMIT case, leading to higher bores. The ComMIT model was run with standard parameters.

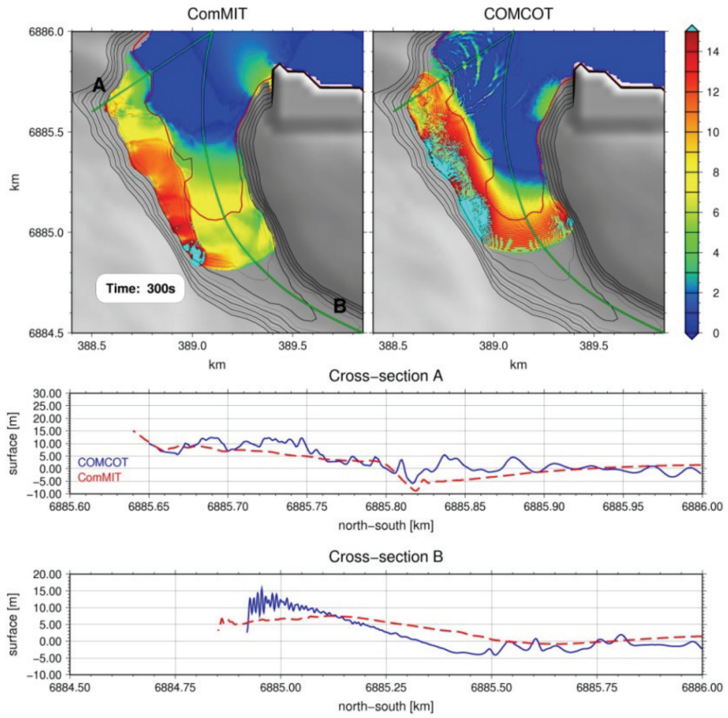

Figure 1.1: Comparison between the ComMIT model (up left) and COMCOT (up right) 300 s after the slide release. The leading wave has started to inundate Hellesylt. The cruve plots shows the comparison of the models with data extracted along the track A and B.

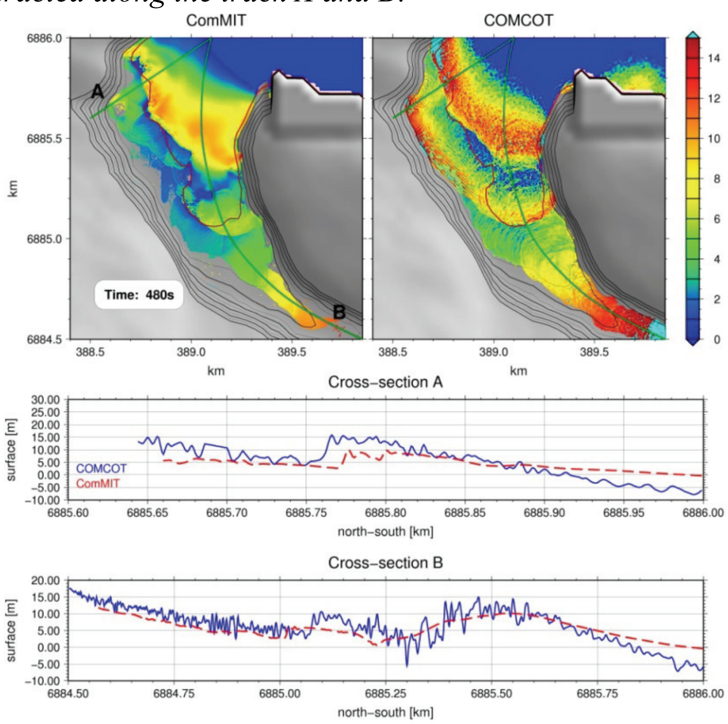

Figure 1.2: Comparison between the ComMIT model (up left) and COMCOT (up right) 480 s after the slide release. See also Figure 1.1.

2 References

ComMIT (2010). URL: http://nctr.pmel.noaa.gov/ComMIT/ (visited 2010-02-11)

Cornell (2009) COMCOT; source code and documentation is found here: http://ceeserver.cee.cornell.edu/pll-group/comcot.htm (visited 2009-09-24).

Appendix E - Modeling detalis

Contents

1 Bathymetry and topography

In this section the data for topography and bathymetry are described. The topography and bathymetry applied for the run-up calculations are filtered using the ComMIT's toolbox labelled "Bathcorr" (see ComMIT, 2010). The filtering is a remedy to avoid potential numerical instability due to bathymetric/topographic variations (especially steep gradients). The filter alters the data slightly only in problematic areas. All data is referenced in UTM 32 coordinates.

The bathymetric data for the inner part of Storfjorden (inside Stordal) are provided by NGU and are based on data with resolutions of both 3 m (in shallow areas) and 6 m. The compilation of these data sets is interpolated onto a uniform grid of 5 m. For tsunami propagation, the data was interpolated onto a grid with resolution 50 m, while for run-up calculations the data was interpolated onto grids with resolution ranging between 5 m and 40 m (depending on grid level). For the outer part of Storfjorden, the bathymetry is based on the best available data from the Norwegian Hydrographic Service (Sjøkartverket) interpolated onto a uniform grid with resolution 50 m. These background data are provided by NGU.

For the topography in the inundation zones (except for Hellesylt, see below), The County Governor of Møre & Romsdal provided the background data. The original data used in the run-up calculations are high resolution 1 m contour lines including the shoreline. In the inundation zones, the patching of the topographic and bathymetric data was performed through the following steps:

- All data seaward the shoreline with a water depth less than 0.5 m was given a value of 0.5 m
- All data landward the shoreline with a height less than 0.5 m was given a value of 0.5 m.
- Both the bathymetric and the topographic data were then transformed onto a single 5 m uniform grid using bi-linear interpolation.

In this manner we obtain a clear definition of the shoreline. Since the available data is originally given as 1 m contour lines only, details in more gentle areas are lost. The use of minimum values of depth/height as described above will to some extent mimic quay structures (a vertical step of 1 m between two adjacent grid points located on different sides of the shore line), and is here a better approach than linear interpolation between the shoreline (height 0 m) and the landward 1 m contour line.

Note that the filtering of the data (applying "Bathcorr", see above) may locally change the bathymetry/topography at very steep locations, see for instance Gravaneset and Dyrkorn in Appendix A.

Smaller islands are not included in the simulations except for the two largest ones in Vegsundet (Flisnesholmen and Furholmen) and the one lying 6 km west of Ørskog (Skotteskjæret).

For Hellesylt, data from NGU with resolution 5 m (raster) is applied for the run-up calculations. This is due to better representation of the topographic details in the valley south of Hellesylt.

2 The energy line approach

In hydraulic engineering the use of energy lines (Bernoullis equation) are common in evaluating the energy dissipation along streamlines. Without going too deep into the theory, the conclusion is as follows: The sum of the potential energy and the kinetic energy is constant at any point along the streamline, if there is no energy dissipation. In real flows however, the difference between the sum of the potential and the kinetic energy from point 1 to point 2 represents the energy dissipation between these two points. Here we describe how to apply a model based on the energy line approach to determine the velocity progression of rock slides.

The potential and the kinetic energy pr unit weight may be expressed in the dimension meter as:

- Potential energy: z (elevation)
- Kinetic energy: $v^2/2g$ (v - velocity, g - gravitational acceleration)

An example is shown in Figure 2.1. The red line is the energy line (assumed piecewise linear), starting at the front of the slide in the initial position and ending at the front of the slide after the slide has come to rest. By assuming a singular loss of the energy when the slide impacts the water (e.g. 10% of the kinetic energy here or 20 m in height), the velocity is easily found by setting $v^2/2g$ to the height difference between the bottom and the energy line. In the work presented in this report, the singular loss of energy at water impact is not taken into account. See also NGI (2008a) – Appendix A and NGI (in prep.).

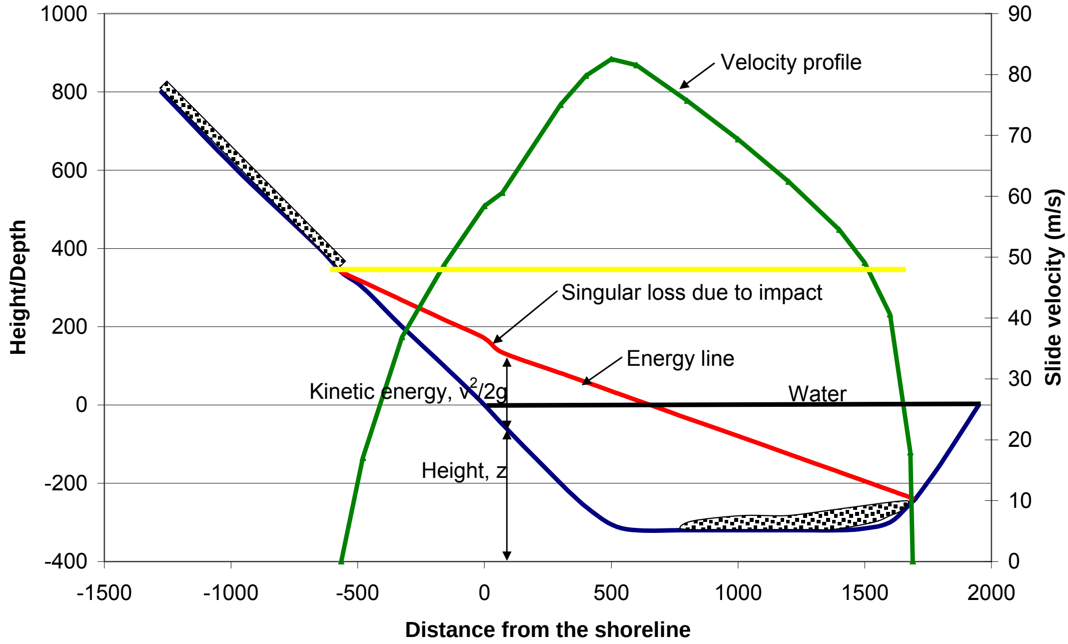

Figure 2.1: Assumed energy line (red) and the resulting flow velocities (green). The energy loss is represented by the distance between the red and yellow line.

3 Numerical models

3.1 Models for tsunami generation and propagation

Tsunamis are often classified as long waves. In other words most of the energy that is transferred from the slide to water motion is distributed on waves with typical wavelength much larger than the characteristic water depth. From this assumption it follows that the pressure is approximately hydrostatic and that the vertical variations of the horizontal velocity are small.

Furthermore, if the characteristic amplitude of the waves is much less than the characteristic water depth except during generation (for rockslide generated waves) and run-up, the surface elevation and the averaged horizontal wave current velocity are determined by the linear, depth-averaged non-dispersive long wave (or shallow water) equations for conservation of mass and momentum (see textbook of Mei, 1989). Models based on these equations are commonly abbreviated as LSW (linear shallow water) models.

However, for the cases where the waves are shorter the pressure is no longer hydrostatic and the waves will be influenced by dispersive effects implying that the speed of wave propagation depends on the wave length; longer waves travel faster than shorter ones. Furthermore, if the characteristic amplitudes are higher than in the LSW regime above, the waves may be influenced by non-linearity. This effect can be seen, e.g., as steepening of waves propagating towards the shore, followed by possible wave breaking. To include these two higher order effects (dispersion and non-linearity) we apply so-called Boussinesq models. By switching the effects of dispersion and non-linearities on and off the model will be run using different mathematical descriptions, as shown in Table 3.1.

In this report we have applied two Boussinesq models. The first model is labelled GloBouss, and is newly developed at NGI/ICG/UiO and is more robust and less computational demanding than the second model labelled DpWaves[1] (applied for instance in NGI, 2008a). Both models have the option of simulating slide generated waves, either as simple slide boxes or more sophistically using output from numerical slide models as input. DpWaves is by now the only model capable to be initiated by the time-history along a boundary (forced input), and is the model applied for simulating waves with input from the laboratory experiments at SINTEF. In all other simulations we apply the GloBouss model. Figure 3.1 shows a comparison of the two models, showing only minor discrepancies for the leading waves. The slide configuration is identical for both runs, but with independent codes for transferring the volume displacement due to the slide motion to the tsunami, and the comparison is hence valuable for the validation of the different tsunami propagation models.

For further information about the models, see NGI (2008a), Langtangen and Pedersen (1998), and Pedersen and Løvholt (2008).

Table 3.1: Overview over combination of the model parameters (non-dispersive and non-linear model types) and the abbreviations applied in this report.. '+' means included while '-' means excluded.

Description	Abbrev.	Dispersion	Non-linearities
Boussinesq model	bouss	+	+
Linear dispersive model	disp	+	-
Nonlinear hydrostatic model	nlin	-	+
Linear hydrostatic model	hydr	-	-

[1] Used in "mild slope" mode to avoid numerical instabilities related to steep depth gradients, see Løvholt and Pedersen (2009).

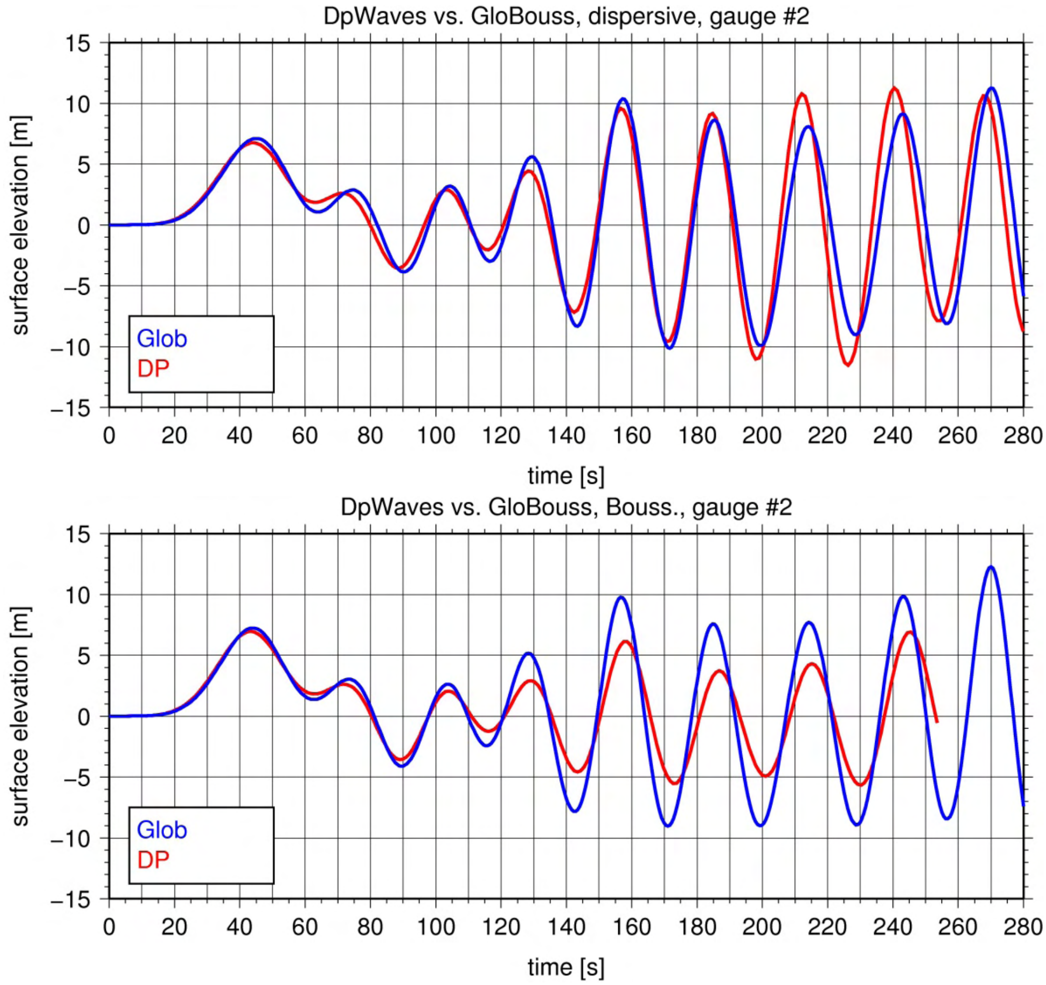

Figure 3.1: Two independent simulations using two different Boussinesq models.”Glob” and “DP” are the GloBouss and DpWaves models, respectively. Gauges 2 is located north of Åknes (see Figure 4.1, page 11).

3.2 Threshold depth

The non-linear terms in the Boussinesq models may lead to instability if the sea-bottom is exposed during simulation. This problem is especially severe in the generation area, but also for waves entering shallow water near shore. Numerically such problems are often handled by defining a so-called threshold depth. Implementation of such techniques is done either by replacing the data for the part of the bathymetry with depth smaller than the threshold value with the threshold value itself, or by moving the shoreline to the threshold depth. At the slide area, we have applied a both radially and linearly decaying threshold depth. First we determine a point at the shoreline below the slide area. From this point ($r=0$, with a threshold value $T=h$) the threshold is linearly decaying to zero ($T=0$) at a distance $r=d$. For each point within the circle ($r<d$), a depth less than the threshold value $T(r)=hr/d$ is replaced by $T(r)$. The effect on the generated waves of some different choices of h and d is shown in Figure 3.2.

At gauge 5 (close and south of the slide area at Åknes, see Figure 4.1 page 11) the different combinations give a variation of the leading wave of only +/- 0-10%, while smaller discrepancies are found for larger distances, e.g., gauge 11 outside Geiranger. We may then conclude that applying a threshold depth as described above has only limited effect on the overall performance. For the Åknes scenario simulations we have applied *d*=4 km and *h*=0.3 km.

In the other parts of the fjord system, we have applied a constant threshold value, typically 50 m for non-linear and 20 m for dispersive simulations, respectively. The effect of the constant threshold depths for the tsunami propagation is quantified in numerical tests, see Section 5.2 in this appendix.

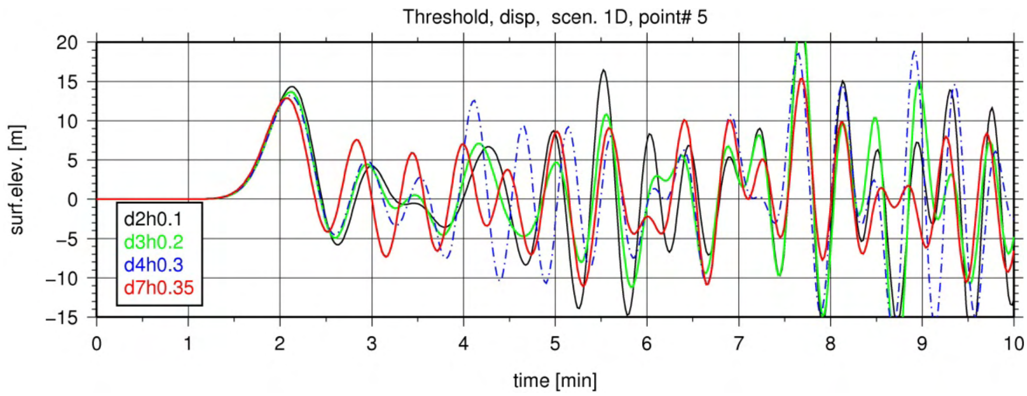

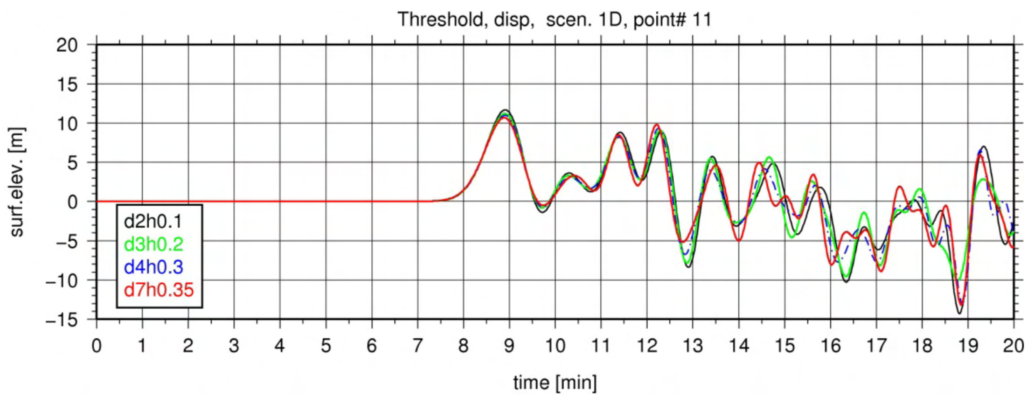

Figure 3.2: Effect of different values for determining the threshold depth close to the slide area. "d" is the radius and "h" is the threshold at the starting point in kilometers, as explained in the text (see Figure 4.1, page 11).

3.3 Model for run-up calculations

For the run-up simulations we have applied the ComMIT model, see Appendix B and the references therein. ComMIT is the graphical user interface (GUI) for the MOST model. Through ComMIT you are allowed to choose input to run-up height calculations for potential earthquake sources along all possible trenches.

For rock slide generated waves modelled in the present work, the input to the inundation model is given by the dispersive GloBouss or DpWaves models. Due to a high number of scenarios and locations for run-up calculations, we have applied the MOST model directly (not trough the GUI) by running the MOST model via input files controlled by scripts written in Python (Python, 2010). The scripts may run a large set of simulations as well as performing the post-processing (projecting data, extracting maximum values, plotting, etc.) automatically.

By using a one way nesting procedure, ComMIT reads the output from the propagation model (GloBouss or DpWaves) over the model boundaries at each time step, see Løvholt et al. (2010). As the propagation and inundation models are generally operating on different grids, the boundary values obtained from the propagation model are interpolated to the run-up model by bi-linear interpolation in space and linear interpolation in time. Technically, the nesting is performed by dumping so-called propagation files from GloBouss or DpWaves, containing time dependent fields of the surface elevations and the two velocity components over a region covering the whole computational domain of the local model. The file format of the propagation files are of the NetCDF type. From GloBouss, NetCDF propagation files compatible with the ComMIT input are produced over a user defined region and with a user defined resolution.

In Appendix B the ComMIT/MOST model is thouroughly compared to another inundation model Geoclaw at Hellesylt using a scenario from Åknes. This work concludes that the two models give quite similar results, with ComMIT/MOST slightly more conservative. The work also revealed some instability problems with ComMIT/MOST during draw-down. If instability occurs, the calculations are stopped before the solution is destroyed. Fortunately, in these cases the strongest impact on land is the leading wave. Terminating the simulation during draw-down has then no influence on the inundation distance and maximum values as long as the maximum inundation is reached. A convergence test for ComMIT/MOST are found in Appendix E.

4 Data from the laboratory experiments

The 1:500 scale model at the Coast and Harbour Reasearch Laboratory at SINTEF (SINTEF, 2008) covers the inner part of Storfjorden (Sunnylvs- and Geirangerfjorden), see Figure 4.1 where also the gauges numbered 1 to 12 are shown. At the northern boundary (y=6900 km) a wave damper extracts the energy to avoid false reflections. Eventually false reflections will occur at the gauges 1-3 and 4-6 after about 2.5 and 4 min after slide release, respectively. The 12 gauges measure the surface elevations using resistive wave sensors. In addition two level sensors measuring the water level are located in the run-up zones at both Hellesylt (coordinates in UTM32: 389092 m, 6885273 m) and Geiranger (406234 m, 6886498 m). Finally, the particle velocity at three gauges was logged during each experiment.

The numerical model applies the slide progression measured in the laboratory experiments directly, SINTEF (2008). The measurement of the slide progression is performed in the laboratory experiments by recording the run-out of a line attached to the rear end of the slide. Since the slide moves in mainly two different planes (one is at the inclined fjord slope and one is at the fjord bottom), the run-out of the line measured as a function of time cannot be related directly to the position of the slide. A rough estimate shows that the velocity of the slide motion in the numerical model is in average about 15 % higher than for the laboratory experiments, leading to slightly more conservative results in the numerical model. From sensitivity analyses, however, we conclude that deviations of these orders are insignificant.

The data from SINTEF were stored in a Excel spreadsheet for the scenarios 1A, 1B, 1C, 1D, 2A, 2B, and 3A as time history with a time-resolution of 0.02 s. Details for the different scenario is given in main report. The data included information about the slide progression, surface elevations (twelve gauges for propagation and two for run-up), as well as the particle velocity (three locations). Examples for gauges 4-6 for scenario 1C and 3A are found in Figure 4.2. Note that gauge 6 is not capable to measure elevations above 18 m (transferred to full scale). However, we believe that for similar large scenarios (1A-1D) this as only limited influence on the overall result when importing the data into the numerical model (see below), since gauge 6 is located close to the shoreline, while the main part of the energy transport is in the middle of the fjord.

The numerical model applies the slide progression measured in the laboratory experiments directly. The measurement of the slide progression is performed in the lab by attaching a line at the rear end of the slide. Since the slide moves in mainly two different planes (one is at the inclined fjord slope and one is at the fjord bottom), the distance measured as a function of time can not be related directly to the position of the slide. A rough estimate shows that the velocity of the slide motion in the numerical model is in average about 15 % higher than for the laboratory experiments, leading to slightly more conservative results in the numerical model. However, from the sensitivity analyses, see Section 5, we conclude that deviations of these orders are insignificant (Compare also the run-up heights of scenario 2A and 2B in the main report). The only difference between these two scenarios is the velocity progression. The impact velocity is 65 and 45 m/s (a divergence of 45%) for scenario 2A and 2B, respectively, but with only minor differences in run-up heights.

To convey the data from the laboratory experiments into the numerical model, the data are processed in following manner:

1. Input to the numerical model is the measured surface elevation at gauges 1-3 (for waves travelling northward) and 4-6 (southward)
2. The data for the numerical model are transferred into a field of two dimensions, space (along the boundary) and time.
    a. Linear interpolation for points lying between the gauges
    b. Constant value is given for the area between the outermost gauges and land
    c. The tsunami model (DpWaves, described above) applies the surface elevation and the velocity potential as primary unknowns. The velocity potential is calculated from the surface elevation using the linear hydrostatic relation.
3. At the boundary at the gauges 1-3 and 4-6 the data are given as forced input along these boundaries.

For more details, see NGI (2008a).

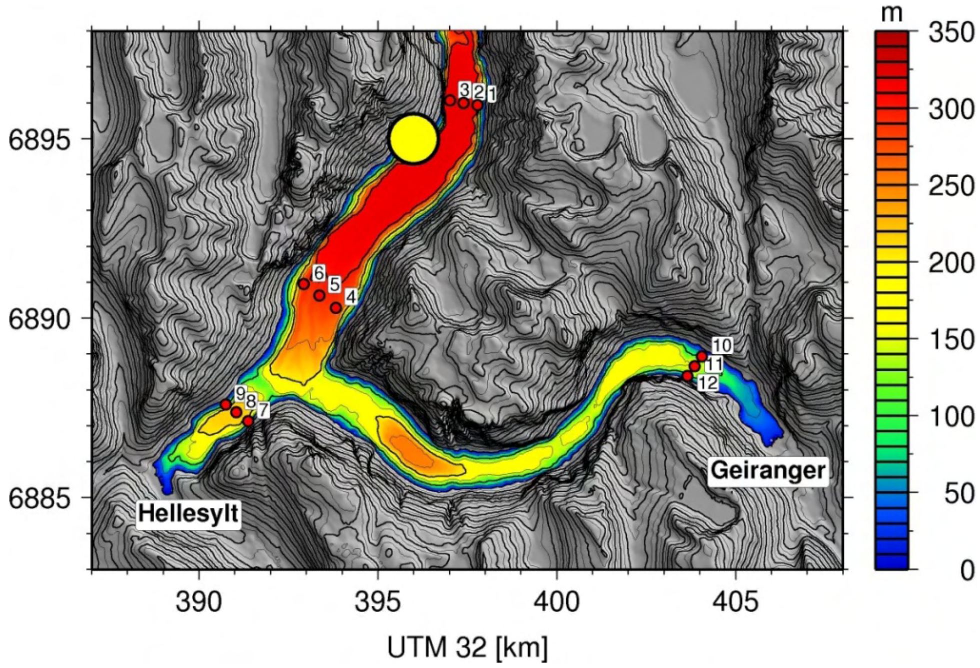

Figure 4.1. Bathymetry and topography for the laboratory experiments. The red bullets (numbered 1 to 12) are the gauges where the surface elevation is measured. The big yellow bullet indicates the location of the potential slide at Åknes.

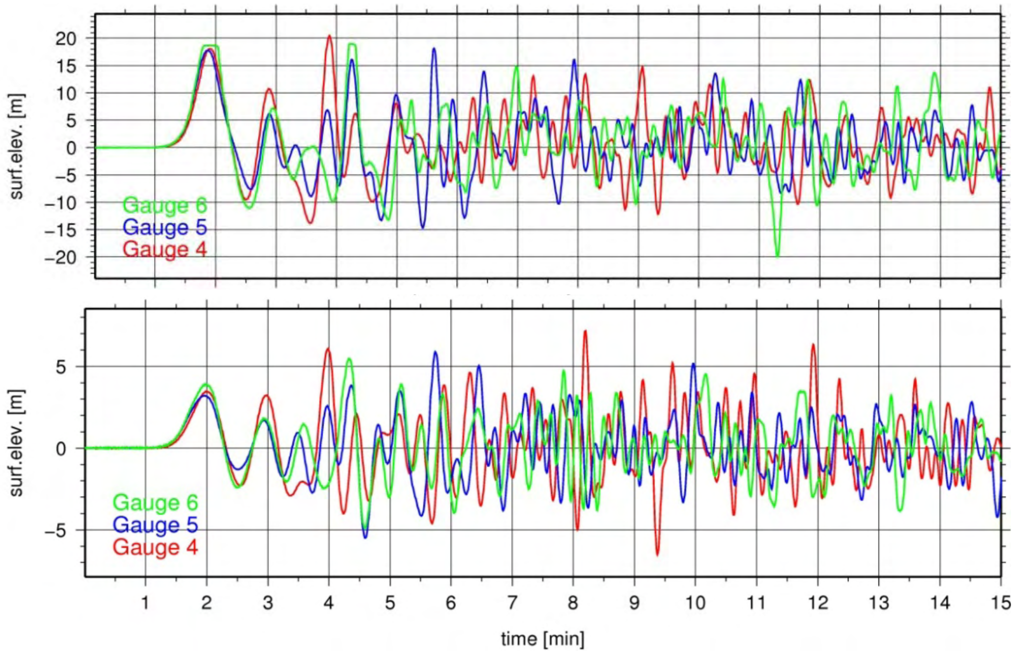

Figure 4.2. Measured surface elevation (transferred to full scale) at gauges 4 to 6. Upper and lower panel show the surface elevation for scenario 1C and 3A, respectively.

5 Sensitivity tests

5.1 Review of sensitivity tests presented in previous reports

During the Åknes/Tafjord project, NGI has performed numerous sensitivity tests. Below we list all the tests, and state the most important findings.

Report NGI (2006):

- Influence of shape of initial condition
- Influence of shape of slide
- Influence of slide run-out distance and velocity
- Effect of non-linearity and dispersion

Report NGI (2008a):

- One horizontal dimension (1HD):
    - Influence of run-out distance
    - Influence of impact velocity of slide
    - Velocity profile for the slide
    - Frontal angle of the slide
- Two horizontal dimensions (2HD):
    - Influence of the run-out distance of the slide (extended compared to NGI, 2006)
    - Effect of skin friction
    - Effect of non-linearity and dispersion in idealized and real bathymetries (extended compared to NGI, 2006)
    - Effect of slide direction

Findings:

- Dispersion in the generation phase may be crucial, especially for waves propagating in the same direction as the slide. Dispersion in the generation phase is less important in narrow fjords, where the waves are filtered through bends, crossovers, variation of fjord width, etc.
- The frontal area of the slide is much more important for wave generation than the impact velocity and the slide volume, e.g., maximum slide velocity of 50 m/s and 70 m/s gave insignificant differences of the run-up.
- The effect of the skin friction at the rock slide/water interface on the generated waves can be neglected.
- A change of the slide direction at Åknes has stronger influence on the waves propagating northward then southward.

5.2 Effect of a constant threshold depth

In the numerical model, we have for the tsunami propagation stage in addition to the special treatment of threshold depth close to the slide area (see main report) applied a constant threshold depth for the GloBouss model along all coastlines of 20 m and 50 m for the dispersive and Boussinesq model, respectively. In the model, the shoreline is moved to the depth contour line equal to the threshold depth, giving a narrowing of the fjord. This effect is of course sensitive to the bathymetry; if the 20 m or 50 m depth contour is located a longer distance from the shoreline (gentle bathymetric slopes), this may lead to a significant narrower fjord. In Figure 5.1 the results for different threshold values of 0 m, 20 m, and 50 m are shown for the 1C scenario (see main report) using the dispersive model. The different heights of the leading wave are mainly due to the volume conservation. Outside Hellesylt (gauge 8) the fjord sides and bathymetry is steep so the different contour lines are close to each other, leading to small differences on the choice of threshold depth. On the other hand, outside Geiranger (gauge 11) the bathymetry is gentler and a larger threshold depth leads to a significant narrower fjord. The volume conservation leads to higher waves for larger threshold depth. However, for the run-up calculations the waves are not restricted by the threshold depth and are also allowed to inundate dry land in all directions, see Figure 5.2. In the latter figure the surface elevations during run-up is measured at one gauge located on land.

By comparing the wave height measured outside Geiranger (gauge 11) and the subsequent run-up, we see that the leading wave at gauge 11 for 20 m and 50 m threshold is 10 % and 22 %, respectively, higher than the solution without a threshold depth. For the run-up the differences are correspondingly -13 % and -15 %. The fact that the solutions for threshold depths of 20 m and 50 m have been through the wave breaking stage while the solution for no threshold depth is still breaking (and may be reduced further) may explain the differences to the solution with 0 m threshold depth here. However, the differences between the threshold depths of 20 m and 50 m seen at gauge 11 are strongly reduced in the run-up stage. Remark that the measured differences are sensitive to the inherent noise. However, it is a clear tendency that it is the total volume of the waves rather then the surface elevations and wave breaking only that have the main influence on the wave impact during run-up.

Another finding from these tests is that a change in threshold depth changes the wave propagation speed. The main parameter for the wave propagation speed is the depth, but for waves in a fjord (or a channel), also the averaged depth across the (“numerical”) fjord affect the propagation speed. A deeper threshold depth will increase the average depth and hence lead to faster wave propagation. This is clearly seen at gauge 11 outside Geiranger in Figure 5.1.

For the tsunami model DpWaves (used for simulating input from the laboratory experiments) the threshold depth is applied without moving the shoreline to a deeper contour line. Instead all values from the contour line (at depths 20 m or 50 m) to the shoreline are replaced by the threshold depth.

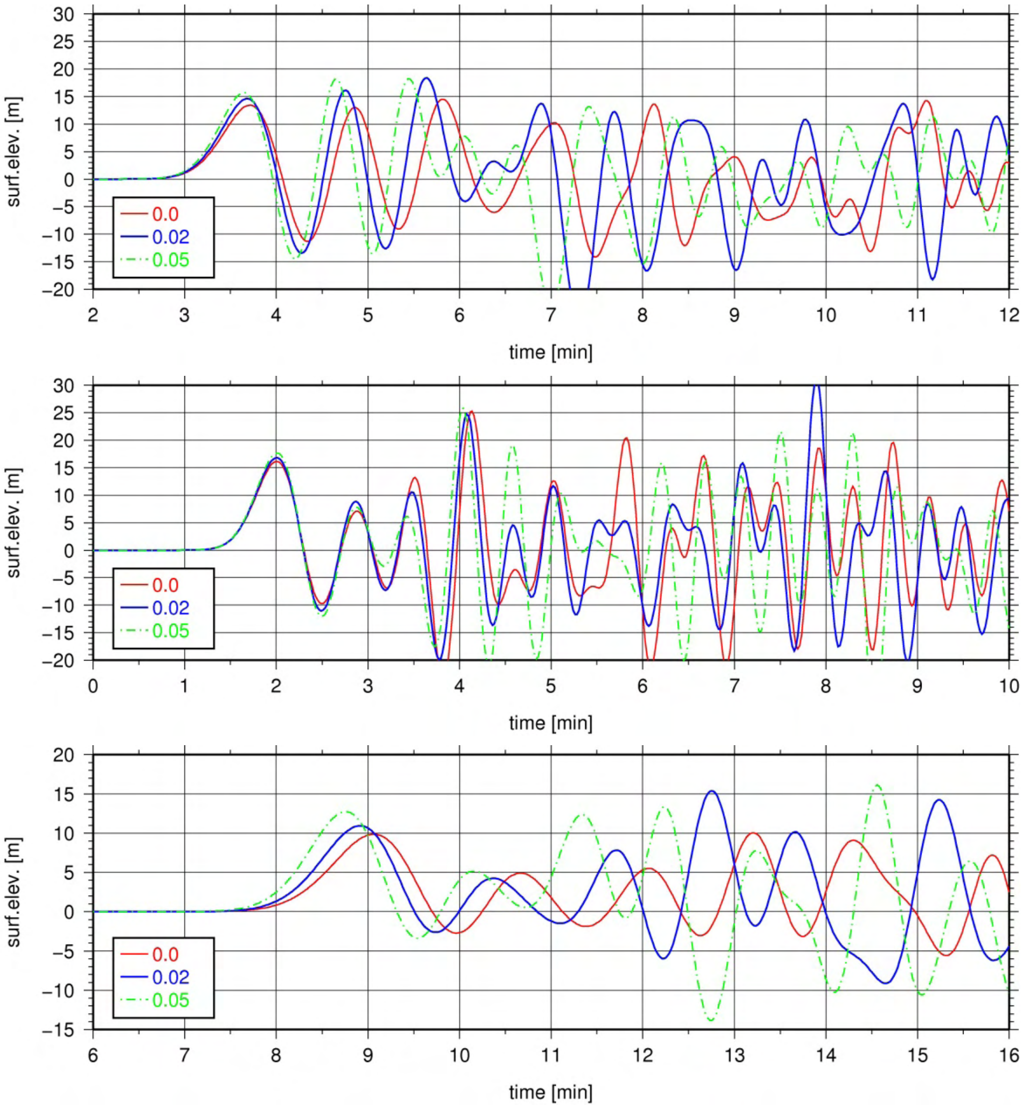

Figure 5.1: Surface elevations at gauges 5 (upper panel), 8 (outside Hellesylt), and 11 (lower panel, outside Geiranger) for three different choices of a constant threshold depth (see legend), as explained in the text. See Figure 4.1 for gauge location.

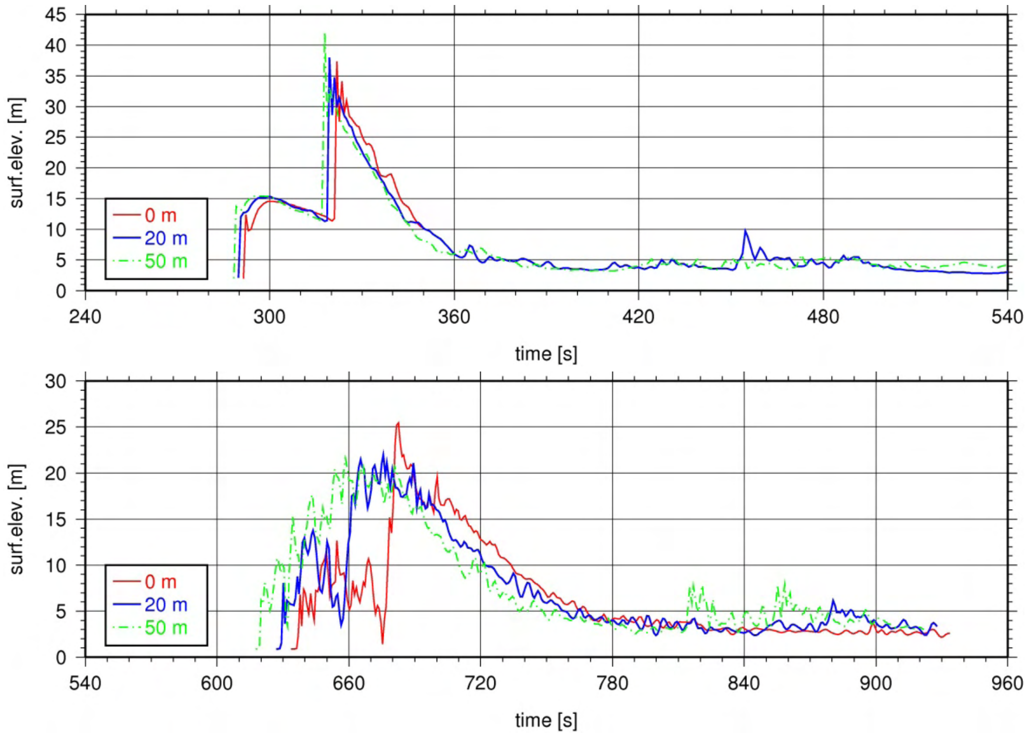

Figure 5.2: Surface elevations for scenario 1C in the run-up zone at Hellesylt (upper panel) and Geiranger (lower) for three choices of constant threshold depth (see legend) for the wave propagation stage. The coordinates for the gauges in the run-up zones at Hellesylt and Geiranger given in UTM32 are (389092 m, 6885273 m) and (406234 m, 6886498 m), respectively.

5.3 Convergence tests

5.3.1 Tsunami propagation

To verify the results found by the numerical simulations, it is crucial to investigate the grid dependence. Without such investigations, the results may seem to be physically correct, but as long as the model has not converged, they might be erroneous. In Figure 5.3 grid refinement tests are shown for the linear dispersive model. The scenario used in these tests is 1C (from Åknes) and the location of the gauges 2, 5, 8, and 11 is found in Figure 4.1. Gauge 2 is north of Åknes, 5 is south of Åknes, 8 is outside Hellesylt while 11 is outside Geiranger. For the leading waves the difference in height at gauge 2 for the 50 m and 100 m resolution is about 2.5% which is satisfactory. At longer distances away from the generation area (gauges 5, 8, and 11) the same difference is ranging from -0.2% to +0.4%. We conclude that a resolution of 100 m is sufficient. In all simulations of the tsunami generation and propagation a resolution of 100 m is applied.

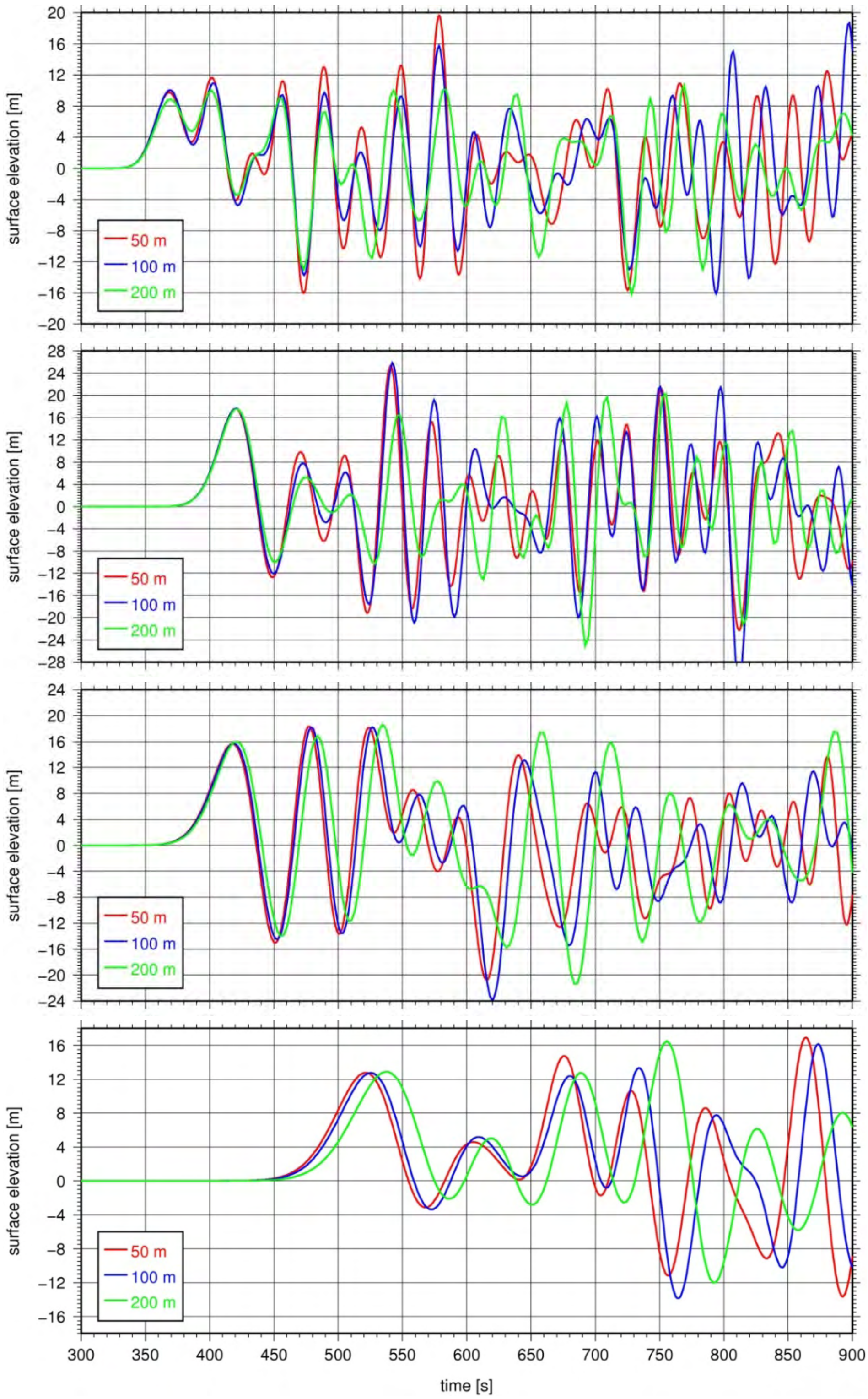

Figure 5.3: Surface elevation at gauge 2 (top panel), 5, 8, and 11 (lower panel) for scenario 1C. The different curves represent simulations with a uniform resolution from 50 m to 200 m. See Figure 4.1 page 11 for gauge locations.

5.3.2 Run-up

In Figure 5.4 the convergence test for run-up calculations is shown by time history of the surface elevation at Hellesylt for scenario 1C. The run-up model ComMIT applied in this report applies nesting of grids on totally three different levels with varying grid resolution. In the convergence test, the resolutions for the coarsest grids A and B is 40 m and 20 m, respectively, while the grid resolution on the finest grid C is varied from 5 m to 20 m. For higher resolution the oscillations are clearly reduced, and we may conclude that at least the solution for the 5 m resolution has converged. During draw-down, the high flow velocity may lead to instability. If we try to use even finer grid than 5 m, the instability problems will increase.

In ComMIT, the time resolution of the calculations for the different grid levels (A, B, and C) can be set individually. In Figure 5.5 the time history for same scenario and same location is shown for different time resolutions. The spatial resolutions used here is 40, 20, and 5 m for grids A, B, and C, respectively. The label “8-4-1” means that the time resolution on grid A and B is 8 times and 4 times the resolution on grid C, respectively. The simulations for label “1-1-1” are using the same time resolution on all levels. In the first case, the resolution in time and space (8x5m, 4x5m, and 1x5m on A, B, and C grid, respectively) is identical leading to a constant Courant number on all levels. The test reveals minor sensitivity to the choice of time resolution relative to the different grid levels, but an important finding is that the solution is more stable if a constant and not too small Courant number (less than 0.2, say) is applied on all grid levels. This is especially true for calculations with extreme large run-up heights.

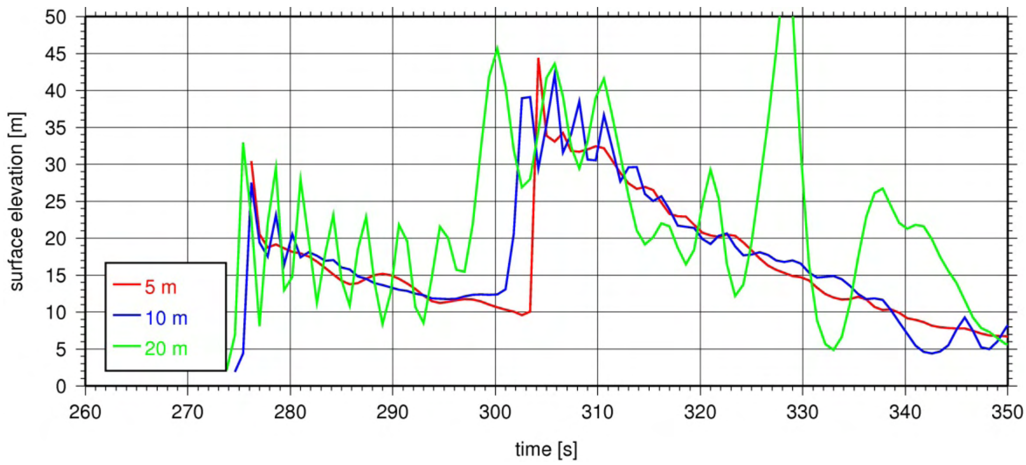

Figure 5.4: Convergence for scenario 1C at Hellesylt. The surface elevations for three different resolutions (in space) are shown.

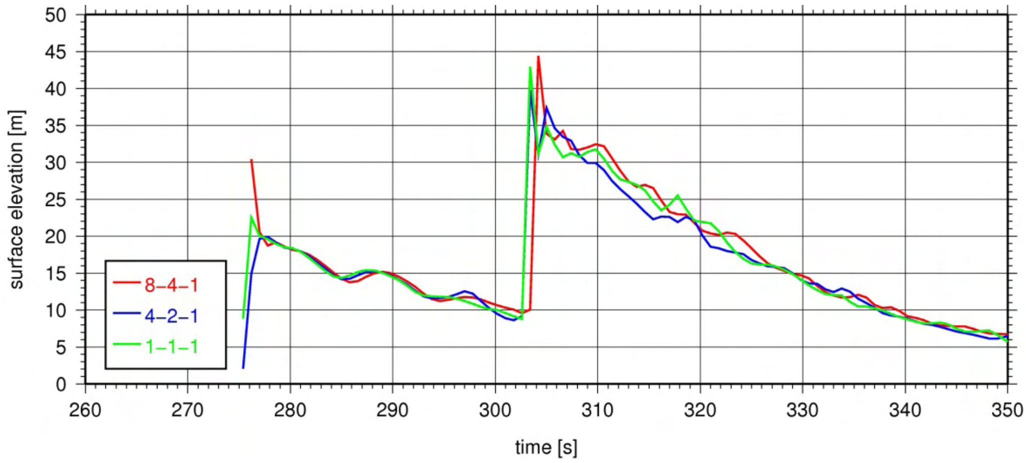

Figure 5.5: Convergence test for scenario 1C at Hellesylt. The surface elevations for three different time resolutions as explained in the text are shown. The three numbers reflect the time resolution (or more precisely ratio to the time resolution on grid C) for A, B, and C grid, respectively.

5.4 Influence of background data resolution on run-up heights

In Figure 5.6 we show the inundation lines for different resolutions of the background data (both topography and bathymetry). For the run-up simulations the resolution on the finest grid is 5 m. For the label “5m” the high-resolution data (see Section 1) are applied. On the other hand, the label “50m” indicates that data based on coarser resolution (old data) are sampled onto a 50 m grid.

For wave impacts where the lines of maximum inundation are found in steeper part of the terrain, the inundation distance is only slightly affected by the resolution of the background data, while (not surprisingly) for cases where the lines for maximum inundation is located in smoother terrain larger deviations are found.

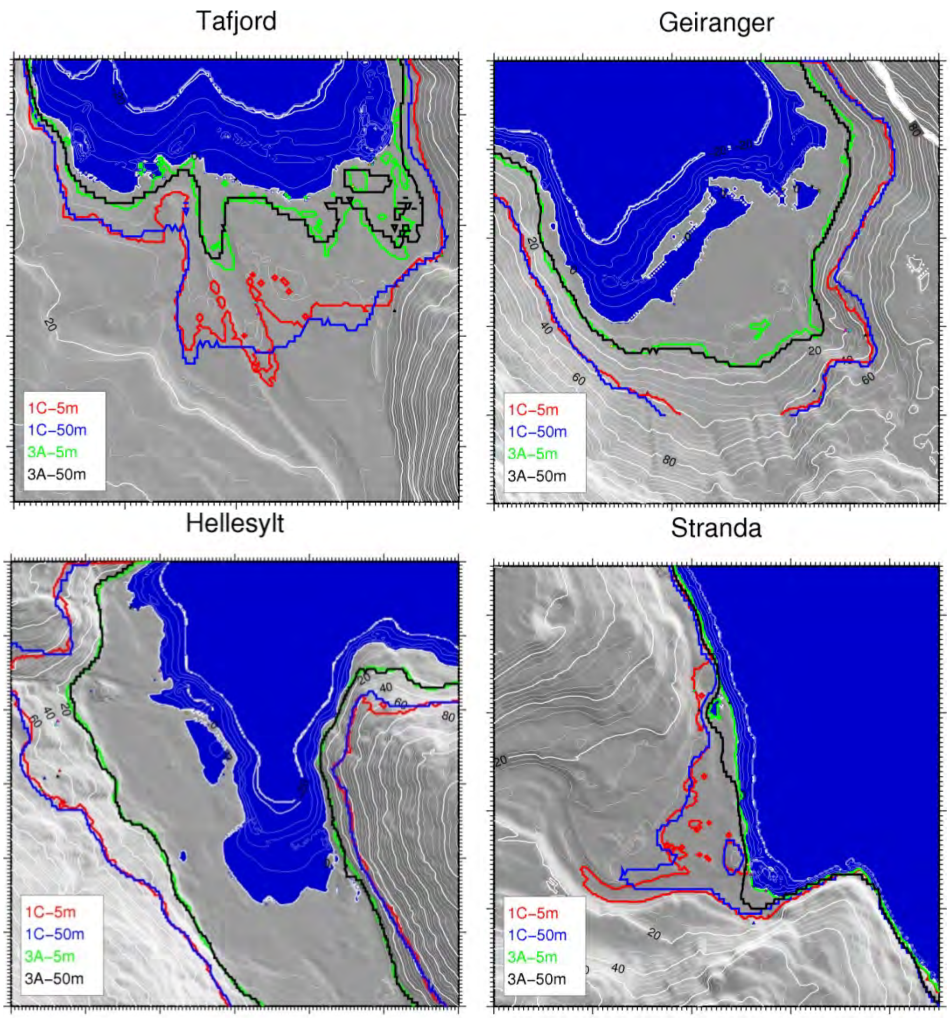

Figure 5.6: Maximum inundation lines for run-up simulations with different resolutions of the background data for scenarios 1C and 3A.

5.5 Significance of slide prolonging

As explained in the main report, there are some problems with instabilities close to the generation area when the tail of the slide enters the fjord. In most cases the problems are cured by using the threshold depth as explained in Section 3.1, while in other problem cases the slide is prolonged.

When a slide moves in the water a depression is formed at the tail which may lead to an exposed fjord-bottom, again leading to instability at least for the non-linear simulations. For the wave generation, the front of the slide (or more precisely the frontal area, see NGI, 2005 and 2008a) is the most important parameter. A way around such instability problems (not cured by the threshold depth) is to prolong the slide. In this manner only the front of the slide will contribute to the generation, since the tail then is not allowed to enter the fjord.

In Figure 5.7 we have shown surface elevations measured at gauges 5 (closer to the generation area) and 11 (outside Geiranger) for prolonged slides ("prolonged") and normal slides ("normal"). As we can se, closer to the generation area the leading peak is not influenced by the lack of the following depression. However, at longer distances the leading peak has been slightly reduced in height by the trailing depression.

For the computations presented in this report, all scenarios from Åknes apply "normal" slides, while the potential slides for Hegguraksla and the slides for the historical scenarios (Tafjord, Skafjell, and Tjelle) are prolonged.

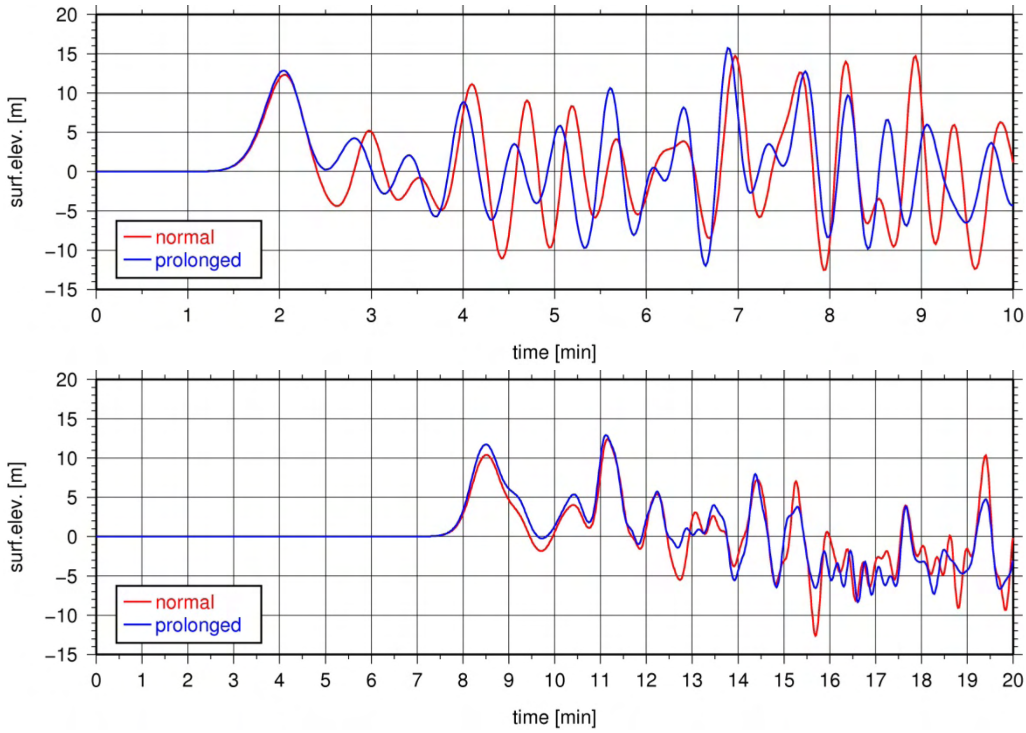

Figure 5.7: Effect of prolonging the slide to avoid numerical instabilities. Comparisons are made for scenario 1A from Åknes at gauge 5 and 11 in upper and lower panel, respectively (see Figure 4.1 page 11).

6 References

ComMIT (2010). URL: http://nctr.pmel.noaa.gov/ComMIT/ (visited 2010-02-11)

Cornell (2009) COMCOT; source code and documentation is found here: http://ceeserver.cee.cornell.edu/pll-group/comcot.htm (visited 2009-09-24).

Harbitz, C., G. Pedersen and B. Gjevik (1993). Numerical Simulations of Large Water Waves Due to Landslides. Journal of Hydraulic Engineering, Vol. 119, No. 12.

Langtangen, H.P. and Pedersen, G. (1998). Computational models for weakly dispersive and nonlinear water waves. Comput. Methods Appl. Mech. Engrg. 160, 337-358.

Løvholt, F., Pedersen, G, and Glimsdal, S. (2010). Coupling of Dispersive Tsunami Propagation and Shallow Water Coastal Response. The Open Oceanography Journal (in press).

Løvholt, F., Pedersen, G, and Glimsdal, S. (2010). Coupling of Dispersive Tsunami Propagation and Shallow Water Coastal Response. *The Open Oceanography Journal* (in press).

Løvholt, F. and Pedersen, G. (2009). Instabilities of Boussinesq models in non-uniform depth. *International Journal for Numerical Methods in Fluids.* Vol. 61 (6), 606-637.

Mei, C.C. (1989). The applied dynamics of ocean surface waves. Advanced Series on Ocean Engineering Vol. 1, 740 pp. World Scientific, London.

NGI (2005). Innledende numeriske analyser av flodbølger som følge av mulige skred fra Åknes. NGI rapport 20031100-2.

NGI (2006). Semi-annual report: Preliminary results using an improved tsunami model. NGI rapport 20051018-1.

NGI (2008a). Semi-annual report: Tsunami impact in the outer part of Storfjorden, testing of numerical models for rock slide and tsunami, coupling to laboratory experiments. 20051018-2.

NGI (2008b). Operational tsunami models with run-up. NGI report 20061073-1.

NGI (in prep.). Evaluation of the flow characteristics of the potential Akneset rock slide, western Norway – Contributions to the design of laboratory experiments on wave generation. NGI report.

Pedersen G, Løvholt F. (2008). Documentation of a global Boussinesq solver. Dept of Mathematics, University of Oslo, Norway.. URL: http://www.math.uio.no/eprint/appl_math/2008/01-08.html

Python (2010). Scripting language, http://python.org/ (visited 2010-02-11).

SINTEF (2008). Notat – rasmodell, dated 2008-09-12.

Kontroll- og referanseside/
Review and reference page

Dokumentinformasjon/*Document information*

Dokumenttittel/*Document title* Numericalsimulations of tsunamis from potential and historical rock slides in Storfjorden; Hazard zoning and comparison with 3D laboratory experiments	**Dokument nr/*Document No.*** 20051018-00-1-R
Dokumenttype/*Type of document* ☒ Rapport/*Report* ☐ Teknisk notat/*Technical Note* **Distribusjon/*Distribution*** ☐ Fri/*Unlimited* ☒ Begrenset/*Limited* ☐ Ingen/*None*	**Dato/*Date*** 21 February 2011 **Rev.nr./*Rev.No.*** 01
Oppdragsgiver/*Client* Åknes/Tafjord Beredskap IKS (ÅTB)	
Emneord/*Keywords* Tsunami, numerical modelling, rock slide	

Stedfesting/*Geographical information*

Land, fylke/*Country, County* Møre og Romsdal	**Havområde/*Offshore area***
Kommune/*Municipality* Stranda	**Feltnavn/*Field name***
Sted/*Location*	**Sted/*Location***
Kartblad/*Map* 1219 II Geiranger	**Felt, blokknr./*Field, Block No.***
UTM-koordinater/*UTM-coordinates* Sone 32 N6895460 E396000	

Dokumentkontroll/*Document control*

Kvalitetssikring i henhold til/*Quality assurance according to* NS-EN ISO9001

Rev./*Rev.*	**Revisjonsgrunnlag/*Reason for revision***	**Egen-kontroll/*Self review* av/*by*:**	**Sidemanns-kontroll/*Colleague review* av/*by*:**	**Uavhengig kontroll/*Independent review* av/*by*:**	**Tverrfaglig kontroll/*Inter-disciplinary review* av/*by*:**
0	Original document	SGl	FL		
01	Revision of document	SGl	FL		

Dokument godkjent for utsendelse/*Document approved for release*	**Dato/*Date***	**Sign. Prosjektleder/*Project Manager*** Carl Bennevie Harbitz

NGI (Norges Geotekniske Institutt) er et internasjonalt ledende senter for forskning og rådgivning innen geofagene. Vi utvikler optimale løsninger for samfunnet, og tilbyr ekspertise om jord, berg og snø og deres påvirkning på miljøet, konstruksjoner og anlegg.

Vi arbeider i følgende markeder: olje,gass og energi, bygg, anlegg og samferdsel, naturskade og miljøteknologi. NGI er en privat stiftelse med kontor og laboratorier i Oslo, avdelingskontor i Trondheim og datterselskap i Houston, Texas, USA.

NGI ble utnevnt til "Senter for fremragende forskning" (SFF) i 2002 og leder "International Centre for Geohazards" (ICG).

www.ngi.no

NGI (Norwegian Geotechnical Institute) is a leading international centre for research and consulting in the geosciences. NGI develops optimum solutions for society, and offers expertise on the behaviour of soil, rock and snow and their interaction with the natural and built environment.

NGI works within the oil, gas and energy, building and construction, transportation, natural hazards and environment sectors. NGI is a private foundation with office and laboratory in Oslo, branch office in Trondheim and daughter company in Houston, Texas, USA.

NGI was awarded Centre of Excellence status in 2002 and leads the International Centre for Geohazards (ICG).

www.ngi.no

Hovedkontor/Main office:
PO Box 3930 Ullevål Stadion
NO-0806 Oslo
Norway

Besøksadresse/Street address:
Sognsveien 72, NO-0855 Oslo

Avd Trondheim/Trondheim office:
PO Box 1230 Pirsenteret
NO-7462 Trondheim
Norway

Besøksadresse/Street address:
Pirsenteret, Havnegata 9, NO-7010 Trondheim

T: (+47) 22 02 30 00
F: (+47) 22 23 04 48

ngi@ngi.no
www.ngi.no

Kontonr 5096 05 01281/IBAN NO26 5096 0501 281
Org. nr/Company No.: 958 254 318 MVA

BSI EN ISO 9001
Sertifisert av/Certified by BSI, Reg. No. FS 32989